Questa Rock Pile Weathering and Stability Project

CHARACTERIZATION OF GOATHILL NORTH ROCK PILE, NEW MEXICO

New Mexico Bureau of Geology and Mineral Resources

Open-file Report OF-523

Prepared for Chevron Mining Inc., Questa, New Mexico

Chevron Tasks: 1.3.3, 1.3.4, 1.4.2, 1.4.3, 1.11.1.3, 1.11.1.4, 1.11.2.3, B1.1.1, B1.3.2

Revised December 13, 2009

Authors

Virginia T. McLemore, Gertrude Ayakwah, Kwaku Boakye, Andy Campbell, Ariel Dickens, Kelly Donahue, Nelia Dunbar, Gabriel Graf, Luiza Gutierrez, Lynn Heizler, Richard Lynn, Virgil Lueth, Eric Osantowski, Erin Phillips, Heather Shannon, Samuel Tachie-Menson, Remke van Dam, Vanessa C. Viterbo, Patrick Walsh, G. Ward Wilson, and Dirk van Zyl

With field and laboratory assistance from Cathy Aimone-Martin, Soloman Ampim, Kojo Anim, George Austin, Jack Adams, Shannon Archer, Dustin Baca, Joann Baker, Brenda Bews, Kwaku Boakye, Lynn Brandvold, George Brimhall, Ariel Dickens, Melissa Dimeo, Frederick Ennin, Prosper Felli, Murray Fredlund, Bonnie Frey, Leann Giese, Gabriel Gomez, Phoebe Hauff, Jan Hendrickx, Glen Jones, Karen Karen, Christian Kruger, Lynne Kurilovitch, Joseph Marcoline, Chris McKee, Christine McLemore, James McLemore, Nancy McMillan, John Morkeh, Mike Ness, Samuel Nunoo, Anthony Oduro-Darkwa, Kayode Olanrewaju, Stacey O'Neil, Frederick Partey, Patty Jackson Paul, Doug Peters, Mike Pullin, John Purcell, James Quarles, Steve Raugust, Amanda Rowe, Farid Sariosseiri, John Sigda, Michael Smith, Dawn Sweeny, Alex Tamm, Ed Truijullo, Karin Wagner, Bruce Walker, Donald Wenner, Nate Wenner, Sean Wentworth, Soloman Wenzel, John Wilson, Shannon Archer Williams, Todd White, and Amber Woodyatt

Project Management by

Terry Chatwin, Jack Hamilton, Virginia T. McLemore, George Robinson

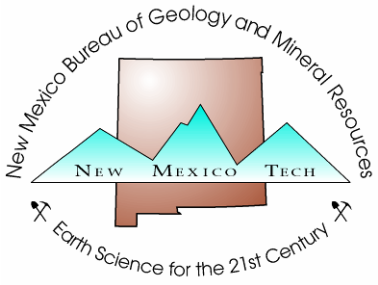

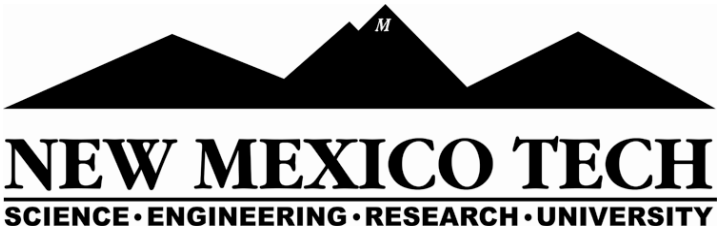

EXECUTIVE SUMMARY

Nineteen trenches were constructed in the Goathill North (GHN) rock pile as it was regraded in 2004-2005. The regrading of GHN provided a rare opportunity to examine, map, and sample the interior of this rock pile. The GHN rock pile is stratified and the strata can be correlated down slope through the rock pile. Rock fragment lithology is generally consistent within mapped units and correlates well with mineralogy and chemistry. Detailed geologic mapping and sampling revealed mappable geologic units in the rock pile, which were correlated between benches and to opposite sides of each trench, and units were correlated down slope through the excavated trenches. Units were defined on the basis of particle size, color, texture, stratigraphic position, lithology, and other physical properties that could be determined in the field. Eighteen geologic units were differentiated, described, and sampled. The units also could be distinguished within the adjacent drill holes.

Weathering is the set of physical and chemical changes, up to and including disintegration of rock by physical, chemical, and/or biological processes occurring at or near the earth's surface (e.g. in the vadose zone at temperatures less than or equal to approximately 70°C) that result in reductions of grain size, changes in cohesion or cementation, and changes in mineralogical composition. In this operational definition, there is no clear distinction between weathering and diagenesis, although the coarse-grained and subaerial nature of the mined rock pile restricts the nature of "diagenetic" reactions compared to, for example, those that might occur in a submarine, saturated system. From this mapping and analyses of samples, four different zones of weathering can be distinguished at GHN:

- outer oxidized zone (included the surface, unit C, and geologic units I and J)
- intermediate zone (included unit N)
- inner, less oxidized, unweathered zone (included units K-W)
- basal oxidized zone (included geologic units R and rubble zone).

The regrading of GHN provided a rare opportunity to examine, map, and sample the interior of this rock pile. The GHN rock pile is stratified and the strata can be correlated down slope through the rock pile. Rock fragment lithology is generally consistent within mapped units and correlates well with mineralogy and chemistry. The majority of geochemical activity appears to be confined to the interface regions of the rock pile, but not all of these regions exhibit weathering effects. The areas most affected by weathering processes are the 1) surface-atmosphere, 2) bedrock-rock pile (rubble zone) areas, and 3) interfaces between fine- and coarse-grained layers in the interior zones where water and/or humid air flow and oxidize the rock pile material. Weathering generally decreased from the outer edge of the rock pile to its interior and then increased toward the base of the rock pile. Where water and oxygen are available, pyrite and calcite are being dissolved by weathering to form gypsum, jarosite and other soluble Fe salts. Oxygen and water are available at and near the surface of the rock piles, at and near the base of the rock pile, in permeable strata within the rock pile, and along cracks and crevasses cutting across the strata that have been formed by slope movement and possibly other means. Stable isotopes of pore water and precipitation indicate that evaporation at and near the surface is an important process in moving water out of the rock pile. Clays are not being generated by weathering in the rock pile, but were formed by hydrothermal alteration of the rocks before mining. Electron microprobe work, mineralogy and chemistry changes within GHN, and chemistry of waters draining from the rock pile have established that incongruent (residue remains or new phase forms) and congruent (dissolution) mineral dissolution have occurred. Authigenic gypsum, jarosite soluble efflorescent salts, Fe oxide minerals and to a lesser extent,

clay minerals liberated from the mined rock material during construction of the rock piles (i.e. pre-mining clay minerals), have cemented parts of GHN rock pile material. The rock fragments typically are not weathered except along fractures.

It is difficult, but possible to distinguish between pre-mining hydrothermal alteration and post-mining weathering, by using detailed field observations and petrographic analysis that includes defining the paragenesis (sequence of events), especially using microprobe analyses. The evidence for weathering in the Questa rock piles includes:

- Change in color from darker brown and gray in less weathered samples (original color of igneous rocks) to yellow to white to light gray in the weathered samples. However, the mineralogical effect of the fast-reacting (less than 40 yrs) weathering pyrite system is to produce precipitates of secondary reaction minerals on the surface of existing rock fragments and within the soil matrix, which result in the yellow to orange color, reflecting the role of ferric iron in the mineral structures. The secondary precipitates form coatings on exterior surfaces, rims, and fill macro- and micro-fractures. Thus, the macro-scale impression of weathering, caused by the discoloration from the observed secondary precipitates is exaggerated.
- Thin yellow to orange, "burnt" layers within the interior of GHN, where water and/or air flowed and oxidized the rock-pile material.
- Paste pH, in general, is low in oxidized, weathered samples and paste pH is higher in less weathered samples.
- Increase abundance of jarosite, gypsum, Fe-oxide minerals and soluble efflorescent salts (locally as cementing minerals), and low abundance to absence of calcite, pyrite, and epidote in weathered samples.
- Tarnish or coatings of pyrite surfaces within weathered samples.
- Dissolution textures of minerals (skeletal, boxwork, honeycomb, increase in pore spaces, fractures, change in mineral shape, accordion-like structures, loss of interlocking textures, pits, etching) within weathered samples.
- Change in bulk textures of the rock-pile material including increase in soil:rock ratio, piping or stoping within the rock pile, and decrease in grain size due to physical weathering.
- Chemical classification as potential acid-forming materials using acid base accounting methods.
- Chemical analyses of water samples characterized by acidic, high sulfate, high TDS, and high metal concentrations (Al, Ca, Mg, Fe, Mn, SO_4).

Friction angle, point load strength index and slake durability index of the GHN rock pile samples decreased as the degree of weathering increased in some samples but not all. However, the decreases were still quite small and suggest that 25-40 years of weathering have not substantially affected the shear strength properties of these rock pile materials. Some, but not all samples located on the outer edge of the rock pile disintegrated more and presented lower durability. Comparison of slake durability and point load indices of fragments in the rock pile to values of un-weathered drill cores of rocks with similar lithologies to those in the pile show that rock fragments in the GHN rock pile have not experienced considerable weathering after emplacement. Therefore, lower values of friction angle, point load strength index and slake durability index of samples from the outer edge of the pile are likely due to post-deposition oxidation, which is consistent with the change in color, loss or obscuring of original igneous texture on the edges and within many rock fragment grains, and increase in weathered minerals

(i.e. gypsum, jarosite). Conversely, the point load strength index and slake durability index values of samples on the interior of the pile are similar to the values of un-weathered drill core samples. Consequently, the samples from the interior of the GHN rock pile are not more weathered since its emplacement. However, the differences in friction angle between the outer and interior units are relatively small. These and other studies suggest that changes in physical properties (i.e. particle size, texture and fabric) have a larger effect than mineralogic and chemical changes on the friction angle than do mineralogic and chemical changes. The shear strength would be expected to increase with increase in cementation. Cementation in the short term is controlled by gypsum, jarosite, and other salts. These less stable minerals could form the building blocks (sites) for further stronger cementation consisting of hematite and goethite. Collectively, these results suggest that future weathering will not substantially decrease the friction angle of the rock piles with time.

TABLE OF CONTENTS

LIST OF APPENDICES

LIST OF FIGURES

LIST OF TABLES

INTRODUCTION

PURPOSE

Rock piles, the preferred term by some in the metal mining industry today, refer to the man-made structures consisting of piles of non-ore overburden material and mineralized rock too low grade to process that had to be removed in order to extract ore. This material, referred to in older literature as mine waste, mine soils, overburden, stockpiles, spoil piles, subore, or proto-ore, does not include the tailings material, which consists of non-ore material remaining after milling. During open-pit mining, the overburden material was removed to gain access to the ore and placed in massive rock piles. Traditionally, this material was discarded in the most efficient and least costly manner possible by dumping in rock piles as close to the open pit as possible to limit haulage costs. Typically, these rock piles were not characterized or studied extensively because they had little significance to the operating mine. However, many rock piles subsequently developed environmental problems including acid rock drainage (ARD), leaching of heavy metals, erosion, slope stability concerns, and undesirable aesthetic views. Now there is a need for basic information and understanding of the construction, characterization, and weathering processes occurring within these man-made features.

Rock piles are some of the largest man-made structures at a mine site by volume, weight and height (Robertson, 1982). Many rock piles have been characterized in the literature in order to:

- Characterize pre-mining background conditions (Briggs et al., 2003).
- Characterize and predict stability and erosion (Dawson, 1994; URS Corporation, 2003).
- Predict acid rock drainage (McLemore et al., 2004b, Shaw et al., 2002).
- Properly dispose of and manage mine overburden material (Dawson, 1994).
- Develop mine closure plans (URS Corporation, 2003; Wels et al., 2002).

Most site characterizations of rock piles are based upon:

- Drilling of the rock piles (Robertson GeoConsultants, Inc. 2000a, b; URS Corporation, 2003)
- Shallow surface test pits (URS Corporation, 2003)
- Composite surface sampling (Smith et al., 2000a, b; Munroe and McLemore, 1999; Munroe et al., 2000; Briggs et al., 2003; Wildeman et al., 2003).

Rarely do these methods of site characterization allow for examination, mapping, and sampling of the interior of large rock piles in situ. The Questa study provided an opportunity to examine the interior of a large rock pile.

The Questa Rock Pile Weathering and Stability Project (QRPWASP) was a scientific research project, focusing on the earth sciences, hydrology, and geotechnical engineering. It was not a site-specific engineering or regulatory analysis of a specific rock pile. The purpose of the QRPWASP is to determine how and to what extent weathering affects the gravitational stability of the Questa mine rock piles over time periods on the orders of 100 and 1000 years. Gravitational stability refers to the static stability evaluated along circular (and other shaped) failure surfaces that are at least 10 m deep. Static stability is evaluated assuming limit equilibrium and the method of slices, which is based on moment and/or force equilibrium of imposed shear stress and available shear strength of the material along an assumed failure surface. Gravitational stability of the rock-pile mass for the QRPWASP analysis does not include considerations of material loss and small surface related failures as a result of erosion, or dynamic loading effects as a result of seismicity. It also does not include consideration of creep displacements and their effects, or failures through weak foundation layers.

The purpose of this report is to describe the structural, stratigraphic, physical, chemical, mineralogical, hydrological, and geotechnical characteristics and extent of weathering of the GHN rock pile. These characteristics will be used to model the GHN rock pile and to model future weathering of the Questa rock piles. The purpose of this report is to understand weathering processes both at the surface of and within the GHN rock pile and determine the geotechnical parameters that control slope stability and how they are affected by physical properties, mineralogy, and chemistry.

The key question to be addressed is, "Will the rock piles become gravitationally unstable over time?" One component of this investigation is to estimate what changes in these conditions and processes, if any, that have occurred since construction of the rock piles, and thereby to extrapolate what future changes might occur in these conditions and processes. As a result, it should be possible to obtain information necessary to provide a scientific basis for determining the effect of weathering on the geotechnical behavior of the rock piles as a function of time and degree of weathering. The technical approach tests the geotechnical behavior of samples across a range of weathering states that are defined by petrology, mineralogy, and chemistry for samples collected from the existing rock piles and elsewhere in the Questa-Red River area.

During the period of open pit mining (1969-1982) at the Questa mine, approximately 350 million tons of overburden rock was removed and deposited onto mountain slopes and into tributary valleys forming nine rock piles surrounding the open pit. Since the rock piles were emplaced, a number of shallow-seated failures, or slumps, have occurred at Questa, and a foundation failure occurred at Goathill North rock pile that resulted in sliding of the rock pile (Norwest Corporation, 2004). This slide was halted by unloading and buttressing of the rock pile, and GHN is now stable. The regrading of the Goathill North (GHN) rock pile at the Questa molybdenum mine provided a rare opportunity to examine, sample, and develop a conceptual model of the undisturbed interior of a large mine rock pile in situ using the trenches cut into the rock pile as regrading progressed.

DEFINITIONS

Alteration is a general term describing the changes in mineralogy, texture, and chemistry of a rock as a result of a change in the physical, thermal, and chemical environment in the presence of water, steam, or gas, including those changes produced by weathering (Henley and Ellis, 1983; Reed, 1994, 1997; Neuendorf et al., 2005; Ludington et al., 2005). The nature of the alteration depends upon (Browne, 1978; Henley and Ellis, 1983; Ludington et al., 2005):

- Temperature and pressure (including amount of overburden or depth) at the alteration site
- Composition of the parent rock
- Quantity and composition of the altering (invading) fluids
- Permeability of the parent rock
- Duration and intensity of the alteration process (i.e. time)
- Distance from the alteration source, resulting in alteration zoning
- Climate.

Hydrothermal alteration is the change in original composition of rock in situ by hydrothermal (warm to hot) solutions during or after the mineralization. In the Questa study, hydrothermal alteration refers to pre-mining conditions. Alteration includes hypogene or hydrothermal (primary), supergene (secondary), and weathering alteration. *Hypogene alteration* occurred below the surface during the formation of the ore body by upwelling (ascending) hydrothermal

or warm to hot fluids (Neuendorf et al., 2005). *Supergene alteration* is the natural weathering, before mining, of the ore body, at low temperatures at and near the Earth's surface by descending fluids (Neuendorf et al., 2005).

Weathering is the set of physical and chemical changes, up to and including disintegration of rock by physical, chemical, and/or biological processes occurring at or near the earth's surface (e.g., within approximately 300 ft of ground surface at temperatures less than or equal to approximately 70°C) that result in reductions of grain size, changes in cohesion or cementation, and change in mineralogical composition (modified from Neuendorf, et al., 2005). *Diagenesis* is a broad term related to the chemical, physical, and biological changes affecting sediment after its initial deposition and during and after its lithification. Diagenesis does not include weathering or metamorphism of the sediment, but does include pedogenesis or the processes that form soils (Neuendorf et al., 2005). In terms of the Questa rock piles (man-made sediment), weathering and diagenetic processes overlap in time and space, especially in cementation of the rock-pile material. Cementation is the diagenetic process where sediments become lithified or consolidated or the binding-together of particles into hard, compacted rocks (Neuendorf et al., 2005). Cementation is important in the Questa study, because cementation could increase the slope stability of the rock piles in both the short (<100 years) and long term (>100 years). In this operational definition, there is no clear distinction between weathering and diagenesis, although the coarse-grained and subaerial nature of the mine rock pile restricts the nature of "diagenetic" reactions compared to, for example, those that occur in a submarine, saturated system.

The general expression of weathering in natural environments is three-fold:

- Transformations of minerals from their pre-depositional character to new compositions and structures in better accord with the new energy environment. For example, pyrite oxidizes in the presence of oxygen and water; the iron and sulfate released in the dissolution process may be re-precipitated elsewhere as secondary minerals such as jarosite or goethite or released in the water as seeps or springs at the base of the rock piles.
- Changes in rock texture due to dissolution, precipitation, or solid-state transformations. For example, a rock containing stockwork veins with pyrite and calcite can weather under oxidizing conditions as the pyrite oxidizes, calcite dissolves, and secondary gypsum and iron oxides precipitate; the mineralogical changes can be observed microscopically or even macroscopically. Especially if there is low confining stress (i.e., near the surface of the rock pile), the large molar volume of gypsum compared to the molar volumes of the parent minerals could fracture the rock along veinlets where this reaction is occurring.
- Changes in rock texture and particle size due to mechanical strain. An example of mechanical strain with a geochemical source was illustrated by the secondary gypsum-wedging example above. Frost-wedging of fractures by ice during winter conditions is a comparable, entirely physical process that can fracture (in fact, "frost-shatter") rocks. If the stress of the overlying column of rock is sufficiently great and lateral confining pressures are low, it also is possible for crushing to occur deep in a rock pile.

SITE DESCRIPTION

The Questa molybdenum mine is located on the western slope of the Taos Range of the Sangre de Cristo Mountains of the southern Rocky Mountains near the edge of the Rio Grande rift in north-central New Mexico (Fig. 1). The mine is on southward facing slopes and is

bounded on the south by Red River (elevation of approximately 7500 ft) and on the north by mountain divides (elevation approximately 10,750 ft; Fig. 2). The Questa rock piles extend from approximately 8000 ft to 9610 ft in elevation, resulting in some of the highest rock piles in the United States (Shaw et al., 2002, 2003). Many of the side slopes of deeply incised valleys in the mine area are steep, with typical slope grades between 2:1 and 1.4:1.

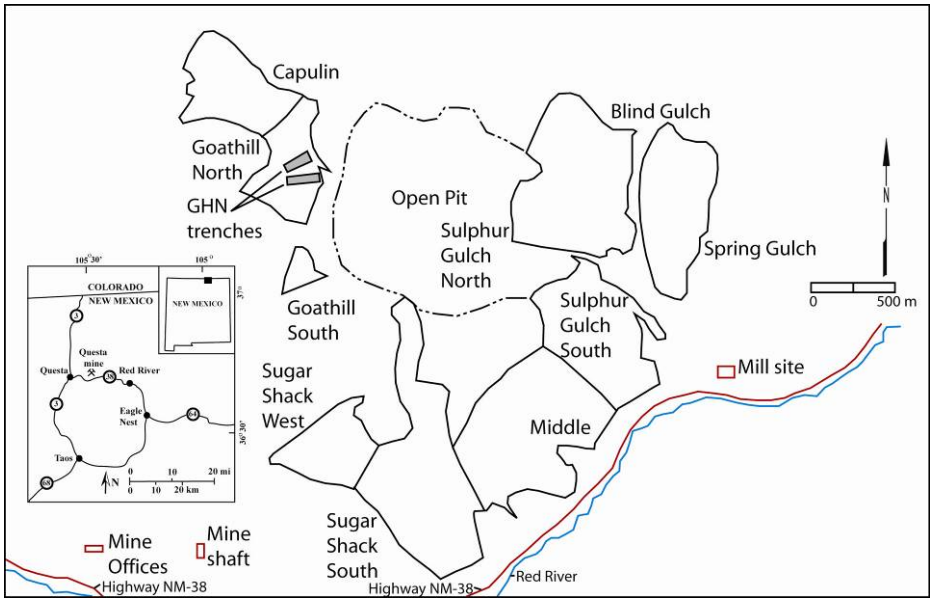

FIGURE 1. Location of the Questa molybdenum mine, northern Taos County, New Mexico.

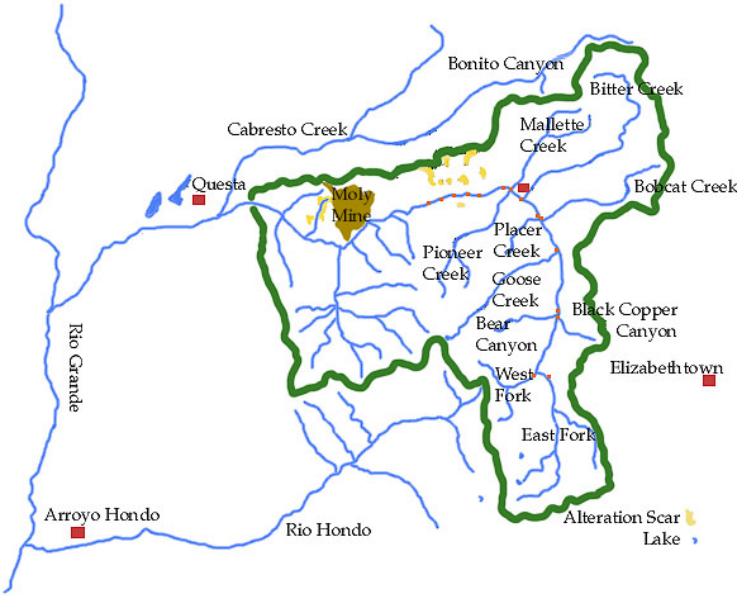

FIGURE 2. Location of the Questa molybdenum mine within the Red River basin. Green line delineates the Red River watershed.

OVERALL TECHNICAL APPROACH

The University of Utah collaborative team was formed to examine the effects of weathering on the Questa rock-pile stability. The team consists of multi-disciplinary scientists from several universities and consulting firms:

- University of Utah (UU, lead university)
- New Mexico Institute of Mining and Technology (NMIMT)/New Mexico Bureau of Geology and Mineral Resources (NMBGMR)
- University of British Columbia (UBC)
- SoilVision Systems
- University Nevada–Reno
- University of California–Berkeley
- R^2, Inc.
- Minnesota Department of Natural Resources
- Geochimica, Inc.

It should be noted that chemical weathering can have at least two qualitatively different influences on slope stability. First, dissolution of feldspars, biotite and other silicate minerals (congruent weathering) by acidic fluids generated by oxidation of sulfide minerals, can result in the reduction of particle sizes and in the generation of clay minerals, both of which have the potential to adversely affect rock-pile stability. Second, secondary chemical precipitates, such as sulfates, Fe-oxide minerals, and oxyhydroxides formed as a result of pyrite oxidation (as well as other reaction products), can form surface crusts that could inhibit infiltration and evapotranspiration and also can cement soil grains. In this case, the additional cohesion due to formation of such cemented aggregates has the potential to increase rock-pile stability (Boakye, 2008). Generation of water-soluble cements (e.g., soluble hydroxysulfates that can form during evaporation in shallow soils) have the potential to increase cohesion during the dry season, but not effectively cement the particles during runoff and snowmelt seasons. Both dissolution and cementation processes are operational at the Questa site and have been observed at many mining sites previously (Ritchie, 1994; Morin et al., 1997; Munroe and McLemore, 1999; Munroe et al., 2000; Fines et al. 2003; Tran et al., 2003).

CLIMATE OF THE RED RIVER VALLEY

The climate at the Questa mine is semi-arid and alpine, with cold snowy winters and moderate warm summers with monsoons during July and August. Summer rains often cause mudslides and flash floods in alteration scar areas that have at times blocked the highway. Since historical climate information can play an important role in determining future impacts of climate on the rock piles at the Questa mine, historical data have been collected from multiple sources and incorporated into a climate database. This database provides information to be used in modeling future climate patterns for the area. Climatic data was downloaded from the National Climatic Data Center (NCDC) for several locations near the Questa mine including Red River, Eagle Nest, Cerro and Taos (Tables 1, 2). These data include temperature, precipitation and snowfall for all four weather stations and evaporation information from Eagle Nest. Additional data for this project were taken from spreadsheets produced by Robertson GeoConsultants, Inc. and Golder Associates, Inc. (2005a, b).

The Red River drainage basin receives an average of 20.4 inches of precipitation per year, concentrated in July and August (Hagan, 2001; based on mean annual precipitation measured between 1931 and 1996). The rock piles from 1965-2003 received an average of 14.2

inches per year (Table 3; Golder Associates, Inc. 2005a, b). The mean maximum annual temperature is 12.4˚C and the mean minimum annual temperature is –5.9˚C, as measured between 1906 and 2001 (Hagan, 2001).

The differences in relief between the rock piles result in large variations in temperature and precipitation each rock pile is subjected to (Golder Associates, Inc. 2005a, b). Temperature extremes tend to be lower for stations at higher elevations than for those at lower elevations, but the precipitation data demonstrate much stronger differences between stations at different elevations. This is shown by the variation in average annual precipitation between several National Weather Service stations located in the area (Tables 1, 2, 3). Cerro receives an average of 16.8 inches of precipitation annually while Eagle Nest, Red River and Taos receive 20.1, 34.6 and 14.7 inches, respectively (Fig. 3). Daily temperature ranges increase with decreasing elevation. When aggregated on a monthly basis, daily lows are much more variable, as represented by the data range for each month, during the colder months (December–April) than the warmer months. Inspection of the monthly rainfall and snowfall data reveals that median and maximum monthly precipitation increases with increasing elevation. Annual rainfall ranged between 15 and 34 inches (Fig. 3). Average annual relative humidity does not vary with elevation, topography or specific location and averages 0.4-0.5% (Golder Associates, Inc., 2005a, b).

Maximum precipitation events also vary greatly across the area. The largest single 24-hour precipitation event recorded in New Mexico occurred on May 18-19, 1955 at Lake Maloya which received 11.28 inches of precipitation (Western Regional Climate Center, 2006). This event also produced the largest single daily (May 18, 1955) precipitation total recorded for Eagle Nest (5.6 inches) and Taos (2.9 inches). The largest single daily precipitation event at Cerro produced 7.5 inches (August 17, 1922) and the largest single daily event at Red River occurred on March 12, 1985 with a precipitation total of 5.61 inches (Fig. 4). The highest multiple-daily precipitation event in the area occurred at Red River from April 28 through May 4, 1999 and resulted in 7.81 inches of precipitation. It should be noted that Red River received 8.25 inches of precipitation between July 14 and September 2, 1929, even though, there was a break in the precipitation from August 3 to August 20, 1929. Other high total, multiple-daily precipitation events occurred at Eagle Nest from February 4-6, 1989 (7.15 inches) and at Taos on May 18-19, 1955 with a total of 4.37 inches of precipitation (Fig. 5). The maximum precipitation the rock piles experienced was in 1979 and averaged 19.2 inches for the year (Table 3; Golder Associates, Inc., 2005a, b).

TABLE 1. Summary of weather stations in the vicinity of the Questa mine. All locations are in NAD 27, UTM zone 13. NWS—National Weather Service. NRCS—Natural Resources Conservation Service

Station	Location	Period	Authority	Elevation (ft)	UTM easting (m)	UTM northing (m)
Lobo Peak	Lobo Peak	1947-1957	NWS	10350	441949.915	4063436.836
Red River	Red River	1915 to present	NWS	8676	461073.137	4067949.792
Midnight mine	Red River mining district	1957-1976		10427	459881.166	4078124.292
TP-1	tailings		Molycorp			
TP-4	Sugar Shack South near WRD-5, upper bench		Molycorp	9280	454219.000	4060731.000

Station	Location	Period	Authority	Elevation (ft)	UTM easting (m)	UTM northing (m)
TP-7	lower bench Sugar Shack South near WRD-3		Molycorp	8705	454245.000	4060396.000
TP-5	Capulin, near WRD-8		Molycorp	9805	453070.900	4063231.000
Taos	Rio Grande valley	1931 to present	NWS	6965	459888.009	4026358.043
Latir Lake	Sangre de Cristo Mountains	1966-1976	NWS	8806	456947.123	4085534.480
Elizabethtown	Sangre de Cristo Mountains	1931-1948	NWS	8470	467246.565	4061453.482
Anchor mine	Red River mining district	prior to 1928	unknown	10600	462852.649	4078110.813
Taos Pueblo	Rio Grande valley	2003-present	NWS	6990	438773.897	4035417.869
TP-2	tailings		Molycorp			
North Costilla	Sangre de Cristo Mountains	1979 to present	NRCS	10600	469988.630	3993041.741
Red River Pass 2	Sangre de Cristo Mountains	1979 to present	NRCS	9850	464307.895	4070708.895
ST-2	midslope on Sugar Shack West near WRD-6		Molycorp	8650	453462.100	4060811.000
Cerro	Sangre de Cristo Mountains	1931-present	NWS	7650	439052.437	4074550.394
Tres Piedras	Sangre de Cristo Mountains	1931 to present	NWS	8140	406246.108	4065601.820
San Cristobal	Sangre de Cristo Mountains	1947-1958	NWS	8110	438933.719	4057911.189
TP-3	tailings		Molycorp			
ST-3	plateau area in Spring Gulch near WRD-1		Molycorp	9075	455737.000	4062543.000
TP-6	lower bench Sugar Shack South near WRD-3		Molycorp	8705	454245.000	4060396.000
Hondo Canyon	Sangre de Cristo Mountains		NWS	10509	453847.464	4061515.211
ST-1	midslope on Sugar Shack South near WRD-4		Molycorp	8915	45440.000	4060607.000
Skardaa		1940-1983	NWS	8280	406388.174	4078544.259
mill site	Questa	1995 to present	Molycorp	8055	456087.000	4061204.000
Eagle Nest	Sangre de Cristo Mountains	1931-present	NWS	8260	468708.669	4054052.550
Philmont Ranch	Sangre de Cristo Mountains	1941-1961	NWS	7610	488090.086	4061399.129

TABLE 2. Average monthly climate summary at Red River from January 1915 to December 2002 (Maest et al., 2004; Western Regional Climate Center, 2006).

Month	Average max temp °C	Average min temp °C	Average total prec (cm)	Average snow fall (cm)	Average snow depth (cm)
January	2.5	-15.4	2.7	50.8	22.9
February	4.1	-13.3	2.9	54.1	22.9
March	6.7	-9.7	4.5	74.4	17.8
April	12.0	-5.6	4.4	55.4	5.1
May	16.9	-1.8	4.4	18.5	0
June	22.6	1.8	3.2	0.3	0
July	24.4	4.9	7.4	0	0
August	23.3	4.6	8.0	0	0
September	20.4	0.9	4.2	1.3	0
October	14.8	-3.8	3.8	21.1	0
November	7.2	-9.9	3.4	47.0	5.1
December	3.1	-14.4	2.9	48.3	15.2
Annual	13.2	-5.2	52.0	370.0	7.6

TABLE 3. Summary of climatic statistics for Questa rock piles (Golder Associates, Inc. 2005a, b).

	Time Period	Precipitation (inches)	Infiltration (inches)	Infiltration %	Evaporation (inches)
Average annual	1911-2003	14.1	1.9	14	12.2
Maximum annual	1979	19.2	5.8	30	13.0
Average annual for rock pile life	1965-2003	14.8	2.1	14	12.6

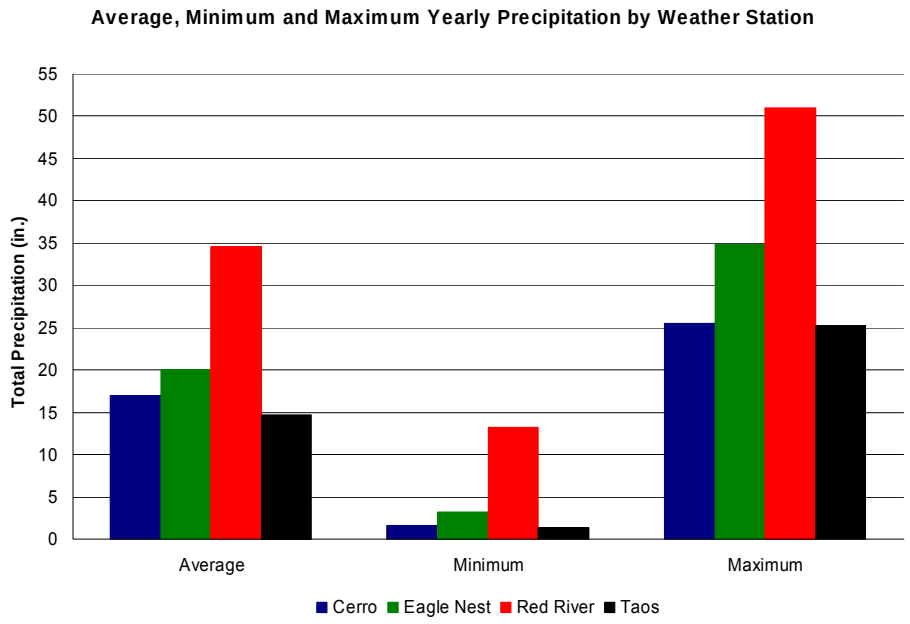

FIGURE 3. Bar chart showing the average, minimum and maximum yearly precipitation for four weather stations near the Questa mine. Red River consistently maintains higher precipitation totals than the other weather stations. The precipitation totals for Cerro and Taos are similar. The data for

all four stations are complete through December 2005. The data for Cerro begins in 1910, Eagle Nest starts in 1929, Red River dates from 1906 and records for Taos start in 1892.

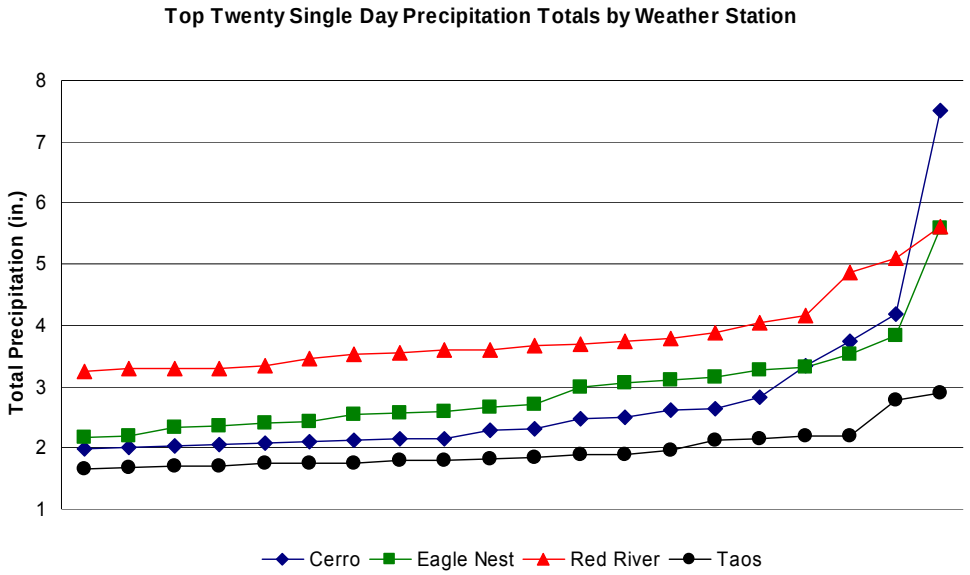

FIGURE 4. The top 20 single-daily precipitation events for four weather stations near the Questa mine. Note the large variation in the single-daily precipitation totals between each station.

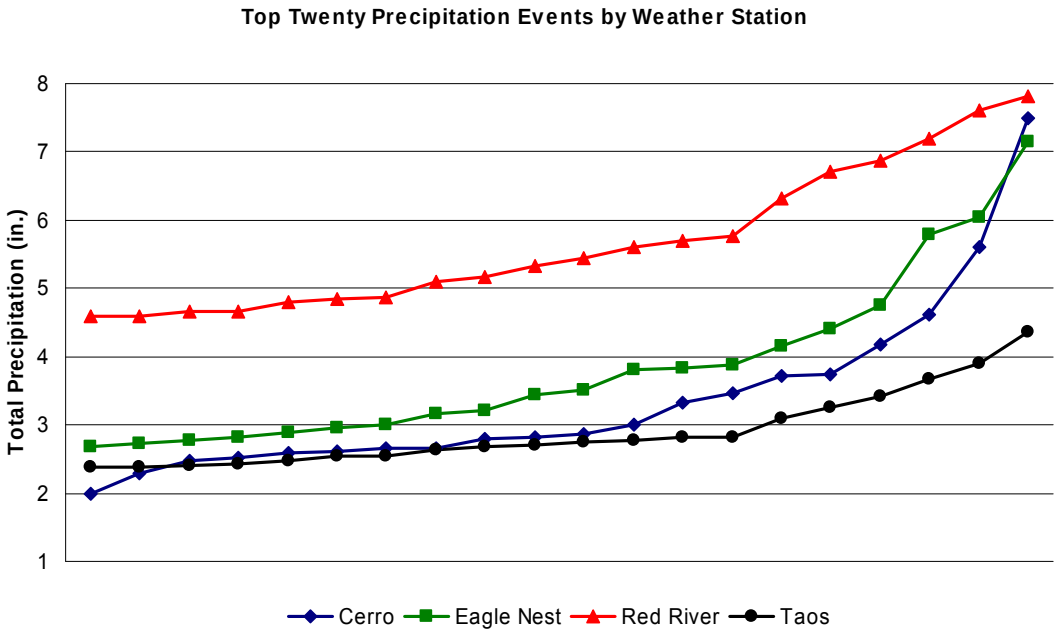

FIGURE 5. This graph shows the top 20 precipitation totals (single- and multiple-day events) recorded by four weather stations in the mine area. This graph further emphasizes the large variation

in precipitation totals in the mine area and the variation between individual precipitation events. These extreme totals confirm that Red River receives the largest amount of precipitation.

GEOLOGIC SETTING OF THE RED RIVER VALLEY

The geology of the Questa-Red River area is complex and described by others (Carpenter, 1968; Clark, 1968; Reed et al., 1983; Lipman, 1988; Lipman and Reed, 1989; Meyer and Leonardson, 1990; Czamanske et al., 1990; Roberts et al., 1990; Meyer, 1991; Meyer and Foland, 1991; Robertson GeoConsultants, Inc. 2000a, b; Ross et al., 2002; Caine, 2003; Rowe, 2005; Ludington et al., 2005; McLemore, 2009). Lithologies likewise are diverse and include metamorphic and volcanic rocks, granites, shales, limestones, and sandstones (McLemore et al., 2009a). The Questa-Red River area, like much of the Rio Grande rift in New Mexico and Colorado, has experienced multiple geologic and tectonic events that resulted in the geology seen today (Table 4, Fig. 6). The regional geology of the Questa-Red River area can be roughly divided into five general tectonic periods: Proterozoic, Paleozoic ancestral Rocky Mountains, Laramide orogeny, Rio Grande rift volcanism including the Questa caldera, and recent Rio Grande rift fill (Table 4; McLemore, 2009). The most important group of rocks in the Red River drainage is the Rio Grande rift-related volcanic rocks. These rocks include the Latir volcanic field, a small and largely eroded series of Miocene (29-18.6 Ma) extrusive and intrusive rocks ranging in composition from basaltic and quartz-latitic flows to welded ash-flows of high-silica alkaline rhyolite (Amalia Tuff) that erupted before, during, and after the Questa caldera. Granitic porphyritic rocks intruded the entire sequence after volcanism ceased.

TABLE 4. Summary of geologic history of the Questa-Red River area (Bauer et al., 2004; Ludington et al., 2005).

Approximate age	Event	Event
2 Ma-present	Pediment and stream deposits	
2.34-5.88 Ma	Taos Plateau volcanic field	
1-16.4 Ma	Santa Fe Group	Miocene lavas
5 Ma to present	Slow extension, basin subsidence	
18.6-5 Ma	Rapid extension of Rio Grande rift	
25-19 Ma	post caldera intrusions and Mo mineralization	
25.7-26.5 Ma	Amalia Tuff (Questa caldera)	peralkaline rhyolite dikes
28-18.6 Ma	Latir Peak volcanic field	Slow extension of Rio Grande rift
27-28.5 Ma	early rhyolite	sedimentary rocks
28.5-33.7 Ma	Early regional extension Rio Grande rift	Transition from crustal shortening to extension
33.7-65 Ma	Laramide orogeny	
1610-1752 Ma	Precambrian rocks	

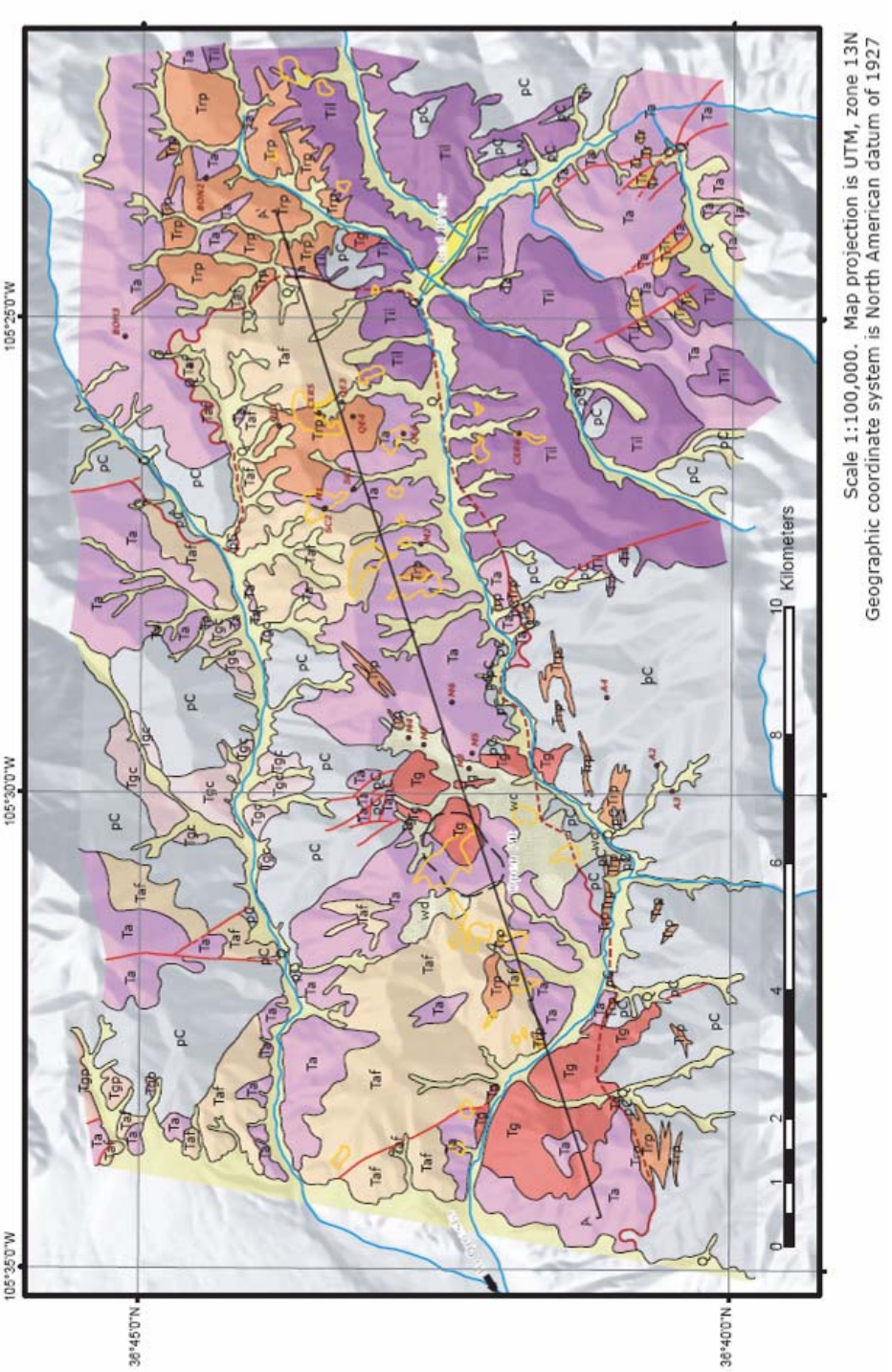

FIGURE 6a. Simplified geologic map of the southern portion of the Questa caldera in the vicinity of Red River, New Mexico from Ludington et al. (2005) modified from Lipman and Reed (1989). The individual rock types shown are a starting point for conceptualizing what could be hydrologically significant units or domains in the study area. Lithologies are described in more detail in the lithologic atlas (McLemore et al., 2009a). Note that the areas impacted by hydrothermal alteration (alteration scars) are outlined in orange. The key is in Figure 6b and cross section A-A' in Figure 6c.

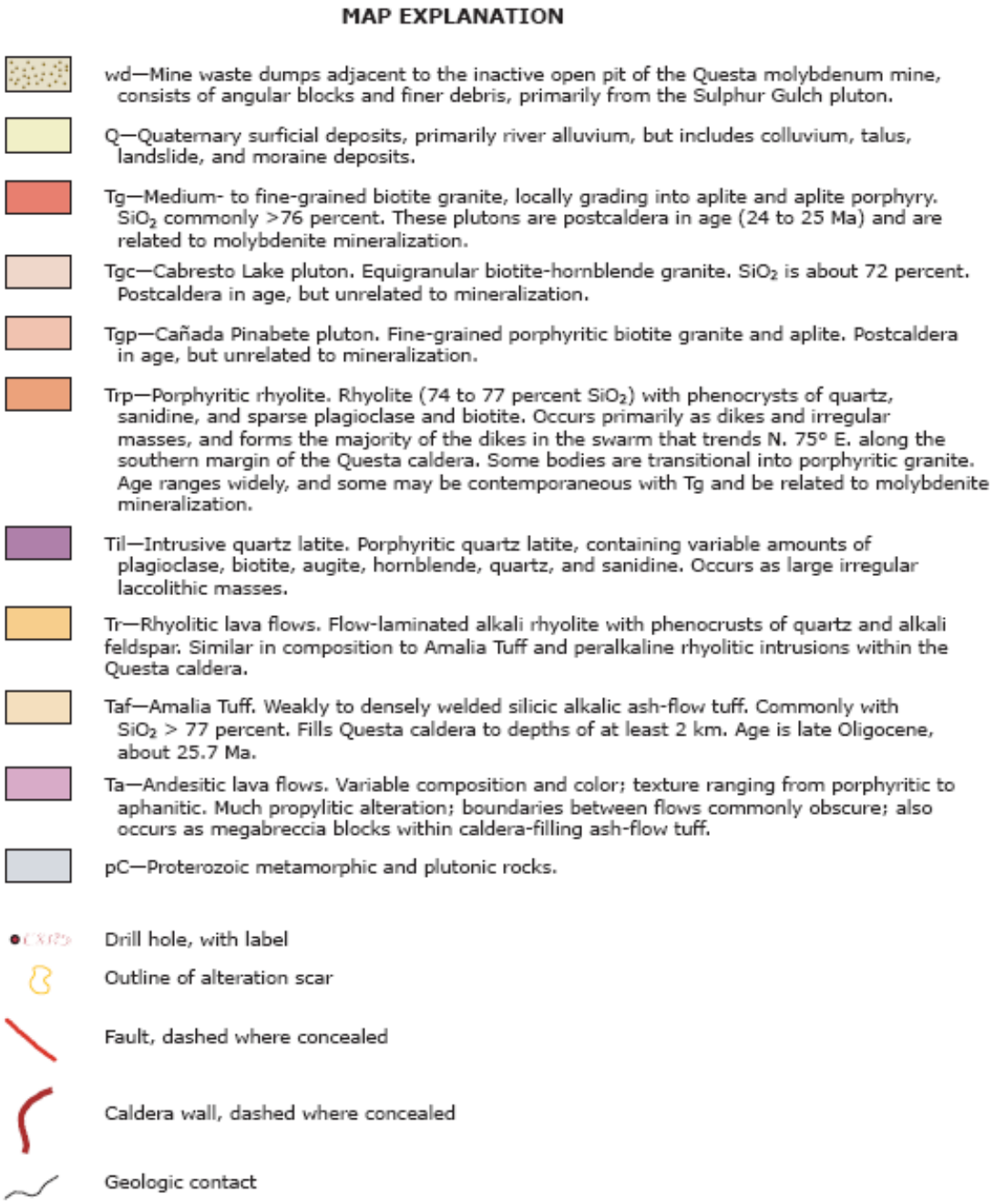

FIGURE 6b. Key to geologic map in Figure 6a, from Ludington et al. (2005) modified from Lipman and Reed (1989).

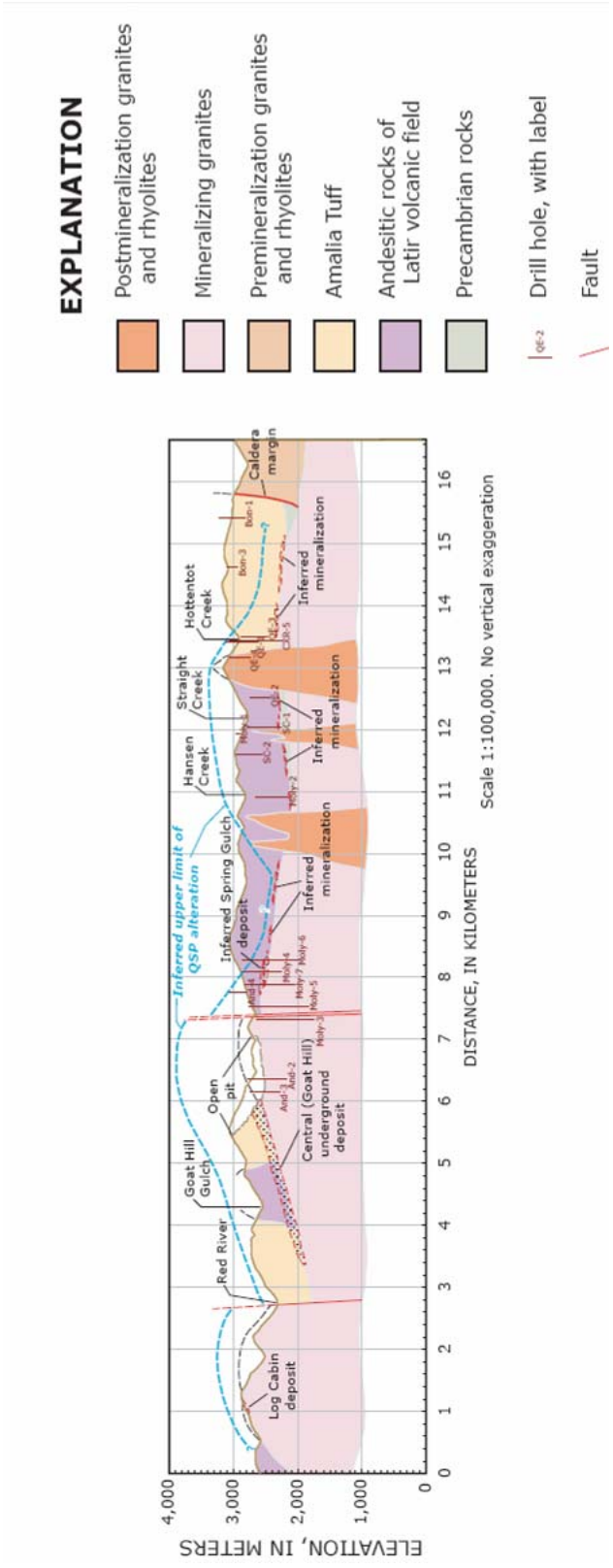

FIGURE 6c. Cross section along line A-A' in Figure 6a, from Ludington et al. (2005) modified from Lipman and Reed (1989).

The Questa deposit is a Climax-type porphyry molybdenum (±tungsten) deposit, which is a large, low-grade (0.1–0.2% Mo) deposit that contains disseminated and stockwork veinlets of molybdenum sulfides and is associated with silica- and fluorine-rich porphyritic granitic intrusions. The deposits formed from hydrothermal fluids that evolved in part from granitic magmas (Mutschler et al., 1981; Johnson et al., 1990; Cline, 1991; Cline and Vanko, 1995; Klemm et al., 2008). All of the mining has been from a horseshoe-shaped system of ore bodies between Goat Hill and Sulphur Gulch, including:

- The original underground mine mined during 1919-1958
- The open pit mined during 1965-1982
- The Goathill ore body mined by block-caving underground during 1983-2000
- The D-ore body, mined by block-caving during 1983-2000
- Remaining reserves, also mined by block caving that are now being developed and mined (Schilling, 1960, 1990; Carpenter, 1968; Molling, 1989; Ross et al., 2002; Ludington et al., 2005; Rowe, 2005; Klemm et al., 2008).

The deposits consist of thin veinlets, fracture coatings, breccia zones, and disseminations in granitic host rock and ore minerals that include molybdenite, powellite, scheelite, beryl, helvite, bismuthinite, and wolframite. Other minerals, typically in adjacent rocks altered by the mineralization, include pyrite, quartz, sericite, chlorite, and fluorite, among others.

Six general types of hydrothermal alteration assemblages are found in the Questa-Red River area, including the overburden rock surrounding the open-pit deposit (Fig. 7; Martineau et al., 1977; Molling, 1989; Meyer, 1991):

- Early and late prophylitic (consisting of chlorite, calcite, pyrite, albite, epidote)
- Argillic (consisting of chlorite, calcite, epidote, quartz, pyrite, clay minerals)
- Potassic (consisting of replacement by K-feldspar and potassium-bearing micas, with fluorite, quartz, and molybdenite)
- Quartz-sericite-pyrite (QSP), also called phyllic, sericitic and silicic (QSP)
- Silicification (replacement by quartz)
- Post-mineral carbonate-fluorite and magnetite-hematite veining (locally with anhydrite).

These are described in more detail by McLemore et al. (2009a).

Pyrite occurs as finely disseminated crystals in the host-rock matrix and as stockwork veins up to 6 inches thick. Younger epithermal quartz veins cut these hydrothermally altered rocks and, locally, fragments of the altered rocks are present in the mineralized veins. The hydrothermal alteration mineral assemblage consists of essential chlorite (producing a green color), quartz, and pyrite, and a variety of additional minerals (including calcite, epidote, adularia, sericite/illite, smectite, etc.) depending upon original host-rock lithology, temperature, and composition of the hydrothermal fluids. In the district, silicification is the most extensive alteration adjacent to and along mineralized veins and veinlets. Locally, chloritization, argillization, and sericitization form a halo surrounding mineralized faults. Epidote is present within this halo and indicates temperatures of formation >200°C (Reyes, 1990; Simmons et al., 1992; Reed, 1994). These altered halos consist of illite, kaolinite, chlorite, quartz, and iron oxides. More detailed descriptions of alteration assemblages are in McLemore et al. (2009a).

Molybdenum was discovered in the Questa district along the Red River about 1914 (Schilling, 1960, 1990). Underground mining of high-grade vein ore occurred from 1919 to 1958, with a production of 0.375 million tons of >4% MoS_2 (Schilling, 1960, 1990; Ross et al., 2002; McLemore and Mullen, 2004). Ore production from the open pit began in 1965 and ended in 1982, at which time approximately 81 million tons of ore with an average grade of 0.191%

MoS_2 had been processed (Schilling, 1960, 1990; Ross et al., 2002; McLemore and Mullen, 2004). Underground block caving of ore commenced in 1982. Molycorp, Inc. continued mining through 1986, when poor market conditions caused the temporary shutdown of the mine until 1989. Mining operations again were placed on standby in 1992 and resumed in 1995 and continues to the present. Production from the Goat Hill orebody from 1983 to 2000 amounted to 21.11 million tons of 0.31% MoS_2. Current production is from the adjacent D-orebody since 2001 with a grade of 0.338% MoS_2. In early April 2005, Chevron-Texaco announced the purchase of UNOCAL, including Molycorp, Inc. and in October 2007, Molycorp, Inc. officially became Chevron Mining Inc. Molybdenum is used in steel alloys and molybdenite, the most common molybdenum mineral, is used as a lubricant.

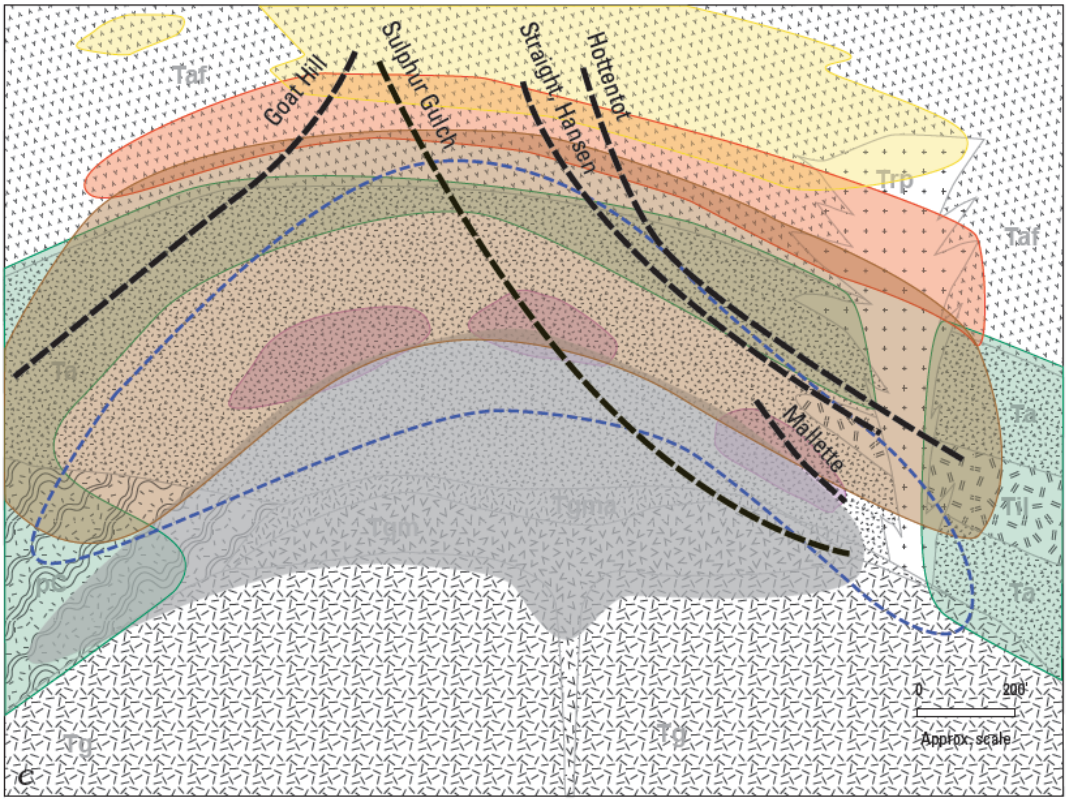

FIGURE 7. Schematic cross section of showing schematic spatial distributions of lithologies, alteration assemblages, and alteration scars in the Red River valley (taken from Ludington et al., 2005, which is modified from Martineau et al., 1977).

GENERAL CONSTRUCTION AND DESCRIPTION OF MINE ROCK PILES

The shape of rock piles is mainly based on the construction method and topography of where they are emplaced. Rock piles can take the shape of one of, or a combination of many different configurations, such as valley-fill, cross-valley, side-hill, ridge, and heaped, depending on the topography of the area (Zahl et al., 1992). The dumping method of rock-pile material can be used to classify rock piles into five basic methods of rock-pile construction (Nichols, 1987; Morin et al., 1991; Quine, 1993; Herasymuik, 1996; Shum, 1999; Tran et al., 2003):

- End dumping (dumping rock over the dump face resulting in particle size segregation down slope towards the toe of the rock pile, with particle size generally increasing down slope)
- Push dumping (dumping from trucks then leveling/pushing by tractors resulting in particle size segregation; finer at the top, coarser at the toe of the rock pile)
- Free dumping or plug dumping (dumping in small piles on the surface of the rock pile, grading the material, and compacting in layers or lifts resulting in dense layers with no real particle size segregation)
- Drag-line spoiling (deposited on the surface without construction of lifts and minimal compaction resulting in dense layers with no real particle size segregation because of the relatively low overall height of the spoil piles; typically used in coal mining)
- Mixing of waste rock with tailings.

Examination of the interior of other end-dumped rock piles have been described by Morin et al. (1991, 1997), Herasymiuk (1996), Fines et al. (2003), Tran et al. (2003), and Wilson (2003), who revealed alternating dipping layers of fine- and coarse-grained material within the rock piles. Most other studies of rock piles involved drilling, surface test pits, and numerical modeling.

Studies by Haering et al. (2004) indicate that mine soils have high abundance of rock fragments (35-70%), low clay, and heterogeneous chemical properties. Soil properties are inherited from overburden (texture, color, pH), while density and drainage typically result from construction method. Weak A soil horizons can develop within one year in a humid climate in coal mine spoils. Horizontal layering was observed in 8 out of 30 profiles. This layering is believed to be spoil layering by construction rather than by pedogenic processes. The sources of the minerals found within rock piles are derived from the original pre-mined altered overburden rock; typically that rock material is hydrothermally altered. However, studies by Mascaro et al. (2001) at Fenice Capanne, Italy (mined from 6-7th century to 1985) indicate that the mine rock piles there have high concentrations of illite and kaolinite, with some kaolinite, smectite, and illite-smectite formed as weathered products in rock piles. Therefore, an understanding of the hydrothermal alteration of the mineral deposit is required to better understand the source of material within the rock pile and the weathering within the rock pile after construction and in the future.

Oxidation rates typically are variable and occur at different rates, even though most of the rock piles oxidize slowly. At Aitik, Sweden, pockets of more oxidized material are found within the rock pile, especially near the edges (Linklater et al., 2005). Geochemical models predict that consumption of sulfide material would take a few hundred to many thousands of years, because of:

- Slow dissolution rates of most sulfide and aluminosilicate minerals
- Rapid dissolution of amorphous oxides and pyrite
- Precipitation of secondary minerals, such as gypsum, jarosite, and other sulfate minerals.

Mineralogical studies of the Laver tailings in Sweden showed (Ljungberg and Ohlander, 2001):

- Low sulfides in the uppermost, oxidized portion
- Sulfide minerals with surface coating of Fe-oxyhydroxides
- Edges of biotite were slightly oxidized
- No other silicate minerals were oxidized.

Mineralogic and chemical studies of the high-sulfide mine-wastes at the Berikul mine in the Kemerovo region, Russia, delineated five zones of weathering (Sidenko et al., 2005):

- Upper-most jarosite zone
- Intermediate zone
- Melanterite zone
- Cemented hardpan zone
- Basal slightly altered waste zone.

These and other studies summarized by McLemore et al. (2009c) indicates that weathering of rock piles is site specific and not always well understood and emphasize the need to examine the effects of weathering on the stability of the Questa rock piles.

CONSTRUCTION OF THE QUESTA ROCK PILES

During the period of open-pit mining (1965-1982), multiple areas of the open pit were mined simultaneously and overburden rock material was dumped in the nine rock piles at the Questa site (Table 5), predominantly as side-hill and valley-fill construction. Records of the quantity, lithology, and rock-pile location of individual overburden material were not maintained during construction of the rock piles, which was normal practice in the industry at the time. An estimate of the construction history of the rock piles was determined by examination of aerial photographs, which is summarized in a report by URS Corporation (2003) and in Table 5.

The GHN rock pile is one of nine rock piles created during open-pit mining and contained approximately 5.5 million yds^3 (16 million tons) of overburden material with slopes similar to the original topography (Table 5, Fig. 8). GHN rock pile was approximately 630 ft high and 200 ft thick (URS Corporation, 2003; Norwest Corporation, 2004). GHN rock pile was constructed during 1964-1974 when material was end dumped in an alteration scar area, which is a natural, actively eroding landslide area caused by acidic weathering (Norwest Corporation, 2004). Material in the alteration scar was rapidly deposited at the base of the scars as scree, talus or colluvial deposits that were later remobilized during storm events as debris flows within the valleys (Fig. 9). GHN was constructed on the slopes and drainages of a west-facing valley, on a debris fan west of the open pit (Fig. 9). GHN was divided into two areas: a stable area and an unstable area (Fig. 9). The unstable portion of the rock pile was an active land slide area, involving 2.5 million yds^3 of material (Norwest Corporation, 2004). Evidence of slope instability and actual sliding of the unstable portion of the GHN rock pile were observed in the 1974, 1976, 1977, 1991, and 1997 aerial photographs. The colluvial foundation at GHN first failed between 1969 and 1973 (Norwest Corporation, 2004). Molycorp stabilized this rock pile by removing material off the top portion of both areas to the bottom of the pile (Norwest Corporation, 2004). This regrading has decreased the slope angle, reduced the load, and created a buttress to prevent future movement of the rock pile.

TABLE 5. Physical characteristics of the Questa rock piles (URS Corporation, 2003).

Rock pile	Maximum height (ft)	Maximum thickness (ft)	Footprint (acres)	Slope area (acres)	Slope	Overall slope	Quantity of rock (million tons)
Sugar Shack West	980	200	43	50.7	1.7 to 1.5H:1V	1.6H:1V	31
Sugar Shack South	1580	400	128.4	151.4	2.1 to 1.4H:1V	1.6H:1V	53
Middle	1300	500	140	155.76	1.1 to 1.4H:1V	2.1H:1V	46
Sulphur Gulch	750	350	70.9	75	3.3 to 1.5H:1V	2.9H:1V	80
Blind Gulch	740	375	128.3	134	2.0 to 1.4h:1V	3.7H:1V	36
Spring Gulch	770	325	84.9	89	2.0 to 1.6H:1V	3.0H:1V	31
Capulin	440	225	44.4	47.6	3.7 to 1.3H:1V	1.7H:1V	26
Goathill North	630	200	56.8	59	5.7 to 1.4H:1V	2.3H:1V	16
Goathill South	500	75	8.8	10	1.9 to 1.5H:1V	1.6H:1V	9

Rock pile	Years placed on benches	Years placed on slopes	Soil loss (tons/acre/year)	Annual soil loss (tons/year)
Sugar Shack West		1969, 1973, 1974, 1976, 1977	32	1376
Sugar Shack South	1974	1973, 1974, 1976, 1979	34.7	4442
Middle	1974, 1979, 1991	1974, 1976, 1077	31.9	4466
Sulphur Gulch	1973, 1974, 1977, 1979, 1991, 1997	1969, 1974, 1976	34.7	2464
Blind Gulch	1973, 1974, 1991, 1997	1976, 1977	12.7	1626
Spring Gulch	1969, 1973, 1974, 1976, 1977, 1991	1976	8	680
Capulin		1974, 1976, 1977	22	968
Goathill North		1964-1974	22.8	1300
Goathill South		1969	21	189

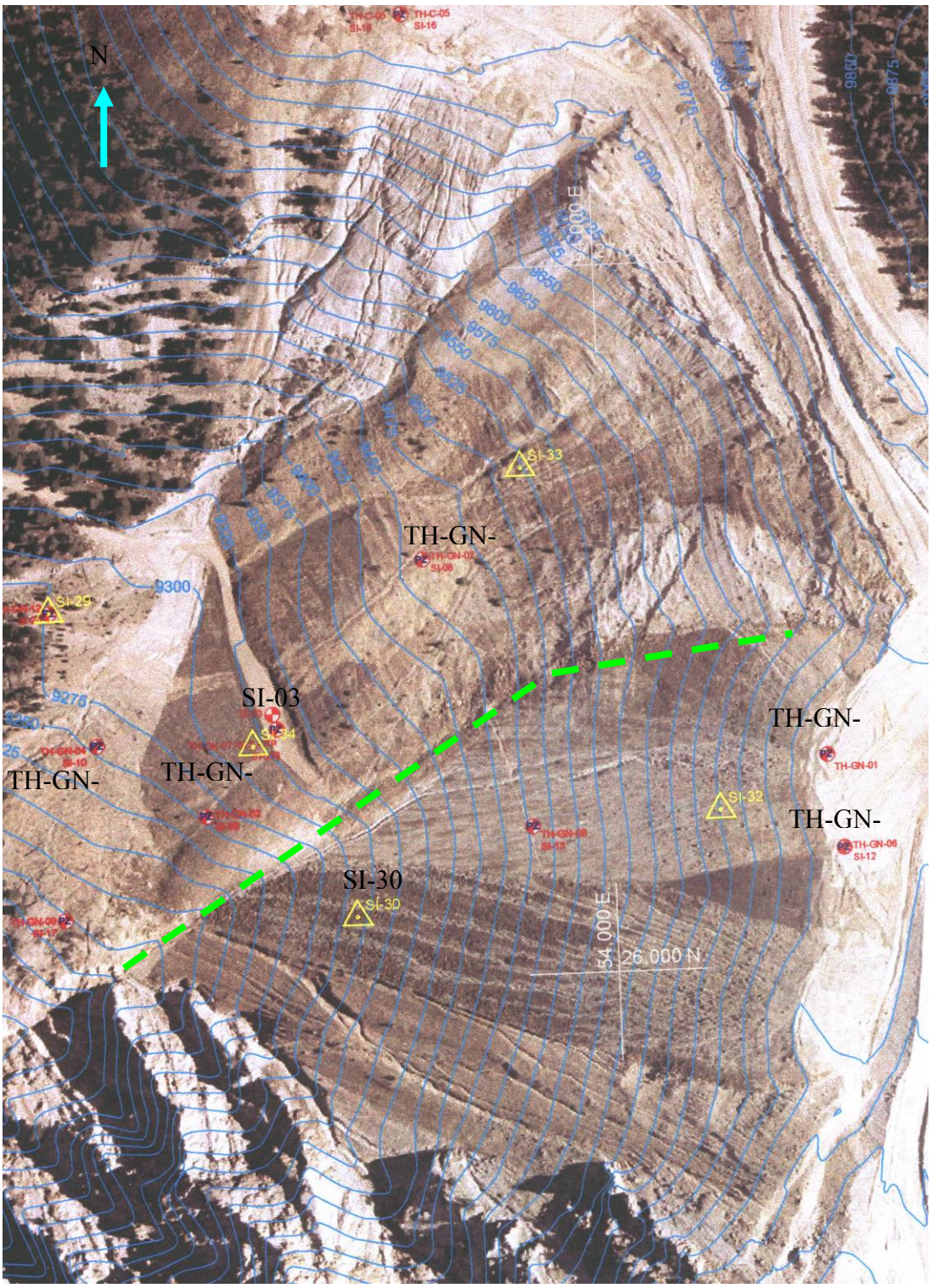

FIGURE 8. Aerial photograph of the GHN rock pile showing colluvium and the locations of boreholes. The yellow triangles are slope inclinometer holes; the red and blue circles are piezometer holes; the blue lines are elevation contours. The bright green dashed line separates the stable portion (south) from the unstable portion (north).

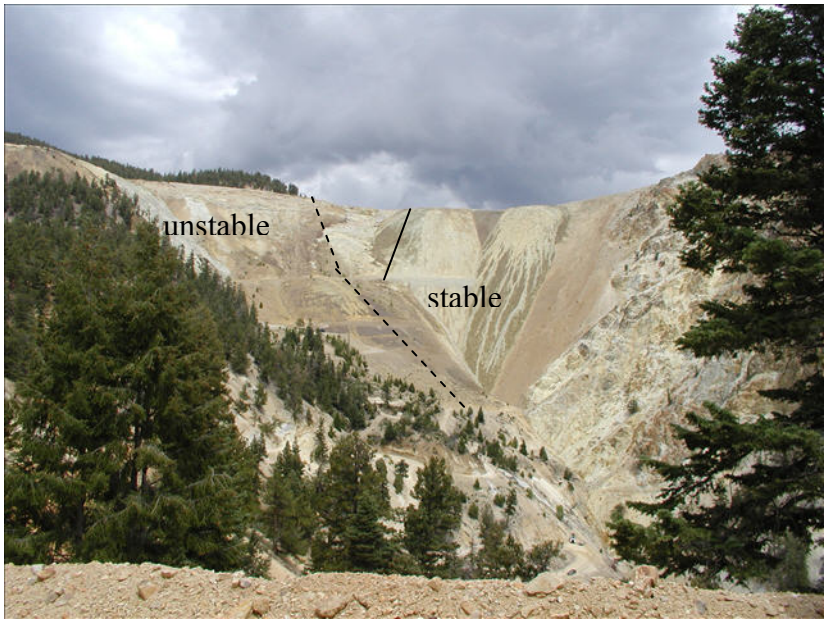

FIGURE 9. GHN before regrading, looking east. Solid line indicates approximate location of trenches constructed in summer-fall 2004; dashed line indicates the boundary between the stable and unstable portions of the rock pile.

The Questa rock piles were constructed using standard mining practices at the time. The piles were constructed primarily by haul-truck end-dumping in high, single lifts, which involved the dumping of rock over the edge of the hill slopes and resulting pile crests (URS Corporation, 2003; McLemore et al, 2005). The rock pile is generally a stratified accumulation of aerially deposited, clastic rock fragments derived from mining of the Questa ore body. Except that the rock fragments have been derived by mining rather than by natural erosion, the rock pile is in all important senses, and behaves as, sediment. The sequence of construction was typically from the top down. The mechanical derivation of the fragments of rock in the rock pile is atypical of natural sedimentary deposits, with the sediment derived by anthropogenic processes (blasting and scooping from rock faces, followed by transport in haulage trucks, during which comminution of particles occurs). End dumping generally results in the segregation of materials with the finer-grained material at the top and coarser-grained material at the base (Fig. 10). The resulting layers are locally at or near the angle of repose and subparallel to the original slope angle. End-dumping results in five zones of segregation (Nichols, 1987; McLemore et al., 2005):

- Upper traffic surface (compacted by heavy equipment and trucks)
- Top of the rock pile where fines were more concentrated than coarser material
- Intermediate zone where material is well graded and evenly distributed
- Toe of the rock pile where mostly coarse material is concentrated
- Basal rubble zone of cobbles and boulders along the contact between the rock pile and the original bedrock or colluvium.

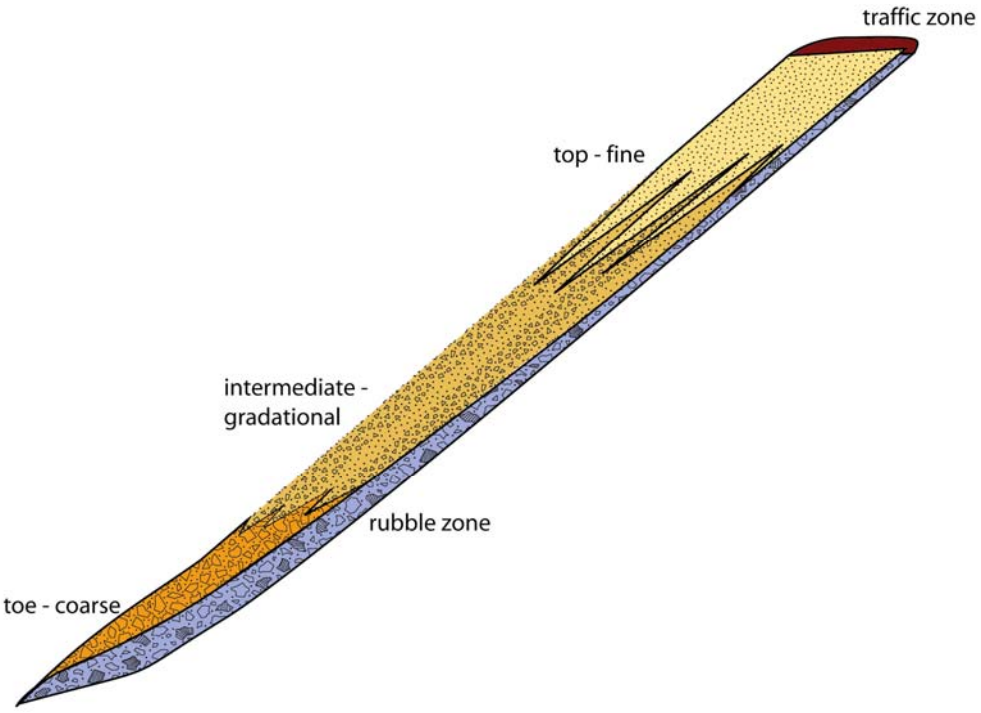

FIGURE 10. Conceptual model of the particle size of the Questa rock piles (from field studies at GHN and from Nichols, 1987). See text below and McLemore et al. (2005) for explanation of zones.

Figure 10 is a particle size conceptual model for an end-dump rock pile over the crest of a natural slope of a hill, similar to the construction of GHN and many rock piles in the world that were constructed by end-dumping (Nichols, 1987; Morin et al., 1991, 1997; McLemore et al., 2009c). End-dumping forms steeply dipping layers of alternating coarse- and fine-grained material. Each layer tends to progressively increase in particle size down slope. During construction, coarser rock settled at the base of the rock pile and is called a basal rubble zone (Morin et al., 1991; Nichols, 1987; Herasymuik, 1996; Wilson, 2003). These conditions were observed in the trenches and test pits at GHN.

LITHOLOGY OF MATERIAL REMOVED FROM THE OPEN PIT

The lithologies mined from the open-pit deposit are grouped into five major rock types: rhyolite (Amalia Tuff), andesite breccia, andesite (including latite and quartz latite), granitic porphyry, and aplite (McLemore et al., 2009b). The proportions of various lithologies that were mined from the open-pit deposit were estimated from company geologic cross sections through the open pit (Table 6, this report). The procedure is summarized below:

- Calculate areas for each lithology within the open pit as mapped on cross sections provided by SRK, using either rectangles or triangles.
- Calculate a volume by multiplying each area by 200 ft (the distance between cross sections). This assumes that each lithology is a simple box.
- Calculate total volume mined and divide each lithology to get a percentage of the lithology mined.

Other lithologies present in the open-pit deposit included volcaniclastic sandstone, shale, and rhyolite and granitic dikes, which were typically included with the andesite breccia or andesite in

Table 6. Field and laboratory analyses indicated that the GHN rock pile consisted primarily of hydrothermally altered andesite and rhyolite (Amalia Tuff) rock fragments.

TABLE 6. Estimates of volume of each lithology mined from the open-pit deposit determined in this study using company cross sections. Explanation of the lithologies and procedures are in McLemore et al. (2008a). QSP—quartz-sericite-pyrite hydrothermal alteration, prop—prophylitic hydrothermal alteration.

Symbol	Lithology	Volume percent	Relative estimate of strength (1 strong, 3 weak)	Comments
Tdqpt-Trt	rhyolite (Amalia Tuff)	10	1	Mostly QSP altered, no ore
Tanbx	Andesite breccia	14	3 2	50% QSP, 50% prop, no ore
Tanfp	Andesite (including latite and quartz latite)	46	3 2	50% QSP, 50% prop, some ore
Thfp	Christmas Tree porphyry	8	2	QSP altered, no ore, pyrite rich
Tpap	Aplite	22	1	Most of ore from this unit
TOTAL		100		

PREVIOUS WORK AT QUESTA

Wagner and Harrington (1995) conducted vegetation and soil surveys of all of the rock piles at the Questa mine. They divided the rock piles into subunits because of the wide range of site conditions. Each subunit was defined by Wagner and Harrington (1995) by surface particle size, substrate color, aspect, and overburden pile. The GHN rock-pile surface consisted of nine subunits (Table 7).

The surficial GHN rock-pile material consists of a wide range of particle size material from boulders and cobbles to silty sands and minor clay. Most of the surficial material is a sandy gravel with less than 20% fines, less than 10% clays, and plasticity index (PI) less than 10 (Table 8); moisture contents as high as 25.5% are reported. In previous studies, paste pH varied from 2.1 to 10, paste conductivity varied from 0.19 to 23,000 ms/cm, and paste TDS varied from 1.9 to 1700 ppm (URS Corporation, 2003). ABA data are summarized in Table 9. The friction angle of the GHN rock-pile material averaged 31º (Table 10; Norwest Corporation, 2004).

Petrographic examination, combined with PIMA spectral analysis and XRD Rietveld analysis, was performed by PetraScience Consultants Inc. (2001) on 10 samples from the surface of the Questa rock piles, including one sample from GHN (GT-1). The sample was an andesite and consisted of 40% ground mass, 30% argillized and sercitized plagioclase, 13% chlorite, 6% sericite, 5% clay and trace to 2% each of jarosite, epidote, pyrite, rutile, chalcopyrite, and zircon. All of the samples were hydrothermally altered. The results of this study indicated the fine-grain portions contained the majority of the sulfate and clay minerals. There was a broad correlation between pH and the amount of sulfate present. Lithology was an important factor in the extent of weathering. Typically, andesite samples contained more sulfate and showed evidence of resorption of pyrite in this section (PetraScience Consultants Inc., 2001).

TABLE 7. Descriptions of GHN surface subunits as defined by Wagner and Harrington (1995). TDS is total dissolved solids.

Molycorp Subunit or zone	Geologic Unit in this report	Vertical projection Acreage	Stability	Average slope angle (degrees)	Rooting zone pH	Rooting zone TDS ppm	Rooting zone Conductivity uS
15	A	4.31	Loose boulders eroding out	39	2.7	1640	2900
14	B	4.64	Boulders eroding out of face	39	2.1	>2000	4300
14A	H	0.55		39			
16	C	4.52	Tension cracks, appearance of past movement	39	3.2	240	410
17	D	0.94	Terraced/slumped appearance	39	2.8	940	1700
18	D	11.93	Open tension cracks, boulders raveling	27	2.7	330	530
19	E	4.89	Boulders weathering out of face	33	2.6	570	1020
18A	D	0.63	Outwash/slide debris	14			
18B	D	1.57	Outwash/slide debris	14			

TABLE 8. Summary of reported physical properties of GHN rock pile (URS Corporation, 2003; Norwest Corporation, 2004). Number=number of samples.

		Particle Size				Atterberg Limits			
Sample description		% Gravel	% Sand	% Fines	% Clay	Liquid limit %	Plasticity index	Moisture Content %	Comments
Mine rock (split spoon, drill cuttings)	Average	55.1	33.9	11.1	5.6	27.7	9.5	6.7	Sandy gravel with cobbles
	Std dev	19.2	13.9	6.6	2.5	3.6	3.4	3.9	
	Number	42	42	42	17	36	36	42	
Colluvium	average			24.1	8.5		11.2		
	Std dev			10.7	4.8		3.6		
	Number			91	50		84		
Weak zone of colluvium	range			36-65	11-34		14-25.3		
	Number			7	7		7		
Mine rock (test pits)	range	35-54	36-49	6-28	2.1-12.8	24-37	4-18	2.6-13.1	Sandy and clayey gravel with cobbles
	Number	28	28	28	28	28	28	28	
Bedrock (highly weathered/ altered andesite)	range			30-49		30-36	12-21	11.4-12	
	Number			4		4	4	4	
Robertson GeoConsultants Inc. (2000)	1 sample (GT-18)	59	19	5	2	28	12	2.7	

TABLE 9. Summary of reported paste pH and ABA results on Questa rock-pile samples (Robertson GeoConsultants Inc., 2000b).

Rock Pile	Drill Hole Number	Paste pH range	Avg. NNP (kg $CaCO_3$/t)	NP/AP	Acid Generation Potential
Spring Gulch	WRD-1	7.8-8.2	0.6	1.2	Uncertain
	WRD-2	4.0-6.4	-73.7	<0.1	Acid- generating
Sugar Shack South	WRD-3	5.8-7.7	-25.7	0.5	Potentially acid-generating
	WRD-4	6.5-7.9	-27.4	0.3	Potentially acid-generating
	WRD-5	4.7-8.0	-31.0	0.3	Potentially acid-generating
Sugar Shack West	WRD-6	4.1-7.8	-42.3	0.2	Potentially acid-generating
	WRD-7	4.5-7.6	-50.9	0.2	Potentially acid-generating
Capulin	WRD-8	3.7-4.5	-29.4	<0.1	Acid- generating
	WRD-9	3.9-5.6	-23.9	<0.1	Acid- generating

TABLE 10. Summary of reported values of friction angle of Molycorp mine rock-pile samples and "weak zone" at GHN and their gradation results (Robertson GeoConsultants, Inc., 2000b; URS Corporation, 2003; Norwest Corporation, 2004).

Sample location	% fines -0.75 mm	% clay -0.002 mm	Plasticity index	Friction angle (degrees)	Cohesion	Type of test	Comments
SSW-2 Sugar Shack West	18.8	6.6	8	36 (average)		Consolidated undrained triaxial test	mine rock
SSM-6 Sugar Shack Middle	29.1	7.7	11			Consolidated undrained triaxial test	mine rock
GT-18 GHN	5	2	12	31	561	direct shear test 2.4 in diameter	mine rock
TH-GH-04S 60-61 ft	36	11	16.6	39.8	0.0	direct shear test 2.41 in diameter	weak zone
TH-GH-04S 69-71 ft	65	34	25.3	22.3		direct shear test	weak zone
TH-GH-02S 137.5-138 ft	49	21	18.5	19.7		direct shear test	weak zone
TH-GH-02S 141-141.8 ft	44	18	15.6	30		direct shear test	weak zone
TH-GH-10S 44.7-45.5 ft	39	20	24.8	27		direct shear test	weak zone
TH-GH-10S 44.7-45.5	39	20	24.8	27		direct shear test	weak zone
TH-GH-14S 90.5-91 ft	39	15	18.2	25		direct shear test	weak zone
TH-GH-14S 94.2-95 ft	40	14	14	29.5		direct shear test	weak zone

METHODS OF STUDY

INVESTIGATIVE APPROACH

The GHN rock pile regrading provided an excellent opportunity to:

- Document the regrading of GHN rock pile, using trenches to map and obtain samples that characterized the structure, composition and material properties of units in the rock pile.
- Define the mineralogic, chemical, isotopic, hydrological, and geotechnical characteristics of spatially distributed samples.
- Identify and quantify zones that can influence fluid and air flow within the rock piles.
- Develop an appropriate conceptual model and data to allow initial modeling of weathering, heat transport and water and gas flow within GHN rock pile.

Prior to field work, team members drafted a sampling plan and standard operating procedures (SOPs; Table 11) to outline the procedures for each type of analysis and to organize the field sampling team's activities. All data collected were entered into the project Access database (McLemore et al., 2004a).

TABLE 11. List of standard operating procedures (SOPs) for the project (available upon request).

Number	Name	Description
MP	Project Management Plan	Overall project management plan
WP	Work plan	Work plan for the project
HASP	Health and Safety Plan	Health and safety plan for field and laboratory work
QAPP	Quality Assurance Project Plan	Quality assurance and quality control plan
FSP	Field Sampling Plan	Field sampling plan
DP1	Drilling plan, phase 1	Drilling plan
DP2	Drilling plan, phase 2	Drilling plan
GMP	Geologic mapping plan	Geologic mapping plan
SOP 1	Data management	entering, reporting, verification, and validation of data to the database
SOP 2	Sample management	procedures of handling samples from field to laboratory to archive
SOP 3	Surveying (GPS)	field procedures using GPS and other surveying methods
SOP 4	Photography	procedures taking photographs in the field and laboratory
SOP 5	Sampling outcrops, rock piles, and drill core	field procedures for taking surface solid samples
SOP 6	Drill logging and sampling of subsurface	field procedures for drilling, logging, and sampling of subsurface samples (solids)
SOP 7	Sample equipment Decontamination	field procedures for decontamination of sampling equipment
SOP 8	Sample preparation	laboratory procedures for sample preparation (solids)
SOP 9	Test pit excavation, logging, and sampling (solid)	field procedures for test pit excavation, logging, and sampling (solid)
SOP 10	Met station maintenance	field procedures for maintaining meteorological station
SOP 11	Paste pH and paste conductivity	laboratory procedures for paste pH and paste conductivity
SOP 12	Field measurements of water	field procedures for measuring water flow, pH, conductivity, alkalinity, temperature when collecting water samples
SOP 13	Water elevation measurements	field procedures for measuring water elevations in drill holes
SOP 14	Field filtration of water samples	procedures for filtering water samples in the field
SOP 15	Surface water and seep sampling	field procedures for collecting samples of surface and seep water samples

Number	Name	Description
SOP 16	Groundwater sampling	field procedures for collecting ground-water samples
SOP 17	Borehole logging	field procedures for borehole logging
SOP 18	Pump testing	field procedures for collecting information during pump testing
SOP 19	Geophysical logging	field procedures for borehole geophysical logging
SOP 20	Well development	field procedures for development of wells
SOP 21	Monitoring well installation	field procedures for installing monitoring wells and instrumentation
SOP 22	Analytical data validation	procedures for data validation
SOP 23	Geophysics with electromagnetic induction	procedures for geophysical surveys
SOP 24	Petrographic analysis	laboratory procedures for describing petrographic samples
SOP 25	Stable isotope analysis	laboratory procedures for stable isotope analyses
SOP 26	Electron microprobe analyses	laboratory procedures use for analyses using the electron microprobe
SOP 27	X-ray diffraction (XRD) analyses	laboratory procedures for mineralogical analyses by x-ray diffraction (XRD)
SOP 28	X-ray fluorescence (XRF) analyses	laboratory procedures for chemical analyses by x-ray fluorescence (XRF)
SOP 29	Clay mineralogy analyses	laboratory procedures for sample preparation and XRD analyses of clay minerals
SOP 30	ICP-OES analyses	laboratory procedures for chemical analyses using ICP-OES
SOP 31	ICP-MS analyses	laboratory procedures for chemical analyses using ICP-MS
SOP 32	Bulk density	laboratory procedures for determining bulk density
SOP 33	Particle size analysis	laboratory procedures for determining particle size analyses
SOP 34	Sampling for the Remaining Pyrite Model	approach, collection of samples and laboratory procedures required for sampling for remaining pyrite model
SOP 35	Volumetric moisture content	collection of samples and laboratory procedures for determining volumetric moisture content
SOP 36	Sample preservation, storage, custody, shipping	procedures for sample preservation, storage, and shipment
SOP 38	DI leach	laboratory procedures for leaching solid samples by deionized water to provide for soluble material
SOP 39	Samples for Pore water measurements	laboratory procedures for collecting samples for pore water measurements
SOP 40	Gravimetric moisture content	collection of samples and laboratory procedures for gravimetric moisture content
SOP 41	Reflectance spectroscopy	field procedures for mineralogical analyses using reflectance spectrography
SOP 42	Porosity	laboratory procedures for determining porosity
SOP 43	Tensiometer and thermal conductivity thermal conductivity sensor installation	field procedures for installing tensiometers and thermal conductivity sensors procedures for argon/argon dating
SOP 44	Argon/argon geochronology	laboratory procedures for argon/argon dating
SOP 45	Moisture retention relation by hanging column	procedures for determining moisture relations
SOP 47	Rain and snow collection for isotope	field procedures for collecting rain and snow
SOP 48	Dye tracer studies	Tracer studies using dyes
SOP 49	Chip tray preparation	How to prepare chip trays of drill cuttings for examination
SOP 50	Direct Shear tests	How to do simple shear box tests
SOP 51	Collecting Thermal images	How to collect thermal images using thermal camera
SOP 52	Static Net Acid Generation (NAG)	NAG test for laboratory

Number	Name	Description
	Test	
SOP 53	Tension Infiltrometer	procedures for tension infiltrometer measurements
SOP 54	Atterberg Limits	procedures for Atterberg Limits
SOP 55	General Microbial Sampling - Solids	General Microbial Sampling - Solids
SOP 56	Classical microbial analysis - solids	Classical Microbial Analysis - Solids
SOP 57	Microbial laboratory safety	Microbial Laboratory Safety
SOP 58	Microbial metabolic profiles - biology	Microbial Metabolic Profiles - Biology
SOP 59	Microbial nucleic acid analysis	Microbial Nucleic Acid Analysis
SOP 60	Slurry pH-redox-condictivity-temperature	Slurry Ph – Redox – Conductivity - Temperature
SOP 61	Neutron density gauge	Describes measurements taken with the nuclear density gauge (density, water content)
SOP 62	Acid-base accounting (ABA)	Procedures for acid base accounting in laboratory
SOP 63	Kelway soil acidity and moisture measurements	Kelway Soil Acidity and Moisture Tester for field measurements
SOP 64	Portable tensiometer	procedures for using field portable tensiometers as opposed to in place monitoring
SOP 65	Sandcone	procedures for sand cone
SOP 66	Gas analyzer	procedures for gas analyzer
SOP 67	Solid sample collection and compound analysis	procedures for solid sample collection and compound analysis
SOP 68	Water analyses	water analyses in lab
SOP 69	Other chemical analyses on solids	other chemical analyses on solids (ammonia, nitrate, fluorine, etc)
SOP 70	Sand replacement	calculates volumetric moisture content and bulk density
SOP 71	Guelph permeameter	procedures for guelph permeameter measurements
SOP 72	SWCC	Soil water characteristic curve (UBC)
SOP 73	Falling head Permeability	Permeability by falling head method
SOP 75	Specific gravity	procedures for determining specific gravity
SOP 76	Slake durability	procedures for slake durability tests
SOP 77	Point load	procedures for point load tests
SOP 78	Humidity cell testing	procedures for weathering cells tests
SOP 79	Sample preparation for humidity cell testing	procedures for weathering cells sample selection and preparation
SOP 90	XRD sample preparation for pyrite reserve model	XRD sample preparation for pyrite reserve model
SOP 91	Color	procedures for obtaining the color of a soil sample

DATA REPOSITORY

A project data repository was developed to incorporate data from the project. The project data repository includes a variety of data, including:

- Access Database (McLemore et al., 2004a)
- External files (files of data that are not completely contained within the access database and are supporting data files)
  - Climate data
  - Datasheet information files (excel spreadsheet files)
  - GIS (and map data)
  - Image files
  - Remote sensing data and reports

- Reports
- URS water chemistry databases.

The data incorporated in the Access database includes locational data, mineralogy, chemical analyses, geologic data on drill holes and test pits, photographs, and other data. Locational data includes GPS (global positioning system) data and locations measured from surveyed points. There are five main collections of tables in the Access database: samples, drill holes/test pits, analytical data, photographs, and bibliography, and more than 70 supporting tables. Each of these main tables is linked to each other, where appropriate, and all of the supporting tables are linked to one or more of the main tables. The Access database is referenced to additional data in other file formats outside of the Access database, such as photographs, reports, laboratory scans, etc. The data for the project data repository is from a variety of published and unpublished reports, miscellaneous files (mostly consultant reports), and newly collected data.

Students and professional staff enter data into the data repository, which can then be converted into GIS or other formats. NMBGMR staff checks the data as they are being populated to make sure that data are being entered accurately. NMBGMR staff also checks the locations of the samples, drill holes, test pits, and other features using USGS topographic quadrangle maps and GIS software. The data repository was backed up daily to avoid data loss. Portions of the database are available upon request.

MAPPING PROCEDURES

The Geologic Mapping and Work Plans describe the mapping and analyses procedures that the team used. Standard geologic mapping techniques were used in this study (Lahee, 1961; McLemore et al., 2005). Surface geologic mapping of GHN was conducted in May-July 2004 by mapping the roads and bench cuts along the GHN rock pile and using aerial photographs. Surface units on the rock piles were identified visually, using Wagner and Harrington (1995) as a guide. Then each unit was examined and described, including the dip, strike, and true thickness of each unit. Longitudinal sections were made of each bench on the GHN rock pile. Each unit boundary was mapped using the combined aerial photograph-topographic maps, Airborne Visible-Infrared Imaging Spectrometer (AVIRIS) data and preliminary hyperspectral remote sensing maps (Appendix 10). Eight surface geologic units were differentiated, described and sampled as described below. The units were differentiated mostly on the basis of color, particle size, composition, stratigraphic position, dip, thickness and other soil properties, which correspond to units described by Wagner and Harrington (1995). Soil color is identified with a Munsell soil color chart. These units are surface units only and no age relationships between them can be determined. The rock piles lie unconformably on bedrock or colluvium, which overlies hydrothermally altered fractured bedrock of andesite and rhyolite (Amalia Tuff), some of which has not experienced subsequent weathering.

Trenches were located on the GHN rock pile (Fig. 11, Appendix 1) based upon:

- Surface geologic mapping
- Location of prior drill holes in the rock pile
- Geophysical surveys (van Dam et al., 2005)
- Company regrading plans (Norwest Corporation, 2004).

Contractors constructed 19 trenches during the regrading of the GHN rock pile (Fig. 11, 12; Table 12). Each Friday afternoon, the sampling team began preliminary mapping and sampling, and company personnel surveyed the trench corners (Appendix 1). Mapping and sampling

activities continued throughout Saturday, Sunday, and Monday as weather conditions permitted. At the beginning of each work day, a designated safety officer inspected the stability of the trench prior to entrance of the field team.

Specific location and construction data for each trench are in the project database and in Appendix 1 and the drill hole locations are in Appendix 2. Two trenches were constructed in the stable portion of GHN in June 2004 prior to regrading to:

- Train personnel in sampling and mapping procedures
- Test mapping and sampling procedures
- Confirm the geophysical studies
- Provide a base line of the structure and stratigraphy
- Aid in locating additional trenches.

Starting in September 2004, five additional trenches were constructed during the regrading of the stable portion of GHN rock pile. In February-April 2005, 12 trenches were constructed in the unstable portion of the rock pile and in the colluvium and weathered bedrock beneath GHN rock pile. Each trench was surveyed, mapped and sampled.

Trenches in the stable portion of GHN typically had four benches, which were approximately 37 ft wide and did not exceed 4 ft in height, to give an overall slope of 1.4 horizontal to 1.0 vertical within the trench (Fig. 13). Each trench was extended for a length sufficient to explore site conditions, maintain the regraded 2:1 slope, and ensure personnel safety. Most trenches in the unstable portion of GHN consisted of only one or two benches (Appendix 1).

Trench walls and benches were surveyed using a differential global positioning system (GPS). For every trench in the stable portion of GHN, geologic maps of the trench (Appendix 3), longitudinal sections (Appendix 4) and logs (Appendix 5) of each bench were created to describe the different subsurface rock pile material units, including the thickness, orientation, stratigraphic position, texture, and spatial extent of the units. Samples are located in the logs in Appendices 5 and 6. Subsurface units were defined based on particle size, color, stratigraphic position, texture, and other physical properties that could be determined in the field. Units were correlated within each trench, and most units were correlated down slope through a series of five successively excavated trenches. Eighteen units were differentiated, described and sampled. Table 12 is a summary of the trenches, benches, and samples collected.

Drill holes were completed before and during regrading and are located in Figure 8. NMBGMR sampled those holes that had cuttings. Appendix 2 contains location and construction data of the GHN drill holes. Appendix 6 contains the drill logs of those holes sampled, with locations of the samples.

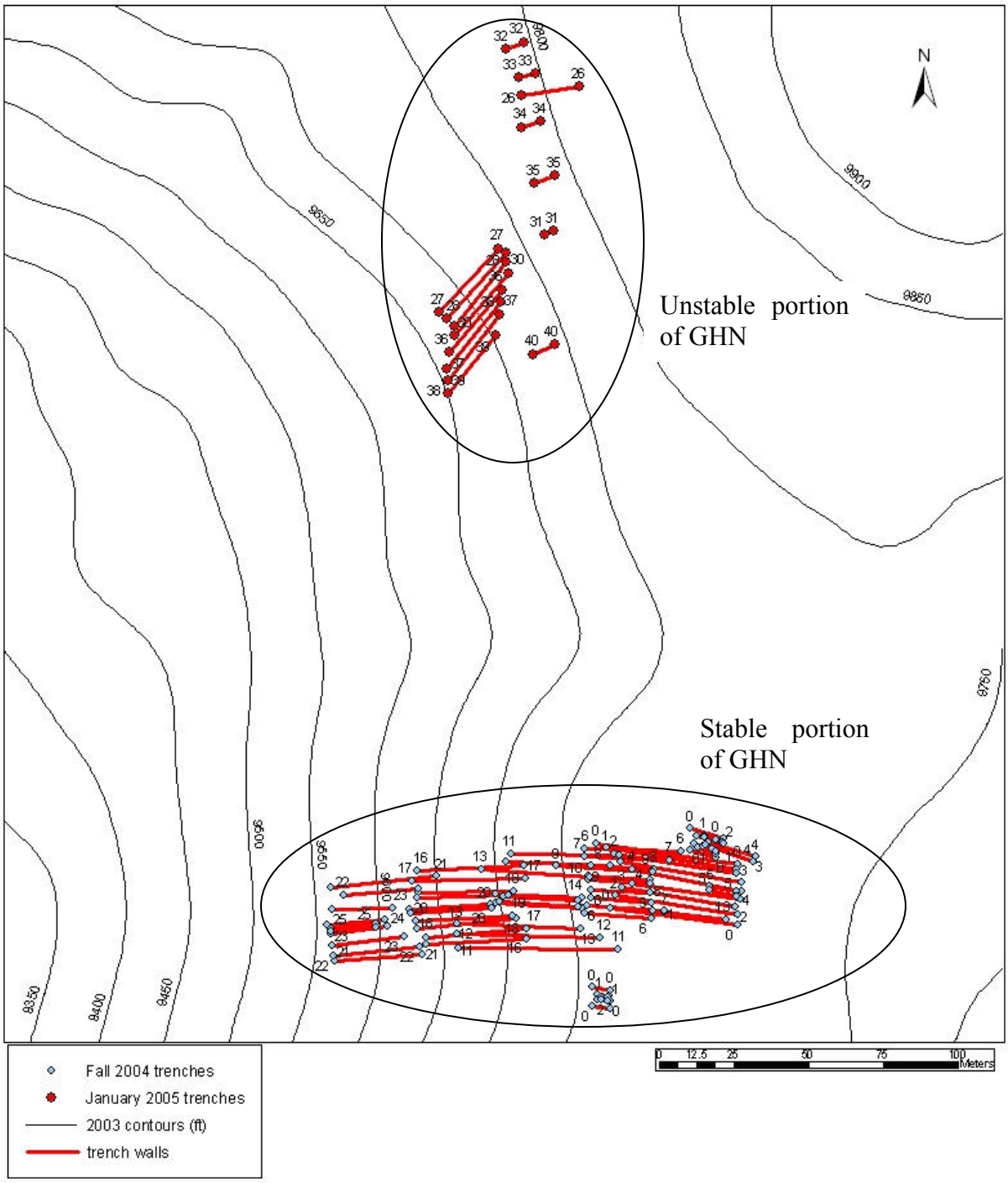

FIGURE 11. Map showing GHN trench locations. Red lines show trench walls. Circles show surveyed trench corner points. Black lines show elevation contours. The unstable portion of GHN lies to the north and the stable portion to the south.

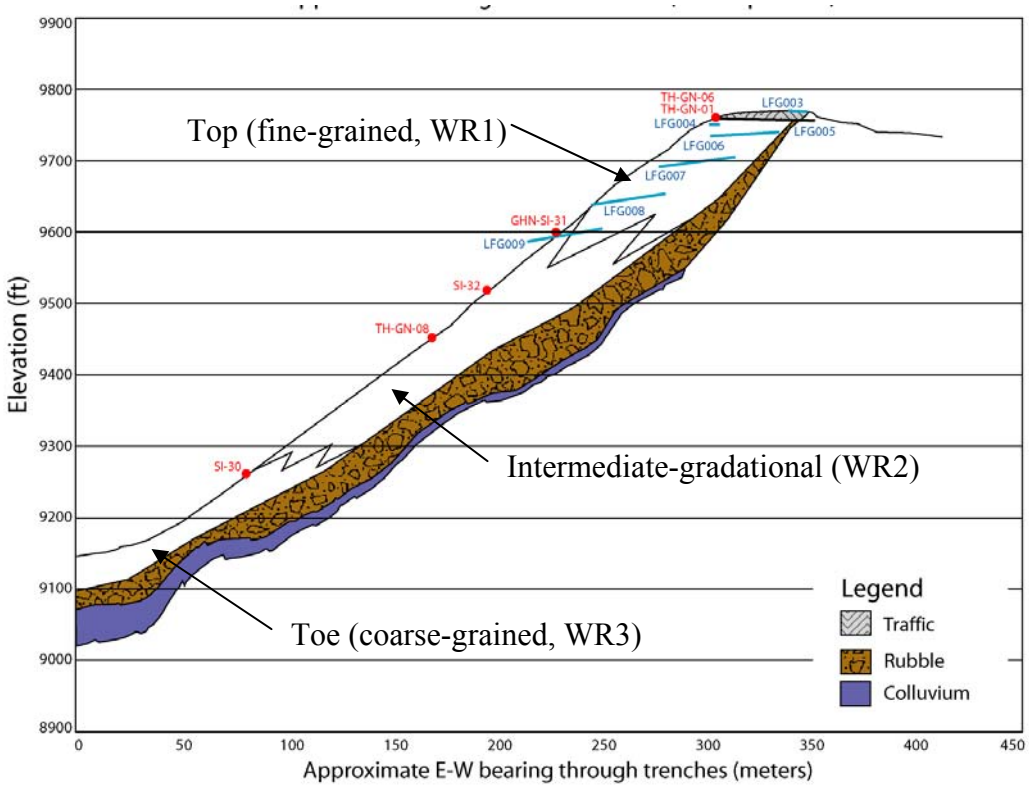

FIGURE 12. Hydrologic conceptual model (cross section) of the Questa GHN rock pile (from field studies at GHN; McLemore and the Questa Rock Pile Weathering and Stability Team, 2008). See text below for explanation of zones. Red dots are drill hole locations. Colored straight lines are trench profiles. The top and bottom surfaces of the rock pile are from the 2003 and 1967 contour maps, respectively. The trenches and drill holes are based upon survey data and the zones are based upon logging of the trenches and drill holes.

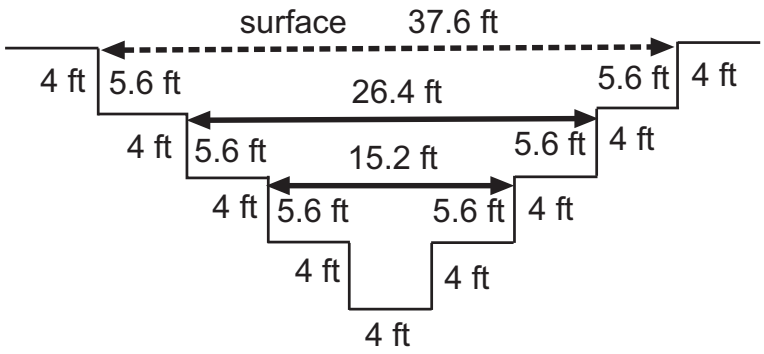

FIGURE 13. Sketch of a typical trench configuration for the GHN rock pile.

TABLE 12. List of trenches, benches and their respective numbers of samples in the stable portion of GHN rock pile.

Trench ID	No. of Benches	Bench nos.	No of samples on bench	Total no. of samples in trench
LFG-003	4	1	3	20
		2	5	
		3	8	
		4	4	
LFG-004	2	1	4	7
		2	3	
LFG-005	5	1	42	156
		2	36	
		3	33	
		4	37	
		5	8	
LFG-006	4	7	27	111
		8	24	
		9	39	
		10	21	
LFG-007	4	12	37	118
		13	32	
		14	34	
		15	15	
LFG-008	4	17	12	82
		18	24	
		19	29	
		20	17	
LFG-009	4	22	25	72
		23	33	
		24	8	
		25	6	
Total number of samples from stable portion trenches				566

SAMPLING PROCEDURES

A sample is a representative portion, subset, or fraction of a body of material representing a defined population (Koch and Link, 1971; Wellmer, 1989; Davis, 1998; Neuendorf et al., 2005; Downing, 2008). A sample is that portion of the population that is actually studied and used to characterize the population. Collecting a representative sample of rock-pile material can be difficult because of the compositional, spatial, and size heterogeneity of the material. It is necessary to define the particle-size fraction of the sample required and analyzed, because of the immense size heterogeneity in many rock piles (Smith et al., 2000a, b). The sampling process is defined in the project sampling plan and SOPs (listed in Table 11) and summarized in Appendix 8. Several different types of samples were collected to characterize GHN:

- Rock-pile material that includes both the soil matrix and rock fragments of mixtures of different lithologies and alteration assemblages
    - Samples collected from the surface and from test pits throughout the rock piles
    - Samples of the rock-pile material collected from trenches in GHN (5 ft channel or composite within a single, selected layer)
- Soil profiles of colluvium/weathered bedrock

- Splits of drill cuttings from holes drilled into the rock piles and underlying colluvium/bedrock
- Samples selected for specific analysis (age dating, stable isotopes, etc.).

Sample locations are in Appendices 3, 4, 5, and 8. Project SOPs (Table 11) provide detailed descriptions of sampling methods and laboratory analysis methods for each type of sample.

Before regrading of GHN, composite surface samples were collected along the road cutting across GHN of each surface geologic unit for characterization. Tensiometer measurements were obtained throughout the surface of GHN (Shannon, 2006) and samples were collected at those sites as well. Splits of drill cuttings from drill holes in GHN were collected from 5-gallon buckets, representing 5- or 10-ft intervals collected during drilling.

During GHN regrading, samples of each of the subsurface units were collected after the unit boundaries were identified. Composite samples were collected from the north wall of the trench for characterization. If there was enough time, samples also were collected along the south wall of the trench as well. Additional samples were collected in 5 gallon buckets of each geologic unit within the trench for geotechnical testing. Samples were collected from each defined unit for geochemical analysis, geotechnical shear box tests, biological analysis, isotopic composition, and electron microprobe analysis. Most samples were channel composites collected along approximately 5-ft-long horizontal slots using a rock hammer to chip material from bench walls placed into a sample bag. Some samples were composites collected along specific layers that were less than 5 ft thick. The entire sample was then typically analyzed by various techniques (Fig. 14), although selected analytical methods required smaller size fractions than normally collected (see SOPs). Sampling procedures, descriptions, and analytical analyses were employed that are typically used for soil profiles because the material in the rock piles appears to be soil-like (i.e. mine soils) (URS Corporation, 2003; Haering et al., 2004; Stormont and Farfan, 2005). *Mine soils* are soils that form from organic matter, mineral soil materials, sediments, and rocks redistributed by humans during or after mining process (Galbraith, 2004).

Different sampling strategies were employed based upon the purpose of each sampling task (Appendix 8). Typically, at each site, a select, grab, or bulk sample of rock or other material was collected for petrographic study and geochemical analyses. A hand sample was collected from some sites for thin section analysis. Each sample was stored in a separate bag or bucket, assigned a unique number (as described below), logged on a field description form, and entered into the project database. Selected sample sites were marked in the field and a digital photograph (SOP 4) was taken at most localities. Photographs provide visual record of the sample site. The photograph form identified site specifics, provided basic location and other data about the photograph (SOP 4). Location information obtained by GPS or surveying by the company, type of sample, and field petrographic descriptions were collected. Geologic observations were recorded on the field description form (see Appendix 8 for the form) and each site was located on a map, if possible (SOP 5). A global positioning system (GPS) reading was recorded as well (SOP 3). Hand sample description provided a record of what was collected, which aided in petrographic descriptions and provided information on the sample for the laboratory analysis. The hand sample description was the preliminary data required to determine what samples required additional detailed analyses.

The following in-situ measurements were taken along either the horizontal or vertical surfaces of each exposed bench and along the base of the trench:

- Sand cone or sand or water replacement (density)
- Tensiometer (matric suction)

- Moisture content
- Particle size
- Infiltration tests
- Nuclear gauge measurements (density, moisture content).

Gravimetric water content samples were collected at many locations, including the locations selected for the measurement of matric suction and infiltration tests.

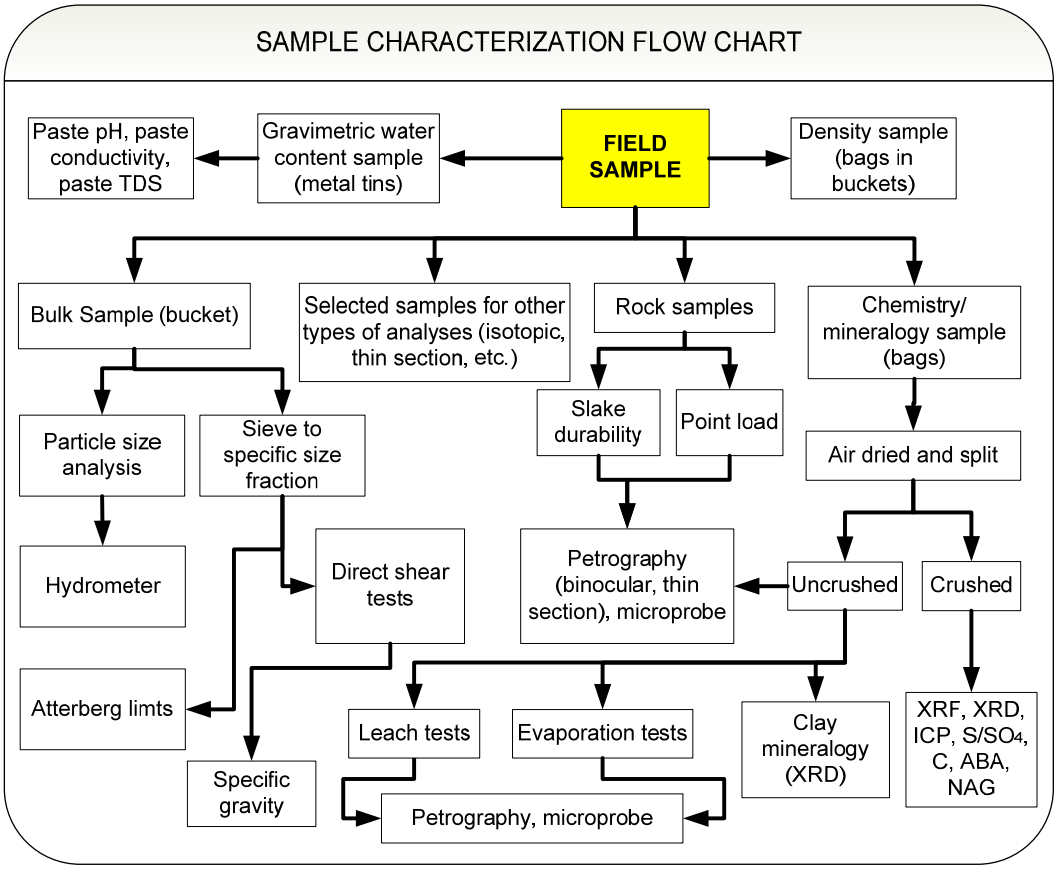

FIGURE 14. Flow chart showing analyses of selected samples. Not all analyses are performed on every sample. Bucket, metal tin, and bags refers to size of sample collected. XRF–X-ray fluorescence analyses, XRD–X-ray diffraction analysis, ICP–Induced-coupled plasma spectrographic analysis, NAG–net acid producing tests, ABA–acid base accounting tests.

GHN rock-pile samples, drill cuttings from holes drilled into the rock piles, and samples collected from test pits throughout the Questa rock piles represent varying degrees of hydrothermally-altered samples that have been exposed to surface weathering since the construction of the rock pile (approximately 25-40 years). The collected samples from the rock piles consisted of a heterogeneous mixture of rock fragments ranging in size from boulders (0.5 m) to <1 mm in diameter within a fine-grained soil matrix. Most rock fragments were hydrothermally altered before mining occurred; some show signs of oxidization and weathering since emplacement in the rock pile.

Sample and Photograph Nomenclature Scheme

Each sample was assigned a unique field identification by the field manager or sample collector (Field ID) number (Table 12; Appendix 8). The Field ID number for Questa samples is comprised of three components, separated by dashes, as described in Table 13 and SOP 2, for example SSW-HRS-0001.

TABLE 13. Scheme for identifying samples collected in the field, designated the Field ID.

Component 1	Component 2	Component 3
Three letter abbreviation for the mine feature, for example SSW for Sugar Shack West.	Three letter initials of the sample collector, for example HRS for Heather R. Shannon.	Sequential four number designation, for example 0001

Each sample is then assigned in the laboratory a separate sample identification number (Sample ID) designating the different sample preparation methods. The first part is identical to the Field ID number and is followed by a sequential two numbers, for example SSW-HRS-0001-01 (Table 14). The two digit lab sample can be correlated to sample preparation methods.

TABLE 14. Scheme for identifying subsamples or splits of the collected field sample for specific laboratory analysis designated the Sample ID.

Component 1	Component 2	Component 3	Component 4
Three letter abbreviation for the mine feature, for example SSW for Sugar Shack West.	Three letter initials of the sample collector, for example HRS for Heather R. Shannon.	Sequential four number designation, for example 0001	Sequential two number designation, for example 01

Photographs are taken of most sample sites (SOP 4) and information is recorded on photograph form. The numbering system for the photograph consists of the Field ID or Test Pit ID number followed by a letter representing the type of image (F-field, T-thin section, P-probe, H-test pit, D-drill core/cuttings, G-general, O- historic) 001 sequentially (Table 15). For example SSW-HRS-0001-F001 is the photograph number 1 that HRS took at sample site number 1. Photographs will be taken at the highest resolution as jpeg or tif.

TABLE 15. Scheme for identifying field photographs and designating the Photo number.

Component 1	Component 2	Component 3	Component 4	Component 5
Three letter abbreviation for the mine feature, for example SSW for Sugar Shack West.	Three letter initials of the sample collector, for example HRS for Heather R. Shannon.	Sequential four number designation, for example 0001.	Sequential two number designation, for example 01.	Letter of image type (F, T, P, H, D, G, O, M), followed by a sequential three number designation, 001.

ANALYTICAL PROCEDURES

Not all samples collected were analyzed in the laboratory. Samples were collected in the field and stored at NMIMT. Specific samples were subsequently selected for analyses depending on the purpose of the project tasks. Not all analyses were performed on each sample because only the specific analyses to address the task were performed. Laboratory analyses were performed on the samples according to project SOPs and are summarized in Table 16 and Appendix 8. The tests were performed in various laboratories using procedures outlined in SOPs for laboratory methods. Data generated from these analyses provides a more comprehensive characterization of the material in the rock piles and ultimately provide insight into weathering

processes and how they affect rock-pile stability. Quality assurance is summarized in Appendix 8.

Petrographic analyses (mineralogy, lithology, hydrothermal alteration, etc.) were performed on both the soil matrix and rock fragments using a binocular microscope; these analyses were supplemented by thin section petrography, microprobe analyses, X-ray diffraction (XRD) analyses, and whole-rock chemical analyses. Modal mineralogy was estimated using standard comparison abundance charts. Clay mineralogy, in terms of the major clay mineral groups, was performed on the complete sample (i.e. both matrix and rock fragments) using standard clay separation techniques and XRD analyses of the clay mineral separate on an oriented glass slide (Hall, 2004; Moore and Reynolds, 1989). However, this method does not liberate or measure the amount of clay minerals within the rock fragments. The concentrations of major and trace elements of the complete sample, except S, LOI (loss on ignition), and F were obtained by X-ray fluorescence (XRF) spectroscopy at the New Mexico State University and Washington State University laboratories. S and F concentrations were determined by ion probe at NMBGMR and LOI concentrations were determined by gravimetric methods at NMBGMR. Total S and C were determined by Leco Furnace and SO_4 was determined by sulfate sulfur-carbonate leach by ALS Chemex. S as sulfide was determined by subtracting sulfate from the total S. Induced-coupled plasma spectrometry (ICP) and other chemical analyses were performed at NMBGMR laboratories. Descriptions of selected samples are in Appendix 9.

Samples for chemical analyses were crushed in jaw crushers and pulverized by tungsten-carbide disc grinders to a particle size of <35 μm. Each sample was homogenized at each crushing step by cone and quarter method. The samples were then sent to the laboratories for analyses. NMBGMR internal (waste rock pile, rhyolite, basalt) and commercial certified standards and duplicates of selected samples were submitted blind to the laboratories with each sample batch of 25 samples to assure analytical quality. NMBGMR has archived a split of all remaining samples for future studies. The quantitative mineralogy was obtained using a modified ModAn technique that is consistent with the petrographic observations, electron microprobe analysis, clay mineral analysis, and the whole-rock chemistry of the sample (Paktunc, 1998, 2001; McLemore et al., 2009b).

TABLE 16. Summary of sample preparation for specific laboratory analyses. XRF–X-ray fluorescence analyses, XRD–X-ray diffraction analysis, ICP–Induced-coupled plasma spectrographic analysis, NAG–net acid producing tests, ABA–acid base accounting tests. Solid materials remaining after the tests were archived. Pulverized and crushing are the steps in SOP 5 that reduce the particle size to <100 mesh required for chemical analysis.

Laboratory analysis	Type of sample	Sample Preparation	Method of obtaining accuracy and precision	SOP
Petrographic analyses	Collected in the field, used split from chemistry sample	Uncrushed, typically smaller than gravel size material used, thin sections made of selected rock fragments	Selected samples were analyzed by outside laboratory	24
Microprobe analyses	Collected in the field or split from chemistry sample	Uncrushed, generally 2 splits; rock fragments and soil matrix	Use reference standards	26
Whole-rock chemical analysis (XRF, S/SO4)	Collected in the field in separate bag, analysis performed on powdered sample	Crushed and pulverized	Use reference standards and duplicates and triplicates	8

Laboratory analysis	Type of sample	Sample Preparation	Method of obtaining accuracy and precision	SOP
Whole-rock chemical analysis (ICP)	Collected in the field in separate bag, analysis performed on powdered sample	Crushed, pulverized, and dissolved in a liquid for analysis	Use reference standards and duplicates and triplicates	8, 30, 31
X-ray diffraction (XRD) analyses (including remaining pyrite analysis)	Used split from chemistry sample	Crushed	Compared to detailed analysis by electron microprobe	27, 34
Clay mineralogy analyses	Used split from chemistry sample	Uncrushed, typically smaller than gravel size material used, thin sections made of selected rock fragments, clay separation obtained by settling in a beaker of DI water	Use duplicate analysis, compared to other results performed by consultant companies, compared to detailed analysis by electron microprobe	29
Particle-size analysis	Bulk sample collected in the field	Sample sieved for each size fraction weighed	Use duplicate analysis, compared to other results performed by consultant companies	33
Paste pH and paste conductivity	Collected in the field, used split from chemistry sample or gravimetric sample	Uncrushed, typically smaller than gravel size material used	Use duplicates, compared with field measurements using Kelway instrument (SOP 63), compare to mineralogical analysis	11
ABA/NAG tests	Used split from chemistry sample	Crushed, typically smaller than gravel size material used	Use duplicate analysis, compared to other results performed by consultant companies	52, 62
DI leach	Collected in the field	Uncrushed, typically smaller than gravel size material used	Use reference standards and duplicate analyses	38
Gravimetric moisture content	Collected in the field in a sealed metal canister	Uncrushed, typically smaller than gravel size material used	Use duplicates	40
Atterberg Limits	Bulk sample collected in the field	Sample sieved to <0.425 mm	Use duplicate analysis, compared to other results performed by consultant companies	54
Bulk density and specific gravity	Collected in sealed buckets in the field	None, typically smaller than gravel size material used	Use duplicate analysis, compared to other results performed by consultant companies	32, 65, 70, 75
Direct Shear Test	Bulk sample collected in the field	Sieved to pass through the no. 6 sieve (<3.35 mm) for 2 inch shear test	Use duplicate analysis, compared to other results performed by consultant companies	50
Slake durability and point load index tests	Rock fragments 40 and 60 g for slake durability tests and approximately 4-10 cm in dimension for point load tests	None	Duplicate tests	76, 77

Laboratory analysis	Type of sample	Sample Preparation	Method of obtaining accuracy and precision	SOP
Stable isotope analysis	Selected mineral grains	See SOP	duplicate analysis and use of international standards	25

In the laboratory, splits of original sample material were used for measurements of moisture content, grain size, Atterberg limits, and specific gravity, according to ASTM standard procedures (Table 16; ASTM, 2001a, b, 2002a, b). Golder Associates personnel made 338 in-situ dry density measurements in the GHN trenches using the neutron gauge (see SOPs). The field team made additional measurements using the sand cone method, the sand replacement method, and the water replacement method. Each method of determining the in-situ dry density followed ASTM guidelines or was adapted from ASTM procedures as described in the appropriate SOP (Table 16). Samples tested included a mixture of rock fragments (18 cm to <1 mm in diameter) and soil matrix. Most GHN samples were collected from the trenches in the upper half of the GHN rock pile. Also, direct shear measurements were conducted on soil matrix samples, while point load strength and slake durability tests were performed on larger rock fragments from these sample splits.

The slake durability test was developed by Franklin and Chandra (1972) and recommended by the International Society for Rock Mechanics (ISRM, 1979) and standardized by the American Society for Testing and Materials (ASTM, 2001c). The purpose of the test is to evaluate the influence of alteration on rocks by measuring their resistance to deterioration and breakdown when subjected to simulated wetting and drying cycles. The durability of rocks can be described as their resistance to breakdown under weathering conditions over time. Slaking is defined as the swelling of rocks containing clay minerals when in contact with water (Franklin and Chandra, 1972). The slake durability index (ID_2) is a measure of durability and provides quantitative information on the mechanical behavior of rocks according to the amount of clay and other secondary minerals produced in them due to exposure to climatic conditions (Fookes et al., 1971). The test consists of a representative sample containing 10 rock pieces, each weighing between 40 and 60 g, with a total sample weight ranging from 450 to 550 g. The sample is placed in a screen drum and oven-dried at a temperature of 110 ± 5°C. After the sample is cooled to room temperature, the drum is immersed in distilled water and rotated at a speed of 20 rpm for 10 min. The sample is then oven-dried to a constant weight. The sample is submitted to 2 such cycles of wetting and drying. The ID_2 is obtained from:

$$ID_2 = \frac{W_A - W_D}{W_B - W_D} \times 100$$

where W_B is the mass of drum plus oven-dried sample before the first cycle, W_A is the mass of drum plus oven-dried sample retained after the second cycle, and W_D is the mass of drum.

All samples were visually described and classified according to the ID_2 values range after the second cycle of the slake durability test. Categories for visual description include (Franklin and Chandra, 1972): Type I, where pieces remain virtually unchanged, Type II, where the sample consists of large and small pieces and Type III with exclusively small fragments. Classification based on ID_2 values is presented in Table 17.

TABLE 17. Slake durability index classification (Franklin and Chandra, 1972).

ID_2 (%)	Durability classification
0 – 25	Very low
26 – 50	Low
51 – 75	Medium
76 – 90	High
91 – 95	Very high
96 – 100	Extremely high

The point load test is a simple test for estimating rock strength. The equipment is comprised of a loading frame that measures the force required to split the sample and a system for measuring the distance between the two contact loading points. The point load test can be performed on samples with different shapes, both cylindrical (core) and irregular shaped (Broch and Franklin, 1972). The point load strength index (Is50) corresponding to a sample of 0.05 m in diameter, given in MPa, is calculated using (ISRM, 1985):

$$Is50 = \frac{P}{D_e^2} \times F$$

where P is the peak load, D_e is the equivalent core diameter, and F is a size correction factor $(D_e/0.050)^{0.45}$. All samples are classified according to the classification index in Table 18.

TABLE 18. Point load strength index classification (Broch and Franklin, 1972).

Is50 (MPa)	Strength classification
< 0.03	Extremely low
0.03 – 0.1	Very low
0.1 – 0.3	Low
0.3 – 1.0	Medium
1.0 – 3.0	High
3.0 – 10	Very high
> 10	Extremely high

The shear strength of granular soil is frequently characterized by its internal friction angle (ϕ). The internal friction angle for granular materials is a function of the following characteristics (Hawley, 2001; Holtz and Kovacs, 2003):

- Particle size (friction angle increases or decreases with increase in particle size)
- Grain quality (weak rock such as shale versus strong rock such as granite)
- Particle shape and roughness of grain surface (friction angle increases with increasing angularity and surface roughness)
- Grain size distribution (well graded soil has a higher friction angle than a poorly graded soil)
- State of compaction or packing (friction angle increases with increasing density or decreasing void ratio).

The determination of the internal friction angle (ϕ) and cohesion (c) is commonly accomplished by direct shear test or triaxial tests. The direct shear test was preferred in the Questa project because of its simplicity, reliability and lower cost. It has been found that soil parameters ϕ and c obtained by direct shear testing are nearly as reliable as triaxial values. Limitations of the direct shear test were recognized and taken in consideration to minimize its effects in the results. One of the limitations identified was the inability to control or monitor pore water pressures during

the direct shear test. Air drying the samples before being tested was adequate to reduce the chance of pore water pressure buildup during the experiment.

Direct shear tests were performed at NMIMT (ASTM test procedure D 3080-98; Gutierrez, 2006) and at UBC. At NMIMT, direct shear tests were performed in a 2-inch shear box using dry samples from GHN with densities ranging from 1.60 to 1.84 g/cm^3, 0.02 in/min displacement rate, and normal load varying from 100 to 500 KPa (Gutierrez, 2006; Gutierrez et al., 2008). At UBC, direct shear tests were performed in a 4-inch shear box using saturated samples at loads ranging from 60 to 500 kPa (G. W. Wilson, written communication, Sept. 2005). At NMIMT, the shear tests were conducted on the air-dried samples that passed sieve No. 6, using 2-inch and 4-inch square shear boxes, using manual operation. A displacement rate of 8.5×10^{-3} mm/sec (0.02 in/min) and a normal stress range of 160 to 800 kPa were used for the tests. A minimum of four splits of approximately 120 g of each sample were used for the tests. A dry density of 1.7 ± 0.2 g/cm^3 was achieved for most samples. This density was based on the nuclear gauge field measurements, for which the dry density ranged from 1.06 to 2.31 g/cm^3 with an average of 1.69 g/cm^3 and standard deviation of 0.15 g/cm^3. A small density range was desired to reduce the number of variables affecting the friction angle. All samples were prepared by lightly compacting three lifts to attain the same relative compression. Each lift was carefully placed by pouring the soil with a spoon in order to minimize segregation. A displacement rate of 0.5 mm/min and normal stress varying from 159 to 800 kPa were adopted for all the tests. For dry samples used in the experiments, the shear rate is not important since no pore water is present. Normal stresses required for testing were estimated by dividing the applied load by the area of the shear box. Loads represented the weight of the rock-pile overburden consistent with the depth of the sample in the rock pile. Using a 50.8 mm shear box, the normal stress varied between 50 kPa and 800 kPa. These values duplicate depths in the rock pile between 3 m and 48 m (considering sample density of 1.69 g/cm^3).

Peak shear stress and residual shear stress were determined from plots of shear stress versus normalized displacement (Fig. 5a). All tests were continued until the shear stress became constant or until a maximum shear deformation of 10 mm had been reached, per ASTM D3080 recommendation (ASTM, 1998). In almost all samples the maximum shear stress was achieved at deformation less than 10 mm. Internal friction angle was obtained using a linear best-fit line from the plot of peak shear strength versus normal stress (Fig. 5b). The residual friction angle was obtained using a similar best-fit line.

The direct shear tests for GHN were performed on the finer-grained material and could introduce a biases. Field in-situ direct shear tests and direct shear tests using a 12-inch shear bow with larger size material were performed along with laboratory direct shear tests on other Questa rock piles for a comparison of methods (Boakye, 2008; Nunoo, 2009).

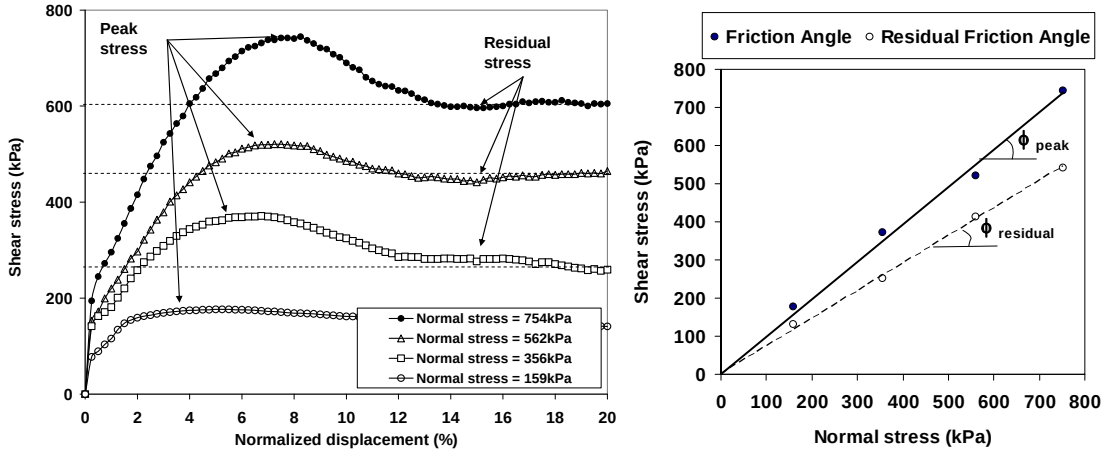

FIGURE 15. a) Example of a shear stress versus shear displacement plot for sample GHN-JRM-0037. b) Example of a Mohr-Coulomb diagram showing the best fit line for the peak internal friction angle and the residual internal friction angle.

MINERALOGICAL DETERMINATION

Petrographic analysis of rocks has been traditionally performed with optical microscopy using thin sections and point counting to provide a modal mineralogy (van der Plas and Tobi, 1965). However, this method typically does not provide accurate and reproducible mineral proportions for sedimentary, volcanic, and soil-like material, because rock fragments, groundmass, and matrix are typically identified as separate phases, not as specific minerals. In addition, groundmass phases in volcanic rocks can be too fine-grained to identify individually, and making thin sections of intact soil-like material is difficult because much of the material is not well cemented.

The modified ModAn technique (McLemore et al., 2009b) provides a quantitative bulk mineralogy that is consistent with the petrographic observations, electron microprobe analysis, clay mineral analysis, and the whole-rock chemistry of the sample. Figure 16 is a flow chart of the characterization procedure for a typical Questa sample collected by the procedures outlined in Figure 14. Unlike most normative mineral analyses, all of the minerals calculated for the quantitative mineralogy are in the actual sample analysis using ModAn. ModAn is a normative calculation that estimates modes "…by applying Gaussian elimination and multiple linear regression techniques to simultaneous mass balance equations" (Paktunc, 1998, 2001) and allows location-specific mineral compositions to be used. Representative mineral compositions for minerals in the Questa samples were determined from electron microprobe analysis and used in ModAn for this study (McLemore et al., 2009b). One of the features of ModAn that makes it appropriate for this study is that it can include a sulfide mineral in the modeling procedure. The results obtained by ModAn were corrected for the addition of other minerals not modeled by the program.

Three techniques were used to test the validity of the modified ModAn method to determine the quantitative mineralogy (Graf, 2008; McLemore et al., 2009b). Quantitative X-ray diffraction (QXRD) was determined on one set of samples from the Hanson alteration scar (Graf, 2008). Petrographic analysis and Rietveld analysis were determined on 14 samples that were used in the weathering (humidity) cells (Mineral Services Canada, Inc., 2008). The mineralogy obtained from the modified ModAn method was compared to these two separate analyses

(McLemore et al., 2009b). Not all methods compared exactly, but all methods provided similar enough results that the method is reliable, to approximately <5% in most samples, with a maximum error in some samples of 10% of the mineral composition in the rock (Appendix 8).

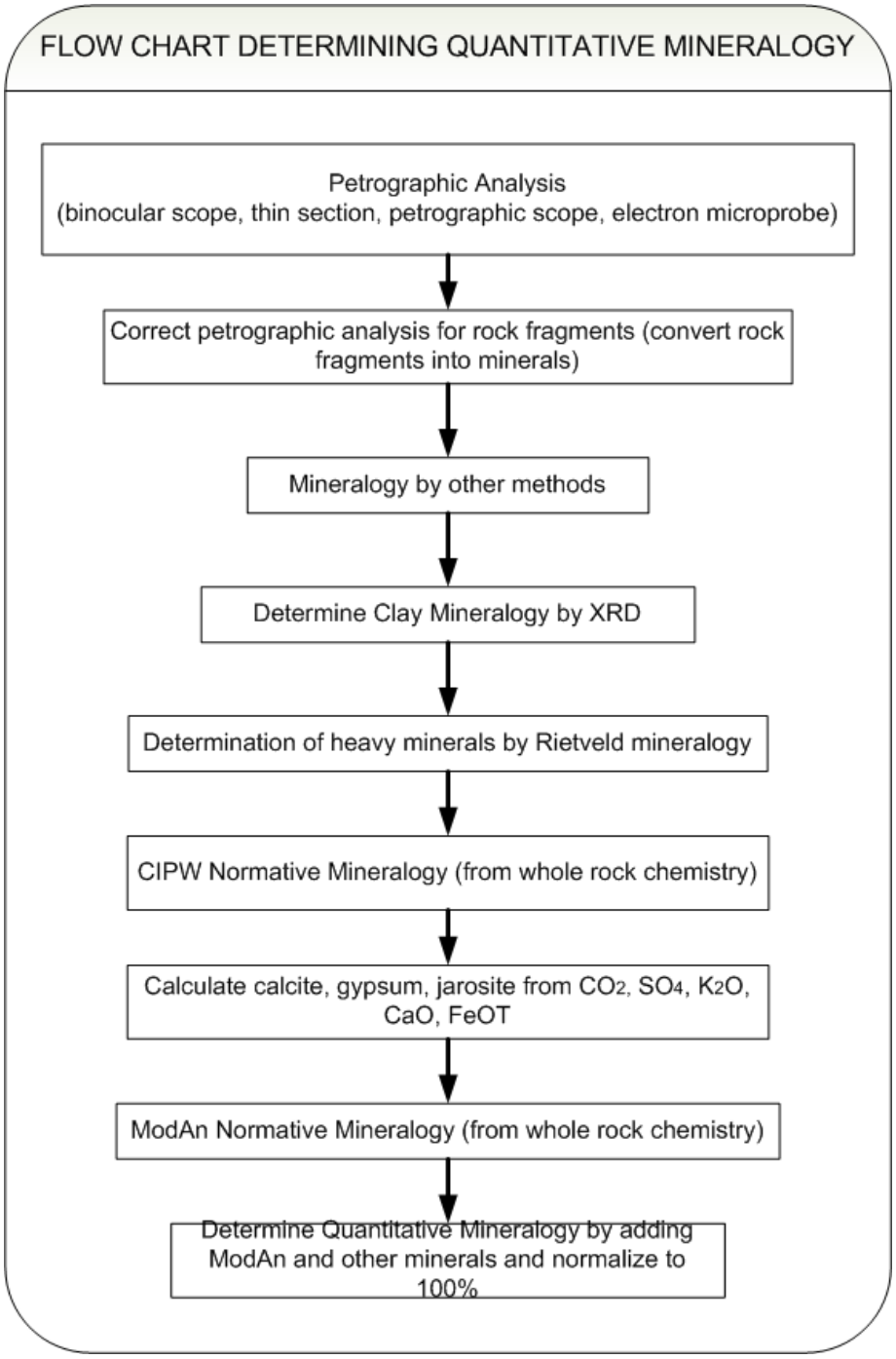

FIGURE 16. Flow chart for determining quantitative mineralogy from starting sample.

QUALITY CONTROL AND QUALITY ASSURANCE PROCEDURES

A standardized protocol was followed after each sample was taken. Each sample was clearly identified and a chain of custody process was followed to assure that all samples were

transported to the laboratory, analyzed, and the results sent back to NMBGMR. The sample number assigned to each sample follows the sample through all phases of analysis. The samples were transported from the field to NMBGMR and stored in a locked trailer until they could be analyzed. Specific details for quality control and quality assurance are summarized in Appendix 8 (also McLemore and Frey, 2008) and described in the project SOPs (Table 11).

The accuracy of the data is how close the measured value is to the true value. Analyzing certified standards as unknown samples and comparing with known certified values monitors accuracy. The precision of an analysis is the repeatability of a measurement. Precision is monitored by multiple analyses of many sample duplicates and internal standards. In general, analyses obtained from the different laboratories and methods are in agreement with certified values of certified standards and precision is excellent between multiple analyses (Appendix 8; McLemore and Frey, 2008). However, some differences between certified standards and duplicate pairs do exist.

Certified samples were submitted to the laboratories as unknowns (Appendix 8). The results obtained by the laboratories compare within error with certified values for most elements. Nugget effects can account for variations in some analyses. A nugget effect is where a small grain of native gold or other minerals occurs in one split and not the other split and produces a higher concentration of that element. Another variation between certified values and the results provided by the laboratories is a result of different analytical techniques. ICP requires acid digestion and analyses of a liquid-base solution. In many cases, not all of the solid rock will be completely digested and will result in a lower value than that obtained by certified values typically done by XRF, which analyzes the powdered sample. Specific analytical techniques also have specific analytical interferences that could affect the reported elemental concentrations.

The precision of chemical analyses is acceptable for most Questa samples. There are numerous reasons why duplicate samples and/standards do not always agree. Some samples, such as rhyolite and basalt, grind into powder more easily than other samples, such as stream-sediment samples and waste-rock samples. Fusion techniques required for XRF analyses vary from lab to lab and also can differ between different personnel that could result in variations between sample pairs. Analytical error is higher for analyses with concentrations close to the detection limit. In addition, rock pile and soil samples can be very heterogeneous and difficult to completely homogenize.

Another potential problem encountered with rock-pile samples, is the variability of sample collection. SOPs and personnel training insured that exact procedures were used to avoid variations between sample collectors. The overall analytical error is within ±5% for most samples, with a maximum error in some samples of 10%.

In order to verify the accuracy of the adopted direct shear test procedure for determining friction angle, some samples were tested in duplicate or triplicate (Appendix 8). In addition, tests were conducted using a calibrated *ELE* direct shear testing apparatus at Kleinfelder Laboratory in Albuquerque, NM. The proving ring for this motorized apparatus is annually calibrated. The purpose of these tests was to provide validation of the tests conducted with the manual *Soiltest* shear box machine in the NMIMT Mineral Engineering Department. The Mohr-Coulomb diagrams for samples GHN-KMD-0014 and GNH-KMD-0017 tested using both machines are shown in Figure 17. The shear test results using the ELE machine fell along the trend lines defined by data generated with the machine at NMIMT. The addition of the corroborating data did not change the ϕ values. Therefore, test results obtained at NMIMT are considered to be representative and reproducible.

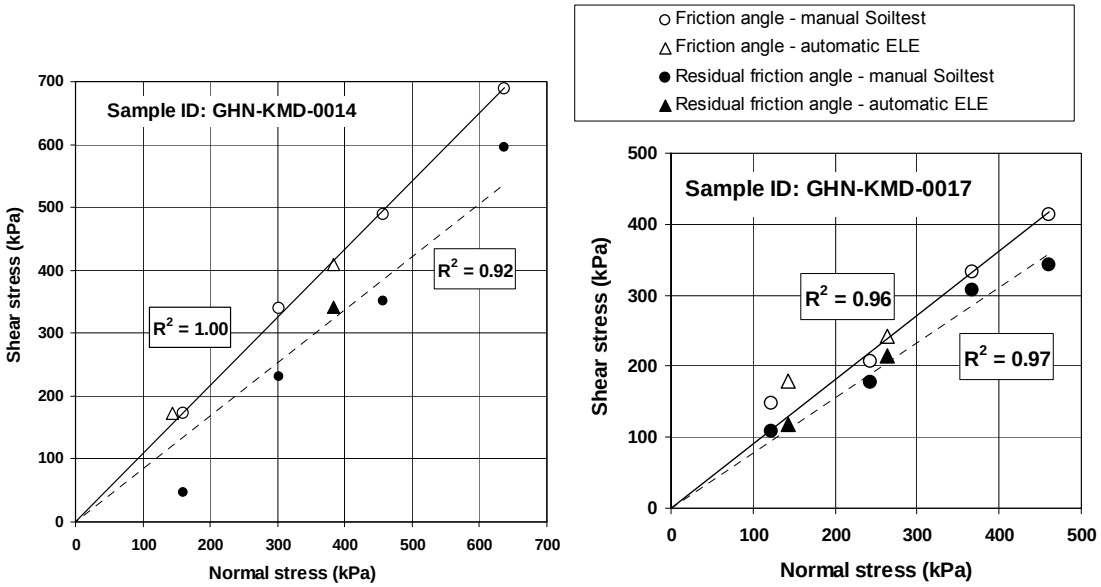

FIGURE 17. Mohr-Coulomb diagrams for two distinct samples using data points generated by both the automatic *ELE* and the manual *Soiltest* shear box equipment.

CHARACTERIZATION OF GHN

GEOPHYSICS AND REMOTE SENSING

Remote sensing

Hyperspectral remote sensing is used to analyze the mineralogy of the Questa rock-pile surfaces and surrounding altered and unaltered bedrock (Appendix 10). These remote sensing data are field verified by analyzing samples with a portable spectrometer. Knowing the distribution of minerals at the surface of the rock piles provides a tie between surface conditions and subsurface variation within the rock piles. Spectral analyses of samples are compared with traditional mineralogical analysis methods. Results indicate that spectral analyses can be used to differentiate between minerals formed by weathering and alteration, specifically the acid-sulfate minerals, such as jarosite and clay minerals. Goathill Gulch and the GHN rock pile are characterized by QSP alteration, especially sericite and pyrite (Livo and Clark, 2002; reflectance spectroscopy data in Appendix 10). Kaolinite and goethite surround the QSP alteration. Jarosite and gypsum occur at the surface of the GHN rock pile (Fig. 18, Appendix 10).

Thermal imagery

Thermal properties of the rock-pile material were measured using the FLIR SC 3000 infrared thermal camera. The thermal camera detection is limited to near surface thermal measurements. Thermal imaging on the rock piles can detect "hot spots" that are venting at the surface as well as layering associated with variations in soil moisture near the surface of the rock pile. Details of the survey can be found in Shannon et al. (2005).

Thermal camera surveys were conducted at three different locations on GHN prior to regrading (Shannon et al., 2005). The tripod location at the first location on the stable part of the rock pile was at coordinates UTM NAD27, zone 13, 0453578E, 4062161N at an elevation of 9498 ft (along the slope rising from the road that was constructed to access a drill hole). The second survey took place on the unstable portion of the rock pile along a road cut across the

middle part of the rock pile, and the third survey area was along a crack-like linear feature that transected the middle bench above the road. The surveys took place during the early morning hours, when it would be expected to encounter the greatest difference between the ambient temperature and any venting in the rock pile. In May, when the GHN rock pile was surveyed, no snow cover was present and no vapor was observed escaping from the rock pile.

The thermal images captured from the three survey locations on GHN indicate temperatures ranging between 4 and 12º C (Table 19). Similar measurements on Sulfur Gulch South range between 16º C in February and 13º C in May (Shannon et al., 2005). The lack of visible venting at the GHN rock pile could indicate that the thermal flux exiting the pile is relatively small compared to the energy added to the pile by solar radiation. The composite images of the stable and unstable portions of the GHN rock pile appear to indicate layering (Figs. 19, 20).

Surface Geophysical Surveys

Electromagnetic induction (EM31) and ground penetrating radar (GPR) geophysical measurements on GHN rock pile were carried out in 2004. Details on the measurement techniques can be found in van Dam et al. (2005). The measurements consisted of an EM31 and GPR reconnaissance survey on the top of GHN rock pile in March, a full-scale investigation on the top of GHN rock pile (using EM31 and GPR) in May, and a GPR survey down the slope of GHN in August before regrading. The objectives of the geophysical study were to:

- Assess the internal structure of the GHN rock-pile material using ground penetrating radar (GPR)
- Measure spatial variability in bulk apparent electrical conductivity
- Find the best locations for digging trenches to study rock-pile characteristics
- Correlate geophysical observations with trench analyses.

Geophysical measurements have been successfully used to characterize the subsurface characteristics of GHN rock pile (Fig. 21, 22; van Dam et al., 2005). The GPR survey imaged the rock-pile stratigraphy up to a maximum depth of approximately 15 ft and identified several areas characterized by steeply dipping structures. The trench locations were selected based on the information provided by the geophysical survey. One trench was dug at the location of geophysical survey Line 1 (Fig. 21). The stratigraphy observed in the trench correlated well with the GPR image.

The electrical conductivity measurements indicate significant variations between the northern and southern part of GHN. For survey lines 1, 2, and 3 on the northern part of the rock pile the electrical conductivity is fairly constant and fluctuates between 5 and 8 mS/m. Profiles 4 and 5 on the southern part of GHN exhibit significant variation in electrical conductivity between the eastern and western side of the rock pile. The conductivity increases from low values (similar to Lines 1-3) in the east towards values between 20 and 30 mS/m in the western end of survey lines 4 and 5. In the absence of topography differences the higher conductivity values between ~30 ft and the end of Lines 4 and 5 can be explained by:

- An increase in water content associated with a larger clay content
- A perched water table
- Different mineralogy
- Different pore water composition
- A change in material density related to the presence of a compacted traffic layer.

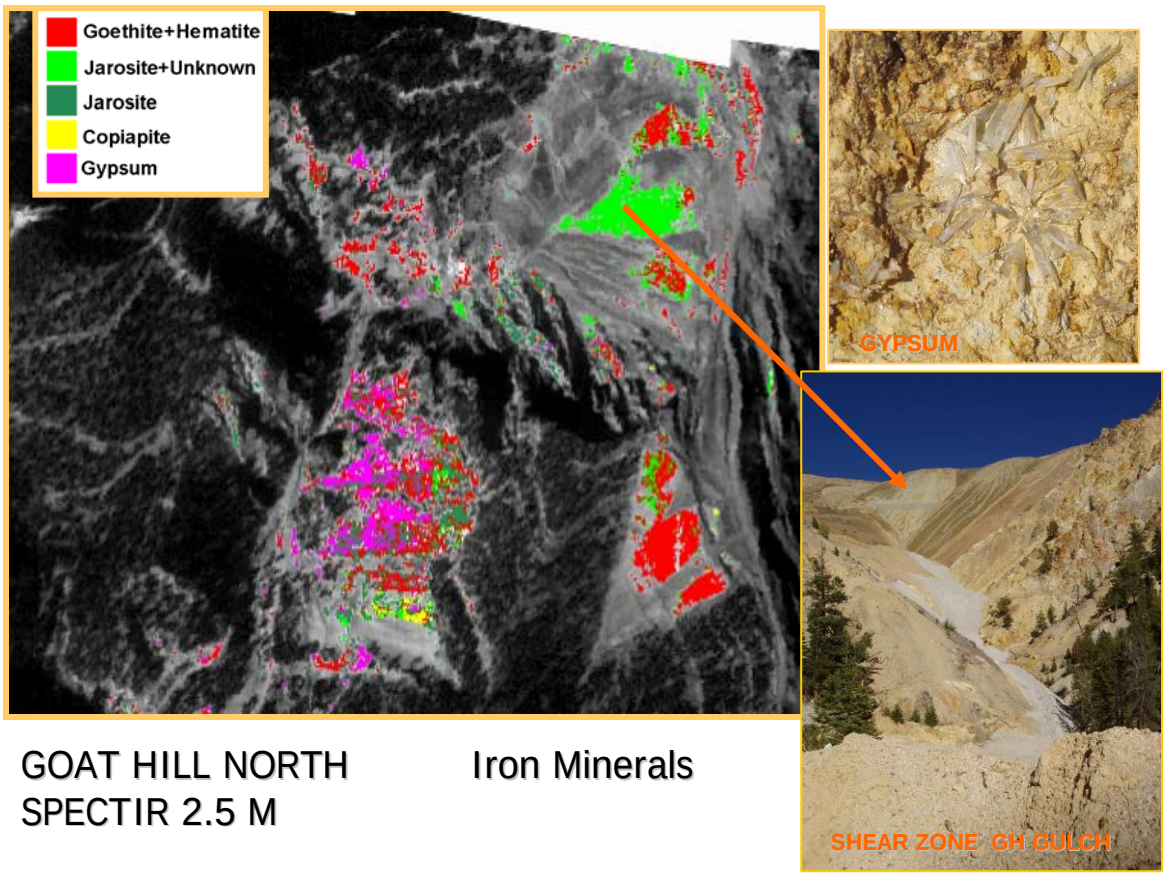

FIGURE 18. Spectir 2.5 M reflectance image of GHN and surrounding area, showing the surface of GHN consisting primarily of jarosite, goethite, and hematite.

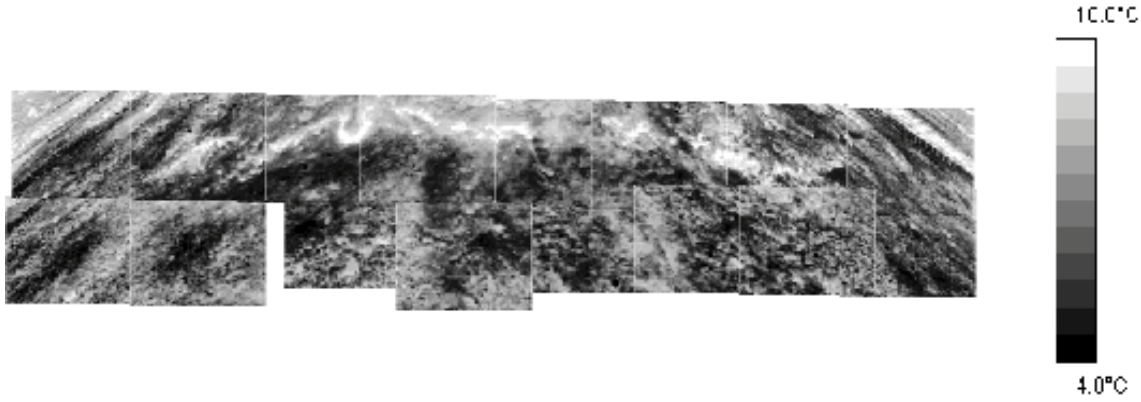

FIGURE 19. Composite thermal image of stable portion of GHN rock pile (Shannon et al., 2005).

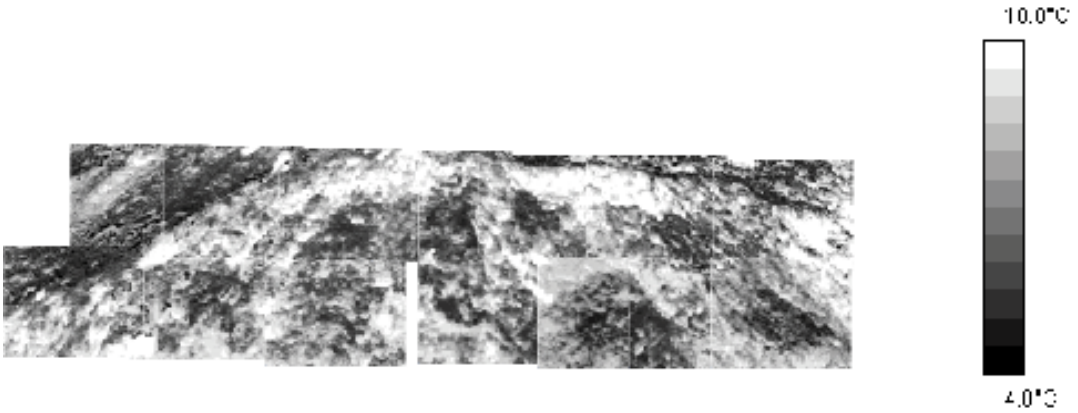

FIGURE 20. Composite thermal image of unstable portion of GHN rock pile (Shannon et al., 2005).

TABLE 19. Temperature ranges for GHN survey areas, May 20, 2004 (Shannon et al., 2005).

Site Description	Maximum temperature (ºC)	Minimum temperature (ºC)
Stable Portion (Unit C)	9.7	4.5
Unstable Portion (Unit D, E)	11	5.4
Crack	10.8	6.2
Excavated Crack	11.9	6.8
Dug Out	11.8	5.7

The three GPR sections on the northern part of GHN rock pile (Lines 1, 2, and 3; Fig. 21; van Dam et al., 2005) were dominated by reflections dipping to the west. These reflections have a similar dip direction as the current slope of the rock pile and reflect the depositional process (avalanching) of the rock-pile material, possibly in combination with secondary processes (e.g., preferential weathering). The reflections can occur due to changes in particle size, compaction, packing, density, or mineralogy. The reflections can be traced to a maximum depth of 15 ft and the maximum dip angle is approximately 30º. However, the dip angles are not consistent, which indicates that not all material was deposited under similar conditions and not all material was deposited at or near the angle of repose. On the southern part of GHN rock pile the GPR reflection character in the zone with high electrical conductivities is dominated by continuous sub-horizontal reflectors and a significantly reduced penetration depth. Because radar-wave attenuation is strongly dependent on the electrical conductivity, the lower signal penetration ties in well with the high electrical conductivities that were found in this area.

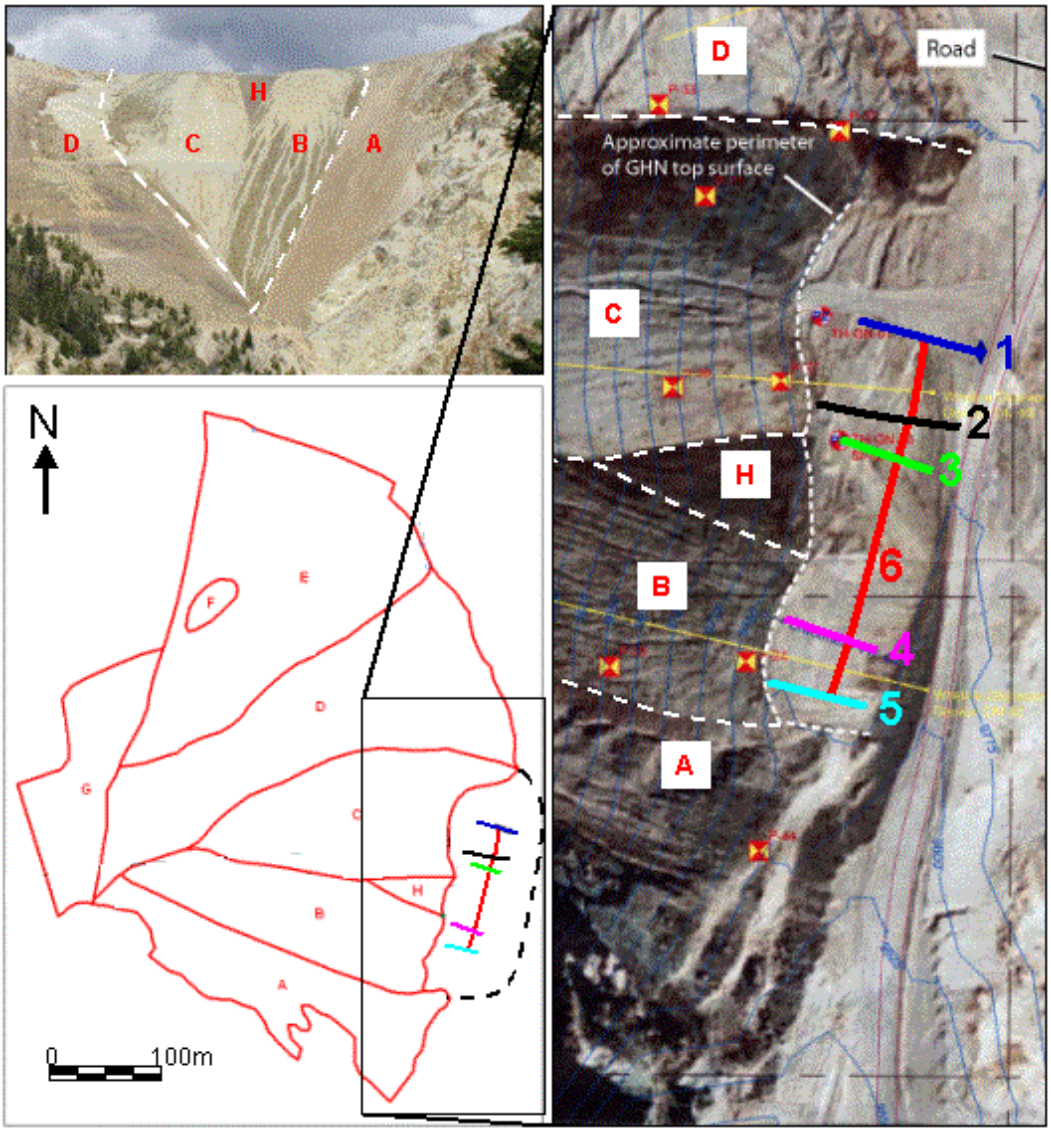

FIGURE 21. The geophysical survey layout on the GHN rock pile (van Dam et al., 2005). Top left: picture of GHN rock pile, looking east. The area studied was between the dashed lines. The letters refer to distinct units on the geologic/structural map of GHN rock pile before regrading (lower left). A description of the units can be found in McLemore et al. (2005, 2006a, b) and below. The boxed area represents the aerial photograph (right), the GHN Drilling and Instrumentation Map (updated 10/06/03). The photograph shows the locations of geophysical survey lines (colored lines and numbers), relative to the different units of the rock pile (boxed letters). Data are based on GPS measurements on May 18, 2004.

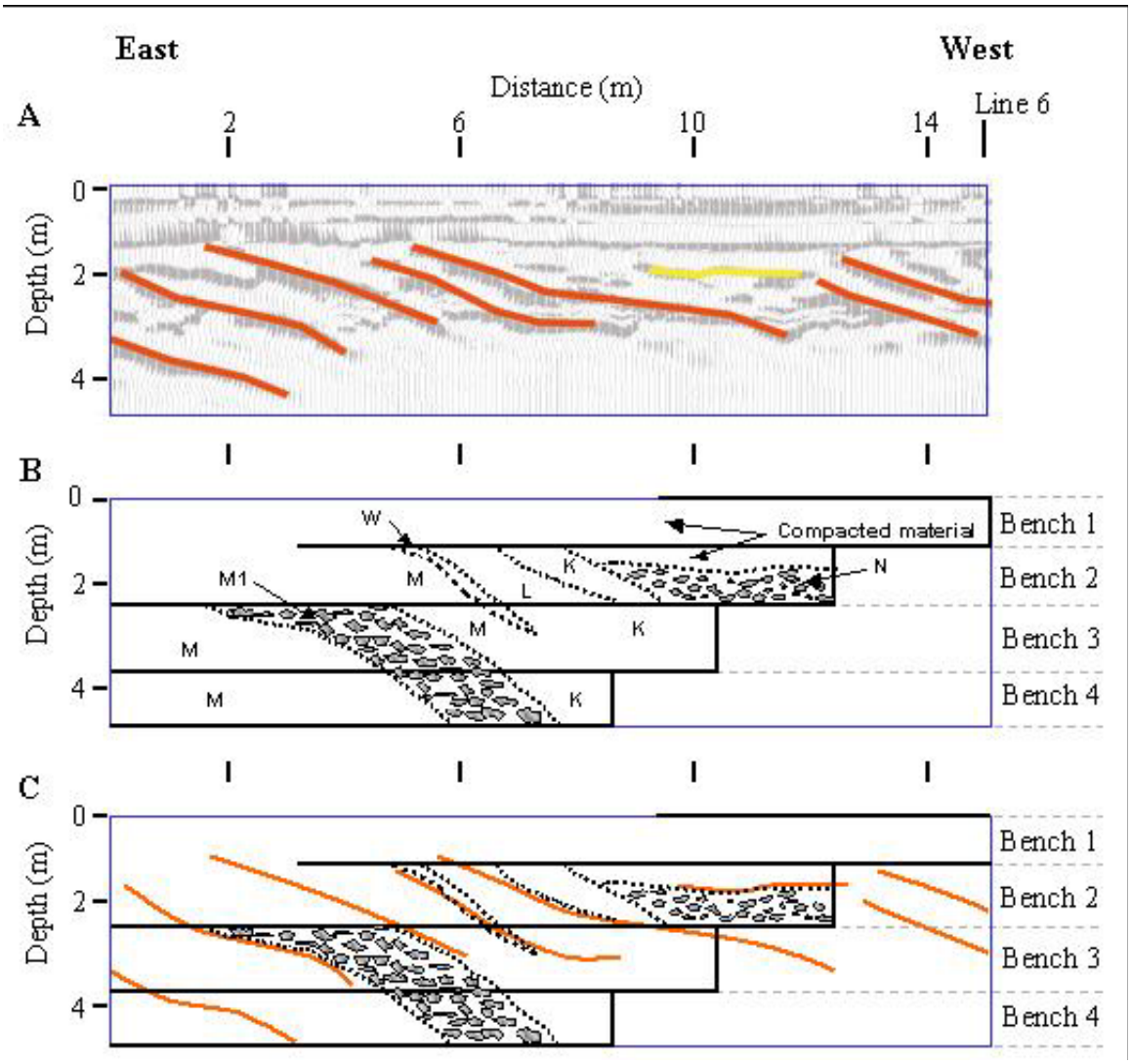

FIGURE 22. Comparison of the 100 MHz GPR survey of Line 1 and the geological section of trench LFG-0003 that was excavated over part of Line 1 (van Dam et al., 2005). A) GPR data and interpretation of reflections. The blue box represents the approximate outline of the trench. B) Geological section of the layers identified in the trench; for a detailed description of the trench units see below and McLemore et al. (2005, 2006a, b). C) Overlay of the GPR interpretation (in red) and the layers identified in the trench.

DESCRIPTION OF SURFACE GEOLOGIC UNITS

The surface of GHN rock pile was a composite of andesite and rhyolite (Amalia Tuff) with variable surficial weathering features that included brown to yellow Fe-oxide layers or streaks, grayish zones with pyrite, black manganese layers or streaks, and white to yellow-brown crusts of soluble salts (Fig. 23; discussed in more detail below). Boulders and cobbles, especially those of andesitic composition, are fragmented along fractures and veins of pyrite that are partially altered to jarosite, Fe-oxides, and gypsum (Fig. 24). These textures are indicative of physical weathering, possibly freeze-thaw or volume changes as a result of formation of new

sulfate minerals (i.e. gypsum), which also decreases the particle size. Similar features are found at other rock piles (Sidenko et al., 2005; Diehl et al., 2006; Farkas et al., 2009).

Eight surface geologic units were differentiated, described and sampled during the surface geologic mapping (Fig. 25). These units are surface units only and no age relationships can be determined between them. Units A, B, C, and H are found on the southern, stable portion of the rock pile where little or no movement has occurred. Units D, E, F, and G are found on the northern, unstable portion of the rock pile, which has slumped at creep rates for the last 25-40 years down slope with total rock pile movement vectors of up to 100 ft or more (Mike Ness, written communication, 4/28/05). The rock pile lies unconformably on colluvium or weathered bedrock, which overlies bedrock of andesite and rhyolite (Amalia Tuff).

High evaporation rates in arid environments can result in a crust that forms on the surface of rock piles, including GHN (Fig. 20). The crusts form by evaporation during dry periods. The crust does not form simultaneously. The crust can take 3-10 days to form depending upon the weather. When there is a heavy rainfall or a snow fall, the cementing minerals forming the crust dissolves and the surface of the rock pile is soft. The crust formation is seasonal and dependent not only by a rainfall event, but requires a heavy rainfall to completely dissolve. The crusts are porous, brittle, and crumble when collected by hand. Fe-oxides and oxydroxides occur as fracture or macro- and micro-cavity fillings; thin films are common. Color varies from red to dark brown, yellow, orange, and black. The change in color is a result of differences in mineralogy (Carbone et al., 2005). The crusts can form in situ up to several centimeters thick. The top surface of the upper layer has many fine desiccation cracks, and includes a discontinuous layer of rock fragments cemented by lathlike crystals (1 mm long) and clusters of crystals of gypsum and other minerals. The minerals found in the crusts include gypsum, jarosite, copiapite, alunite, melanterite, and schwermannite, along with feldspar, quartz, clay minerals, Fe oxides, rutile, apatite, and local pyrite. Gypsum occurs as clear, euhedral, tabular, needle-like crystals. Twinned and skeletal varieties are less common. Cracking of the crust is common and increases the surface area for evaporation (Carey et al., 2005). The upper layer is upwarped, buckled and blistered, partly separating it from the underlying yellowish sulfate, which has formed underneath it. All of these characteristics suggest a process of mineral precipitation by surface evaporation accompanying the capillary rise of water (Joeckel and Ang Clement, 1999; Joeckel et al., 2005).

FIGURE 23. Surficial zones of white to yellow-brown soluble salts, gypsum, and jarosite on GHN.

FIGURE 24. Boulder of andesite that fell apart along veins filled with pyrite, partially altered to jarosite and Fe oxides, gypsum, and calcite. This is a result of physical weathering.

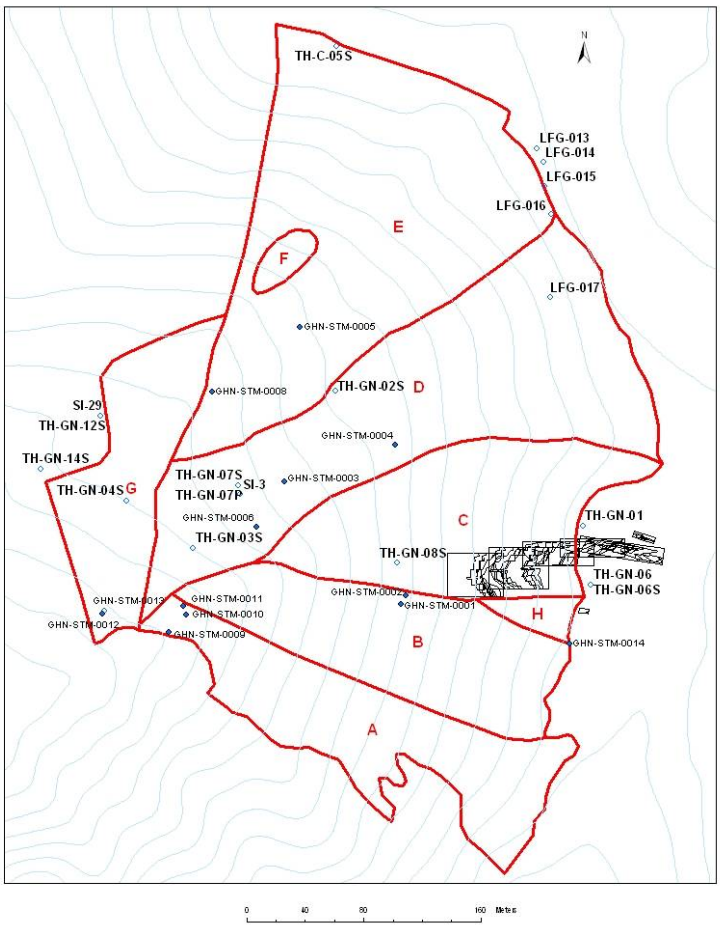

FIGURE 25. Geologic map of GHN rock pile before regrading showing locations of drill holes, samples, and trenches. Open circles indicate drill holes, closed circles indicate sample locations, solid lines outline geologic maps of trenches shown in Appendix 3. Survey and construction data are in Appendices 1 and 2.

DESCRIPTION AND STRUCTURE OF SUBSURFACE GEOLOGIC UNITS EXPOSED IN TRENCHES AND DRILL HOLES (STABLE PORTION OF GHN)

Descriptions of the subsurface units identified in the trenches in the stable portion of GHN rock pile are summarized in Table 20. Appendices 5 and 6 contain logs of the individual benches and drill holes with their descriptions. The descriptions combine geologic and engineering terms to assist in characterizing the units relative to slope stability. During trench mapping, team members identified several consistently correlative units down slope through approximately 200 vertical ft of rock pile material (Fig. 26). A geologic cross section of the upper portion of GHN (area of trenches and drill holes) is in Figure 26 and was constructed from logging of the trenches and drill holes (Appendices 1, 4). Section drawings and lateral measurements of unit boundaries provided data used to compile geologic maps of each trench. Plan maps of individual trenches show a “v-shape”, indicating the westward dipping character of the beds on each bench with an apparent offset between benches due to the vertical walls separating benches (Appendix 3). Unit boundaries have been projected onto an east-west cross section to show the vertical extent of units within the rock pile (Fig. 27; Appendix 3).

A zonation of the rock pile is visible in Figures 28, 29, and 30 (Phillips et al., 2005). The outer units (west, Units C, I, J) are lighter-colored, yellow to orange-brown to light gray, oxidized with very little pyrite, except in some rock fragments. The outer, oxidized units consist of highly leached and oxidized rock comprised mainly of quartz and secondary Fe sulfates, with smectite and mixed layer illite-smectite. This zone is characterized by low paste pH, low acid neutralizing potential, and high acid generating potential. Extensive interchange of water and oxygen occurs in this zone, which enhances pyrite oxidation. Internal to the leached zone is a zone of slightly increased clay-size material accumulation (unit J). The clays are predominantly illite and chlorite with increasing smectite toward the center of the pile, as described below. The origin of this clay-size material accumulation is problematic and it is uncertain whether the material represents originally mined and dumped fine-grained material or an accumulation of fine-grained material washed into the pile from the upper zone. This unit is typically green to orange with moderate to low paste pH. In between the outer, oxidized and interior, unoxidized zone is an intermediate zone (Unit N) of light to dark brown material that is moderate to well cemented by clay minerals and sulfate minerals. It contains local zones of bright orange to punky yellow oxidized sandy clay. Clays are dominated by smectite and chlorite. Proximal to the interface are zones of dark brown to black accumulation of Fe- or Mn-oxide material that coats grains and clasts. This accumulation of Fe and Mn oxides can represent a zone of reduction. Typically, the inner, unoxidized units (east, units K-W, excluding unit N) of the piles are darker colored and uniformly gray to light brown to dark orange-brown with visible pyrite in both the matrix and rock fragments and are interbedded with occasional yellow to gray zones of oxidation associated with little or no pyrite in the soil matrix. The inner, unoxidized zone typically contains abundant calcite, chlorite, epidote and clay minerals and accordingly, has high paste pH values and low acid generating potential. Apparently chemical reactions within the main portion of the rock pile are controlled by the availability of oxygen and water.

The units are generally youngest to oldest, from west to east; the units in the east were deposited first. The upper portion of the rock pile (WR1, traffic zone in Fig. 12) is matrix supported with interbeds of clast-supported material (Figs. 27, 28). The traffic zone is a surface zone on the rock pile of compacted material, where trucks and heavy equipment traveled upon. The remainder of the rock-pile material down slope exhibits a clast-supported matrix (Figs. 31, 32; WR2, WR3, rubble zone in Fig. 12). The samples increase in particle size down slope of the rock pile. Cementation in the rock piles varies from none to moderate, with local discontinuous, well-cemented layers. Unit boundaries ranged from horizontal to vertical, but most dipped between 20 and 40º westward to northwestward. The layers did not have a consistent dip because of compaction of the rock-pile material, irregularities of the material that allowed for different depositional dips, pinchouts in layers, and in some cases apparent dips were measured. Locally, thin units pinched out or graded vertically and laterally.

TABLE 20. Descriptions of geologic units at GHN. No relative age relationships could be determined between surface units A-H. GHN rock-pile material consisted primarily of hydrothermally altered andesite and rhyolite (Amalia Tuff) rock fragments.

Geologic Unit in this report	Description	Structure	Lithology	Location
Surface units				
A	Light brown unit with approximately 60% covered by cobbles or larger sized rocks with vegetation growing	Layered in some of the rills near the	mixed volcanic rocks	Southern-most surface unit of the stable part

Geologic Unit in this report	Description	Structure	Lithology	Location
	upon the surface.	base.		
B	Massive, light brown to gray to yellow-brown unit containing crusts of soluble acid salts. Approximately 65% is covered by cobbles or larger sized rocks. Consists of clayey sand with gravel and cobbles and is locally cohesive.	Shallow rills (0.2-1 m deep) of finer grained material are cut into the surface.	quartz-sericite-pyrite (QSP) altered Rhyolite (Amalia Tuff) (70%) and andesite (30%)	Surface unit of stable portion of the GHN rock pile
C	Grayish-brown to yellowish-gray unit consisting of fine-grained materials (sand with cobbles and gravel) and approximately 15% boulders. Locally is cohesive and well cemented by clays and soluble minerals.	Massive alternating zones, up to 10 ft thick.	rhyolite (Amalia Tuff) (70%) and andesite (30%)	Surface unit of stable portion of the GHN rock pile
D	Yellow-brown gravely sand unit that differs from Unit C by a marked increase in cobbles and boulders (approximately 30-40%).	Massive	rhyolite (Amalia Tuff) (80%) and andesite (20%)	Surface unit of unstable portion of the GHN rock pile
E	Orange-brown unit with patches of gray sandy clay containing approximately 15% cobbles and boulders.	Massive	70 % moderate to strong QSP altered rhyolite (Amalia Tuff) and 30% weakly altered Rhyolite (Amalia Tuff)	Surface unit of unstable portion of the GHN rock pile
F	Similar to Unit A, consists of dark brown, silty sand with some gravel.	Massive	andesite	Surface unit of unstable portion of the GHN rock pile
G	Orange-brown to yellow-brown sandy gravel with some cobbles, includes colluvium material.	Massive	andesite	Surface unit of unstable portion of the GHN rock pile
H	Dark gray to red-brown V-shaped unit with oxidized orange zones and consists of poorly sorted, well graded, weakly cemented, gravel sand with some fine sand to fine sand with clay and contains approximately 80% cobbles or boulders.	Massive	andesite	Surface unit at the top of stable portion of the GHN rock pile
Outer, oxidized zone				
I	Light-gray, poorly sorted, well graded clayey to sandy gravel, medium hard with weak cementation, and no plasticity. The matrix is locally sandy clay with medium to high plasticity. The unit is less cemented and finer grained than the overlying unit C.	Overlain by Unit C, up to 10 ft thick	andesite and rhyolite (Amalia Tuff)	Subsurface oxidized unit of stable portion of the GHN rock pile
J	Dark orange-brown, poorly sorted, well graded coarse gravel with clay matrix and weak cementation. The top of the unit locally is a bright orange oxidized layer, 2-4 inches thick.	Overlain by unit I, 3-12 ft thick	primarily andesite	Subsurface oxidized unit of stable portion of the GHN rock pile
Interior zones				
N	Light to dark brown moderately sorted, uniformly graded, moderately hard sandy clay with cobbles, with moderate to high plasticity and well	Heterogeneous with numerous coarse and fine	andesite and rhyolite (Amalia Tuff)	Subsurface unit of stable portion of the GHN rock pile

Geologic Unit in this report	Description	Structure	Lithology	Location
	cemented by clay; contains zones of bright orange to punky yellow oxidized sandy clay.	layers, 5-10 ft thick		
K	Distinctive purplish-brown gravelly sand with cobbles and is weakly cemented and very coarse containing almost no clay. Cobble layer is locally overlain and underlain by finer gravelly sand layers; contacts are gradational.	grades into Unit O, 0-4 ft thick	primarily andesite	Subsurface unit of stable portion of the GHN rock pile
L	Brown-gray, poorly sorted, well graded gravelly sand with cobbles.	Grades into Unit O	andesite	Subsurface unit of stable portion of the GHN rock pile
O	Brown, poorly sorted, sandy gravel matrix in coarse gravel and cobbles. Numerous coarse and fine layers at varying dips and thicknesses appear in the mass of the unit. The unit has cobbles and clay layers, is deformed and heterogeneous, with numerous S-shaped clay lenses and coarse layers.	Variable dip of individual beds	primarily andesite	Subsurface unit of stable portion of the GHN rock pile
M	Orange-brown to brown, poorly sorted, well graded sandy gravel with boulders (up to 1 m diameter). Sandy gravel forms a matrix between boulders and cobbles. The fines are generally gritty.	Unit locally flattens with 20 degree dip	andesite and rhyolite (Amalia Tuff)	Subsurface unit of stable portion of the GHN rock pile
P	Dark brown, poorly sorted, well graded, sandy gravel with medium hardness and no to weak cementation	Pinches out, 0-3 ft thick	andesite	Subsurface unit of stable portion of the GHN rock pile
Q	Dark brown, poorly sorted, well graded, sandy gravel with cobbles with medium hardness and no to minor cementation.	Steeply dipping	andesite	Subsurface unit of stable portion of the GHN rock pile
R	Orange-gray, poorly sorted, well graded sandy gravel to gravel with cobbles with moderate to weak cementation by clay.	Pinches out, 0-3 ft thick	primarily andesite	Subsurface unit of stable portion of the GHN rock pile
S	Dark gray, poorly sorted, well graded sandy silt with no cementation or plasticity.	Pinches out, 0-4 ft thick	primarily andesite	Subsurface unit of stable portion of the GHN rock pile
T	Dark gray, poorly sorted, well graded sandy gravel.		andesite	Subsurface unit of stable portion of the GHN rock pile
U	Brown poorly sorted well graded, sandy gravel with cobbles.	Pinches out, 0-2 ft thick	andesite	Subsurface unit of stable portion of the GHN rock pile
V	Gray to brown-gray, poorly sorted, sandy gravel.	Pinches out, 0-10 ft thick	andesite	Subsurface unit of stable portion of the GHN rock pile
W	Olive gray clay zone, similar and possibly correlated to Unit S.		andesite	Subsurface unit of stable portion of the GHN rock pile
rubble zone	Orange-brown, angular cobbles and large boulders (15 cm in diameter) with little sand or clay, cobble-supported rubble zone. Unconformably on top of either soil	Unconformable, up to 7 ft thick	andesite, rhyolite (Amalia Tuff)	Basal subsurface unit of stable portion of the GHN rock pile

Geologic Unit in this report	Description	Structure	Lithology	Location
	developed on weathered andesite or colluvium that is similar to the alteration scars.			
Shear zone, alluvium, colluvium	Dark gray to brown clayey soil developed on weathered andesite or a yellow to orange brown clay to sandy clay colluvium that is similar to the alteration scars.	1-3 ft thick	andesite	Original surface, material beneath the rubble zone
bedrock	Gray to dark gray to greenish gray, porphyritic to fine-grained andesite.	Locally fractured	andesite	Original andesite bedrock beneath the soil, alluvium, colluvium

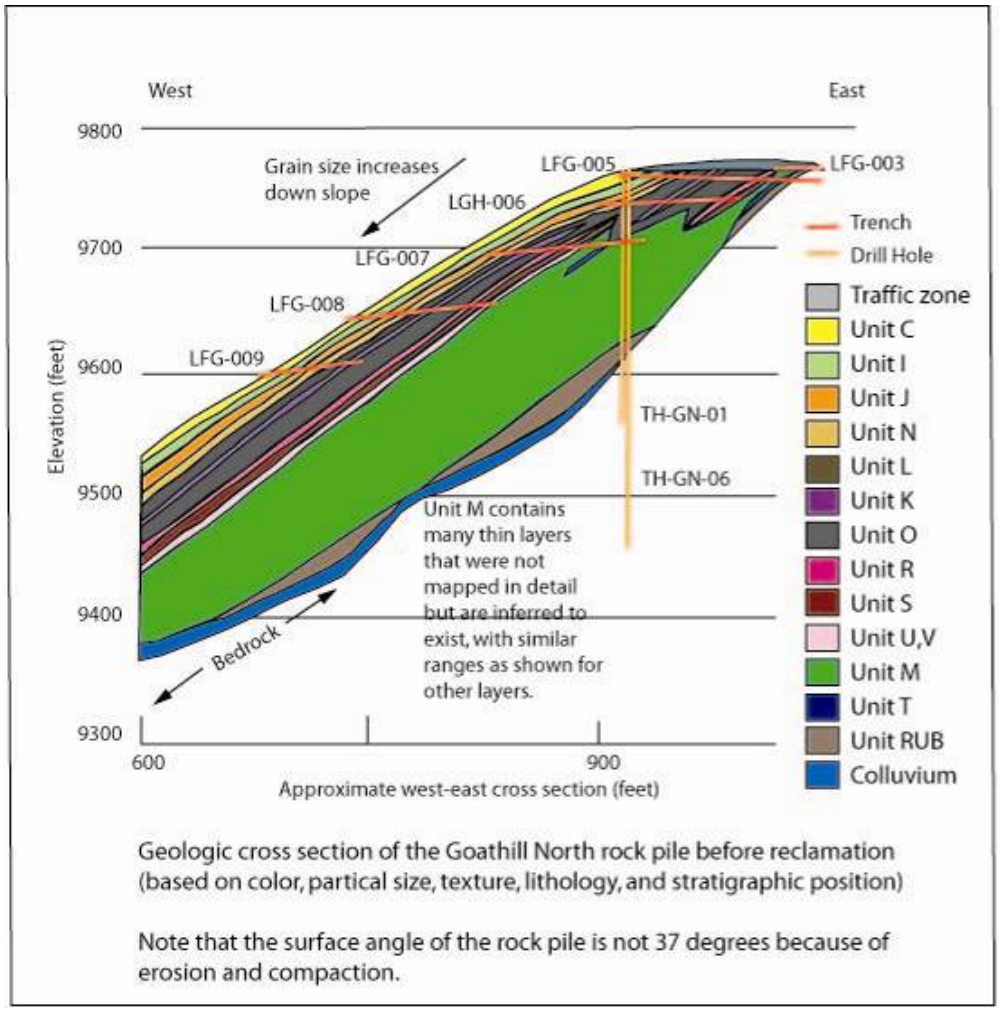

FIGURE 26. Detailed geologic cross section of the upper portion of the stable portion of GHN rock pile (based on mapping of the drill holes and trenches, upper third of the rock pile). Rock material was generally placed at angle of repose (approximately 36º), but the dip of the individual layers was not consistent. The layers ranged in measured dip from 20° to 40°. Some variations are due to compaction of the rock-pile material, irregularities of the material that allowed for different

depositional dips and pinchouts in layers, but some variation also is due to apparent dips being recorded. Units are described in Table 20.

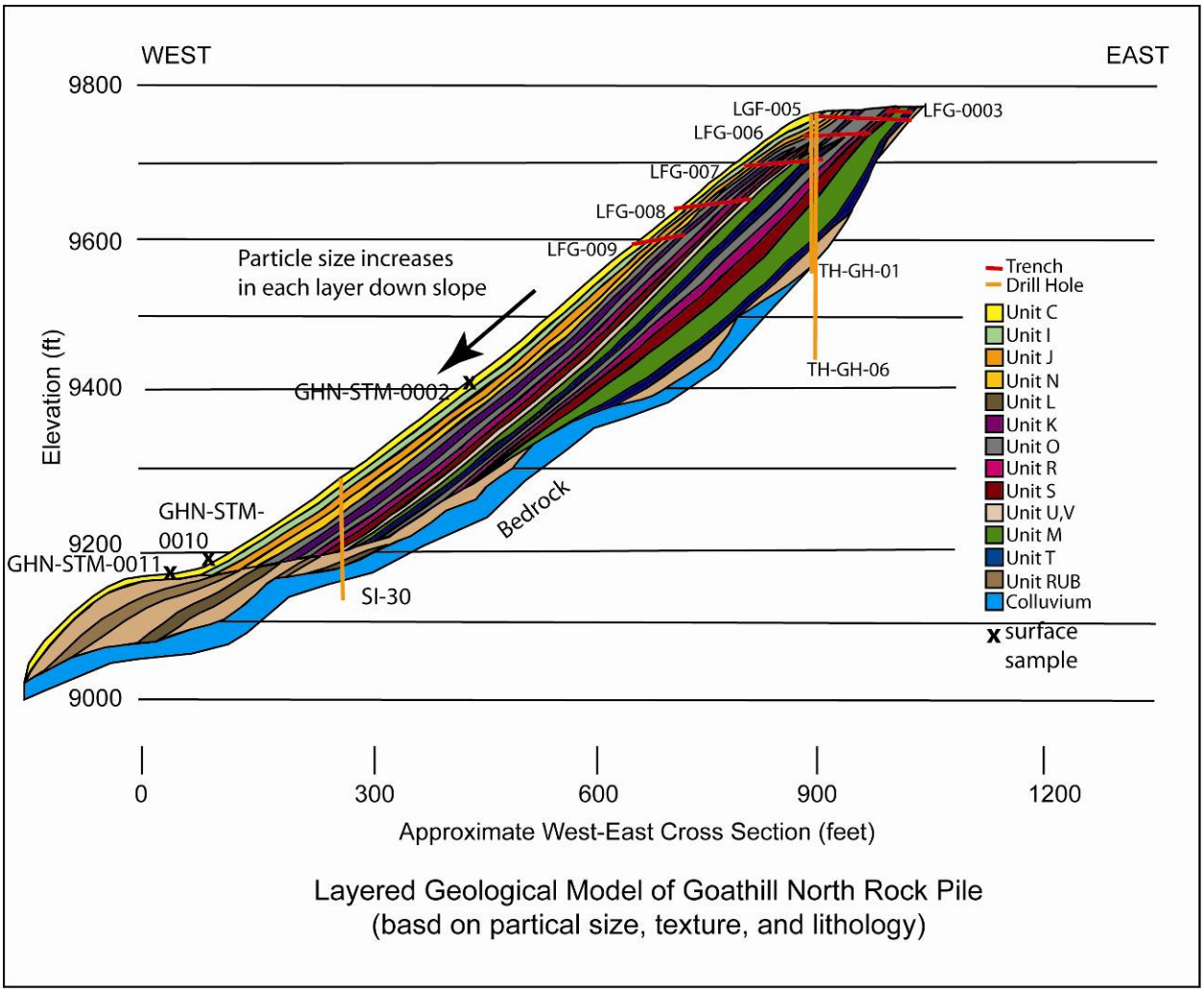

FIGURE 27. Conceptual geological model of GHN rock pile showing sample locations, as interpreted from surface mapping, detailed geologic cross section (Fig. 26), trenches, drill holes, construction method, and observations during regrading of GHN (McLemore and the Questa Rock Pile and Stability Team, 2008).

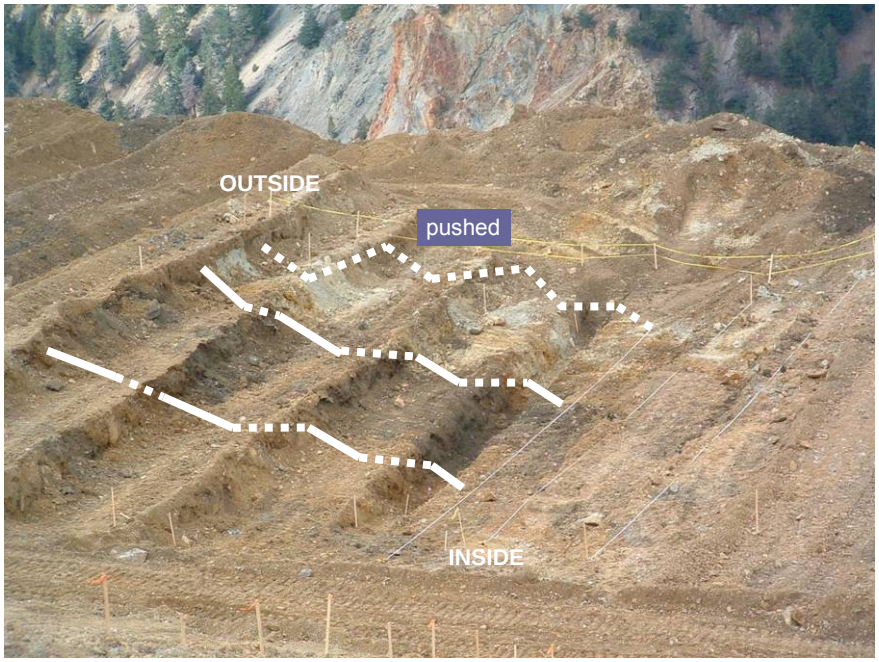

FIGURE 28. Southwestward view of zonation exposed within a typical trench at the outer margin of the GHN rock pile. Note that a trench contains four benches. The white to light gray zone inside the yellow tape represents the outer margin of the original dumped pile (pushed material beyond the white zone). Color zones from outer zone to interior of the rock pile: oxidized, leached zone–white to gray to yellow (Unit C, I); oxidized, sulfate accumulation–orange (Unit J); intermediate zone–dark brown (Unit N), internal zones–brown (Units K-W, excluding N). See conceptual model and cross-section given in Figure 12. Geologic units are described in Table 20.

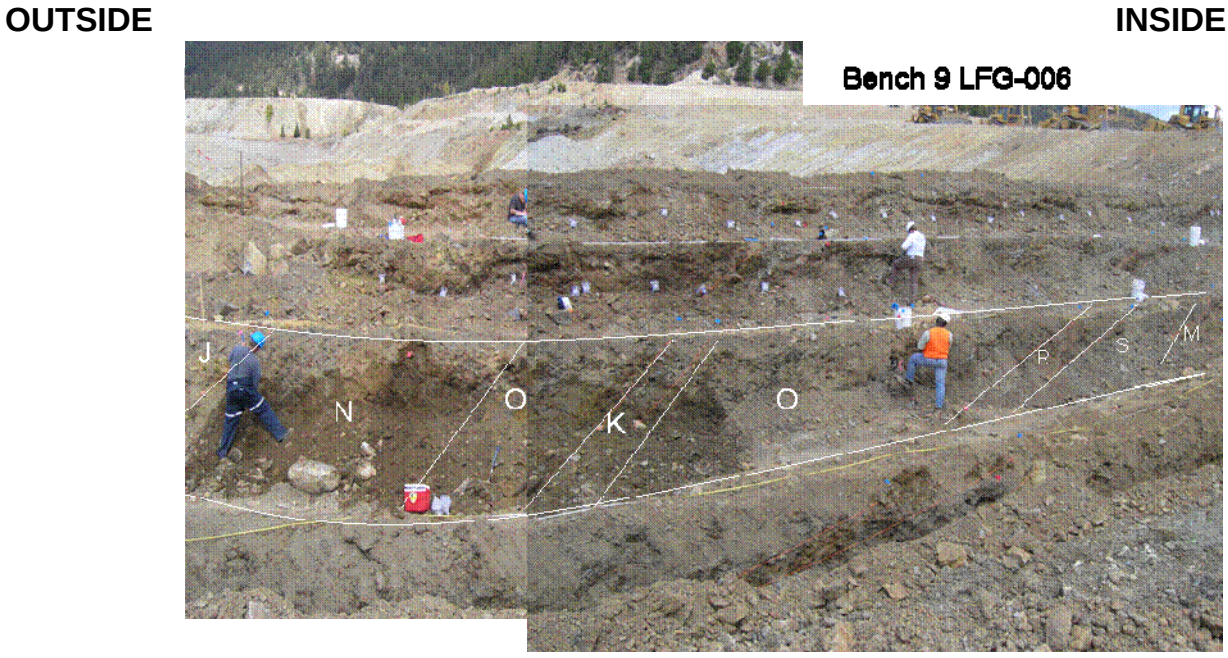

FIGURE 29. North-looking view of bench 9, Trench LFG-006, GHN showing geologic units described in Table 20.

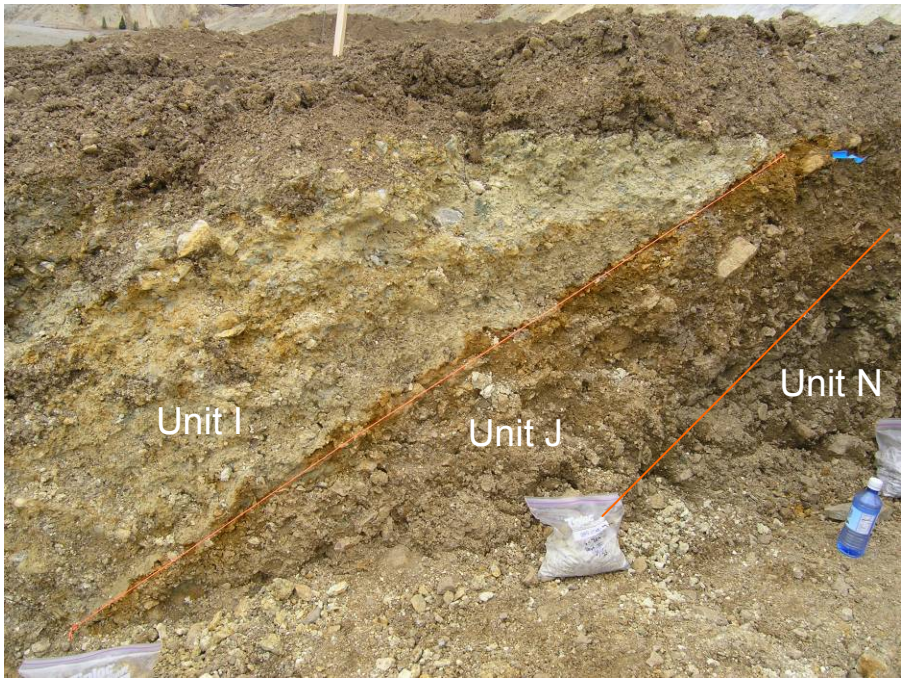

FIGURE 30. Contact between units I, J and N in trench LFG-006, GHN.

DESCRIPTION OF THE TOE OF THE GHN ROCK PILE

The toe of the rock pile was exposed in shallow test pits before reclamation of GHN and examined using cuttings from drill holes. The toe of the GHN rock pile consisted of cobble-supported gravel through boulder-sized material (Fig. 31, 32), similar to the basal rubble zone lying unconformably on top of a dark gray to brown clayey soil developed on weathered andesite. The toe of the rock pile contained mostly andesite and rhyolite (Amalia Tuff) cobbles, jarosite, and gypsum with poor sorting, and very little clay- to sand-size matrix.

FIGURE 31. Toe of GHN rock pile (2/10/03).

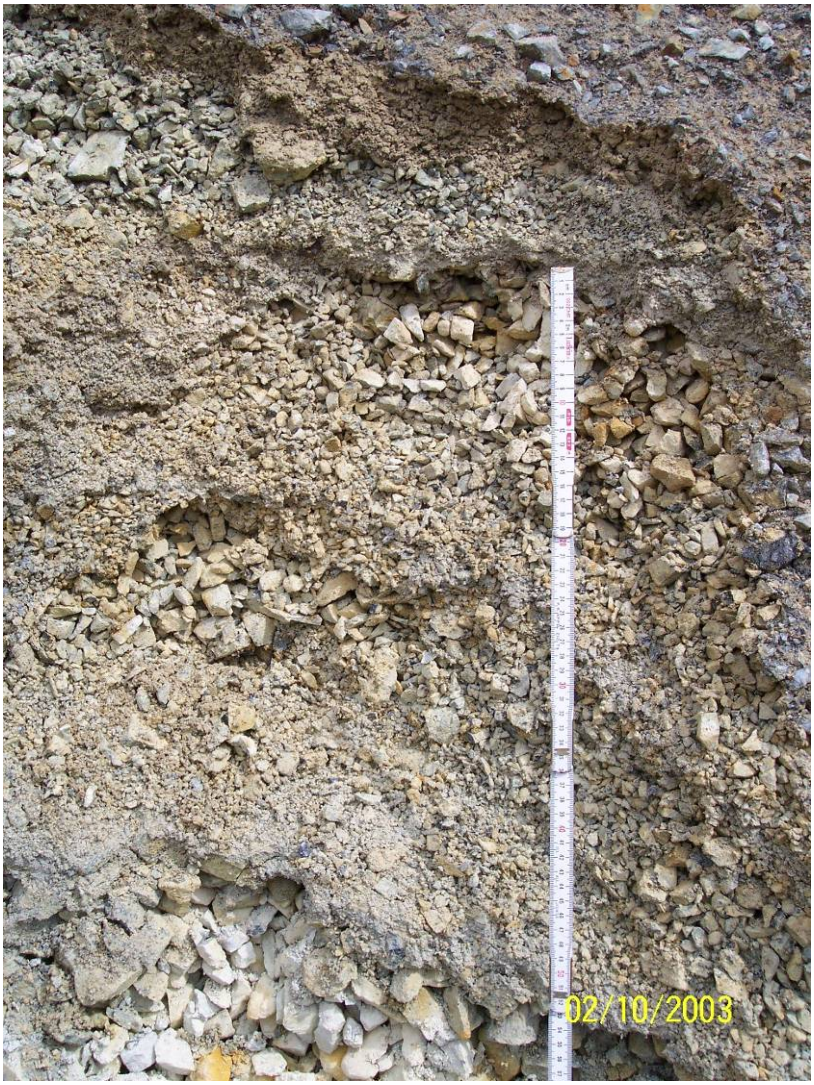

FIGURE 32. Toe of GHN rock pile (2/10/03).

DESCRIPTION OF CONTACT BETWEEN ROCK PILE AND COLLUVIUM/ WEATHERED BEDROCK (FOUNDATION)

The contact between the GHN rock pile and weathered bedrock/colluvium was exposed and examined in various trenches in several places:

- At the top of the stable portion of GHN
- In trenches throughout the unstable portion of GHN
- At the toe of GHN.

Drill holes also incepted the basal contact. Observations in the various trenches that cut into the base of the rock pile and the weathered bedrock indicated that the basal portion (Unit RUB) of the GHN rock pile consisted of a cobble-supported, coarse, rubble zone of gravel through boulder-sized material lying unconformably on top of either a dark gray to brown clayey residual soil developed on weathered andesite (Fig. 33; McLemore, 2009) or a yellow to orange-brown clay to sandy clay colluvium that is similar to the natural alteration scars found along the Red River valley (Fig. 34; Meyer and Leonardson, 1990; Graf, 2008). The rock-pile material

observed in trenches in the stable portion of GHN overlaid yellow to orange-brown acid-weathered or oxidized soil/weathered bedrock or colluvium. The coarse rubble zone near the base of the rock pile contained mostly andesite cobbles, jarosite, and gypsum with poor to moderate sorting, and minor clay- to pebble-size matrix that was developed on top of the weathered bedrock (Fig. 35). Figure 35 shows the profile exposed in the trench on the north wall of trench LFG-019 in the unstable portion of GHN described by McLemore (2008b). The saprolitic andesite is developed on top of fractured andesite bedrock.

FIGURE 33. Close-up of the rubble zone at the base of the GHN rock pile on top of the yellow colluvium. Boulders are up to 3 ft across. See Figure 34 (trench LFG-0003).

FIGURE 34. Coarse, rubble zone of the rock pile lying unconformably on top of yellow colluvium (trench LFG-0003).

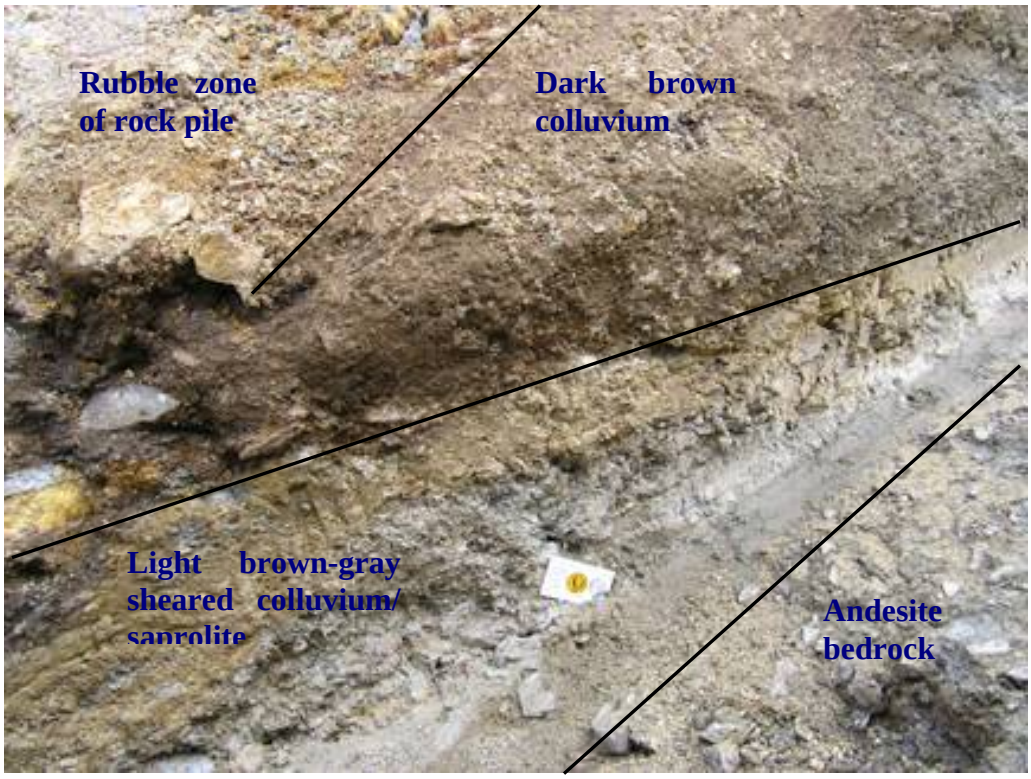

FIGURE 35. The profile on the north wall of trench LFG-019, described in more detail by McLemore (2008b). Entire profile is approximately 3-4 ft thick.

MIGRATION OF FINES WITHIN GHN

Local, discontinuous lenses of fine-grained material are found throughout the rock pile and the origin of these lenses is likely a result of several processes that occurred during and after rock-pile construction. The fine-grained material in these lenses consist of more than clay minerals, including small particles of rock fragments and various minerals found in the rock pile. Fine-grained material was likely deposited in local fine-grained lenses during runoff events during construction of the rock piles (Fig 36). During natural compaction of the GHN rock pile, clay minerals and other fine-size particles locally were squeezed in between the cobbles and boulders, forming lenses of finer-grained material. Water moving within local layers of the rock pile, also could have transported fine-grained material into lower portions of the lenses. Evidence of transport or squeezing of fine-grained material includes clay coatings around grains, clay drapes around mineral grains and rock fragments (Fig. 37), fine-grained material partially filling voids, and amorphous material settling out of suspension and forming distinct lenses.

FIGURE 36. Dark gray zone above Patrick's head consists of fine-grained material possibly deposited by water flowing off of the rock pile during construction.

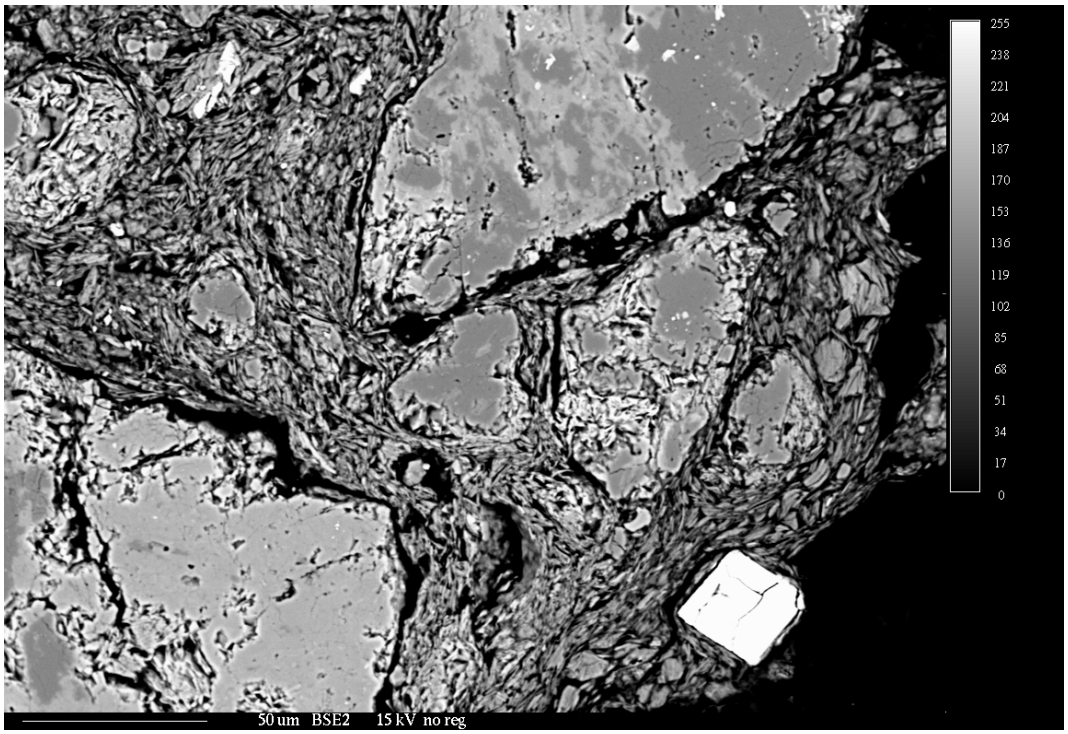

FIGURE 37. Back-scattered electron image of GHN-NWD-0019 showing chlorite and illite surrounding and draped around rock clasts and mineral grains. The clay minerals are the "felted" looking areas between the smoothly-polished rock and mineral clasts. The bright white cube is pyrite. The brightness scale is relative to the atomic number of the material with the brighter areas representing higher atomic number. Lower magnification image is in Figure 85.

ROCK PILE STRUCTURE OF THE UNSTABLE PORTION OF GHN

In the northern unstable portion of GHN, significant structural differences were observed and documented as a result of the slide compared to the stable portion of the rock pile (Fig. 38). Units in the stable portion were westward dipping and not apparently folded or faulted. Units in the unstable portion show apparent deformation by folding as well as both synthetic and antithetic faulting. Faults and folds had similar orientations with measured fault planes striking 355° and 21° and a fold axis orientation of 350°. Complex deformation, winter weather, and time constraints prevented complete mapping within the unstable part of GHN. Only a few tests on samples collected from the unstable portion of GHN have been performed (Tachie-Menson, 2006). This portion of GHN is not described in this report.

GRAIN SHAPE

Grain shape was assessed by petrographic methods and the electron microprobe, involving examination of the grain shape of the finer-grained soil component of the samples, as well as the rock fragments within the rock-pile material. A more detail analysis of shape was performed by Nunoo et al. (2009). The shape of particles has a significant effect on the shear strength and deformational characteristics of granular materials. For rock-pile samples, the classification of the shapes of clasts was based on the AGI comparison chart by Powers (1982) for estimating roundness and sphericity. Based on this classification, sphericity of rock-pile material is mostly subangular, subdiscoidal, and subprismoidal; roundness ranged from very angular to subrounded (Figs. 39-42). Backscattered electron images allow detailed examination of grain shape and texture at small scales. In general, these images revealed a predominance of angular to subangular clasts compared to rounded clasts. The sphericity and angularity of the rock fragments of the older analogs are similar to those of the younger rock piles (Nunoo et al., 2009). These results suggests that short-term weathering (<100 years) has not noticeably changed the particle shapes at the test locations.

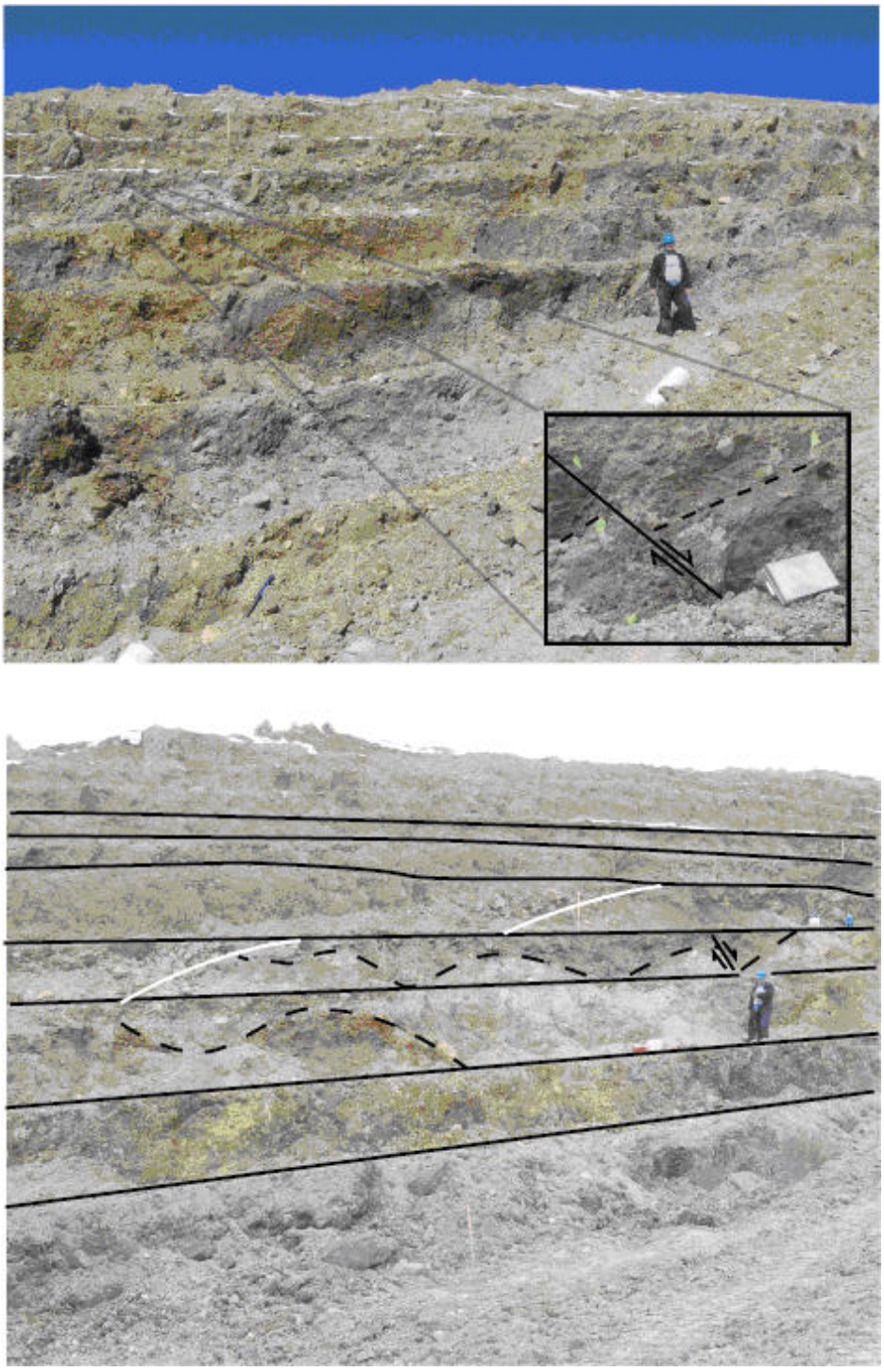

FIGURE 38. Northwest looking photographs showing apparent deformation in trenches cut in the unstable portion of the GHN rock pile. Solid black lines show trench wall tops, white and dashed black lines show unit contacts. a) Faults and b) folds had similar orientations with measured fault planes striking 355º and 21º and fold axis orientation of 350º.

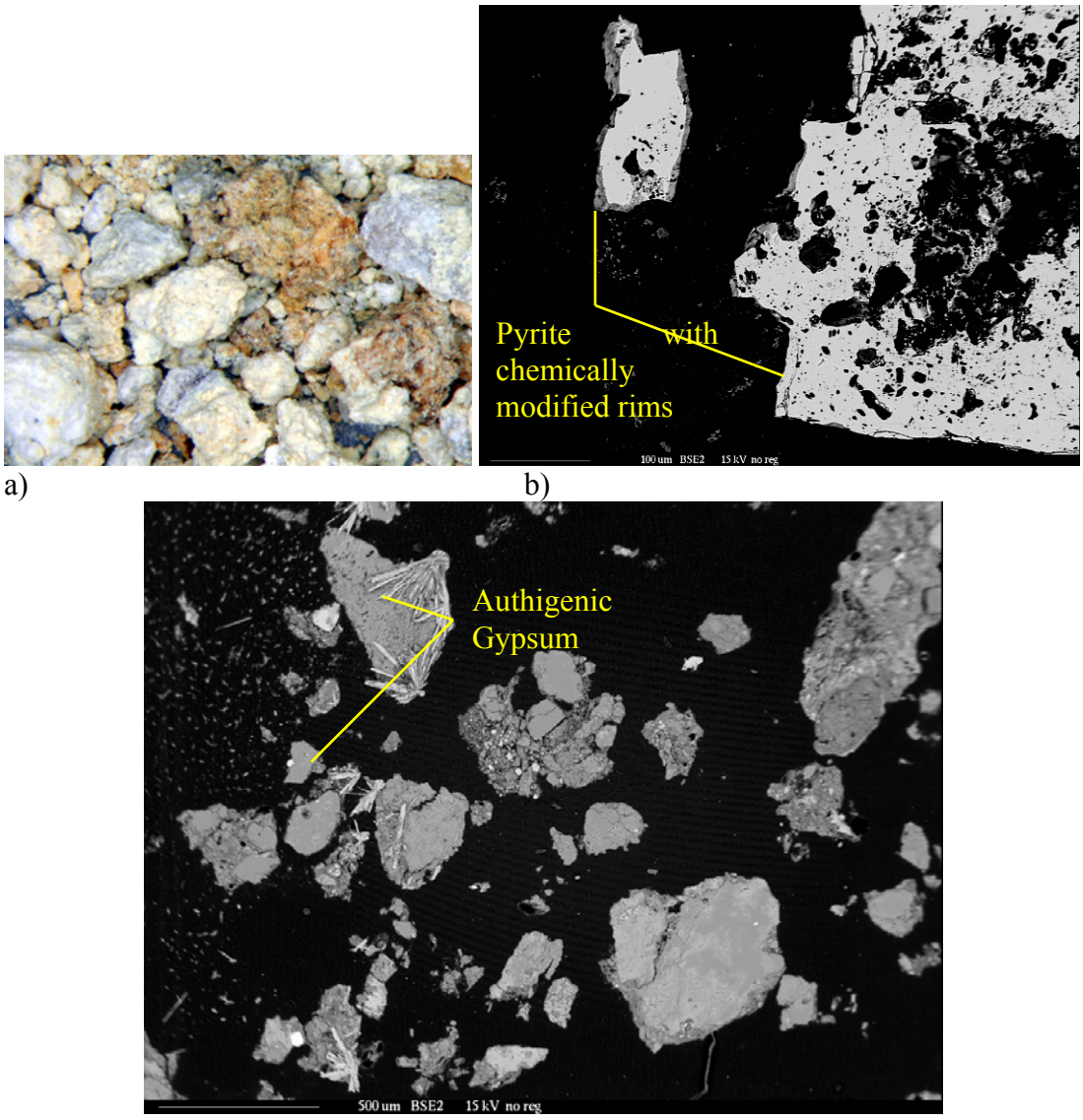

a) b)

c)

FIGURE 39. a) Sample GHN-VTM-194-T001 from unit I (outer GHN), showing predominant color of pale yellow, subprismoidal to subdiscoidal and angular to subrounded shape, bench 9. Field of view is 6 mm. b) Backscattered electron images of pyrite with rims from Unit I. c) Backscattered electron image of rock pile sample from unit I, GHN. Bladed, prismatic crystals are authigenic gypsum. It is unlikely that these delicate crystals would survive blasting, haulage, and dumping, therefore, these are weathered gypsums.

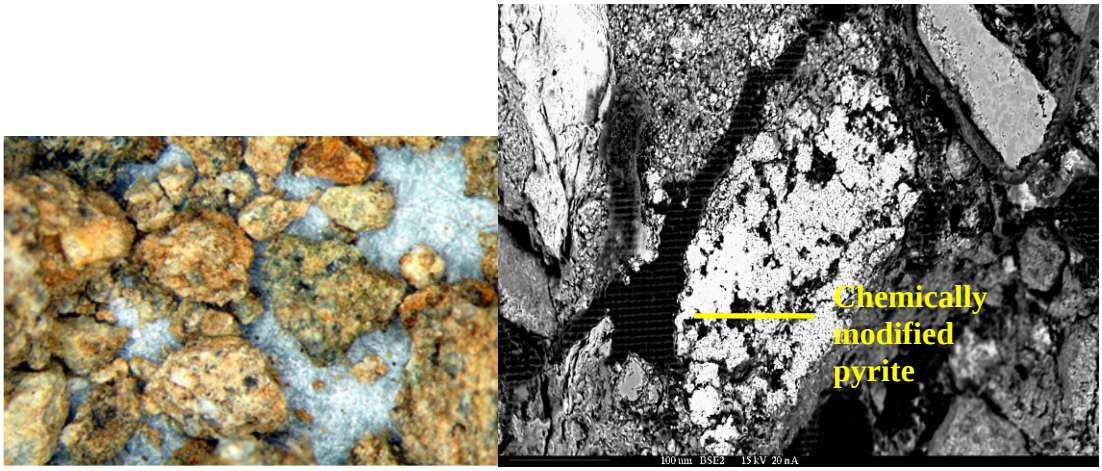

a) b)

FIGURE 40. Sample GHN-VTM-197-T001 from unit N with predominant color of light olive brown, subprismoidal to subdiscoidal and angular to subrounded shape, bench 9, GHN. Field of view is 6 mm. b) Backscattered electron images of highly modified pyrite grain from unit N.

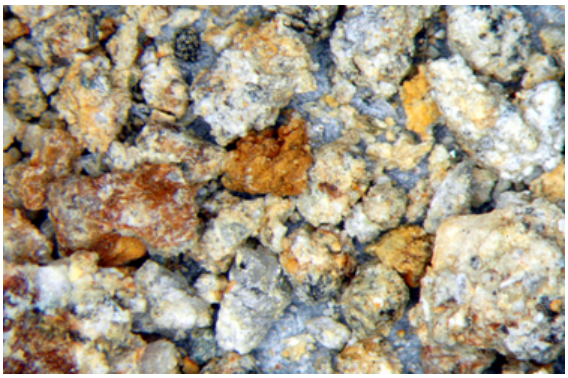

FIGURE 41. Photograph number GHN-VTM-200-T001 (unit N), sample with predominant color of light yellowish brown, subprismoidal to subdiscoidal and very angular to subrounded shape, bench 9, GHN. Field of view is 6 mm.

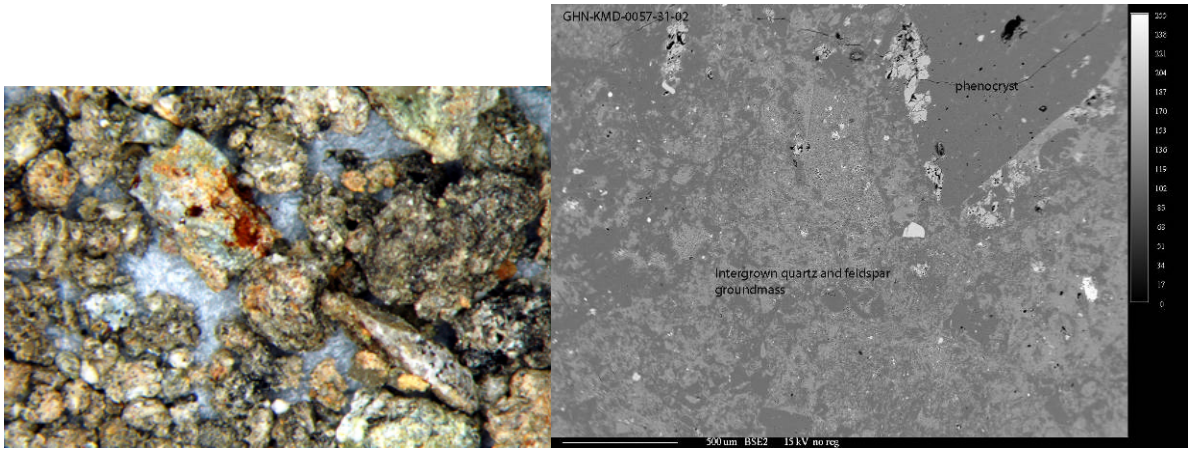

FIGURE 42. Sample GHN-VTM-212-T001 from interior unit O, with predominant color of dark grayish brown, subprismoidal to subdiscoidal and angular to subrounded shape, bench 9, GHN.

Field of view is 6 mm. b) Backscattered electron image of hydrothermally-altered, but unweathered andesite, sample GHN-KMD-0057 from unit O. Darkest areas represent quartz and albite, medium gray represents potassic feldspar and brightest areas are epidote and pyrite.

PETROGRAPHY AND MINERALOGY

Petrographic analyses of rock-pile material characterized rock-fragment and soil matrix lithology, texture, and mineralogy, especially those minerals that are pertinent to the study of weathering. Soil petrography (Delvigne, 1998), aided by electron microprobe, reflectance spectroscopy, XRD, and chemical analyses, provide both a better understanding of variations in the original rock pile and a means to identify the potential mineralogic and chemical effects of weathering. Three sources for mineral phases and chemical elements found in the Questa samples include:

- Primary minerals crystallized in the magma chamber and preserved in the rock (feldspar, quartz, pyroxene, amphibole, magnetite, apatite, etc.)
- Minerals produced before mining by hydrothermal alteration of volcanic rocks (feldspar, pyrite, clay minerals, quartz, epidote, apatite, rutile, Fe- and Mn- oxides, etc.)
  - addition of new elements by the hydrothermal fluids at different times
  - redistribution of elements dissolved from primary minerals
- Minerals that formed in the rock piles by weathering after mining (gypsum, Fe- and Mn-oxides, clay minerals, jarosite, etc.)
  - addition of new elements by meteoric fluids (weathering)
  - redistribution of elements dissolved from primary or hydrothermal phases.

Minerals found in the GHN rock-pile material are listed in Table 21 and grouped according to their relative stability in the hydrothermal and weathering environments. Table 22 contains representative chemical analyses of some of the more common minerals found in the rock piles.

A series of samples, considered representative of the rock pile, was examined from a traverse along a single bench (bench 9) within a rock-pile trench (LFG-006) on GHN (Fig. 43). The geologic map of trench LFG-006 is shown in Appendix 3. Eight mappable units were identified along this bench. Mineralogy, lithology, chemical and other analyses for samples from bench 9 are included in Appendix 7 and sample descriptions are in Appendix 9. This suite of samples is useful because it provides a profile from the outer margin of the rock pile inward, which allows the comparison of rock fragment lithology and mineral abundance across the rock pile.

TABLE 21. Relative stabilities, approximate concentrations, and compositions of minerals found in Questa rock pile deposits (NMBGMR electron microprobe results in bold, other elements by Molling, 1989; Shum, 1999; Piché and Jébrak, 2004; Plumlee et al., 2006). Tr=trace, Approx=approximate concentration in the Questa rock-pile materials.

Relative stability	Mineral	Approx %	Primary elements	Trace elements	Formula
Easily weathered	pyrite	0-8	**Fe, S**	**Cu,** Te, Co, Pb	FeS_2
	calcite	0-5	**Ca, CO**	**Sr, Al, Mg, Mn, Fe, Si, Ba,** P	$CaCO_3$
	anhydrite	tr	Ca, S		$CaSO_4$
	hornblende	0-tr	Mg, Fe, Ca, Al, Si	Ni, Co, Mn, Sc, Si, V, Zn, Cu, Ga	
	Biotite/ phlogopite	0-13	K, Mg, Fe, Al, Si	F, Rb, Ba, Ni, Co, Li, Mn, V, Zn, Cu, Ga	$KFe_3AlSi_3O_{10}(OH)_2$
	apatite	0-1	**Ca, P, F**	**Si, S, Mn, Fe, Sr, Cl,** REE, Pb, Y	$Ca_5P_3O_{12}\cdot OH$
	jarosite	0-0.5	**Fe, S, H, K**		$KFe_3(SO_4)_2(OH)_6$
	alunite	0-0.5	S, K		
	copiapite	0-0.5	Fe, S		$Fe^{+2}(Fe^{+3})_4(SO_4)_6(OH)_2\cdot 20H_2O$
	sphalerite	0-0.1	**Zn, S**	Cd	ZnS
	chalcopyrite	0-0.1	**Cu, Fe, S**		CuFeS
	melanterite	0-0.1	Fe, S		$Fe(SO_4)\cdot 7H_2O$
	schwermannite	0-0.1	Fe, S		$Fe_8O_8(OH)_6SO_4\cdot nH_2O$
	galena	0-0.1	Pb, S	Ag	PbS
Moderately weathered	fluorite	0-0.1	Ca, F	Y	CaF_2
	dolomite	0-0.1	**Mg, Ca, CO**	**Sr, Al, Mg, Mn, Fe, Si, Ba**	$MgCa(CO_3)_2$
	rhodochrosite	0-0.1	**Mn, Ca, CO**		$MnCO_3$
	albite		**N, Al, Si**	Cu, Ga, **Ba, Sr,**	$NaAlSi_3O_8$
	orthoclase	0-24	**K, Al, Si**	Rb, **Ba, Sr,** Cu, Ga	$KAlSi_3O_8$
	anorthite	0-20	**Ca, Al, Si**	**Ba, Sr,**	$CaAl_2Si_2O_8$
	Muscovite (sericite, illite)	0-30	**K, Al, Si**	**F, Cl, Ti, Cr, Mg, Na, Ca, Mn, Fe**, Rb, Ba, Sr, Ga, V, Be?, Li?	$KAl_2(Si_3Al)O10(OH)_2$
	magnetite	0-1	**Fe, Ti**	**Al, Mg, Ca, Mn,** Zn, Co, Ni, **Cr**, V	Fe_3O_4
	Epidote	0-16	**Ca, Al, Si**	**Cr, Mg, Mn, Fe, Na, Ti**	$CaFeAl_3(SiO_4)_3(OH)$
	chlorite	0-12	Fe, Al, Mg, Si, Be?	F, Be?, Li?, various	$Mg_3Fe_2Al_2Si_3O_{10}(OH)_8$
	smectite	0-24	**Si, Al, Mg, Ca, Na, K,** Be?	**P, S, Ti, Mn, Fe, F, Cl,** Be?, Li?	$Ca0_{.33}(Mg0_{.66}Al_{3.34})(Si_8)(OH)_4$
	chromite	0-0.1	Fe, Cr		$FeCrO_4$
	titanite	0-0.1	Ca, Ti, Si		$CaTiSiO_4\cdot OH$
	rutile	0-0.1	Ti		TiO_2
	beryl	0-0.01	Be		BeO
	barite	0-0.01	Ba, S	Sr	$BaSO_4$
	actinolite	0-1	Ca, Mg, Si, OH		$Ca_2Mg_5Si8O_{22}(OH)_2$
Very stable	quartz	0-66	Si		SiO_2
	kaolinite	0-7	**Al, H, Si**	F, Cl	$Al_2Si_2O5(OH)_4$
	gypsum	0-20	**Ca, S**	**Sr, Ba**	$CaSO_3\cdot H_2O$

Relative stability	Mineral	Approx %	Primary elements	Trace elements	Formula
	ferrihydrite	0-0.01	**Fe**		$Fe(OH)_3$
	hematite	0-10	**Fe**	Various	
	goethite	0-1	Fe	Various	FeOOH
	FeMnTi oxides	0-10	Fe, Mn, Ti	various	
	molybdenite	0-0.1	Mo, S		MoS
	Amorphous Si, Fe, Mn, Al	?	Si, Fe, Mn, Al	various	various

TABLE 22. Representative mineral compositions as analyzed by electron microprobe.

FELDSPAR	SiO2	Al2O3	CaO	FeO	SrO	BaO	Na2O	K2O	Total					
Potassic														
Andesite ghn-nwd-0002-14	64.26	19.49	0.06	0.13	0.07	0.52	2.89	12.27	99.69					
Andesite ghn-nwd-0021-20	64.12	19.18	0.00	0.00	0.00	0.04	0.47	16.77	100.57					
Rhyolite ghn-kmd-0051-31-01	64.61	18.78	0.03	0.05	0.07	0.09	0.26	16.38	100.27					
Rhyolite ghn-nwd-0023-03	63.37	18.76	0.02	0.00	0.00	0.13	0.42	16.63	99.33					
Sodic														
bcs-vwl-0002-03	63.15	23.28	3.73	0.05	0.17	0.04	9.08	0.54	100.03					
ghn-nwd-0021-21	67.62	20.23	0.19	0.03	0.04	0.01	11.51	0.22	99.85					
CLAY	**P2O5**	**SiO2**	**SO2**	**TiO2**	**Al2O3**	**MgO**	**CaO**	**MnO**	**FeO**	**Na2O**	**K2O**	**F**	**Cl**	**Total**
Chloritic														
ghn-nwd-0008-20	0.00	30.90	0.00	0.01	16.42	15.96	0.15	1.16	16.87	0.99	0.29	0.60	0.02	83.36
ghn-nwd-0017-13	0.02	27.76	0.06	0.00	16.26	18.21	0.11	0.64	19.08	0.00	0.00	0.35	0.01	82.50
Illitic														
ghn-nwd-0021-14	0.00	46.65	0.01	0.08	26.44	1.42	0.25	0.09	2.00	0.33	8.93	0.10	0.03	86.34
ghn-nwd-0021-15	0.04	47.95	0.00	0.07	25.53	1.57	0.15	0.05	2.22	0.51	9.34	0.43	0.03	87.89
Kaolinitic														
ghn-nwd-0018-30-39	0.00	43.10	0.24	0.00	31.23	1.04	0.61	0.00	1.49	0.05	0.11	0.23	0.22	78.33
ghn-nwd-0024-30-14*	0.47	45.46	0.37	0.00	33.24	1.95	1.03	0.04	4.76	0.02	0.63	0.00	0.01	88.00
Smectitic														
ghn-nwd-0020-30-13	0.00	50.48	0.07	0.01	22.17	2.10	1.27	0.02	2.58	0.07	0.34	0.25	0.15	79.50
ghn-nwd-0020-30-14	0.00	54.10	0.06	0.05	23.79	2.09	1.42	0.08	4.09	0.87	0.18	0.42	0.16	87.31

Pyrite	S	Fe	Cu	Total
ghn-vwl-0003-20	53.30	46.35	0.02	99.67
ghn-vwl-0003-21	53.24	46.28	0.00	99.52

Calcite	Si(CO3)2	Al2(CO3)3	Mg(CO3)	Ca(CO3)	Mn(CO3)	Fe(CO3)	Sr(CO3)	Ba(CO3)	Total
ghn-nwd-0006-10	0.52	0.03	0.13	99.52	0.10	0.34	0.14	0.04	100.82
ghn-nwd-0002-11	0.16	0.00	0.00	97.74	1.77	0.38	0.00	0.04	100.10
ghn-vwl-0003-18	0.00	0.01	0.03	85.11	12.14	0.53	0.70	0.00	98.52

Epidote	SiO2	TiO2	Al2O3	Cr2O3	MgO	CaO	MnO	FeO	Na2O	Total
ghn-nwd-0006-08	37.01	0.00	20.92	0.00	0.05	22.95	0.11	15.83	0.01	96.88
ghn-nwd-0017-25	37.60	0.00	23.99	0.02	0.09	23.05	0.23	12.50	0.00	97.49

Fe-oxide	P2O5	SiO2	TiO2	Al2O3	Cr2O3	Fe2O3	MgO	CaO	MnO	NiO	SO2	Total
ghn-kmd-0048-31-34		0.06	5.39	0.45	0.15	90.11	1.99	0.05	0.23	0.03		98.46
ghn-kmd-0051-31-36		0.14	2.35	0.13	0.00	96.63	0.05	0.01	0.00	0.00		99.31
ghn-kmd-0056-32-17		2.56	0.00	0.06	0.03	90.49	0.02	0.03	0.00	0.03		93.21
SSW-AAF-0001-30-13	7.71	4.68	0.36	5.75		68.62	0.02	0.17	0.00		4.89	92.20
SSW-AAF-0001-30-22	5.65	5.88	0.98	7.65		64.35	0.06	0.05	0.72		2.60	87.94
SSW-AAF-0001-30-23	6.09	2.66	0.34	10.80		70.36	0.08	0.08	0.15		1.91	92.47
SSW-AAF-0001-30-50	2.92	7.33	0.02	3.42		73.98	0.13	0.08	0.02		1.00	88.90
GHN-JRM-0001-30	0.00	1.92	1.37	0.71		88.17	0.09	0.02	0.04			92.32
SSS-VTM-0600-30a	0.21	3.92	0.03	1.57		78.19	0.00	0.03	0.05			83.98
SSS-VTM-0600-30b	4.38	6.07	0.02	3.04		79.94	0.05	0.21	0.03			93.73
SSS-VTM-0601-30b	0.21	3.76	0.00	0.25		85.10	0.11	0.09	0.02			89.53
SSW-AAF-0001-30a	2.79	2.83	0.04	1.25		80.16	0.04	0.05	0.04			87.20

Gypsum	SO2	CaO	SrO	BaO	H2O	Total
ghn-kmd-0071-30-12	42.70	39.53	0.04	0.05	18.37	100.69
ghn-kmd-0056-30-04	44.43	38.71	0.00	0.03	18.71	101.88

Jarosite	P2O5	SiO2	Al2O3	TiO2	Fe2O3	CaO	MgO	MnO	Na2O	K2O	SO3	Total
GHN-JRM-0001-30	0.46	1.19	0.79	0	44.47	0.01	0.03	0.05	0.3	5.12	25.63	78.04
PIT-VWL-0001-31	0.45	0.19	0.15	0.01	46.89	0	-0.02	0	0.2	4.36	27.80	80.03
MID-AAF-0003-30	0.44	2.88	1.49	0.05	37.48	0.04	0.06	0.01	0.58	4.55	20.51	68.10
SSW-AAF-0001-30	2.2	0.01	0.45	0.01	49.87	0.17	0	0.01	2.3	2.72	24.95	82.69

Analytical totals of less than 100% for a group of minerals indicate the presence of an unanalysed component, usually H2O, in the mineral phase. Porosity in mineral phases will also reduce analytical totals

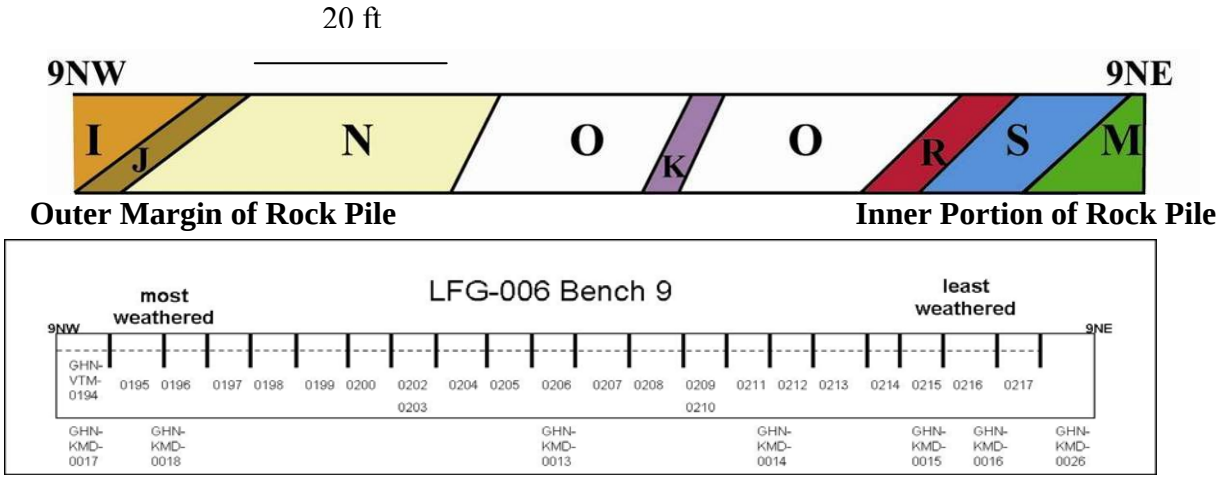

FIGURE 43. Geologic cross section of bench 9, trench LFG-006. Samples used for petrographic and chemical analysis were obtained at approximately 5 ft intervals. Refer to this figure for subsequent plots. Description of geologic units is in Table 20. Photo of bench 9 is in Figure 29.

LITHOLOGY AND HYDROTHERMAL ALTERATION

There is conspicuous variability in the color of the different rock-pile material within GHN, which is illustrated in bench 9 (Figs. 28-30, 39-42). Color is one of the easiest and most obvious characteristics of different intensities of weathering because it reflects differences in mineralogy and texture (Fontes and Carvalho, 2005). The original color of the igneous rocks reflects the original mineralogy, which is typically related to the presence or absence of mafic and feldspathic minerals. The color of soils weathered from igneous rocks is somewhat dependent upon oxidation of these mafic and feldspathic minerals, especially Fe and Mn oxides. Reds, browns and yellows typically reflect the different oxidation states and abundances of Fe- and Mn- oxides.

Numerous studies in the literature have used color as an indication of the intensity of weathering. Shum and Lavkulich (1999) used red color to estimate iron content and as a weathering indicator. Yokota and Iwamatsu (1999) showed that red colors increased with weathering. Yokoyama and Nakashima (2005) showed that color of weathered materials increased towards yellowish-brown with increased weathering as ferrihydrite weathers to goethite. Fontes and Carvalho (2005) describes various color indices and the relationship to weathering. Martín-Garcia et al. (1999) used a visual degree of weathering (DW, 0-3) based upon reddening, cracks, mineral alterations, compactness and roundness of the clasts. There was a lightening of color, red pigmentation, increase in cracks, decreased compactness and increased roundness with increase in weathering. Martín-Garcia et al. (1999) further showed that weathering profiles in pyrite-bearing rock consist of a less weathered reduced zone, dissolved zone, and more weathered oxidized zone in areas where the H_2O and O_2 fluxes are in the same direction. If the H_2O and O_2 fluxes are in opposite direction then the oxidized and dissolved zones overlap. Tonui et al. (2002) used color to differentiate between three different types of weathering of saprolite in regolith at the Northparkes deposit in New South Wales, Australia. Scheinost and Schwertmann (1999) used a colorimeter to determine that color is useful in identifying goethite, hematite, lepidocrocite, jarosite, maghemite, and feroxyhite but not as useful in identifying ferrihydrite, akaganeite, and schwertmnnite.

Thus, the color variations are probably the result of a combination of heterogeneous starting material and alteration processes, including weathering that occurred after the material is

emplaced in rock piles, and is primarily attributed to the formation of secondary Fe-oxides, jarosite, and copiapite. Hydrothermal alteration intensity and rank (i.e. mineral assemblage) also have an effect on color in the Questa samples. The two main hydrothermal alteration types in GHN are prophylitic and QSP. The color of secondary Fe-oxide minerals varies among the GHN samples and includes black, orange, red, yellow, and brown material. The abundance of Fe-oxides does not appear to vary in a systematic fashion across bench 9 (Fig. 44), although jarosite and copiapite are more abundant in units I and J then in the interior units (Fig. 44). These color differences are an important initial observation that can contribute to our understanding of mineralogic variation in the rock pile (Shum and Lavkulich, 1999; Scheinost and Schwertmann, 1999). However, the mineralogical effect of the fast-reacting (less than 40 yrs) weathering pyrite system is to produce precipitates of secondary reaction minerals on the surface of existing rock fragments and within the soil matrix, which result in the yellow to orange color, reflecting the role of ferric iron in the mineral structures. The secondary precipitates form coatings on exterior surfaces, rims, and fill macro- and micro-fractures. Thus, the macro-scale impression of weathering, caused by the discoloration from the observed secondary precipitates is exaggerated.

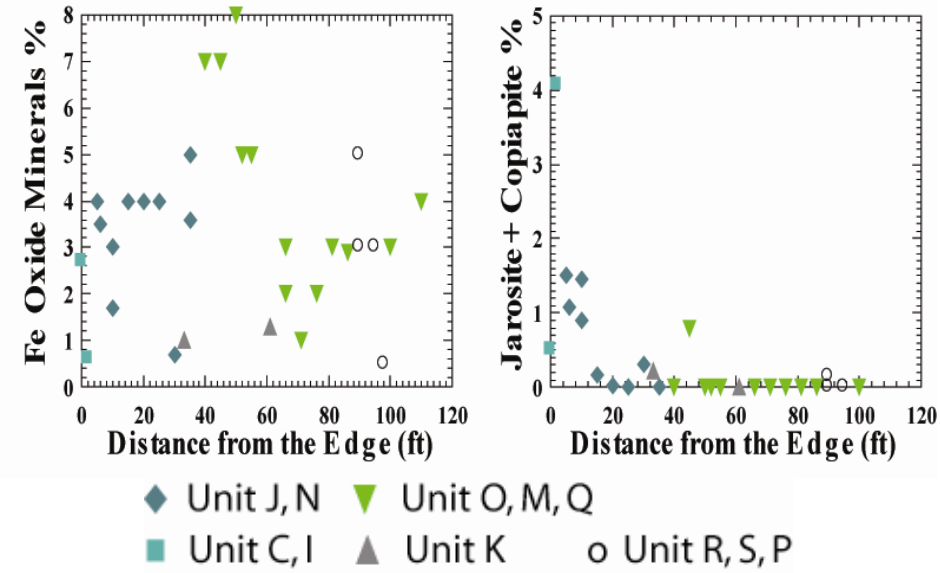

FIGURE 44. Variations of Fe oxide minerals and jarosite+copiapite across bench 9, GHN. Mineralogy is determined from the modified ModAn method of samples that included both rock fragments and soil matrix (McLemore et al., 2009b). See Figure 43 for geologic cross section and Table 20 for description of geologic units.

The composition of rock fragments and the intensity of hydrothermal alteration are characteristics inherent to rock-pile material and were present in the rocks before they were emplaced in the rock pile. Understanding these characteristics is important in order to obtain baseline conditions from which weathering can be assessed. Rock fragments in the GHN samples are comprised of two main lithologies, which are andesite and rhyolite (Amalia Tuff). Intrusive rocks, although present within colluvium/weathered bedrock, alteration scar, debris flows and other rock piles, are minor to absent within the GHN rock pile. The rock types exhibit original igneous textures, although the andesite fragments have typically undergone significant hydrothermal alteration, whereas the rhyolite (Amalia Tuff) fragments are relatively pristine or consisted of QSP alteration. The rhyolite (Amalia Tuff) fragments consisted of large (~mm size)

quartz and feldspar phenocrysts, surrounded by a devitrified glass matrix. Figure 45a shows the variation in lithology with respect to geological units identified within the rock pile. The units are shown in progression from the outermost units of the rock pile (Unit I) towards the inner most units (Unit M). Andesite is the predominant lithology overall. Noted exceptions are Units J and M, in which Amalia Tuff dominates. More details with histograms are in Appendix 11.

Three types of alteration have been described, including prophylitic, quartz-sericite-pyrite (QSP), and argillic, although relict igneous textures are typically preserved (McLemore et al., 2009a). Rough estimates of the intensity of these three alteration styles in the GHN rock pile were made petrographically (Fig. 45b). Although the ranges of intensity of alterations styles within a single rock-pile unit are large, QSP alteration is the most prevalent style, and argillic is relatively minor (Appendix 11). Prophylitic alteration is present throughout the pile, although, on average, at a lower intensity than QSP and argillic alteration. There appears to be slightly more prophylitic alteration in the interior rock pile units.

The rock fragments exhibited hydrothermal alteration textures, consisting of fine-grained intergrowth of quartz and K-feldspar. Feldspar compositions are generally alkaline, and show evidence of alteration from original igneous compositions (Table 23). This alteration is thought to be a result of hydrothermal alteration of the original igneous feldspar composition. Feldspars contain abundant clay-rich pockets, and the clay compositions are consistent with formation by hydrothermal processes.

Chlorite and illite occur in many of the samples, in some cases intergrown and in others as distinct crystals. Chlorite shows no systematic variation across bench 9, whereas illite is more abundant in the outer units of bench 9 (Fig. 46). These two clay minerals are typically associated with hydrothermal alteration. Many of the andesitic-rock fragments contained considerable concentrations of clay minerals replacing original igneous phenocrysts, but also as small pockets within the matrix of the samples. These rocks also contained dispersed blocky epidote and pyrite crystals. Large areas of well-crystallized epidote are present in many of the andesite samples, usually as clusters of crystals, locally associated with clay minerals. Epidote is a hydrothermal mineral that typically indicates temperatures of formation >200°C (Reyes, 1990; Simmons et al., 1992; Reed, 1994). Epidote is more abundant in the interior units of the GHN rock pile than the outer units (Fig. 46). Calcium carbonate, typically Mn-bearing, is associated with epidote or occurs as discrete, well-crystallized grains and is more abundant in the interior units of bench 9 (Fig. 46). Although many of the rock fragments are fractured, many fractures are empty.

In addition to rock fragments, the matrix or soil component of a number of samples also was investigated by electron microprobe analysis. The soil samples are composed of small mineral or rock fragments in a clay-rich matrix. Typically, the mineralogy of the small mineral and rock fragments in the soil is similar to the larger rock fragments from the same sample. However, the soil component tends to be more clay-rich. The clay compositions are similar to those observed in the rock fragments and drill core of the deposit before mining (see below). This clay can be a result of breaking of rock fragments and resultant removal of clay from within the rock during blasting and dumping of the mined material.

It is possible to recognize some mapped units based on their relative proportions of the two lithologies and alteration assemblages found within GHN (Fig. 43, Table 20). For example, all samples from unit O contained ≥70% andesite rock fragments. Prophylitic (chlorite + epidote ± calcite) and QSP are the most common types of hydrothermal alteration found in these samples. The intensities of both types of hydrothermal alteration vary considerably across bench 9 (Figs. 45b, 47). QSP hydrothermal alteration intensity appears to be relatively consistent within

mapped units (Fig. 47). QSP alteration is related to the amount of illite (sericite) and quartz found in the samples (Fig. 48). In addition, QSP and prophylitic hydrothermal alteration intensities are inversely related and samples with the most QSP hydrothermal alteration usually contain a greater proportion of rhyolite (Amalia Tuff) (Fig. 49).

a)

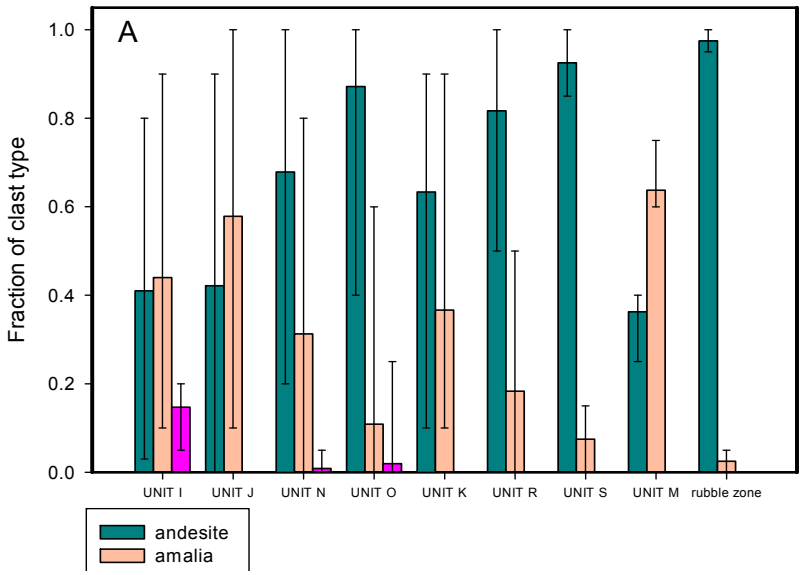

b)

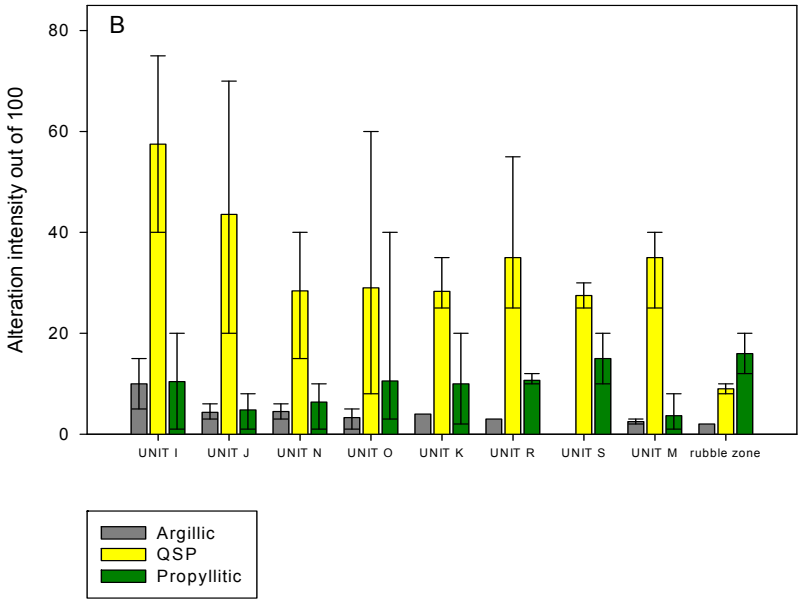

FIGURE 45. Variations of a) lithology and b) alteration intensity by type for geologic units in the GHN rock pile (samples from the stable portion). Averages (colored bars) and range (line) shown. See Figure 43 for geologic cross section and Table 20 for description of geologic units. Histograms are in Appendix 11.

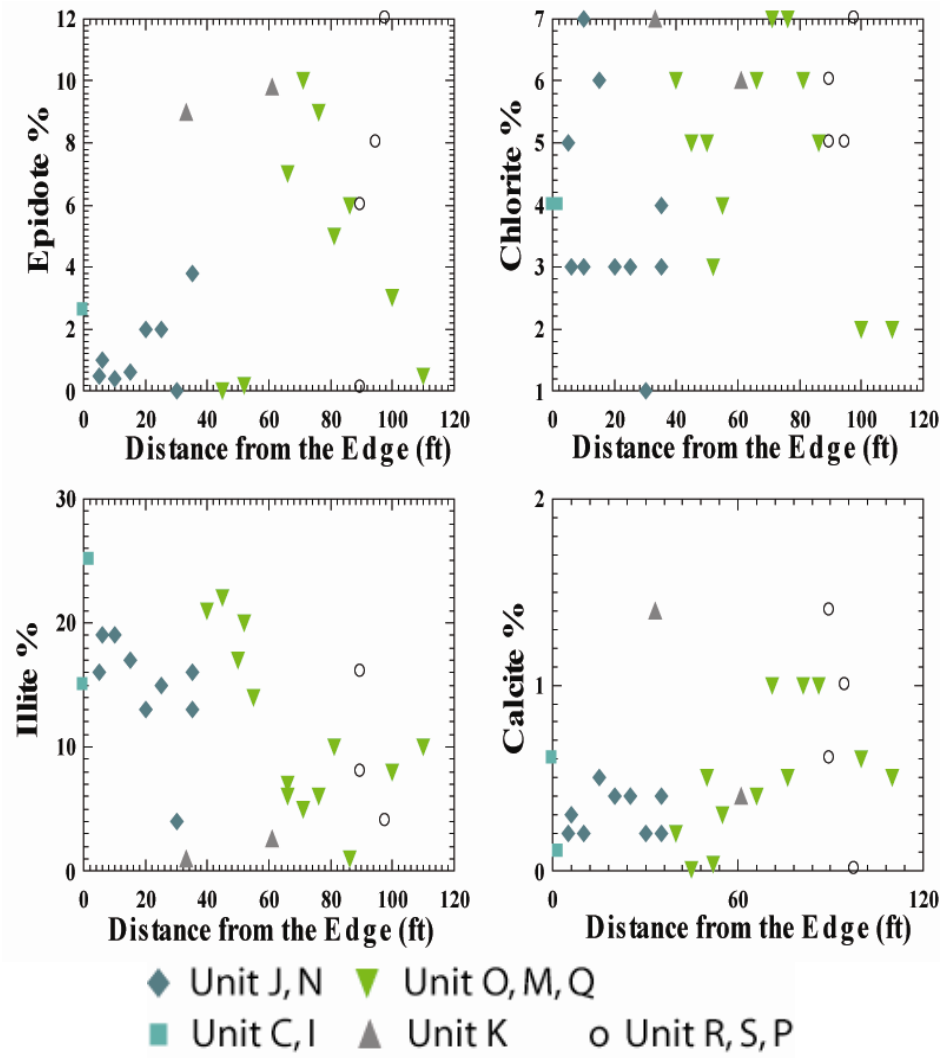

FIGURE 46. Variations of epidote, chlorite, illite, and calcite across bench 9, GHN. Mineralogy is determined from the modified ModAn method of samples that included both rock fragments and soil matrix (McLemore et al., 2009b). See Figure 43 for geologic cross section and Table 20 for description of geologic units.

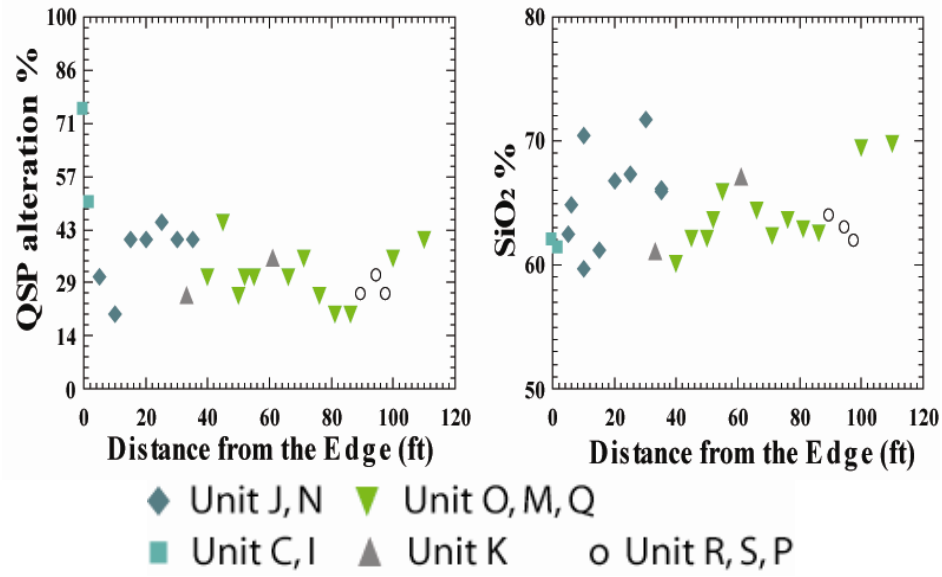

FIGURE 47. Variation of QSP (quartz-sericite-pyrite) hydrothermal alteration intensity (defined by petrographic analysis as the percentage of hydrothermal alteration minerals that have replaced primary minerals in the rock fragments and soil matrix) and SiO_2 across bench 9, GHN. QSP and SiO_2 have similar trends because QSP hydrothermal mineral assemblage contains predominantly quartz. Mineralogy is determined from the modified ModAn method of samples that included both rock fragments and soil matrix (McLemore et al., 2009b). See Figure 43 for geologic cross section and Table 20 for description of geologic units.

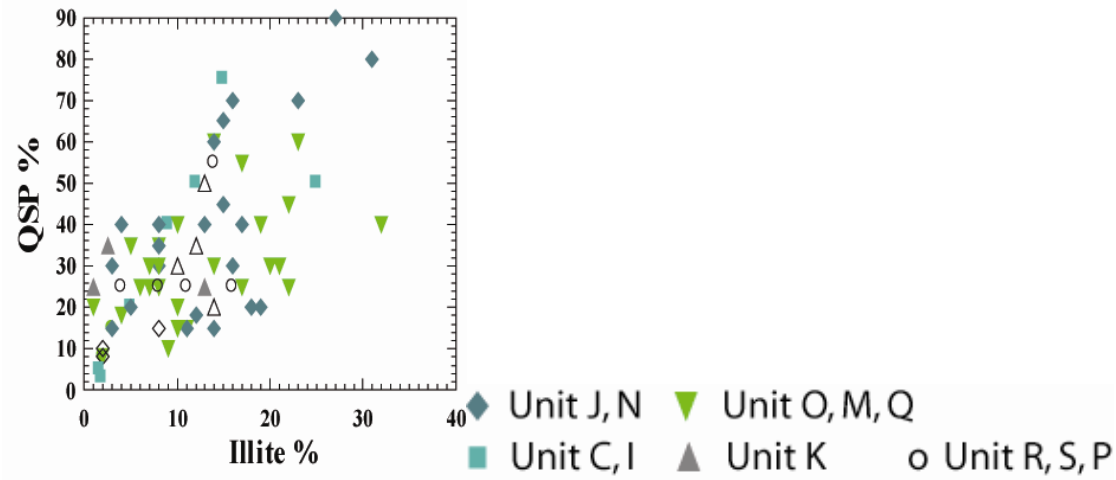

FIGURE 48. Scatter plot of QSP hydrothermal alteration and illite (illite is a form of sericite) in the rock fragments and soil matrix in all of GHN samples. See Table 20 for description of geologic units.

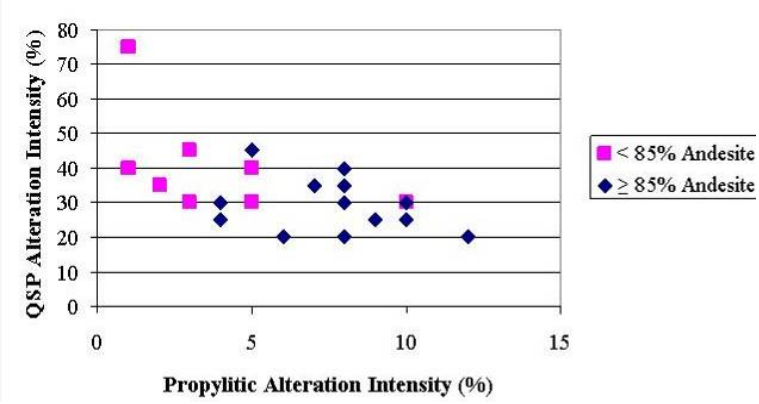

FIGURE 49. Intensity of prophylitic hydrothermal alteration versus intensity of QSP hydrothermal alteration for rock pile samples from bench 9, GHN. QSP alteration is more predominant in the rhyolite, whereas prophylitic alteration is more predominant in the andesite.

PYRITE AND OTHER HEAVY MINERALS

Pyrite concentrations within GHN rock pile typically are less than 3%, with a mean value of 0.8% and no systematic variation within GHN rock pile (Figs. 50, 51, 52, Table 23; Appendix 7, 11). The pyrite distribution differs from rock pile to rock pile (Appendix 11). The pyrite distributions vary with depth within drill holes in the rock piles, but an increase in pyrite is found in the hot zone of SI-50 (Appendix 11). Pyrite is not abundant in rock pile samples from bench 9, comprises up to 2% of unit I (the outer unit), and otherwise occurs only in minor amounts (Fig. 51). Appendices 5 and 6 contain logs of the individual trenches and drill holes with their distribution of pyrite.

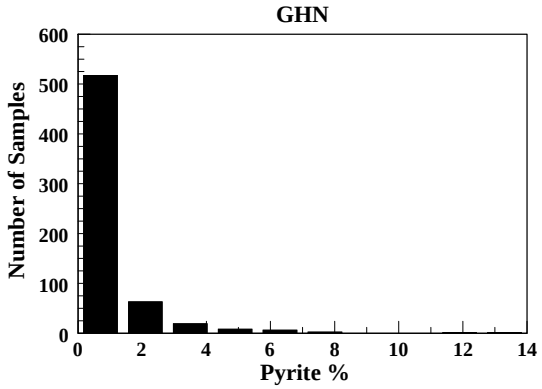

FIGURE 50. Pyrite abundance of whole rock samples from GHN, determined by Rietveld XRD (Oerter et al., 2007) and modified ModAn method of samples that included both rock fragments and soil matrix (McLemore et al., 2009b). Additional histograms for each unit are in Appendix 11.

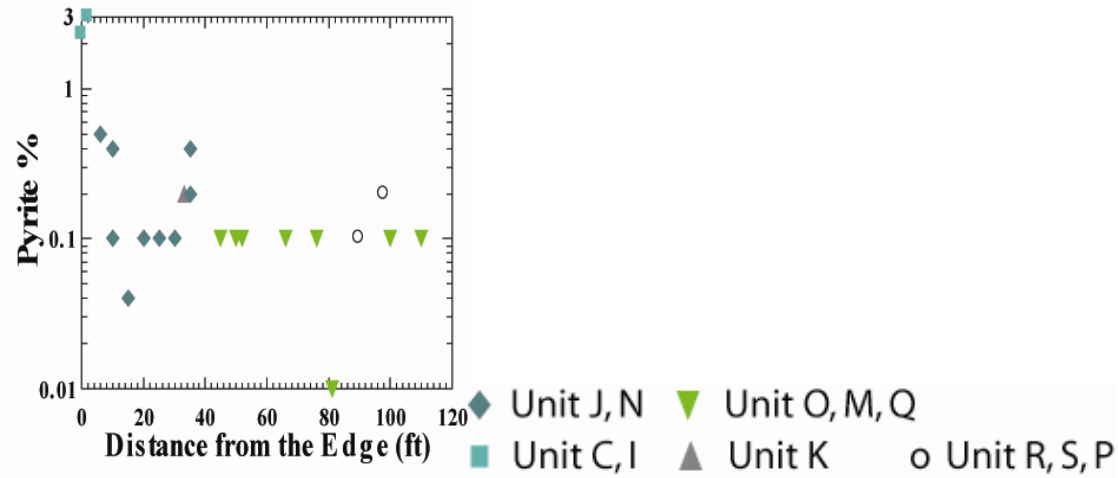

FIGURE 51. Variations of pyrite across bench 9, GHN. Mineralogy is determined from petrographic analysis, Rietveld XRD (Oerter et al., 2007) and modified ModAn method of samples that included both rock fragments and soil matrix (McLemore et al., 2009b). See Figure 43 for geologic cross section and Table 20 for description of geologic units.

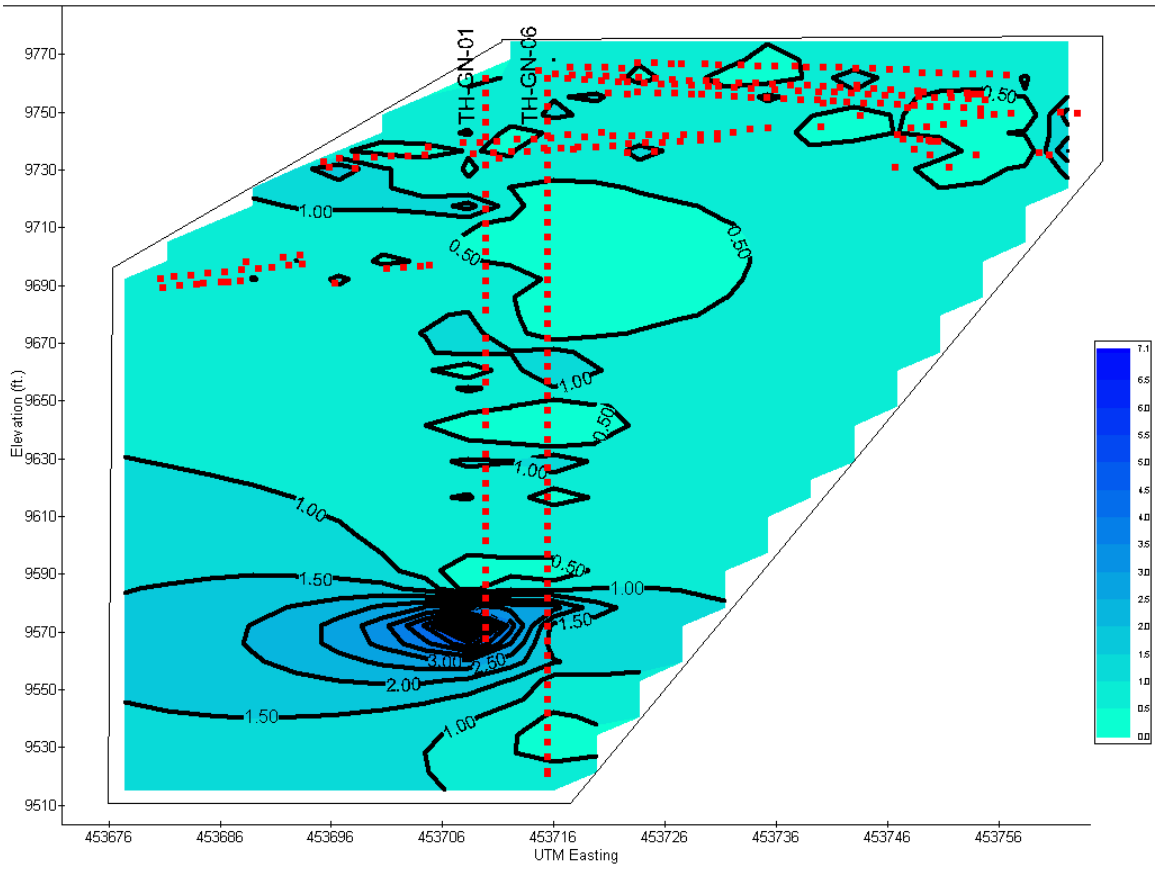

FIGURE 52. A contour diagram of a cross section of the top of the stable portion GHN showing the variation of pyrite (%) in the area of trenches LFG-0003 through LFG-006 and drill holes TH-GN-01 and TH-GN-06. The red points identify sample locations.

TABLE 23. Descriptive statistics of % pyrite by geologic unit (Appendix 11).

Unit	Mean	Median	Standard Deviation	Standard Error	Minimum	Maximum	Number of Cases
traffic	0.6	0.6	0.16	0.04	0.13	0.78	20
Unit C	0.6	0.6	0.24	0.07	0.22	0.55	11
Unit I	1.6	0.9	1.72	0.31	0.22	7.50	30
Unit J	0.8	0.6	0.84	0.17	0.09	3.80	25
Unit N	0.6	0.4	0.62	0.10	0.00	3.00	36
Unit O	0.6	0.5	0.53	0.06	0.00	2.89	75
Unit M	0.5	0.4	0.42	0.06	0.00	1.47	50
Unit Q	0.7				0.69	0.77	2
Unit K	0.7	0.5	0.68	0.15	0.00	2.44	22
Unit L	0.9	0.9	0.21	0.06	0.63	1.4	13
Unit P	0.8						1
Unit R	0.7	0.7	0.31	0.12	0.05	1.03	7
Unit S	0.7	0.8	0.27	0.09	0.05	0.96	9
Unit T	0.5	0.6	0.25	0.11	0.20	0.84	5
Unit U	0.4	0.3	0.33	0.15	0.11	0.34	5
Unit V	0.4	0.4	0.21	0.08	0.11	0.72	7
Unit W	0.7						1
Unit RUB	0.6	0.5	0.49	0.09	0.00	1.91	31
colluvium	0.9	0.5	1.06	0.10	0.00	6.04	113
weathered bedrock	3.6	3.6	3.20	0.49	0.00	3.61	44
Stable GHN	0.6	0.5	0.56	0.03	0	4	380
Unstable GHN	1.5	1.0	1.9	0.12	0	13.5	232
Entire GHN	0. 9	0.6	1.3	0.05	0.0	13.5	617
Questa rock piles	1.1	0.7	1.3	0.04	0	13.5	943
Alteration scars	1.1	0.2	1.3	0.26	0	11	60
Debris flows	0.2	0.09	0.36	0.07	0.01	1.9	27
All Questa materials	1.1	0.7	1.4	0.4	0	13.5	1175

Pyrite is observed in many samples and varies from grains with no apparent alteration (pristine or "clean") to significantly altered grains. The genesis and timing of pyrite alteration, as well as distribution of altered pyrite within rock piles, is uncertain, but likely a result of two or more stages of hydrothermal alteration (Molling, 1989; McLemore et al., 2009a). Pyrite occurs as individual free grains within the soil matrix and as well-crystallized cubes or groups of cubes within rock fragments (Fig. 53). Fresh, unoxidized pyrite grains are common in most rock fragments throughout the entire rock pile, but not in the soil matrix. In some samples, the majority of pyrite has a cubic, eudral shape, whereas in other samples, the pyrite grains are rounded and abraided. Pyrite also occurs as vein and fracture coatings (Fig. 54).

Pyrite exhibits a range of alteration styles, as a result of hydrothermal alteration and weathering, or both, and, in many cases, it can be difficult to distinguish which process has

occurred. Pyrite in the rock-pile soil matrix tends to be more altered than pyrite in the rock fragments from the same sample. Some pyrite grains display oxidized rims, suggesting alteration that is proceeding from the outside inward (Fig. 55). In other samples, void areas around pyrite grains suggest that alteration has taken place, but that the resultant alteration material has been completely removed (Fig. 56). Some pyrite grains in soil matrix samples appear almost completely oxidized, and due to their skeletal appearance, oxidation appears to have taken place in situ (Fig. 57). The unlikelihood that these delicate forms would have survived transport and deposition in the rock pile is the strongest evidence observed that pyrite oxidation occurred after rock pile deposition. It is not uncommon to find pyrite partially or completely replaced by Fe-oxide, typically goethite. Chemical modification of pyrite grains was commonly observed in electron microprobe images (Fig. 58). It is unclear whether this modification was a result of prior alteration or in situ weathering of grains. Pitting is relatively rare, even in the highly weathered outer edges of the rock pile.

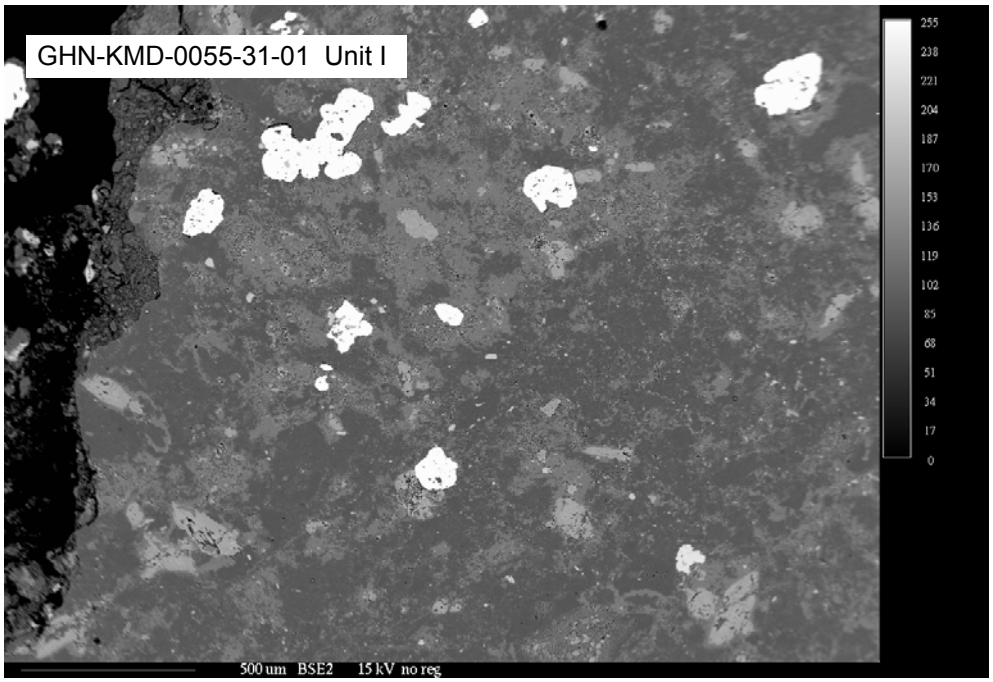

FIGURE 53. Backscattered electron image of fresh pyrite in rock-fragment sample. Brightest areas on image are pyrite grains, which are of uniform brightness and display distinct grain margins.

FIGURE 54. Pyrite and quartz vein.

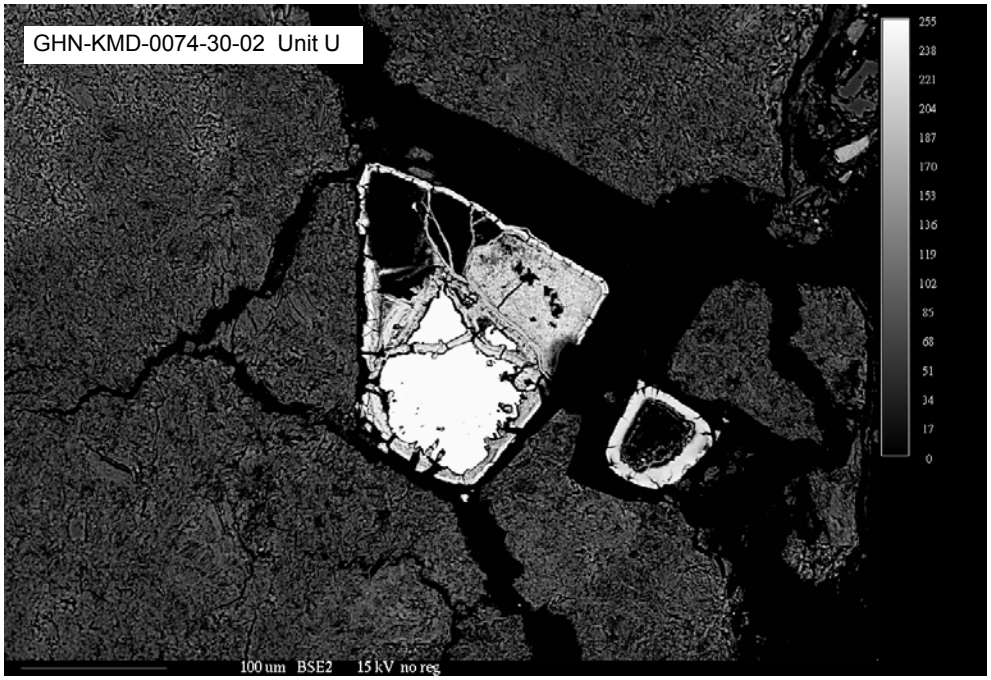

FIGURE 55. Backscattered electron image of residual pyrite core with oxidized rim in soil matrix. Brightest area of image is pyrite, and slightly darker surrounding area is oxidized pyrite.

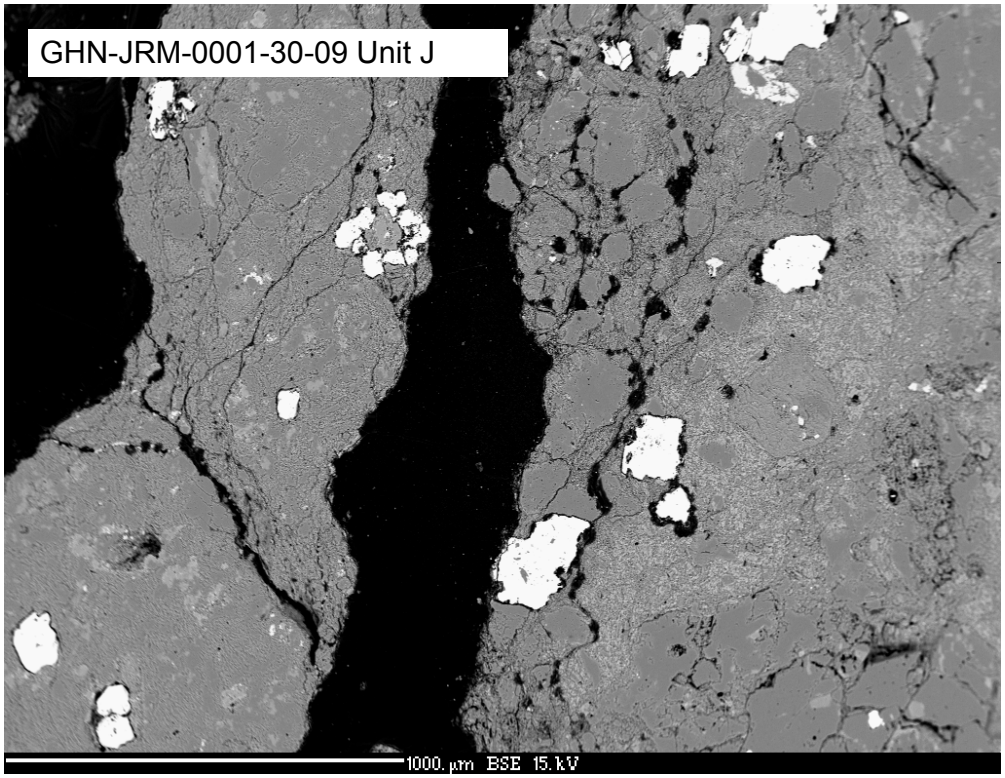

FIGURE 56. Backscattered electron image of pyrite grains in rock fragments. Pyrite is brightest areas of image. Dark rims around pyrite are void spaces, probably a result of dissolution during weathering.

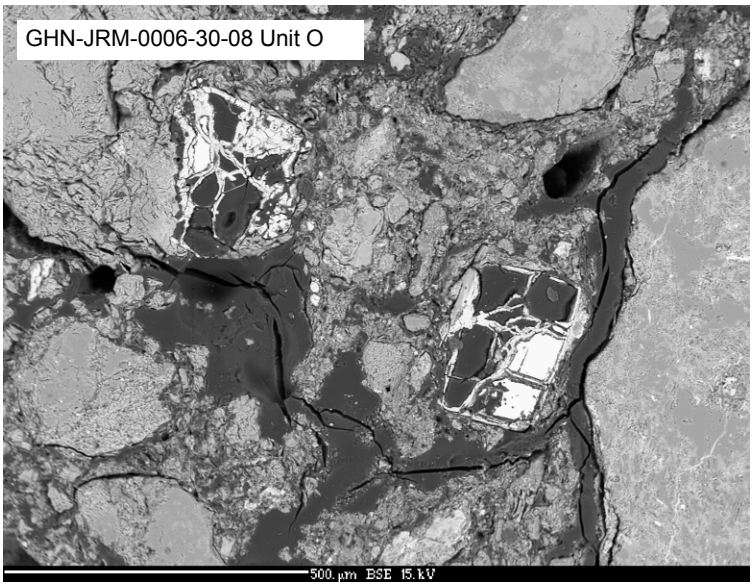

FIGURE 57. Backscattered electron image of altered pyrite grain within soil matrix. Brightest area is residual pyrite, but the outline of the original grain, outlined in an oxidized pyrite skeleton, is visible.

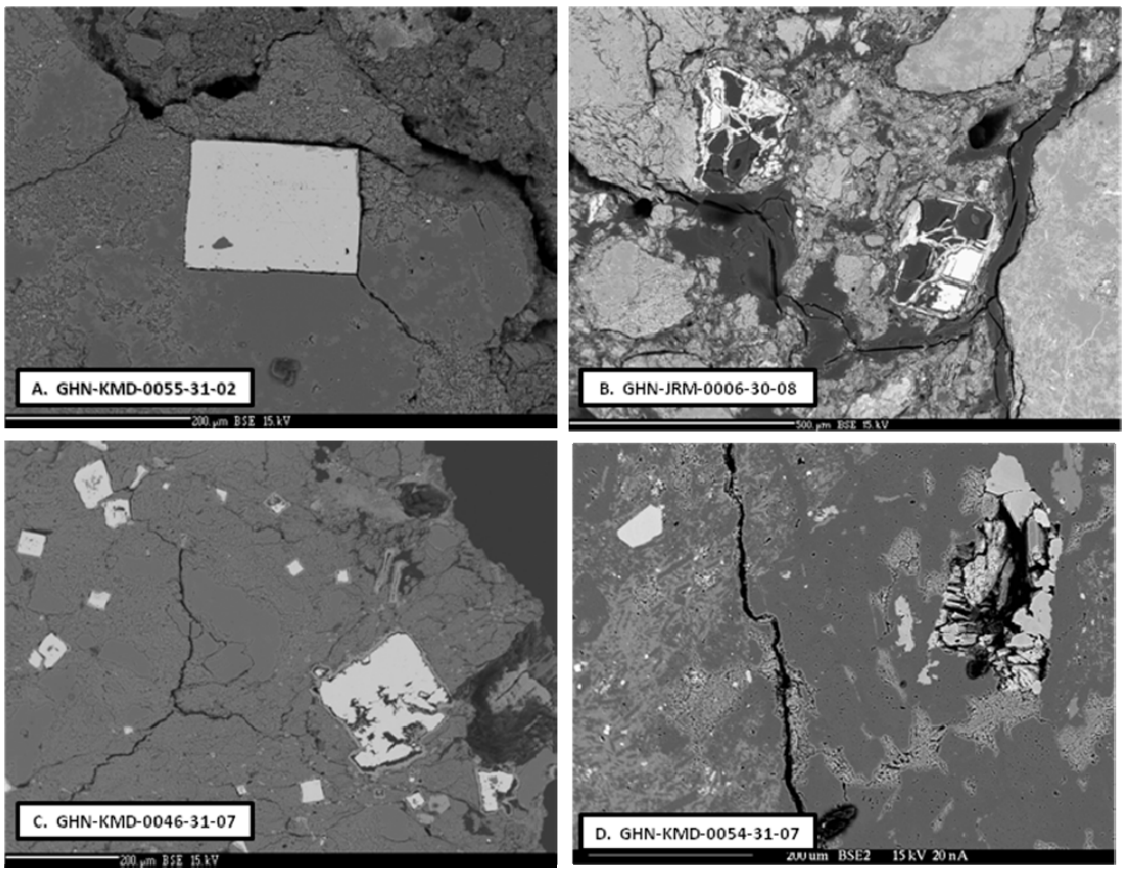

FIGURE 58. Backscattered electron images showing a) A "clean" or unaltered pyrite cube; b) Skeletal pyrite crystals in soil matrix; c) Variably altered pyrite crystals. Intensity of alteration increases with distance from the edge of rock fragment; d) A partially dissolved epidote phenocryst with associated apatite. Figures b through d are indicative of post-mining weathering.

Some pyrites within the Questa rock piles are visibly tarnished. An apparent thin tarnish or oxidation layer is visible along scalloped edges of pyrite grains in the backscattered electron image in Figure 59. Based on the tarnished edge of the grain in the lower left of the image (Fig. 59) the thickness of the tarnish appears to be ~5 μm or less. The chemical composition of oxidized rims on pyrite also has been investigated, and suggests that during the oxidation process, S is lost from the pyrite, but that the resulting Fe-oxide (goethite, hematite) can contain significant Si, Al, and P (Heizler et al., 2007). Weathered samples from unit I and J (outer zone) tend to have more tarnished pyrite and jarosite than unoxidized samples from the intermediate and interior zones.

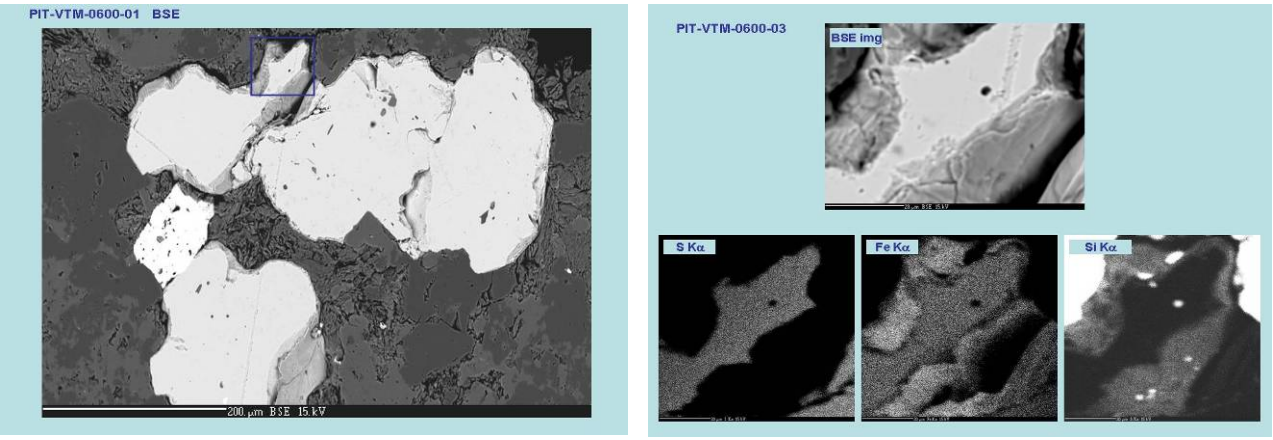

FIGURE 59. Backscattered electron image of pyrite grains showing thin tarnish. b) Backscattered electron image and corresponding S, Fe, and Si chemical maps. Scale bar=20 µ.

The pristine pyrites in the GHN rock pile are relatively chemically pure with minor trace elements (Table 22). Locally, the pyrites contain minor amounts of Cu and As. Studies have shown that the more heterogeneous the pyrite, the faster the pyrite will oxidize, especially with high concentrations of As (Kwong, 1993). These studies indicate that Co and Ni concentrations tend to protect the pyrite from weathering, whereas As and, to a lesser degree, Cu enhances oxidation.

Additional heavy minerals were found in the GHN rock pile as determined by a combination of heavy liquid mineral separation, powder XRD with Rietveld method refinement (Oerter et al., 2007), petrography, and modified ModAn (McLemore et al., 2009b) and included jarosite (≤4%), copiapite (≤0.2%), goethite (≤0.2%), hematite (≤0.4%), apatite (≤0.8%), fluorite (≤0.2%), sphalerite (≤0.05%) and molybdenite (≤0.01%). These minerals were distributed variably throughout the rock pile (Fig. 60).

Whole-rock chemical analyses (Appendix 7, project database) of GHN samples provided insight into the concentrations of metals and, therefore, minerals containing these metals (Table 21). Fluorine ranges from 551 to 1749 ppm in GHN samples and shows a positive correlation with LOI (loss on ignition or loosely bound water, Fig. 60). This relationship reflects F and LOI being found in fluorite, apatite, clay minerals, chlorite, and biotite (Table 21), which is confirmed by electron microprobe analysis. Arsenic concentrations ranged from 0.6 to 6.6 ppm and also show a positive correlation with LOI and no correlation with S (as sulfide). This relationship indicates that As is found in other minerals besides sulfide minerals. Zinc concentrations ranges from less than 1 to 1320 ppm and shows no correlation with S (Fig. 60), indicating that Zn is found in other minerals besides sphalerite. Lead concentrations range from less than 1 to 512 ppm and show no correlation with S (Fig. 60), indicating that Pb is found in other minerals in addition to galena. Copper concentrations range from less than 1 to 215 ppm and also is found in other minerals in addition to chalcopyrite. Other heavy minerals found in the GHN rock pile are listed in Table 20.

POST-MINING WEATHERING

It is difficult, but possible to distinguish between pre-mining hydrothermal alteration and post-mining weathering, by using detailed field observations and petrographic analysis that

includes defining the paragenesis (sequence of events), especially using microprobe analyses. The evidence for weathering in the Questa rock piles includes (McLemore et al., 2006a, b):

- Change in color from darker brown and gray in least weathered samples (original color of igneous rocks) to yellow to white to light gray in the weathered samples (Figs. 29-30, 39-42). However, the mineralogical effect of the fast-reacting (less than 40 yrs) weathering pyrite system is to produce precipitates of secondary reaction minerals on the surface of existing rock fragments and within the soil matrix, which result in the yellow to orange color, reflecting the role of ferric iron in the mineral structures. The secondary precipitates form coatings on exterior surfaces, rims, and fill macro- and micro-fractures. Thus, the macro-scale impression of weathering, caused by the discoloration from the observed secondary precipitates is exaggerated.
- Thin yellow to orange, "burnt" layers within the interior of GHN, where water and/or air flowed and oxidized the rock-pile material.
- Paste pH, in general, is low in oxidized, weathered samples and paste pH is higher in least weathered samples.
- Increase abundance of jarosite, gypsum, Fe-oxide minerals and soluble efflorescent salts (locally as cementing minerals), and low abundance to absence of calcite, pyrite, and epidote in weathered samples.
- Tarnish or coatings of pyrite surfaces within weathered samples (Figs. 58-59; Heizler et al., 2007).
- Dissolution textures of minerals (skeletal, boxwork, honeycomb, increase in pore spaces, fractures, change in mineral shape, accordion-like structures, loss of interlocking textures, pits, etching) within weathered samples (McLemore et al., 2009b).
- Change in bulk textures of the rock-pile material including increase in soil:rock ratio, piping or stoping within the rock pile, and decrease in grain size due to physical weathering.
- Chemical classification as potential acid-forming materials using acid base accounting methods (Tachie-Menson, 2006).
- Chemical analyses of water samples characterized by acidic, high sulfate, high TDS, and high metal concentrations (Al, Ca, Mg, Fe, Mn, SO_4).

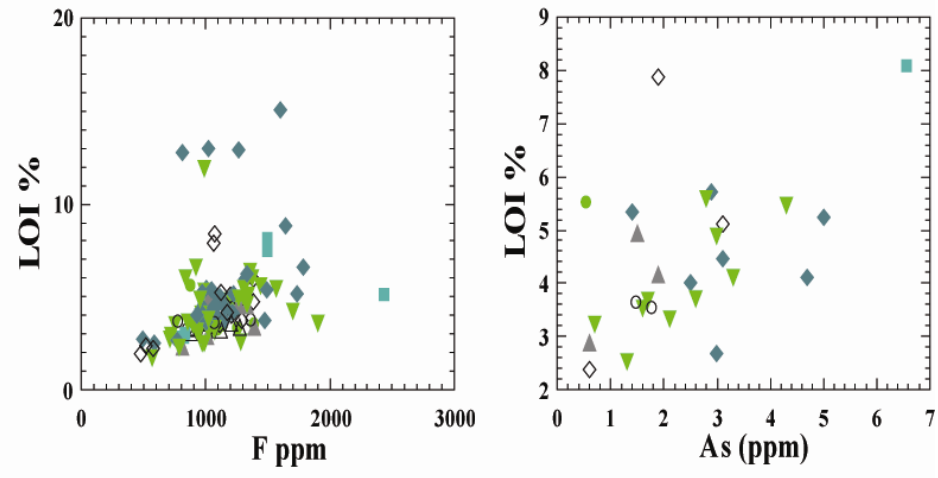

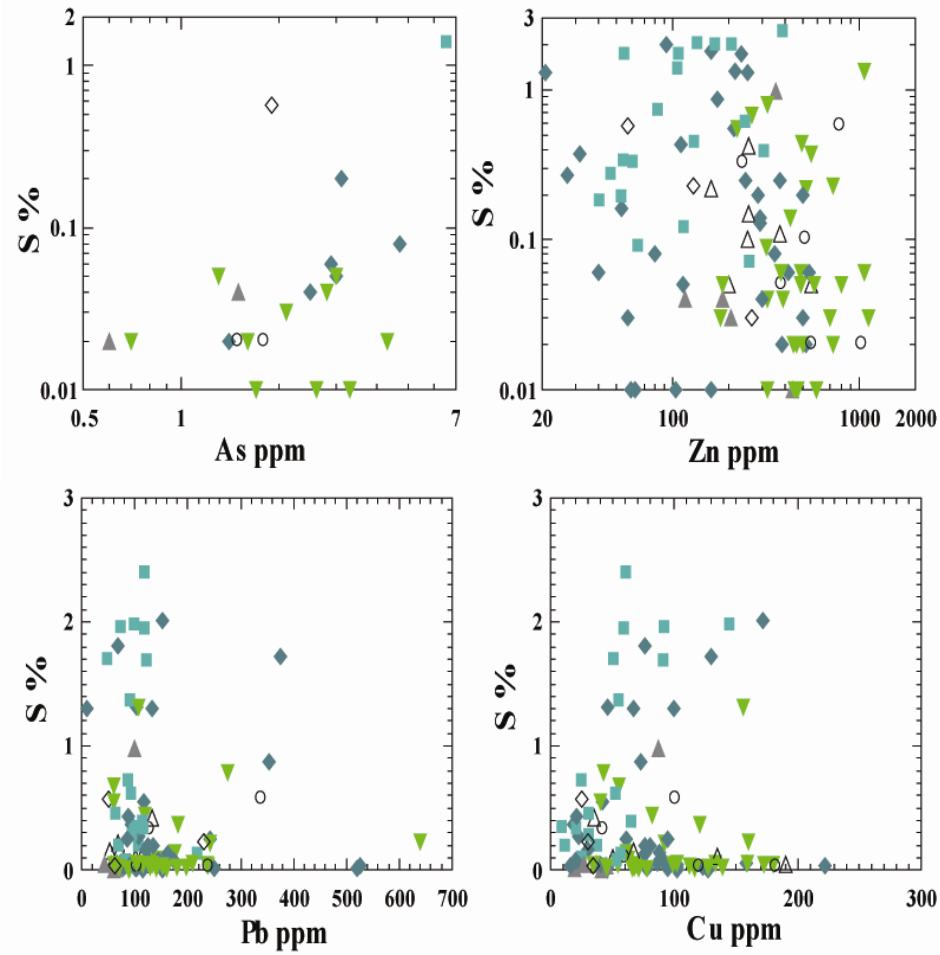

FIGURE 60. Scatter plots showing the relationship between LOI (Loss on Ignition), F, S (as sulfide), As, Zn, Pb, and Cu for samples in GHN. More weathered samples (Units I, J, N; Figure 43) have higher LOI, S, and F than less weathered, interior samples. The lack of correlation between Zn, Pb, As, Cu, and S indicates that these metals are in other minerals in addition to sulfide minerals. Chemical analyses are performed on the entire sample, including soil matrix and rock fragments. See Table 20 for description of the geologic units.

The gypsum-pyrite-carbonate mineral assemblage provided insight into the process of post-mining weathering that has occurred since the material was emplaced in the rock pile. In the time since rock-pile deposition, a number of mineralogical changes have demonstrably occurred. These include alteration of pyrite (discussed in previous section) and dissolution of carbonate, as well as in-situ formation of gypsum, jarosite, copiapite, Fe-oxides, and soluble Fe salts (Table 21). Some of these phases can provide cementation of the matrix, or soil, component of the rock pile. The fine-grained soil matrix typically is more weathered than the rock fragments. Even in highly weathered material, the interior of rock fragments are typically unweathered (Fig. 5), although the intensity of hydrothermal alteration will vary.

Gypsum is found in every soil-matrix sample analyzed thus far by soil petrography, whereas it was not observed in any rock fragment. Gypsum occurs in the piles in distinctly different crystal habits. Stable isotope studies (Fig. 61; $\delta^{18}O$, $\delta^{34}S$) show that the clear, prismatic gypsum crystals are authigenic, forming after material was emplaced in the rock pile (Figs. 61,

62, 63; Pandy, 2004; Campbell et al., 2005; Campbell and Lueth 2008). The authigenic gypsum is likely a product of weathering and is isotopically and texturally distinct from the detrital gypsum, which typically appears as milky, rounded grains (Fig. 62). Authigenic gypsum abundances generally decreased from the outer, oxidized margin to the interior units of the rock pile (Fig. 64). However, the differentiation between detrital and authigenic gypsum is difficult because much of the gypsum is too small to properly identify by petrographic techniques. Conversely, carbonate abundance showed a general increase from the outside to the inside of the rock pile (Fig. 46), reflecting dissolution of calcite during weathering of the outside of the rock pile.

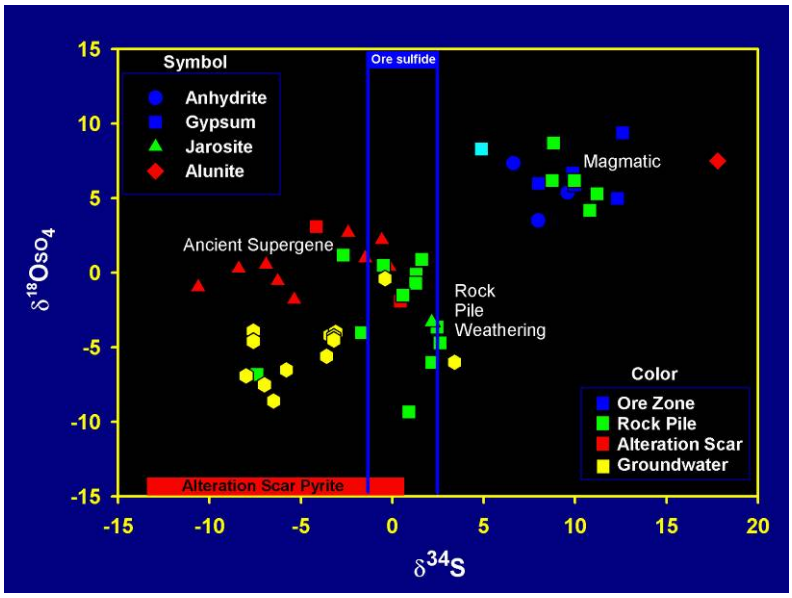

FIGURE 61. This isotopic plot differentiates between hydrothermal, and supergene alteration and post-mining weathering (Campbell and Lueth, 2008).

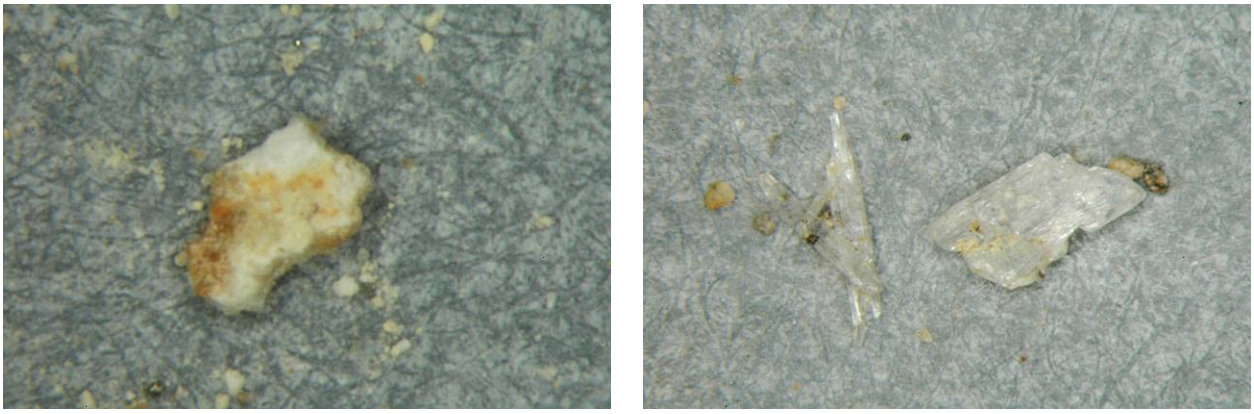

FIGURE 62. Detrital (or old) gypsum (GHN-VTM-194-T004) on the left and authigenic (or new) gypsum (and GHN-VTM-198-T004) on the right. These crystals are approximately 1-2 cm long.

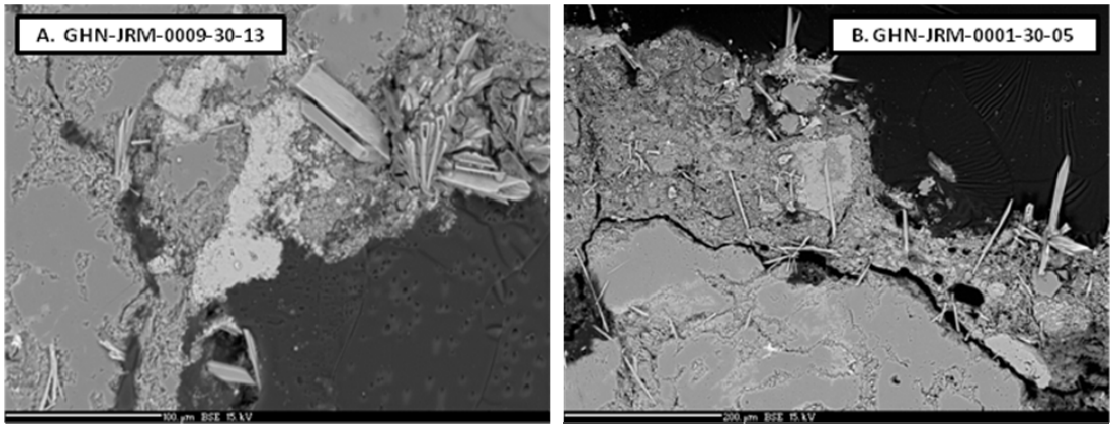

FIGURE 63. Backscattered electron image a) delicate gypsum blades with intergrown jarosite cement (bright phase) and b) feathery blades in adhered soil matrix. It is unlikely that these morphologies could survive blasting and dumping, therefore, these are indications of weathering.

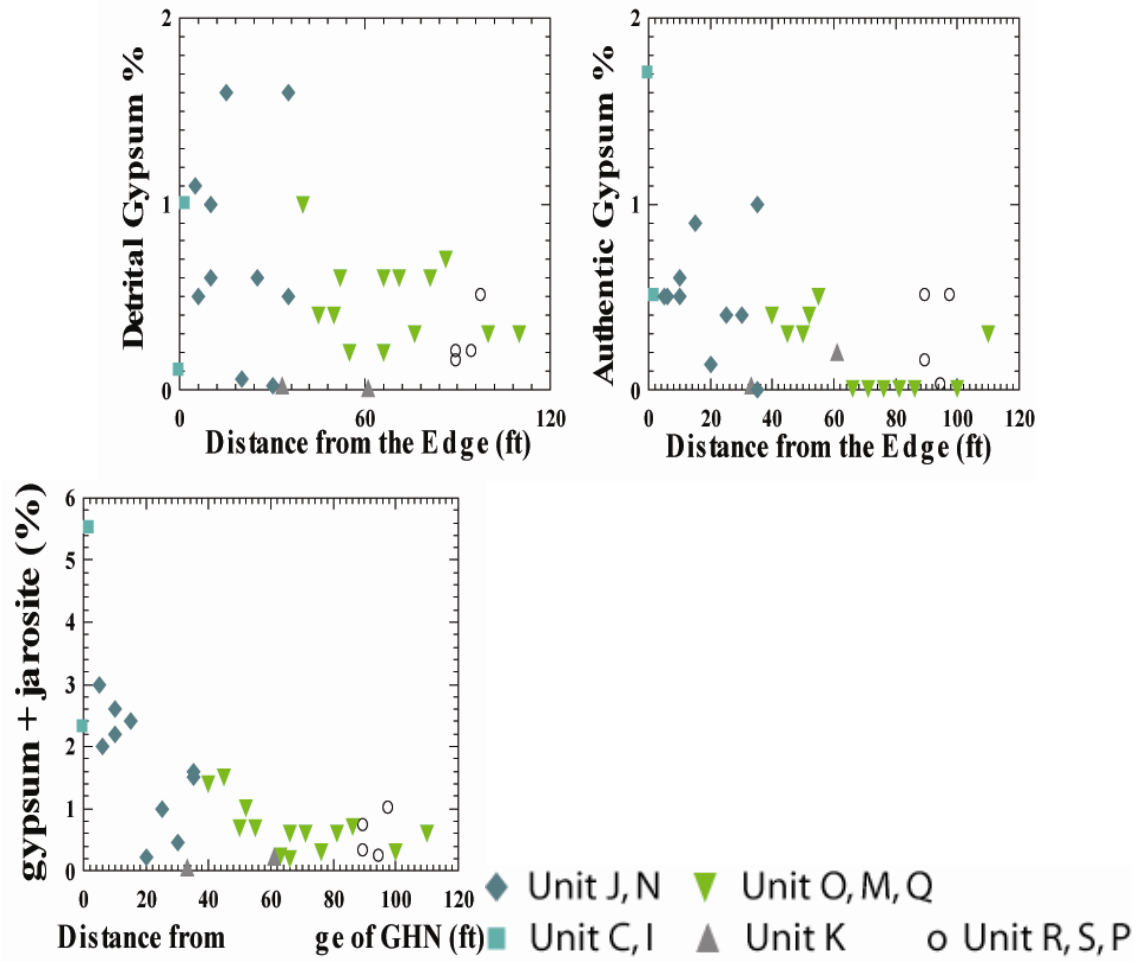

FIGURE 64. Variations in authigenic and detrital gypsum and sum of gypsum and jarosite in weight percent across bench 9, GHN. More weathered samples (units I, J, N) on the outside of the rock pile (left side of diagram) have slightly higher concentrations of authigenic gypsum. The difficulty in determining the abundances of detrital and authigenic gypsum is that much of the gypsum is too

small to properly identify by petrographic techniques. See Figure 43 for geologic cross section and to Table 20 for description of geologic units.

Fe-oxides are present throughout the rock pile. Definitive identification of this phase using the electron microprobe is problematic because analytical totals are consistently low, suggesting the presence of elements that cannot be directly analyzed, particularly O and H. However, based on the association of this phase, as well as the chemical composition based on the elements that are analyzed, this phase consists largely of the mineral goethite (which is a Fe oxyhydroxide). The reflectance spectroscopy analysis also indicates that goethite is more prevalent than hematite, although both are present (project database, Phoebe Hauff, written communication, 7/7/04). Some of this goethite is probably inherited from the source rocks, but some, particularly where replacing pyrite, it thought to be forming in the rock pile during weathering. The observed goethite exhibits striking chemical variability, and can contain up to 10 wt% of SiO_2, Al_2O_3, P_2O_5 or SO_2 (Table 22).

The goethite in these samples occurs in a number of forms. Goethite is directly associated with pyrite grains, probably as the result of pyrite oxidation (Figs. 65, 66). Goethite also occurs as complete replacement of grains that were probably originally pyrite, but in which the pyrite has been completely altered (Fig. 67). Goethite also occurs as fracture fillings (Fig. 10) and as coatings on rock fragments (Fig. 68).

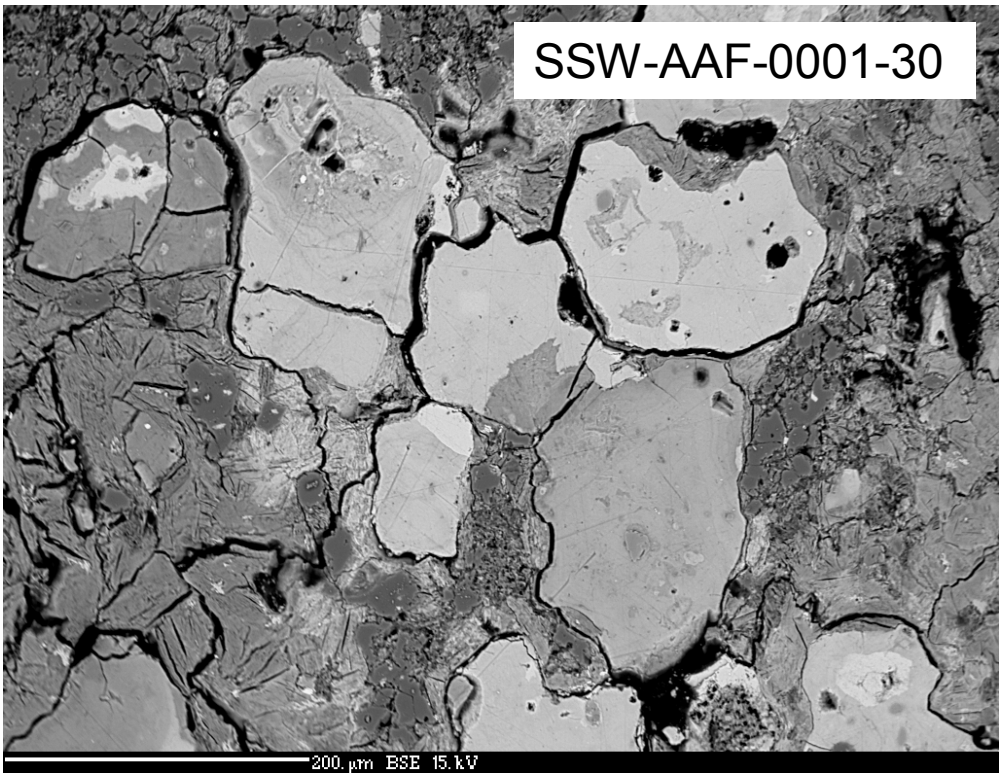

FIGURE 65. Goethite grains (bright areas) that appear to have replaced pyrite.

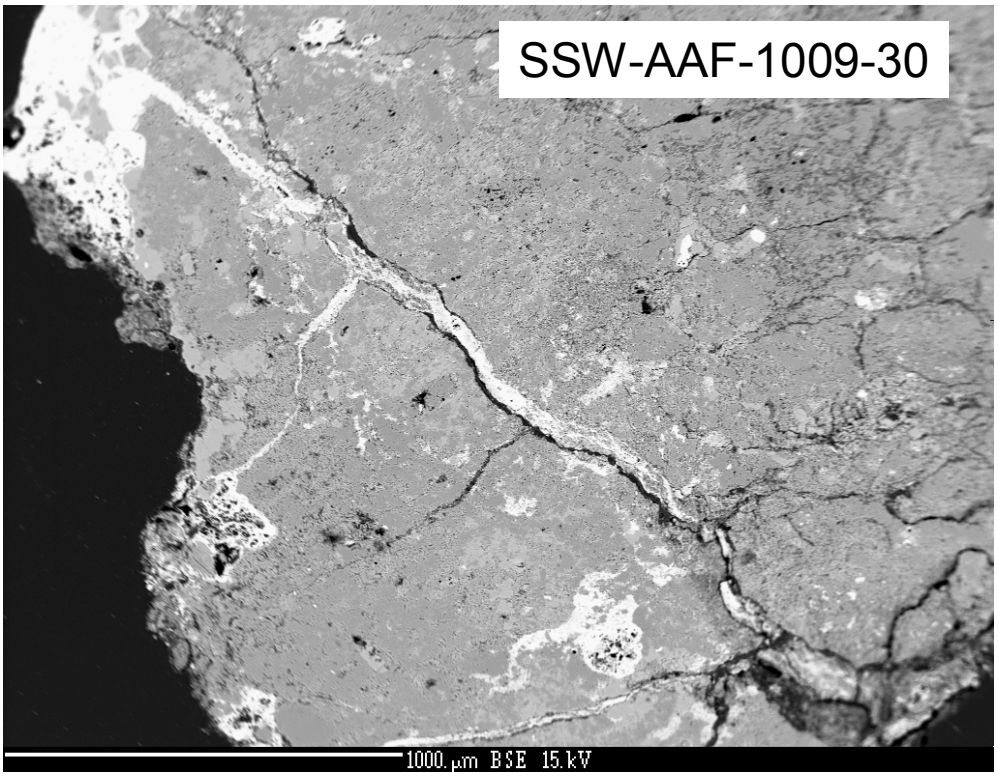

FIGURE 66. Goethite (bright areas) filling a fracture.

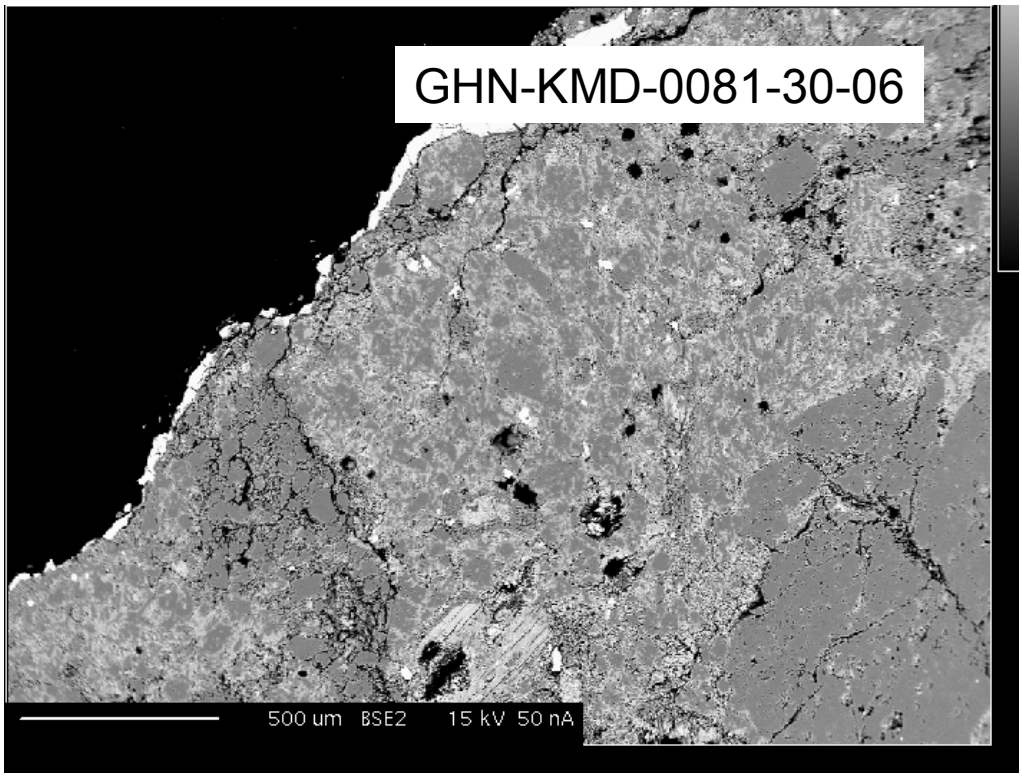

FIGURE 67. Goethite (bright areas) along the edge of a rock fragment.

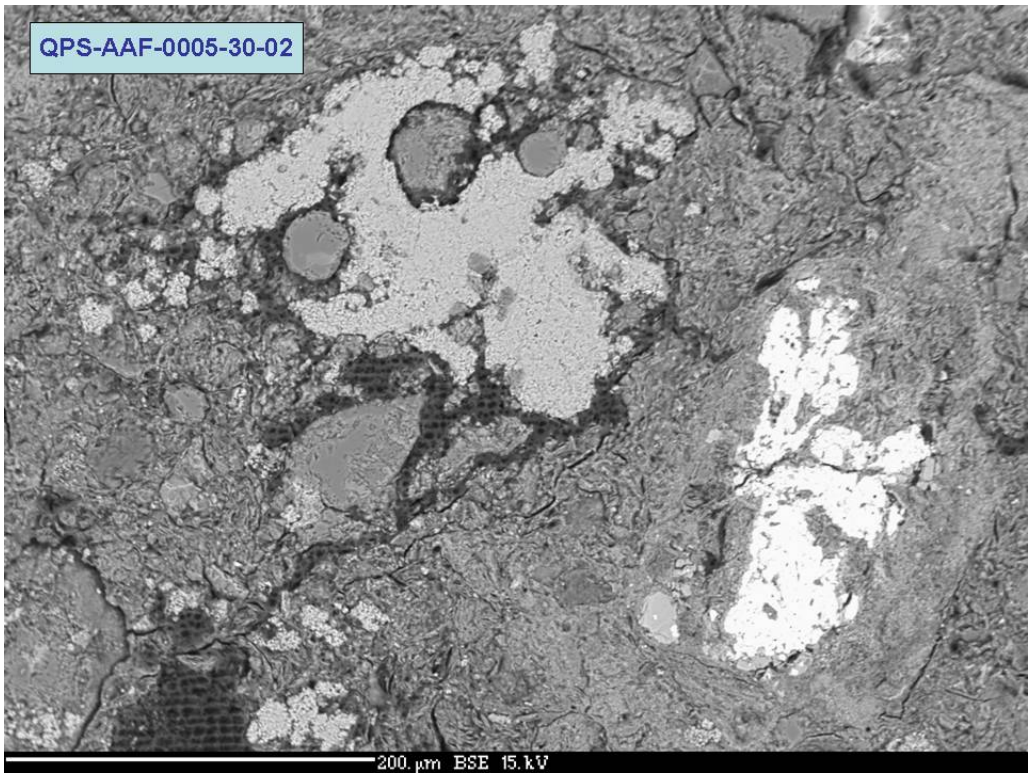

FIGURE 68. Backscattered electron image of granular jarosite (light gray) and P-bearing goethite (brightest grain) in soil matrix.

Goethite found in rock-pile samples can have multiple origins. The delicate goethite that is found replacing pyrite grains is likely to be formed in the rock pile because it would be difficult for such delicate structures to survive transport. In some rock fragments, goethite is more abundant near the margin of the rock fragment than in the core. This also argues for formation in the rock pile. The same argument can be made for goethite that is found as a coating on rock fragments. However, loose fragments of goethite in the matrix, fracture-filling goethite, and massive goethite replacing pyrite can be inherited from the hydrothermally altered source rocks. A notable aspect of the goethite in the rock pile and scar samples is that the chemical compositions are variable. Most goethite contains Si in addition to Fe and Al is also typically observed (Table 23). The abundance of the oxides of Si, Al, P and S can be as high as 10 wt. %. There does not appear to be any systematic correlations between the four elements, but this has not been investigated in detail. As can be seen in Figure 65, many goethites appear banded in backscattered electron imaging, suggesting compositional variability over a short distance.

The abundance of secondary jarosite is strongly linked to location within the rock pile. Jarosite is found in samples from the outer units of, as well as beneath the GHN rock pile and is rare to absent in the interior units (Fig. 44). Several morphologies of jarosite are observed, all of which are interpreted to be authigenic. Jarosite is commonly present in irregular patchy areas, typically with rounded edges, in the matrix of soil samples (Fig. 68). These patchy areas locally occur in association with goethite. These isolated patches may not substantially affect cementing or sample cohesion. The patches shown in Figure 68 consist of very fine masses of jarosite granules. In some samples, granular jarosite forms within the soil matrix and also fills fractures within altered rock fragments, in which case the jarosite can contribute substantially to cohesion (Fig. 69). Jarosite also occurs as a replacement phase within relict pyrite cubes (Fig. 70).

Tiny distinct euhedral crystals of jarosite are occasionally present in the soil matrix (Fig 71), but more commonly jarosite is finely intermixed with clay. Intermixed jarosite is thought to contribute to overall sample cohesion. Jarosite is sometimes observed as localized patches of cement intergrown within the soil matrix (Fig. 72) or as vein filling within altered rock fragments, often in association with goethite. Both morphologies appear to add to sample cohesion. In some samples, jarosite occurs in association with gypsum. Figure 73 shows a jarosite vein in association with finely intergrown gypsum.

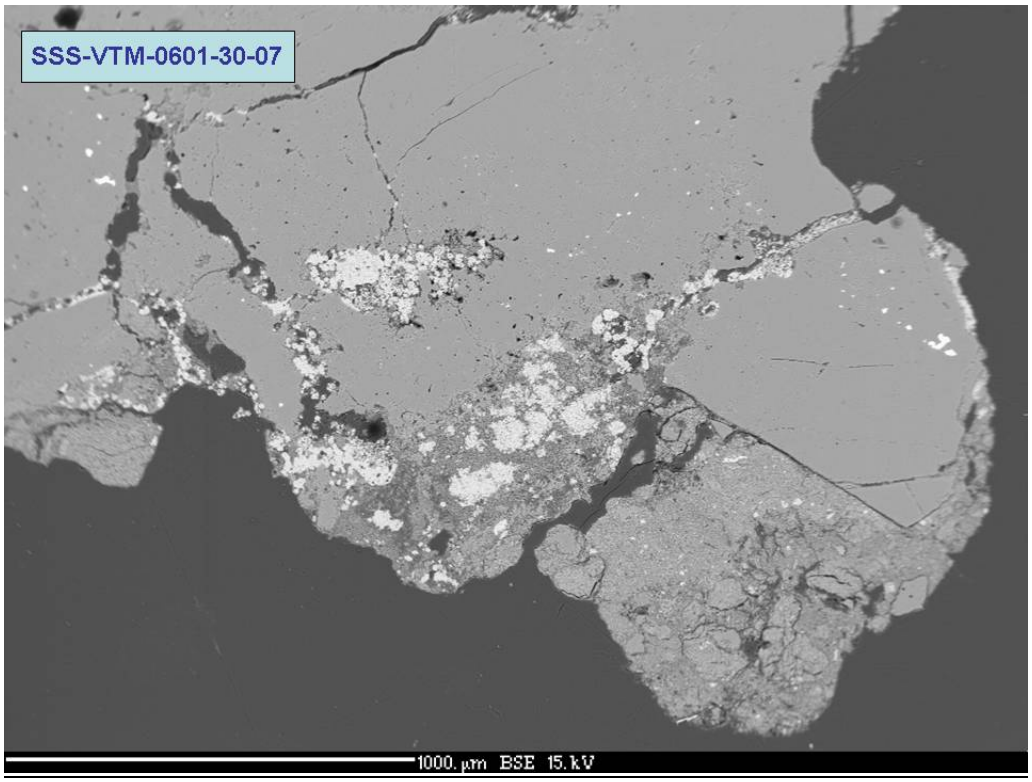

FIGURE 69. Backscattered electron image of jarosite (bright areas) aggregate intergrown in soil matrix and filling fractures in altered rock.

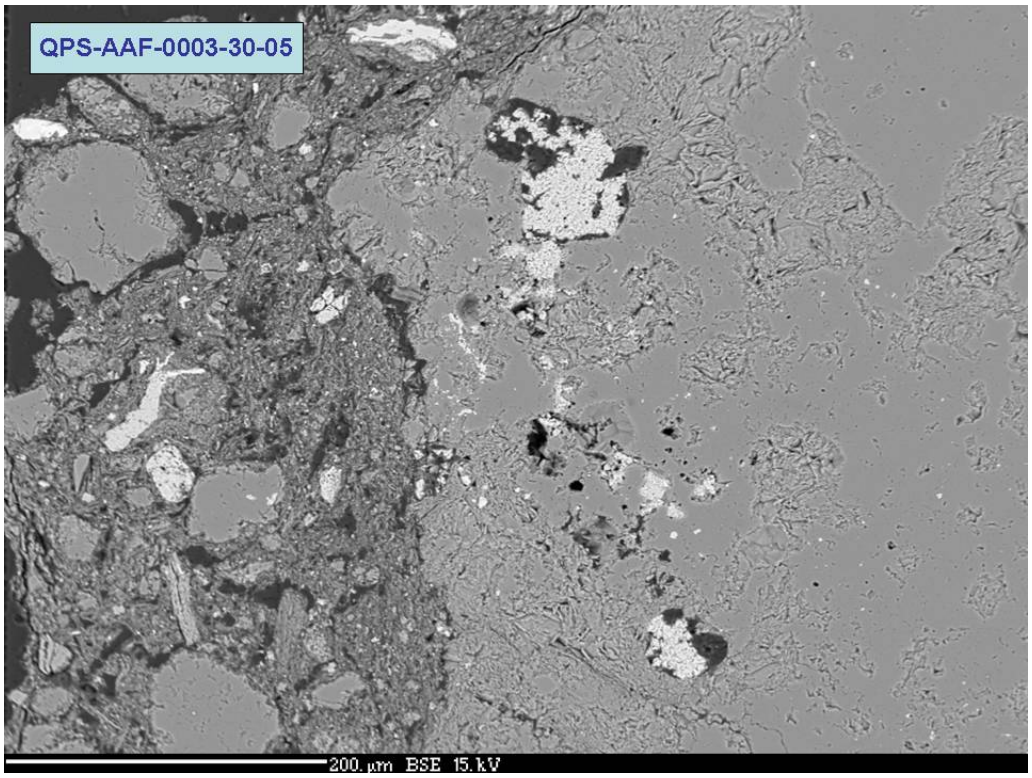

FIGURE 70. Backscattered electron image showing partial replacement of relict pyrite cubes by jarosite (bright areas).

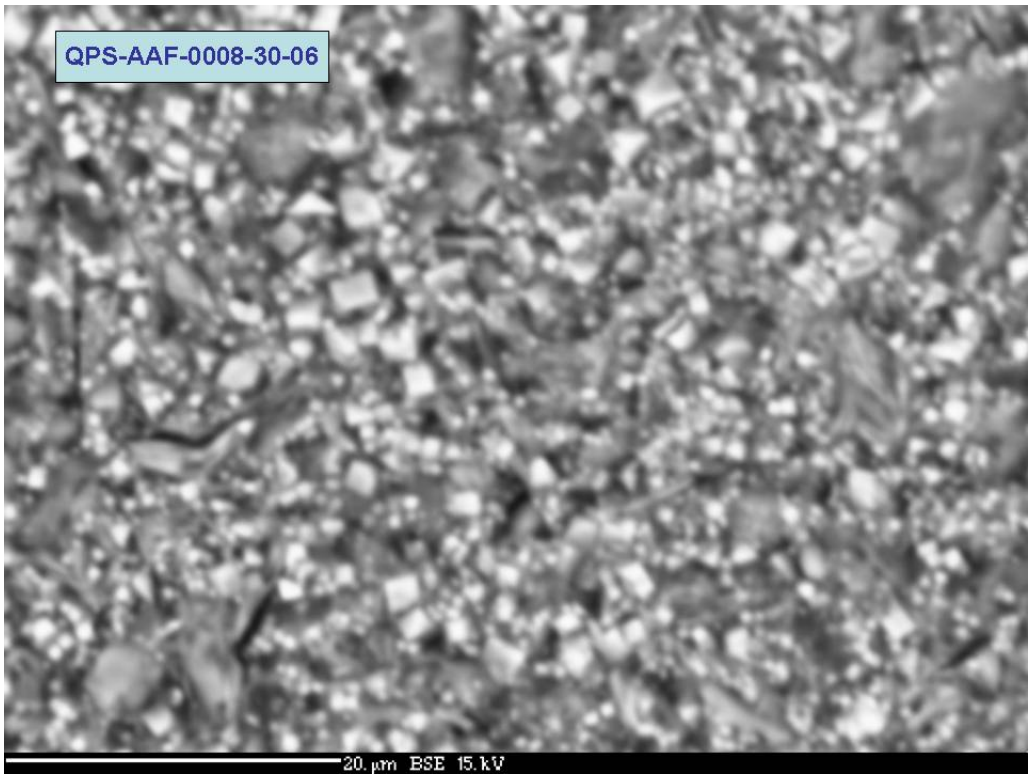

FIGURE 71. Backscattered electron image of tiny euhedral jarosite crystals (bright areas) intergrown in soil matrix.

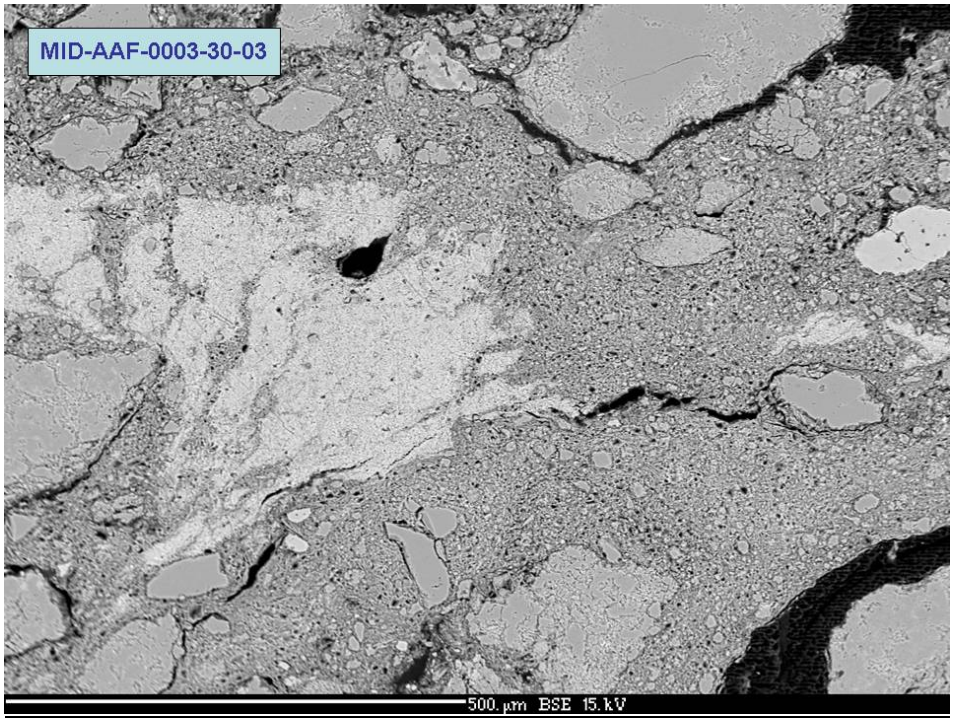

FIGURE 72. Backscattered electron image of jarosite cement (bright areas) within finely intermixed jarosite/clay soil matrix (speckled areas).

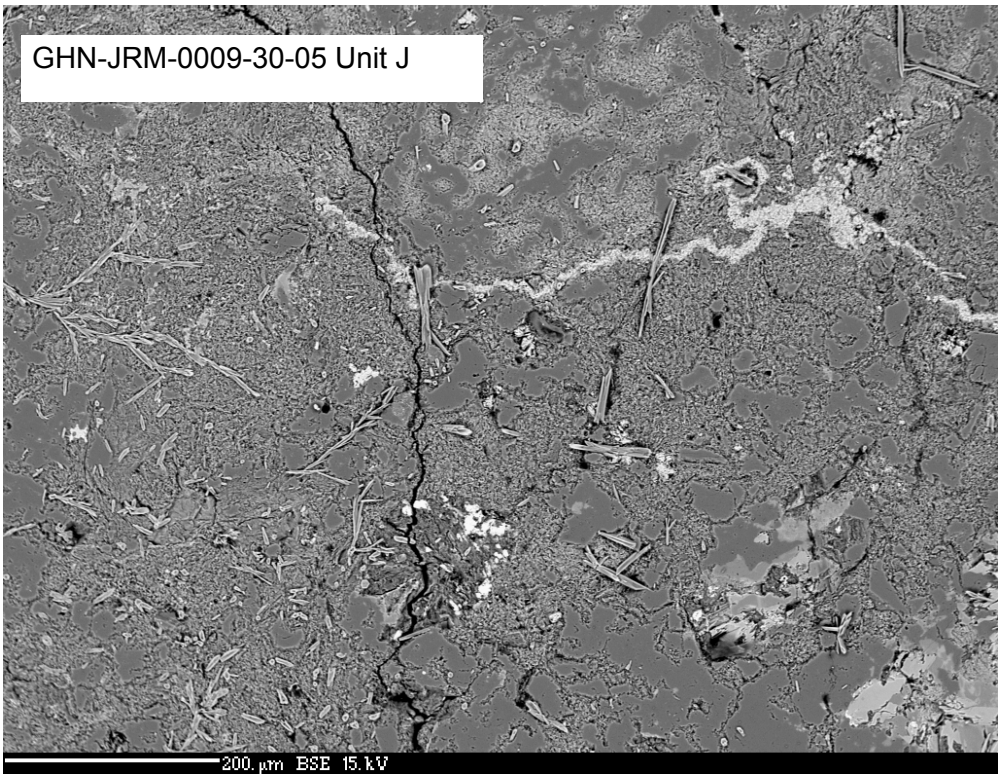

FIGURE 73. Backscattered electron image of gypsum needles intergrown in matrix of altered rock fragment in soil sample. The bright, thread-like vein in the upper part of the image is jarosite.

SIMPLE WEATHERING INDEX

A simple weathering index (SWI) was developed to differentiate the weathering intensity of Questa rock-pile materials (SWI=1, fresh to SWI=5, most weathered; Table 24; Gutierrez et al, 2008). The five classes described in Table 24 describes the SWI classification for the soil matrix at the Questa mine based on relative intensity of both physical and chemical weathering (modified in part from Little, 1969; Gupta and Rao, 2000; Blowes and Jambor, 1990). Samples from the outer units of GHN tend to have a SWI of 4 (weathered) and the interior units have lower SWI (Fig. 74).

TABLE 24. Simple weathering index for rock-pile material (including rock fragments and matrix) at the Questa mine.

SWI	Name	Description
1	Fresh	Original gray and dark brown to dark gray colors of igneous rocks; little to no unaltered pyrite (if present); calcite, chlorite, and epidote common in some hydrothermally altered samples. Primary igneous textures preserved.
2	Least weathered	Unaltered to slightly altered pyrite; gray and dark brown; angular to sub-angular rock fragments; presence of chlorite, epidote and calcite, although these minerals are not required. Primary igneous textures still partially preserved.
3	Moderately weathered	Pyrite altered (tarnished and oxidized), light brown to dark orange to gray: more clay- and silt-size material; presence of altered chlorite, epidote and calcite, but these minerals are not required. Primary igneous textures rarely preserved.
4	Weathered	Pyrite very altered (tarnished, oxidized, and pitted); Fe-hydroxides and oxides present; light brown to yellow to orange; no calcite, chlorite, or epidote except possibly within center of rock fragments (but the absence of these minerals does not indicate this index), more clay-size material. Primary igneous textures obscured.
5	Highly weathered	No pyrite remaining; Fe-hydroxides and oxides, shades of yellow and red typical; more clay minerals; no calcite, chlorite, or epidote (but the absence of these minerals does not indicate this index); angular to sub-rounded rock fragments

The SWI accounts for changes in color, texture, and mineralogy due to weathering, but it is based on field descriptions. Some problems with this weathering index are:

- It is subjective and based upon field observations.
- This index does not always enable distinction between pre-mining supergene hydrothermal alteration and post-mining weathering.
- The index is developed from natural residual soil weathering profiles, which typically weathered differently from the acidic conditions within the Questa rock piles and, therefore, this index may not adequately reflect the weathering conditions within the rock piles.
- This index refers mostly to the soil matrix; most rock fragments within the sample are not weathered except perhaps at the surface of the fragment and along cracks.
- The index is based primarily upon color and color could be indicative of other processes besides weathering intensity.
- This index was developed for the Questa rock piles and may not necessarily apply to other rock piles.
- Weathering in the Questa rock piles is an open not a closed system (i.e. water analysis indicates the loss of cations and anions due to oxidation).

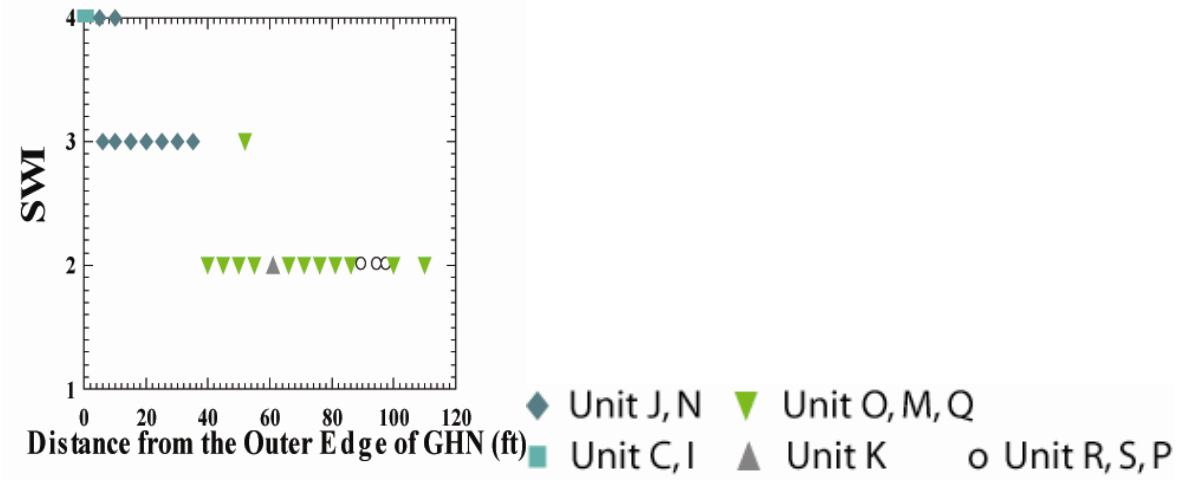

FIGURE 74. Variation of SWI (Simple Weathering Index) along bench 9, GHN. See Figure 43 for the geologic section and Table 20 for description of geologic units.

CEMENTATION

Authigenic gypsum, jarosite soluble efflorescent salts, Fe-oxide minerals and to a lesser extent, clay minerals liberated from the mined rock material during construction of the rock piles (i.e. pre-mining clay minerals), have cemented parts of GHN rock pile material. Cementation in the rock piles varies from none to moderate, with local well-cemented layers. In the short term, cementation at the surface is controlled by jarosite, gypsum and soluble efflorescent salts. The repeated wetting and drying cycle (infiltration, drainage, evaporation, and oxidation) is the major influence on precipitation and dissolution of these soluble minerals (Nordstrom et al., 1979; Nordstrom, 1982; Perkins et al., 1995). These minerals form a thin, hard crust at the surface of the rock piles, which can be partially or completely dissolved during wet periods. During infiltration into the rock piles, these soluble minerals are dissolved and carried farther into the rock pile and re-precipitated, in some cases precipitated as less soluble Fe oxide minerals (Perkins et al. 1995). These less stable minerals could form the building blocks for longer-term cementation consisting of Fe oxides, such as hematite and goethite, and amorphous Fe and Mn material (Delvigne, 1998).

Electron microprobe analysis shows cementation by Fe-oxide minerals and gypsum. The Fe-oxide cement consists of a fine veining network of Fe-oxide intergrown with the clay in the soil matrix (Figs. 75-77). Although the cementation that is observed in the rock-pile material is in close association with rock fragments, it is not typically observed in the rock fragments themselves. Gypsum is observed in a number of rock-pile samples, but typically occurs as individual bladed crystals (Fig. 63). However, gypsum cement has been noted in one rock sample (Fig. 78), where, gypsum appears to be intimately intergrown with the soil matrix.

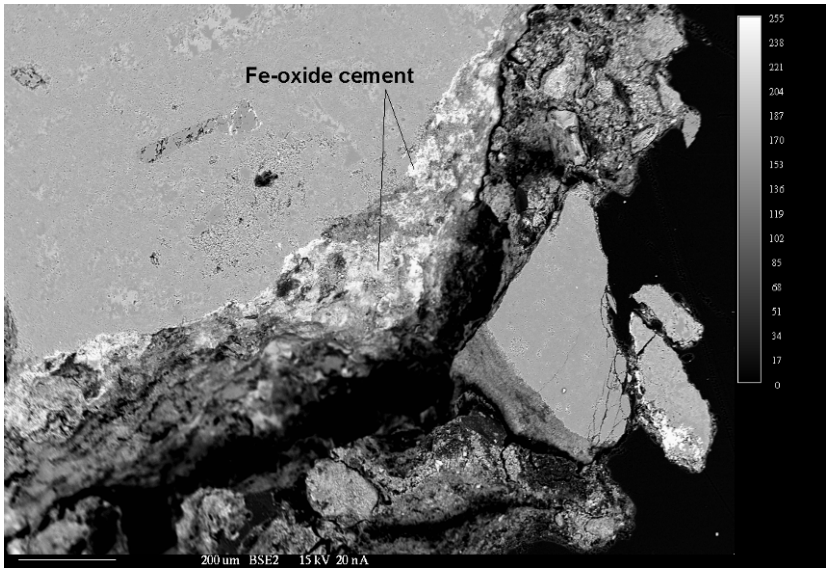

FIGURE 75. Backscattered electron image showing tabular Fe-oxide cement intergrown with clay in soil matrix. Image GHN-NWD-0014-30-02.

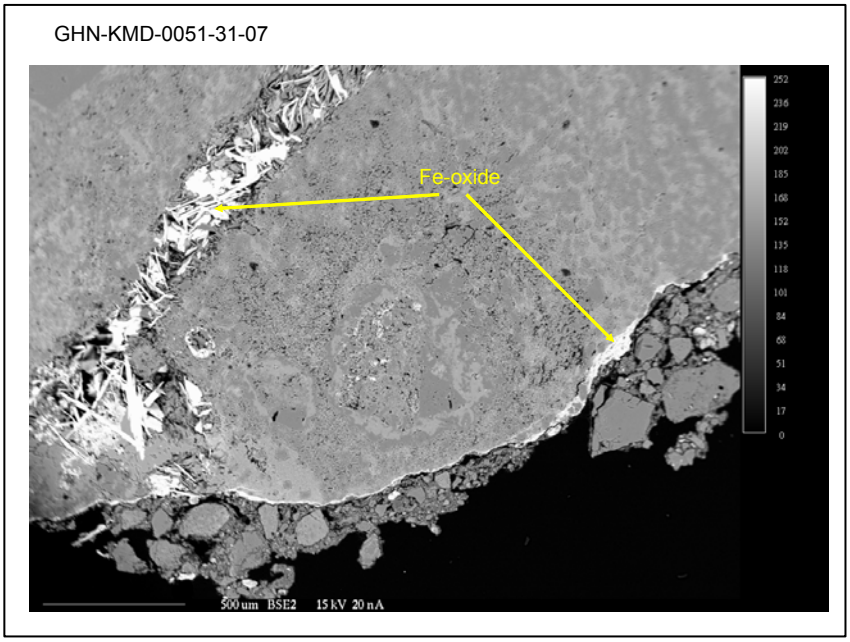

FIGURE 76. Backscattered electron image showing Fe-oxide cement (bright areas) intergrown with clay in soil matrix. Image GHN-KMD-0051-31-07. This delicate bladed morphology is likely post-mining weathering because these bladed crystals probably would not withstand blasting, hauling, and end-dumping.

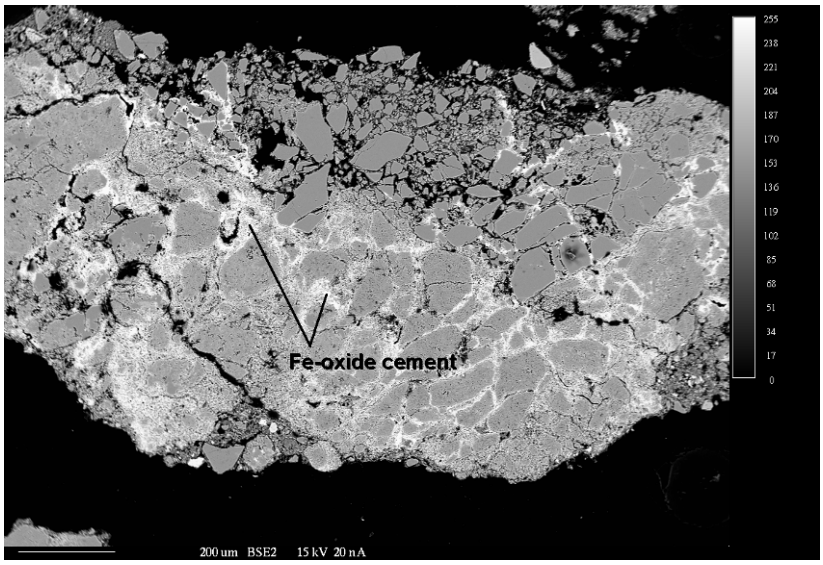

FIGURE 77. Backscattered electron image showing Fe-oxide cement (bright areas) intergrown with clay in soil matrix. Image GHN-NWD-0020-30-08.

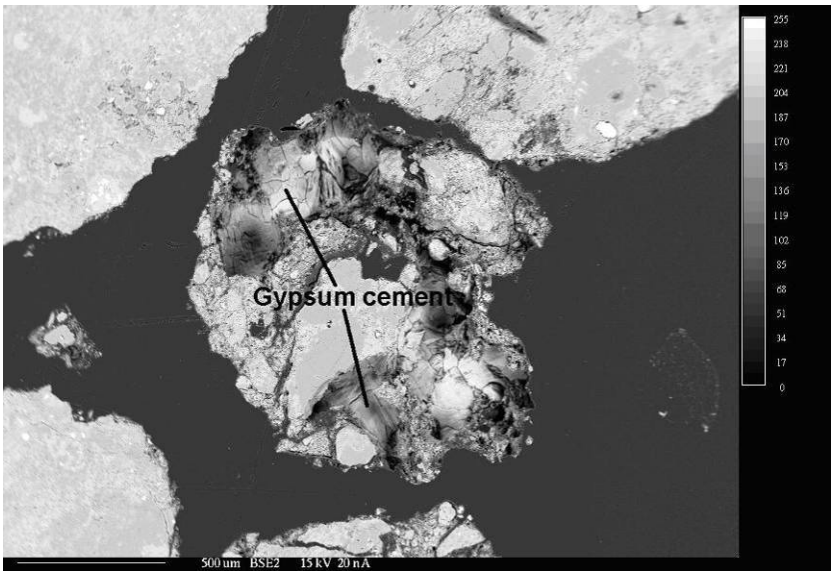

FIGURE 78. Gypsum cement intergrown (mottled gray areas) with soil matrix. Image GHN-NWD-0024-30-05.

Ferricretes are accumulations of secondary Fe-oxyhydroxides that can occur as cemented sandstone or conglomerate or as ferruginous duricrust (Yager et al., 2005; Beauvais, 1999). They are clast- or matrix-supported and typically cemented by goethite or hematite. Ferricretes are prominent features in many alteration scars (Graf, 2008) and have been encountered in drill holes in the front rock piles and in a limited number of rock pile samples from GHN and underlying colluvium. Ferricretes in the rock-pile samples are orange to brown in color and usually exhibit an overall angular to subangular shape (Fig. 79). Ferricretes can provide information regarding a potential end product of both weathering and cementation, because their formation occurs in saturated conditions.

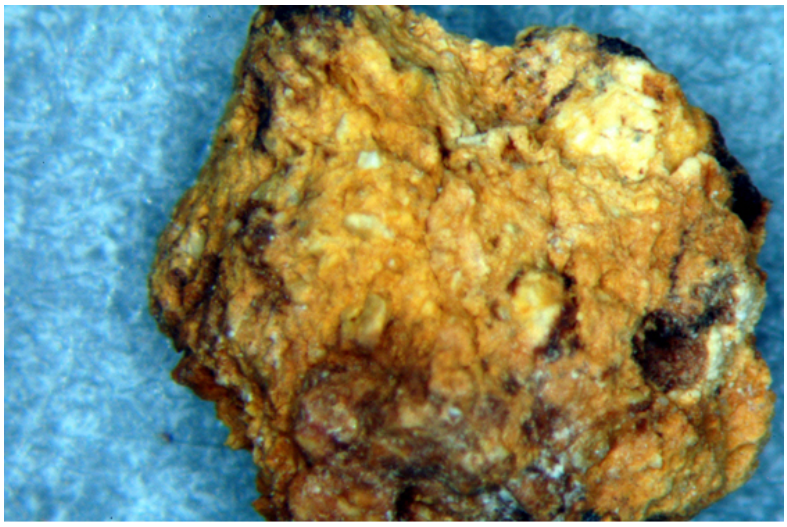

FIGURE 79. Ferricrete from GHN rock pile. Field of view is 6 mm. Photo number is GHN-VTM-205-T003.

CLAY MINERALOGY

Clay mineral analyses by XRD and near-IR spectroscopy for the Questa rock-pile material and nearby natural alteration scars indicate the presence of five phyllosilicate mineral groups: kaolinite, smectite, illite (mica), chlorite, and mixed-layered clays (predominantly illite-smectite). Clay mineralogy analysis, in terms of the major clay mineral groups, was performed on the complete sample (i.e. both matrix and rock fragments) using standard clay separation techniques and XRD analyses of the clay mineral separate on an oriented glass slide (Hall, 2004; Moore and Reynolds, 1989)**.** This method does not liberate or measure the amount of clay minerals within the rock fragments. Based on electron microprobe analysis, clay minerals are present in the soil component of all samples, as well as in rock fragments. The soil component of samples contains a clay matrix surrounding rock fragments. Large relict igneous feldspar crystals contain isolated pockets of clay minerals and the groundmass of rock fragments also contains pockets of clay. Fresh or slightly tarnished pyrite is locally surrounded by clay minerals. Clays in rock fragments invariably occurs in isolated pockets, and, other than chlorite, does not occur as concentrations in through-going fractures in the rock. Chlorite veinlets are common in hydrothermally altered andesite. Similar results were found by petrographic, PIMA spectroscopy and XRD Rietveld analyses by PetraScience Consultants Inc. (2001) on samples from the front rock piles. The mechanical particle size reduction from blasting and dumping the rock-pile material can physically release the clays contained within the silicate phenocrysts resulting in more "free clay" in the soil matrix within the rock piles.

The results of the clay mineralogy analyses indicates that the types and abundances of clay types within the GHN rock pile are indicative of the hydrothermal alteration to the host rock type prior to emplacement in the pile. Within the rock piles, yellow-orange to brown oxidized zones (most common on the outer units) contain more abundant kaolinite and mixed-layer smectite (Fig. 80), most likely a result of preferential placement. Chlorite is of greater abundance within darker brown to gray units more common to the interior of the rock piles (Fig. 80). The abundance of QSP altered rhyolite (Amalia Tuff) rock fragments correlates to a higher

abundance of illite, kaolinite, and minor smectite; whereas a higher abundance of propyllitically-altered andesite correlates to a higher abundance of chlorite, illite, kaolinite, and smectite.

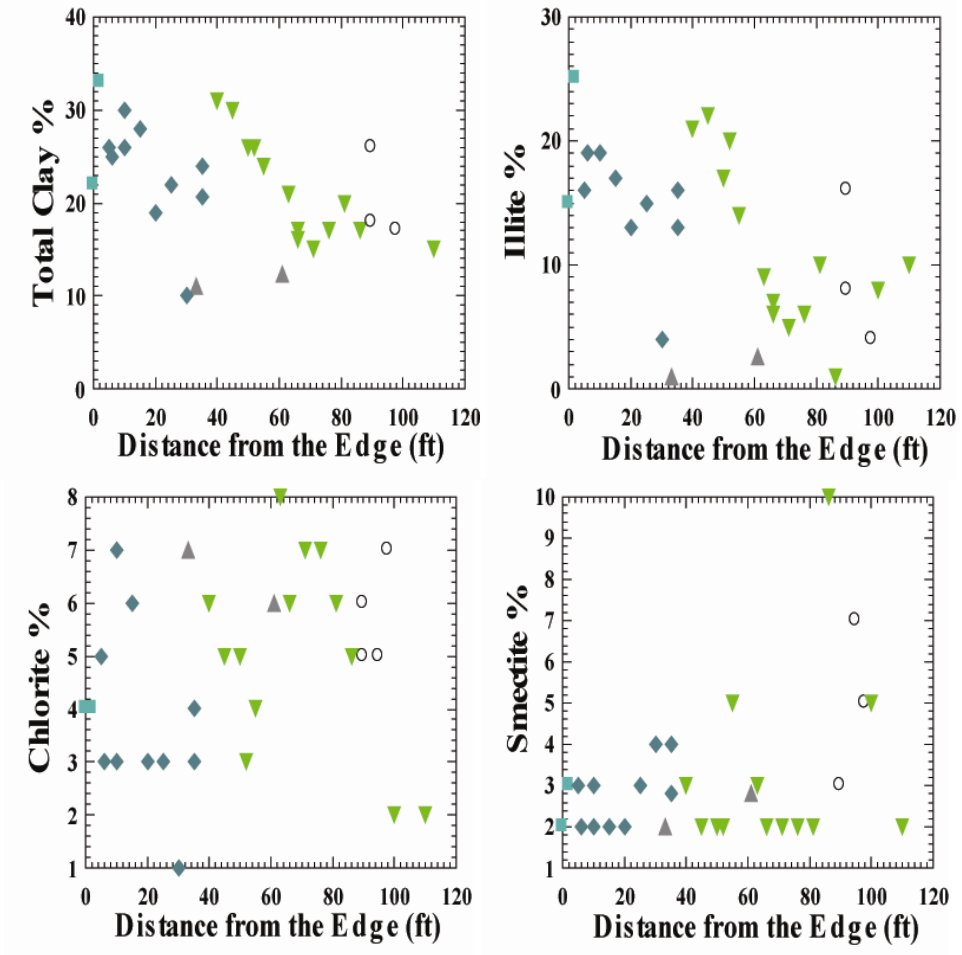

FIGURE 80. Variations of clay minerals along bench 9, GHN. Mineralogy is determined from the modified ModAn method of samples that included both rock fragments and soil matrix (McLemore et al., 2009b). See Figure 43 for geologic cross section and Table 20 for description of geologic units.

Clay types and abundances

Twenty-one samples taken along bench 9 of trench LFG-006 were analyzed for relative abundances of clay minerals (Figs. 81, 82). The inner layers of the rock pile are darker in color and contain more abundant chlorite and smectite. Very few samples from the GHN rock pile contain abundant kaolinite. Soil petrographic analyses for lithology and alteration types from bench 9 were compared to the relative clay mineral types and abundances determined by XRD for the same samples on bench 9 (Figs. 81, 82). The results indicate that the relative abundances of the clay minerals are most likely controlled by the host rock lithology and hydrothermal alteration. Samples with higher percentages of propylitically altered andesite typically have higher amounts of chlorite, while samples with higher percentages of QSP altered rhyolite (Amalia Tuff) have higher amounts of illite and smectite (Figs. 81, 82).

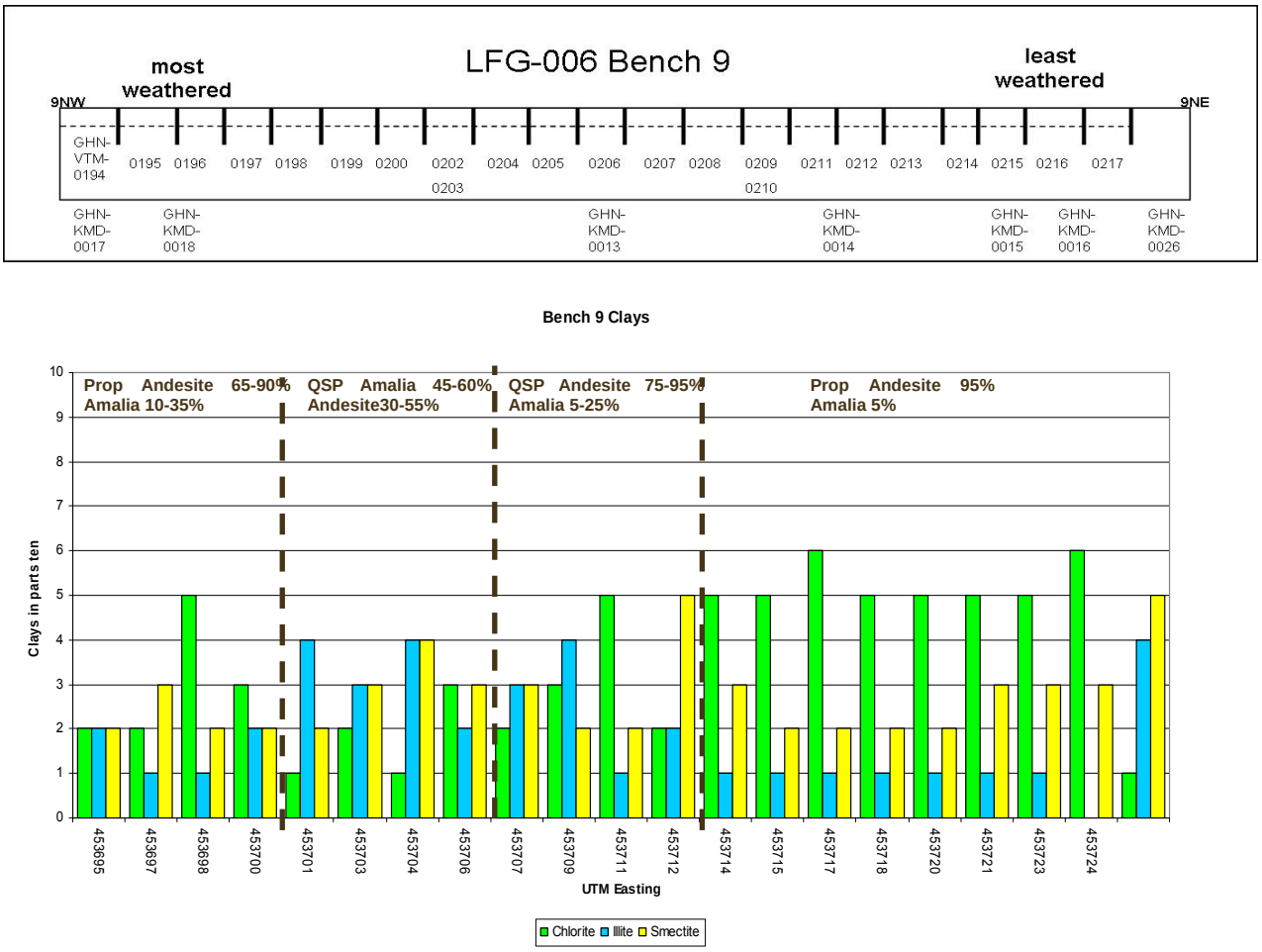

FIGURE 81. The relative clay abundances of chlorite, illite and smectite for bench 9 samples, GHN. Only the soil matrix was analyzed for clay minerals. The major host rock lithologies and hydrothermal alteration type (prop = prophylitic, QSP = quartz-sericite-pyrite) are from soil petrographic descriptions of rock fragments within the samples from bench 9. Sample numbers are located in the scaled figure representing bench 9.

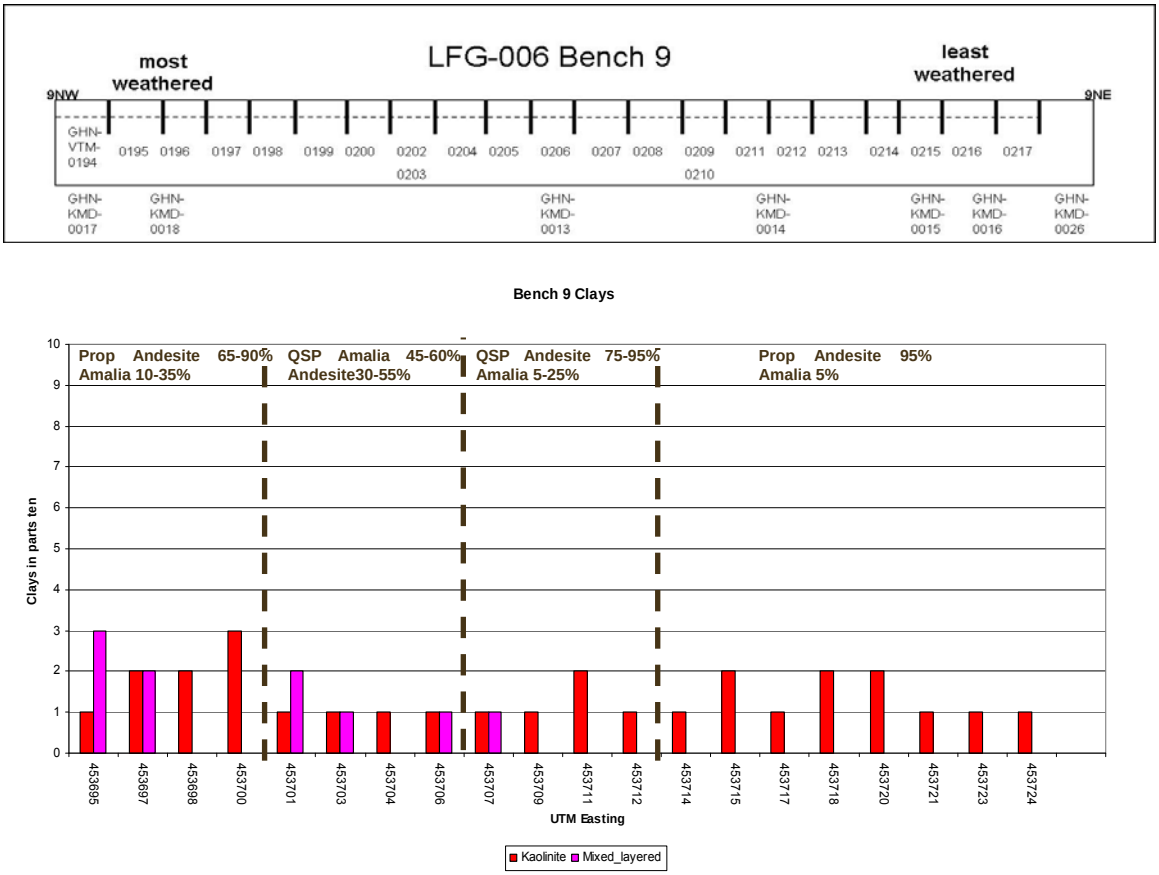

FIGURE 82. The relative clay abundances of kaolinite and random mixed-layer clays for bench 9 samples (GHN). Only the soil matrix was analyzed for clay minerals. The major host rock lithologies and hydrothermal alteration type (prop = prophylitic, QSP = quartz-sericite-pyrite) are from soil petrographic descriptions of rock fragments within the samples from bench 9. Sample numbers are located in the scaled figure representing bench 9.

The XRD results for Goathill North samples indicate that illite, chlorite, smectite and kaolinite clay minerals found in the fine-grained soil matrix also can be found in the rock fragments (Fig. 83). The XRD scans for the Goathill North samples can be grouped together into two general groups of samples based on the relative abundances of illite and chlorite from XRD analysis. The fine-grained soil matrix samples with high relative abundances of illite and low relative abundances of chlorite are from geologic units that contain higher percentages of QSP-hydrothermally altered rhyolite rock fragments. The XRD scans of the corresponding rock fragments splits also have high relative abundances of illite. Fine-grained soil matrix samples with higher relative abundances of chlorite are within geologic units that typically contain higher percentages of propyllitically-altered andesite rock fragments.

To identify the effects of weathering on clay abundances, unweathered drill core samples were crushed and analyzed for clay mineralogy to identify the clay types within the bedrock. The results indicate that for each major lithology (Amalia Tuff and andesite), the same clay minerals are present in the rock pile samples as are present in the pre-mining drill core samples. The QSP altered rhyolite (Amalia Tuff) only contains illite and minor amounts of kaolinite. The andesite,

both prophylitic and QSP altered, contains each of the four main clay minerals and random mixed-layer clays. The clay minerals within sample PIT-KMD-0007 (drill core) are mostly illite (sericite) and chlorite. The XRD diffractogram of PIT-KMD-0007 shows the only major clay type is illite with minor chlorite and other minerals such as quartz and gypsum (Fig. 84).

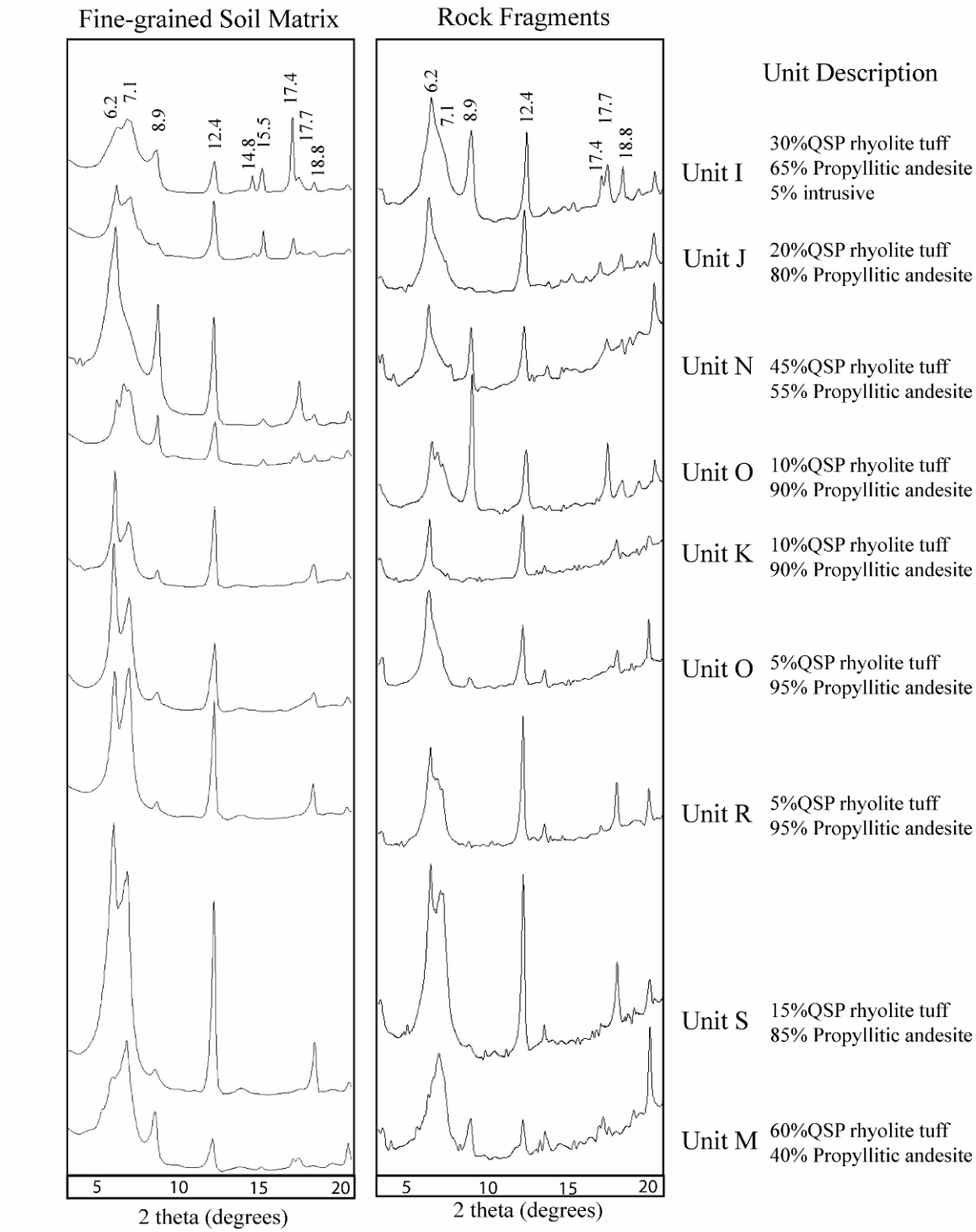

FIGURE 83. X-ray diffraction results of the fine-grained soil matrix and rock fragment samples from bench 9 trench LFG-006 in the Goathill North rock pile. Unit descriptions are of the rock

fragment lithology and dominate hydrothermal-alteration estimated visually using a binocular microscope.

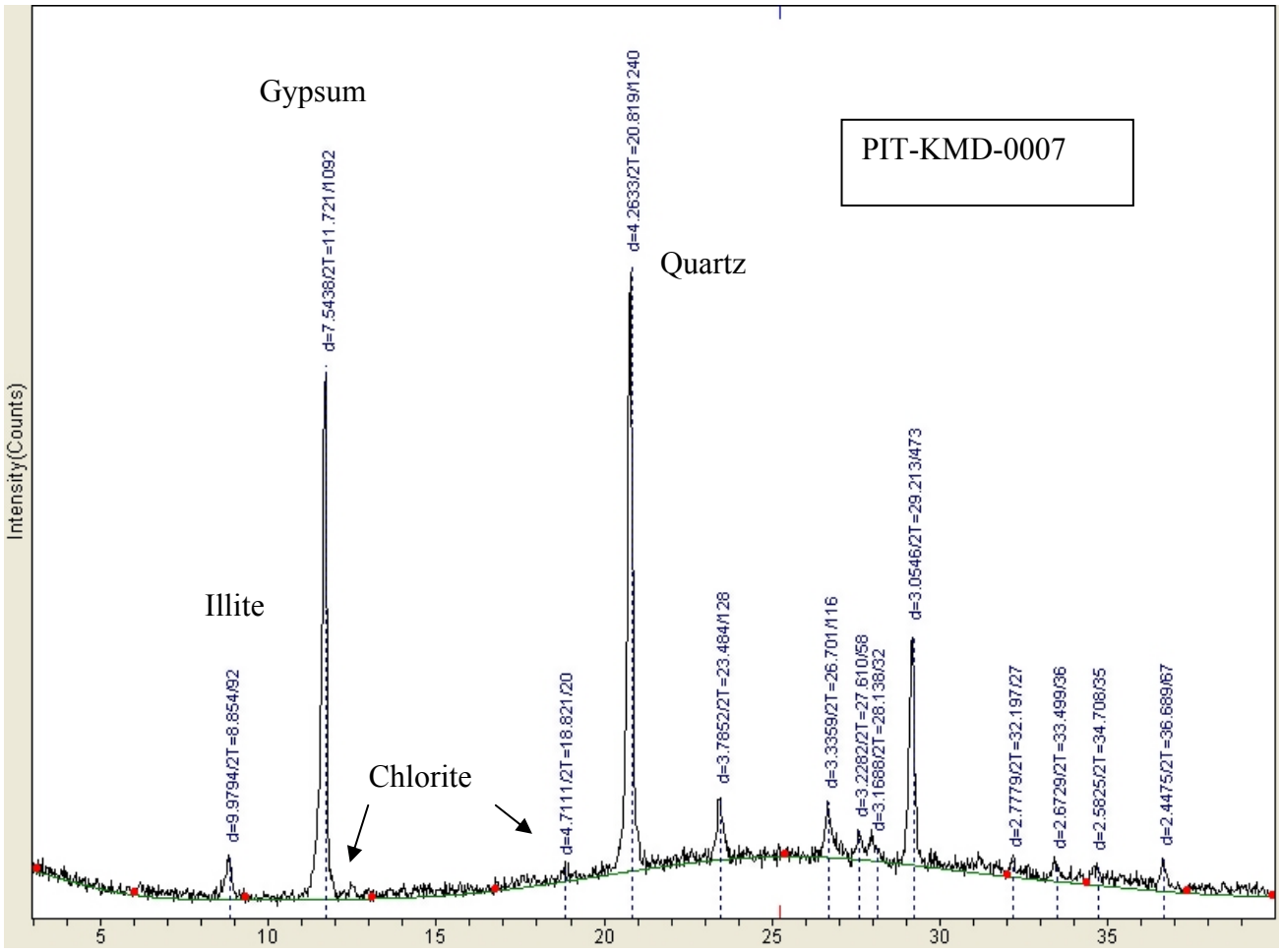

FIGURE 84. X-ray diffractogram of drill core sample PIT-KMD-0007 showing the presence of illite and chlorite with other minerals such as gypsum and quartz. Kaolinite and smectite are minor clay types within this sample.

Clay mineral chemistries

The GHN clay minerals from the fine-grained soil matrix and rock fragments have similar clay mineral chemical compositions and are also chemically similar to the drill core clay minerals (Fig. 85; Table 25). The microprobe beam width during chemical analyses was set between 20-25 µm and is broader than the size of individual clay mineral grains. Therefore the clay minerals chemical analyses could represent a mixture of clay mineral phases particularly for the fine-grained soil matrix samples. The occurrence of Fe-bearing phases such as jarosite or iron-hydroxides mixed within the GHN fine-grained soil matrix samples were noted by analyses with low Al and high Fe content points.

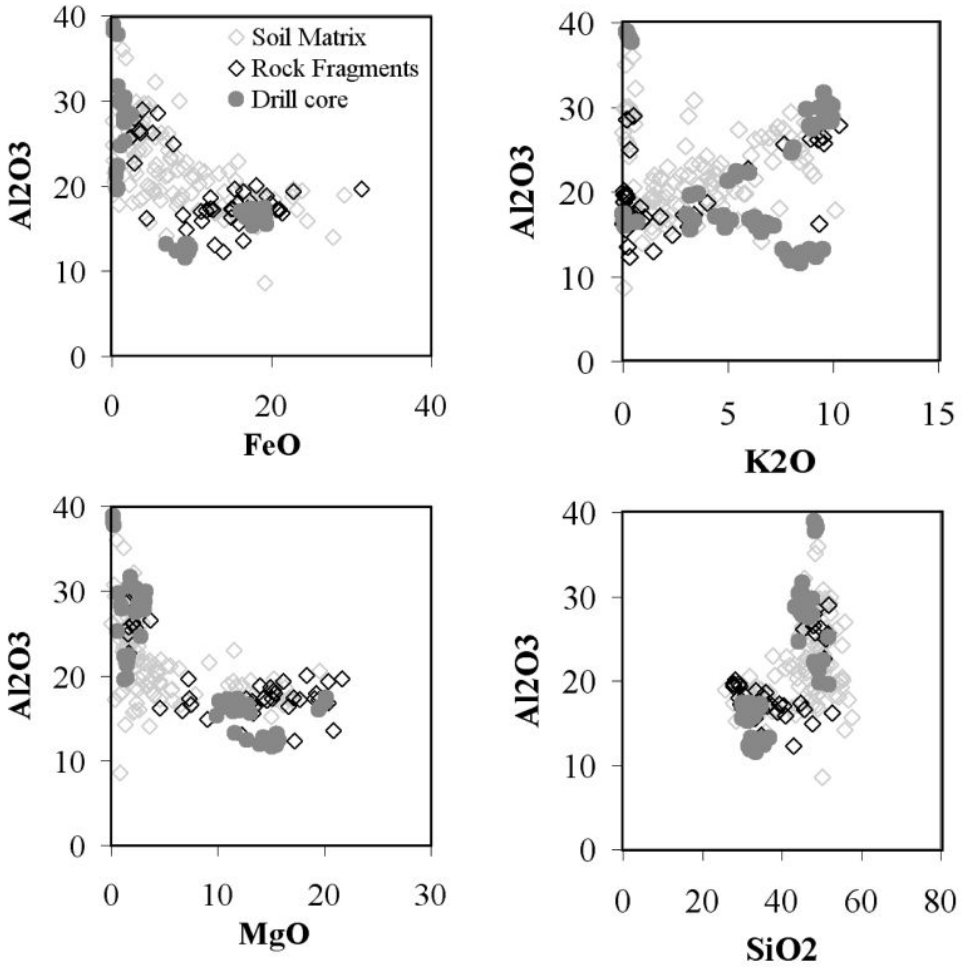

FIGURE 85. Plots of clay mineral chemistries determined using SEM analysis for Goathill North (GHN) fine-grained soil matrix samples (open gray diamond), rock fragments (open black diamonds) and drill core samples (filled gray circles).

Clay textures

The backscattered electron images of the fine-grained soil matrix samples from GHN are characterized by sand to silt-size rock and mineral fragments in a clay-size matrix (Fig. 85). Microprobe analyses of rock fragments within the soil samples indicate clay minerals are replacing primary igneous phenocrysts and groundmass (Fig. 86). The clay minerals within a propyllitically altered andesite drill core sample (Fig. 87; PIT-KMD-0007) are mostly contained within the silicate phenocrysts and not as clay veins or pockets. The contacts around the sand-size rock and mineral grains are sharp and do not indicate the in-situ breakdown of the minerals into the clay-sized matrix. Within GHN fine-grained soil matrix samples untarnished pyrite grains are surrounded by clay-sized material. A likely origin of these clay minerals is that they were released from larger rock fragments during the blasting, transporting, and dumping process.

TABLE 25. Representative clay mineral chemistries determined from SEM quantitative analysis in weight percent. Percentages calculated assuming 12% structural water. QSP = Quartz-sericite-pyrite alteration, Prop = Politic alteration, GHN soil matrix = Goathill North Rock pile fine-grained soil matrix sample, GHN rock frag = Goathill North Rock pile rock fragment sample. Units refer to the geologic units described in Table 20. Scar samples are from the Straight Creek alteration scar profile.

Sample Type	Mineral	SiO_2	TiO_2	Al_2O_3	FeO	MnO	MgO	CaO
QSP drill core	kaolinite	48.57	0.03	38.62	0.18	0.00	0.13	0.06
QSP drill core	illite	44.52	0.19	28.31	2.50	0.07	0.90	0.01
Prop drill core	illite	44.33	0.00	24.67	1.08	0.11	2.75	0.15
Prop drill core	chlorite	35.09	2.23	13.14	9.53	0.53	15.45	0.33
Prop drill core	chlorite	30.17	0.20	16.89	19.09	0.48	20.13	0.34
Overprint drill core	illite	44.89	0.07	29.97	0.84	0.00	3.27	0.16
Overprint drill core	chlorite	32.51	1.64	15.98	17.84	0.22	11.68	0.05
Overprint drill core	smectite	49.47	0.05	19.76	0.73	0.16	1.48	1.69
GHN soil matrix Unit I	illite	55.47	0.11	20.11	2.11	0.10	3.03	0.06
GHN soil matrix Unit I	chlorite + illite	45.99	0.29	22.77	9.34	0.20	2.45	0.20
GHN rock frag Unit I	illite	46.48	0.17	27.43	2.54	0.14	2.63	0.06
GHN rock frag Unit I	chlorite	31.52	0.53	18.94	15.38	0.66	19.48	0.16
GHN soil matrix Unit O	chlorite	27.69	0.58	19.46	23.83	2.15	13.03	0.16
GHN soil matrix Unit O	illite	54.81	0.09	19.24	5.26	0.23	1.69	0.72
GHN rock frag Unit O	chlorite	30.82	0.03	18.38	20.28	1.76	15.05	0.03
GHN rock frag Unit O	illite	49.71	0.18	26.27	5.05	0.04	2.02	0.30
Scar soil matrix	illite	46.05	0.03	27.31	1.58	0.26	6.12	0.09
Scar soil matrix	chlorite	38.82	0.07	23.67	1.37	0.85	18.26	0.02
Scar bedrock	illite	48.61	0.09	29.39	0.06	0.00	1.34	0.19

Sample Type	Mineral	Na_2O	K_2O	P_2O_5	SO_2	Cl	F	Total
QSP drill core	kaolinite	0.02	0.21	0.00	0.02	0.02	0.10	87.96
QSP drill core	illite	0.07	9.90	0.04	0.02	0.02	0.31	86.86
Prop drill core	illite	0.99	8.03	0.02	0.03	0.04	0.20	82.40
Prop drill core	chlorite	0.14	8.86	0.01	0.22	0.07	1.90	87.50
Prop drill core	chlorite	0.03	0.04	0.24	0.07	0.01	0.30	88.00
Overprint drill core	illite	0.34	9.38	0.00	0.00	0.02	0.28	89.22
Overprint drill core	chlorite	0.07	6.78	0.00	0.00	0.21	0.47	87.45
Overprint drill core	smectite	5.21	3.58	0.06	0.03	0.02	0.17	82.41
GHN soil matrix Unit I	illite	0.41	5.30	0.42	0.42	0.07	0.37	87.98
GHN soil matrix Unit I	chlorite + illite	0.10	4.44	0.13	1.24	0.60	0.25	88.00
GHN rock frag Unit I	illite	0.14	7.61	0.30	0.07	0.03	0.39	88.00
GHN rock frag Unit I	chlorite	0.22	0.44	0.12	0.15	0.06	0.35	88.00

Sample Type	Mineral	Na_2O	K_2O	P_2O_5	SO_2	Cl	F	Total
GHN soil matrix Unit O	chlorite	0.11	0.10	0.13	0.08	0.03	0.66	88.00
GHN soil matrix Unit O	illite	0.34	4.52	0.12	0.03	0.79	0.15	87.99
GHN rock frag Unit O	chlorite	0.49	0.45	0.07	0.11	0.02	0.49	88.00
GHN rock frag Unit O	illite	0.04	8.94	0.02	0.03	0.03	0.28	92.91
Scar soil matrix	illite	0.02	5.22	0.65	0.20	0.03	0.45	88.01
Scar soil matrix	chlorite	0.05	3.94	0.18	0.22	0.01	0.56	88.02
Scar bedrock	illite	0.00	7.76	0.00	0.00	0.00	0.48	87.94

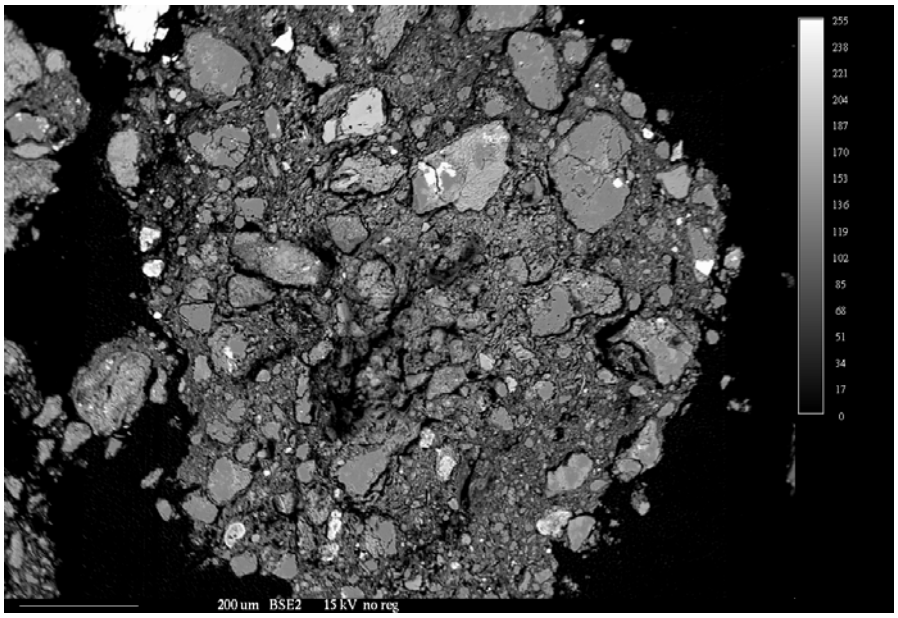

FIGURE 86. Back-scattered electron image of a soil sample (GHN-NWD-0019) showing the abundant clays surrounding rock clasts and mineral grains. The clay minerals are the "felted" looking areas between the smoothly-polished rock and mineral clasts. The brightness scale is relative to the atomic number of the material with the brighter areas representing higher atomic number. Higher magnification image is in Figure 37.

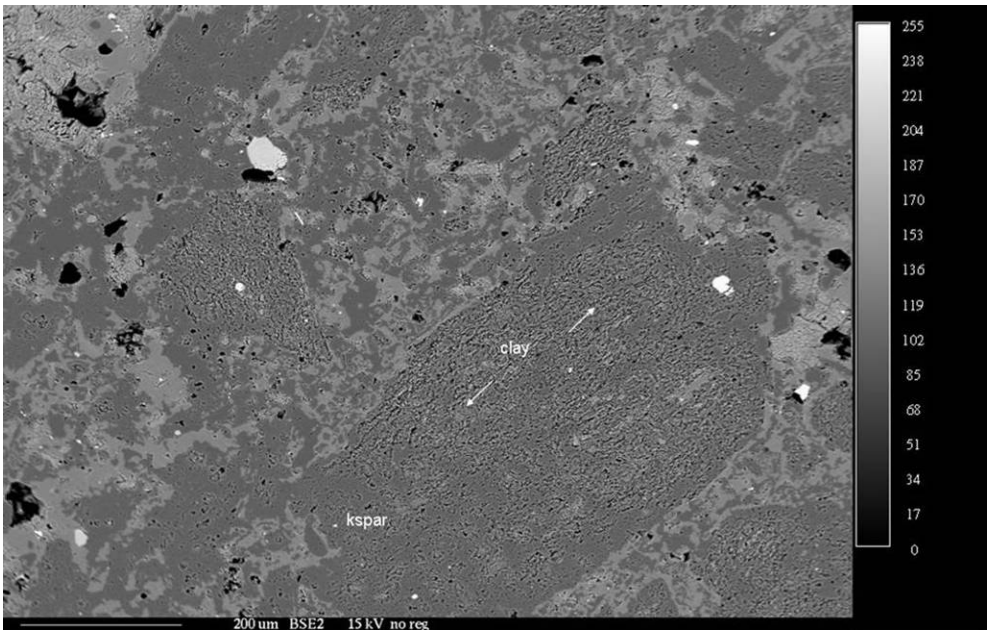

FIGURE 87. Back-scattered electron image of a drill core sample (PIT-KMD-0007) showing clay minerals contained within a feldspar phenocryst. Clays are represented by the rough-appearing areas of the sample surface.

Evidence for weathering of clays

There is evidence to suggest the clay minerals have undergone some degree of weathering at the surface in the GHN rock pile. The 1W smectite clay mineral (~7.1° 2θ) is not found in the drill core samples and also is not as abundant in the rock fragments from GHN, suggesting the formation of the 1W smectite is occurring in the rock pile. An increase in the abundance of 1W smectite can be obtained at temperatures as low as 25°C with almost total dehydration of 2W smectite to 1W smectite occurring at 55°C (Ferrage et al. 2007). Relative humidity also influences the hydration state of smectites (Tamura et al., 2000). The process of smectite dehydration evolves as a two-step process with different thermodynamic thresholds for the transition from 2W-1W smectite and the transition from 1W-0W smectite (Ferrage et al., 2007). The dehydration processes is not congruent and can result in more than one hydration phase being present in a single clay mineral structure (Tamura, et al, 2000; Ferrage et al., 2007). Modeling of samples from GHN indicates the possibility of multiple smectite hydration phases. The high altitude and semi-arid conditions found at the Questa mine could be affecting the smectite hydration state of the clay minerals in the GHN rock pile. Ferrage et al. (2007) noted the dehydration of the smectite clay mineral was reversible up to the energy threshold where the 1W to 0W transition occurs. However the GHN samples did not rehydrate simply by rewetting the clay material during sample preparation. The dehydration of the smectite clay minerals could decrease the smectite clay minerals susceptibility to dissolution at low pH. The dissolution rate of smectite decreases as the number of dehydrated (non-swelling) smectite mineral layers increases (Komdel et al., 1996).

The high abundance of 1W smectite found in the rock fragments of the sample from the innermost unit (Unit M) could be an indication of supergene weathering prior to being placed in the rock pile. The rock pile material closest to the base of the rock pile is the material that was

first stripped off of the open pit deposit and had the highest degrees of supergene alteration. Another possible explanation for the increase in 1W smectites is an increase in the temperature in the rock pile. Other rock piles on the Questa mine site have localized hot zones at various depths due to the exothermic reaction of pyrite oxidation (Norwest Corporation, 2005; Reiter, 2009).

Stable isotopes

Stable isotope analyses of hydrogen and oxygen of clay-mineral separates from rocks throughout the Questa area show that, to the limit of analytical detection, all clay minerals tested are hydrothermal in origin, with minimum temperatures of formation >100ºC (Fig. 88; Graf, 2008). The meteoric water line in Figure 88 depicts the interdependence of H- and O-isotope ratios in meteoric waters on a global scale (Hoefs, 2004), which was first described by Craig (1961). Local meteoric waters can vary locally, but generally fall on or near the meteoric water line. The kaolinite line describes the isotopic composition of kaolinite forming at 20ºC in equilibrium with meteoric waters. This line is plotted using the fractionation factors defined by Sheppard and Gilg (1996). The supergene/hypogene line describe the isotopic composition of kaolinite forming in equilibrium with meteoric water at 35ºC. This line is termed the supergene/hypogene line because 35ºC is the maximum temperature for kaolinite forming at the earth's surface. Samples plotting to the left of this line are termed hypogene because these temperatures are representative of hydrothermal alteration temperatures and not supergene weathering temperatures. The lines showing T=70°C, 100°C and 200°C describe the isotopic composition of a kaolinite forming at these temperatures in equilibrium with meteoric waters.

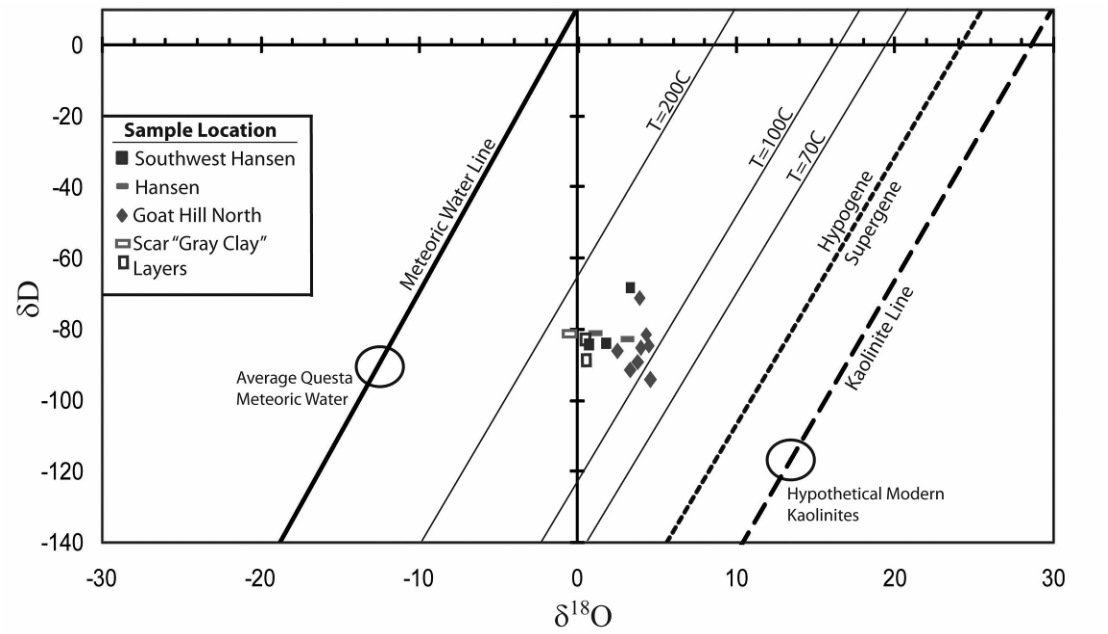

FIGURE 88. δD-δ^{18}O diagram for clay minerals from rock pile and alteration scar. These clays plot in the hypogene field, indicating an origin consistent with hydrothermal alteration. There is no isotopic evidence that clay minerals formed as a result of weathering in either the alteration scars or the rock piles.

Origin of clay minerals

The clay minerals within the fine-grained soil matrix of the GHN rock pile are predominantly of hydrothermal origin and are the result of the liberation from highly fractured mined rock during mining activities and subsequent physical weathering. The majority, if not all of the clay minerals are not formed as the result of chemical precipitation in the rock pile under low pH during weathering over the last 25-40 years, but were formed by hydrothermal alteration of the rocks before mining. There are seven principal lines of evidence that the clays in GHN are predominantly from the hydrothermal alteration of the host lithologies prior to excavation and emplacement in to the GHN rock pile and not formed by weathering (Donahue et al., 2007, 2009):

- Electron microprobe back-scatter (BSE) images of the drill core samples shows evidence of primary igneous minerals being replaced by pre-mining, hydrothermal clay minerals. The contacts between the sand-size rock and mineral grains within the fine-grained soil matrix are sharp and do not indicate the in-situ formation of the clay minerals into the fine-grained soil matrix. There is no petrographic, mineralogic, or isotopic evidence for formation of new clay minerals by chemical weathering in either the rock piles or in the natural analog materials. Isotopic evidence does suggest some alteration of the clay minerals during weathering, but not the formation of new minerals.
- Presence of fresh or lightly tarnished pyrite sounded by clay minerals (Heizler et al., 2007).
- The GHN clay minerals from the fine-grained soil matrix and rock fragments have similar clay mineral chemical compositions and are chemically similar to the clay minerals within the unweathered drill core.
- The unweathered drill core and samples from GHN have similar types and abundances of clay mineral groups based on XRD analyses. Chemical analyses from electron microprobe analysis reveal similar chemical compositions for the clays from the two environments (unweathered drill core versus weathered GHN rock pile material).
- Stable isotope analyses of hydrogen and oxygen of clay mineral separates from rocks throughout the area show that, to the limit of analytical detection, all clay minerals are hydrothermal in origin, with minimum temperatures of formation >100ºC (Fig. 6; Graf, 2008).
- Pre-mining hydrothermal clays will dissolve in a sulfuric acid environment (Donahue, 2008).
- Persistence of $2M_1$ illite and pyrophyllite in the alteration scars and fine-grained soil matrix indicates the hydrothermal clay minerals predominate in the fine-grained soil matrix.
- Tritium isotopic values from porewater, interlayer water, and structural hydroxyl sites of the clay minerals are consistent with pre-mining hydrothermal origin of the clay minerals and not with modern formation of clay minerals by weathering (Marston, 2009).

During physical weathering in the rock pile, the rock clasts are broken down, releasing more hydrothermal clay minerals into the matrix as well as reducing the particle size to clay-sized particles of other minerals, such as quartz and feldspar. The mechanical particle size reduction from mining activities can release the clays contained within the silicate phenocrysts resulting in more “free clay” within the rock piles. Geotechnical testing of the rock fragments within the GHN rock pile indicate the rock fragments are highly durable (discussed below; Viterbo, 2007; Viterbo et al., 2007).

There is no conclusive evidence to suggest there are clay minerals forming today in the rock pile from the weathering of feldspars or other minerals in the GHN rock pile since its emplacement. Weathering of feldspars is relatively slow and requires abundant acidic water; feldspars will not oxidize in humid air as pyrite does (Perkins et al., 1995). The possibility of an increase in clay mineral percentage due only to chemical weathering in the rock pile is very low. It is possible that neoformation of clay minerals due to the dissolution of silicate minerals is occurring in the rock pile. However, if new clay minerals are forming, it is in such small amounts that the techniques used for this study cannot distinguish the newly formed clay minerals from the hydrothermal clay minerals. The persistence of hydrothermal clay minerals, such as $2M_1$ illite and pyrophyllite, in the alteration scars indicates that even on long-term weathering scales, new clay minerals do not appear to be forming in detectable abundances. However, in the future clay minerals can be produced from such mineral weathering in the presence of water. Clay minerals can weather faster than the feldspars (Perkins et al., 1995) and could in effect be releasing some of the elements observed in the waters draining from the rock piles.

CHEMISTRY

The whole-rock chemical composition reflects the mineralogy of the sample (Table 21), which is controlled by the lithology, hydrothermal alteration, and weathering. Linear trends with strong correlations in the scatter plots (Figs. 89-90) are not always observed, because the samples are a mixture of andesite and rhyolite with different degrees of hydrothermal alteration and weathering, all of which have varying chemical signatures. However, some trends can be defined.

Several chemical elements show similar trends with mineralogy across bench 9, GHN. CaO and Sr, components of calcite (Table 20), increase in concentration across bench 9 (Fig. 89), similar to the increasing trend in calcite (Fig. 40). K_2O decreases across bench 9 (Fig. 89) and reflects a similar decrease in illite and K-plagioclase across bench 9 (Fig. 40, 90). MgO increases across bench 9 (Fig. 89), reflecting the increase in epidote across bench 9 (Fig. 40). K-feldspar and Al_2O_3 show little change across bench 9 (Fig. 90), whereas plagioclase and Na_2O shows a minor increase in concentration across bench 9. Many of the major minerals in GHN contain Al_2O_3 (Appendix 7). SO_4 decreases across bench 9 and all samples in GHN (Fig. 91), reflecting the decrease in authigenic gypsum (Fig. 64) and jarosie+copiapite (Fig. 44) across GHN, which are indications of weathering across GHN.

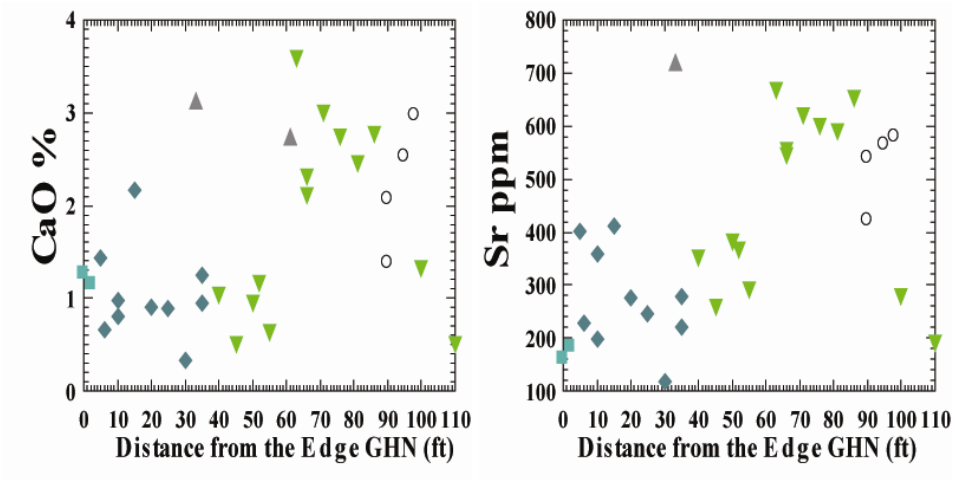

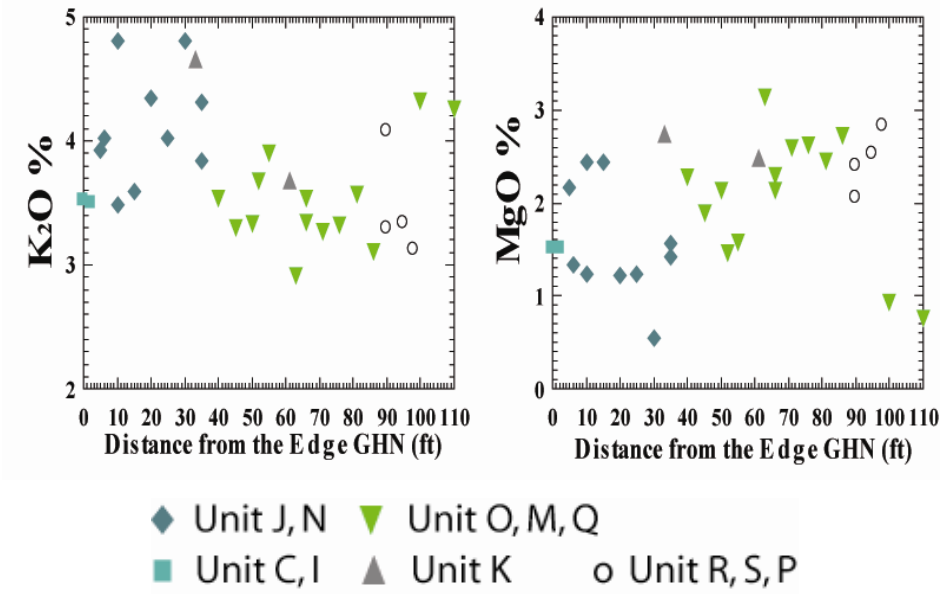

FIGURE 89. Variations of CaO, Sr, K_2O and MgO across bench 9, GHN. These trends are similar to trends in calcite, illite, and epidote across GHN (Fig. 40). Refer to Figure 43 for geologic cross section and Table 20 for descriptions of the geologic units.

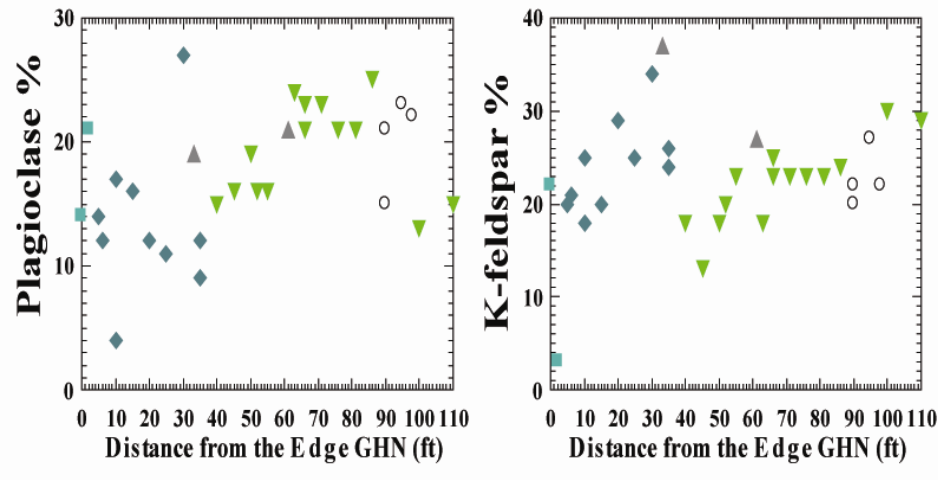

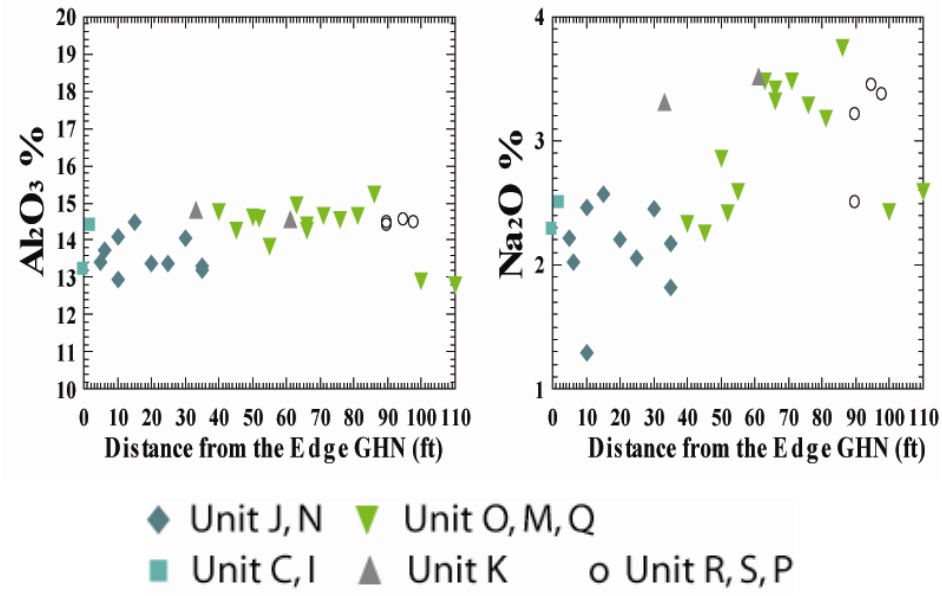

FIGURE 90. Variations in plagioclase, K-feldspar, Al_2O_3 and Na_2O across bench 9, GHN. Refer to Figure 43 for geologic cross section and Table 20 for descriptions of the geologic units.

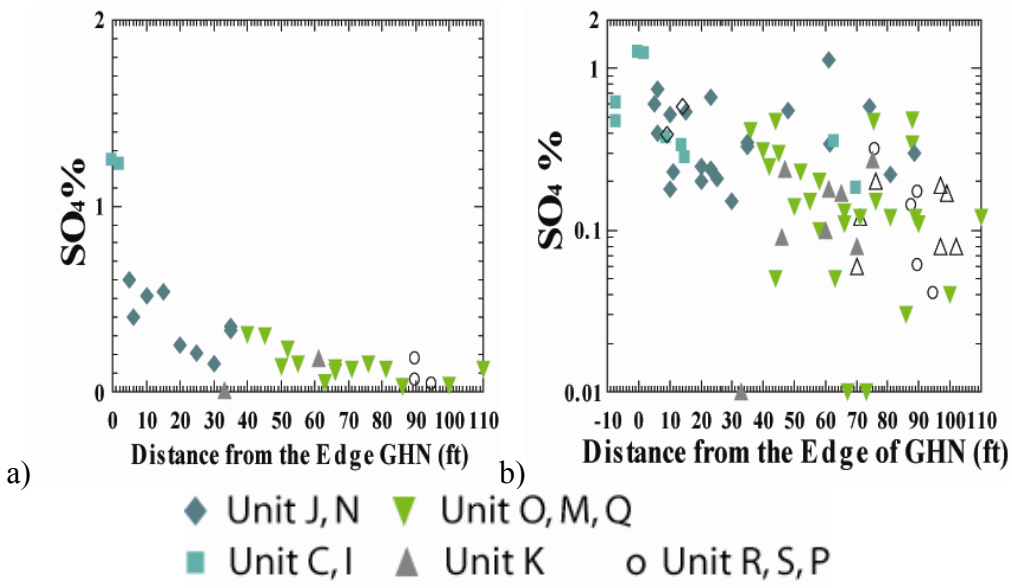

FIGURE 91. Variations in SO_4 across a) bench 9 and b) all samples from GHN. Refer to Figure 43 for geologic cross section and Table 20 for descriptions of the geologic units.

PASTE TESTS

Paste pH and paste conductivity are another indication of oxidation and weathering used in this project, but they have limitations as well. Paste pH and paste conductivity are the pH and conductivity measured on a paste or slurry that forms upon mixing soil material and deionized water. A known volume of deionized water is added to a known mass, or volume, of soil and stirred to form the paste. A calibrated pH meter with an electrode is used to measure the paste pH and conductivity. Paste pH is a simple test used to assess the presence of soluble acid salts. The primary controls of paste pH are sulfide amount and distribution and carbonate amount and

distribution (Borden, 2001). In an acidic material, such as the pyrite-bearing rock piles at the Questa mine, paste pH is an approximate measurement of the acidity of a soil material that is produced by the oxidation of pyrite and other sulfides at the time of measurement. Six common variables that affect the measurement of paste pH and conductivity are 1) the dryness of the sample before testing, 2) the soil:water ratio used, 3) soluble salts content, 4) seasonally influenced carbon-dioxide content, 5) the size of the soil particles, and 6) electrode junction potential (Price et al., 1997; Haby et al., 1997). Many of these can be controlled by applying rigorous testing procedures and the same equipment for the measurements. The four weathering factors that affect the paste pH and conductivity of a material are 1) sulfide texture, concentration and distribution of sulfur, 2) surface age, and 3) calcite concentration and distribution (Borden, 2001; Weber et al., 2004). Sulfides in the soil matrix that are readily available to water tend to react faster than sulfides within rock fragments. Paste pH and conductivity is not always indicative of in-situ weathering, because the minerals that control the paste pH and conductivity could have formed elsewhere in the rock pile.

Paste pH and conductivity were determined on most samples collected from the trenches within the GHN rock pile and other Questa materials. Samples tested consist of a mixture of rock fragments (1 ft to <1 mm in diameter) and soil matrix. Some samples were grab samples of a particular layer and other samples were channel samples collected every 5 ft within a particular layer. Most samples were collected from the trenches in the upper half of the GHN rock pile (Fig. 23). Appendices 5 and 6 contain logs of the individual trenches and drill holes with their distribution of paste pH for the stable portion of GHN.

Results of paste pH and paste conductivity are summarized in Table 26 and Figures 92-99. In the unstable portion, the pH is generally lower and persists throughout the whole thickness of the rock pile except for the lower part where there are a few high pH values (Tachie-Menson, 2006). The sliding movement of the rock pile has contributed to increased permeability that resulted in periodic oxidation of the unstable portion of GHN. These results indicate that generally, the stable portion of GHN had higher paste pH and conductivity than the unstable portion, which is consistent with the hypothesis that humid air circulation was more prevalent in the unstable rock pile compared to the stable rock pile. Similar paste pH values have been reported from other mine sites that are similar to the Questa rock-pile materials (Borden, 2001).

In the stable portion of GHN, the lowest pH values are found in Units A to H at the surface; Units I, J, and N, near the face; and Units M, T and V near the base of the pile (Figs. 92, 93; Table 26). Typically, paste pH increased with distance from the outer, oxidized units (west) towards the interior units (east) of the stable portion of GHN rock pile (Figs. 92, 93; Phillips, et al. 2005). A low paste pH (2-3) along with yellow to orange color and the presence of jarosite, gypsum, and low abundance to absence of calcite is consistent with oxidized conditions in the Questa rock piles. A high paste pH (>5) along with the darker colors and locally the presence of calcite, epidote, and chlorite indicates relatively little oxidation of the rock-pile material (McLemore et al., 2006a, b). This oxidation can be a result of both pre-mining hydrothermal alteration (i.e. pre-rock pile emplacement) as well as post-mining weathering (i.e. rock pile emplacement) in the rock pile. Paste conductivity is not clearly linked to the units.

Low paste pH samples (more oxidized) have low FeO (as total Fe), MgO, CaO, and P_2O_5 than high paste pH samples (less oxidized, Fig. 99). This suggests that paste pH is controlled not only by carbonate and sulfate minerals, but also by other minerals.

TABLE 26. Descriptive statistics of paste pH by geologic unit (updated from McLemore et al., 2005, 2006a, b; Tachie-Menson, 2006). Descriptions of geologic units are in Table 20. Details of the statistics are in Appendix 11.

Unit	Mean	Median	Standard Deviation	Standard Error	Minimum	Maximum	Number of Cases
traffic	4.4	4.3	1.0	0.18	2.5	6.1	29
unit C	2.9	2.9	0.4	0.08	2.3	3.5	20
unit I	3.1	3.0	0.7	0.13	2.2	4.8	31
unit J	3.4	3.2	0.7	0.10	2.1	5.8	56
unit N	3.5	3.5	0.6	0.07	2.2	5.5	74
unit K	4.8	4.3	1.5	0.3	2.4	7.2	36
unit L	6.9	7	1.2	0.4	4.8	8.7	12
unit M	4.5	4.3	1.5	0.2	2.4	9.6	71
unit O	5.4	5.2	1.7	0.1	2.4	9.4	182
unit Q	5.4	5.6	0.7	0.4	4.6	5.8	3
unit P	5.9						1
unit R	6.1	6.7	1.9	0.5	3.2	9.6	17
unit S	6.2	6.4	2.1	0.4	2.5	9.8	22
unit T	4.2	4.2	0.3	0.1	4.0	4.8	6
unit U	3.9	3.9	0.9	0.2	2.5	5.5	17
unit V	4.4	4.4	0.6	0.2	3.4	5.8	11
unit W	6.6						2
Unit RUB (rubble zone)	3.7	3.6	1.1	0.2	2.4	8.6	42
colluvium	3.8	3.3	1.3	0.1	2.4	8.6	45
bedrock	4.1	3.3	1.9	0.3	1.8	9.6	36
Entire GHN	4.5	4.1	1.6	0.1	2.1	9.8	641

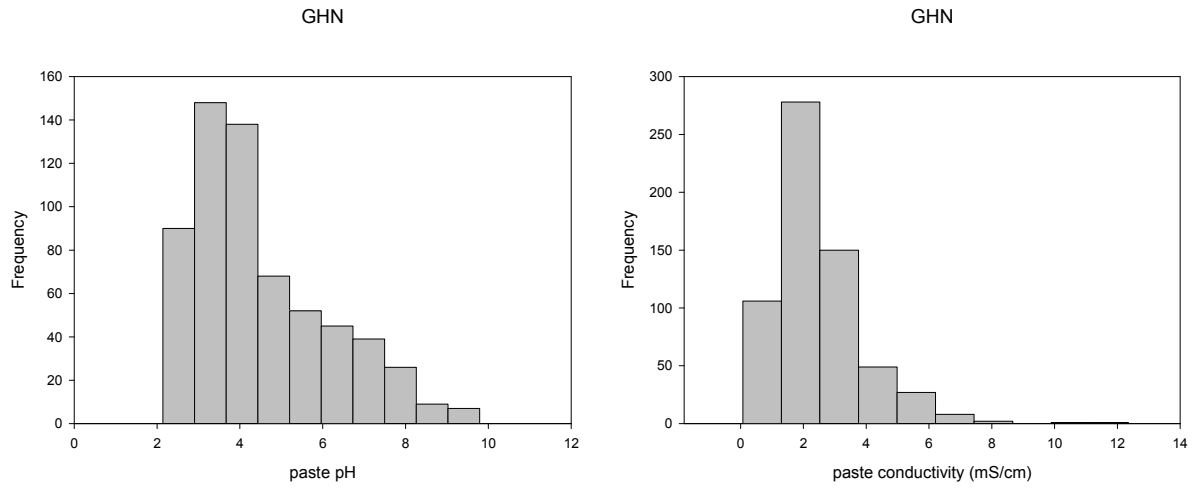

FIGURE 92. Histogram of paste pH and paste conductivity for samples from the stable portion of GHN. Summary statistics are in Table 26. Additional histograms by unit are in Appendix 11. n=641

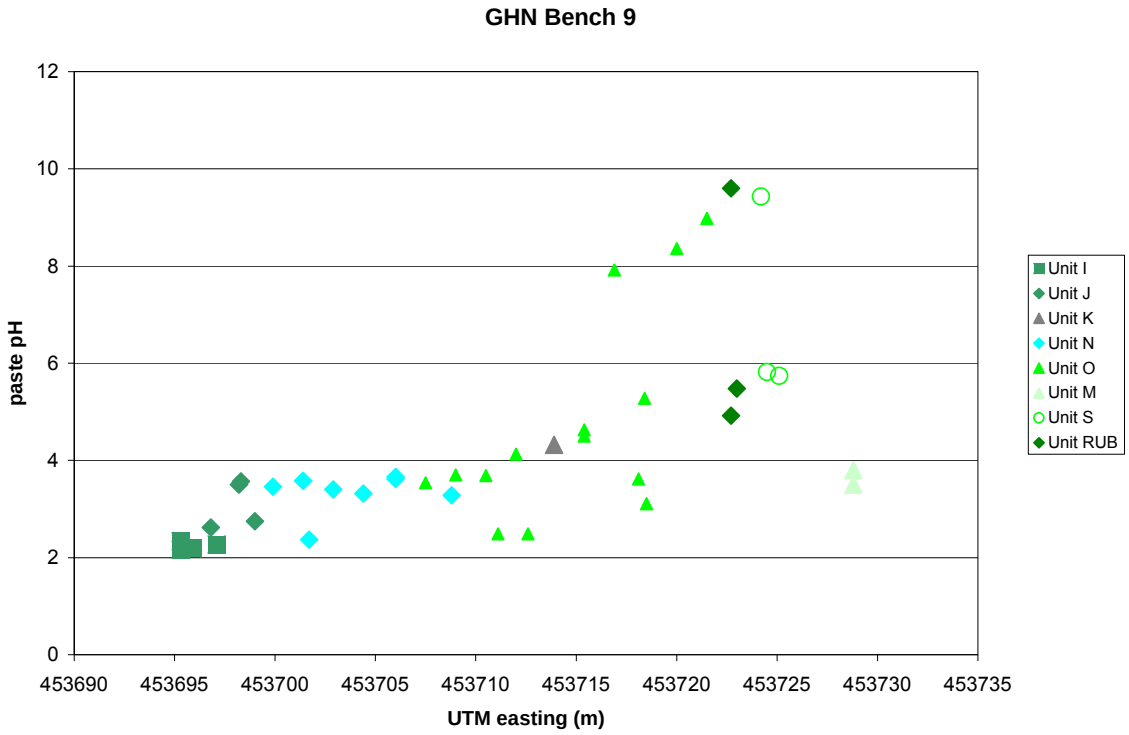

FIGURE 93. Paste pH across bench 9, trench LFG-006. Symbols in the graph refer to geologic units in Table 20 and Figure 43. This graph indicates an increase in paste pH from the outer, oxidized units towards the less weathered, interior of the rock pile.

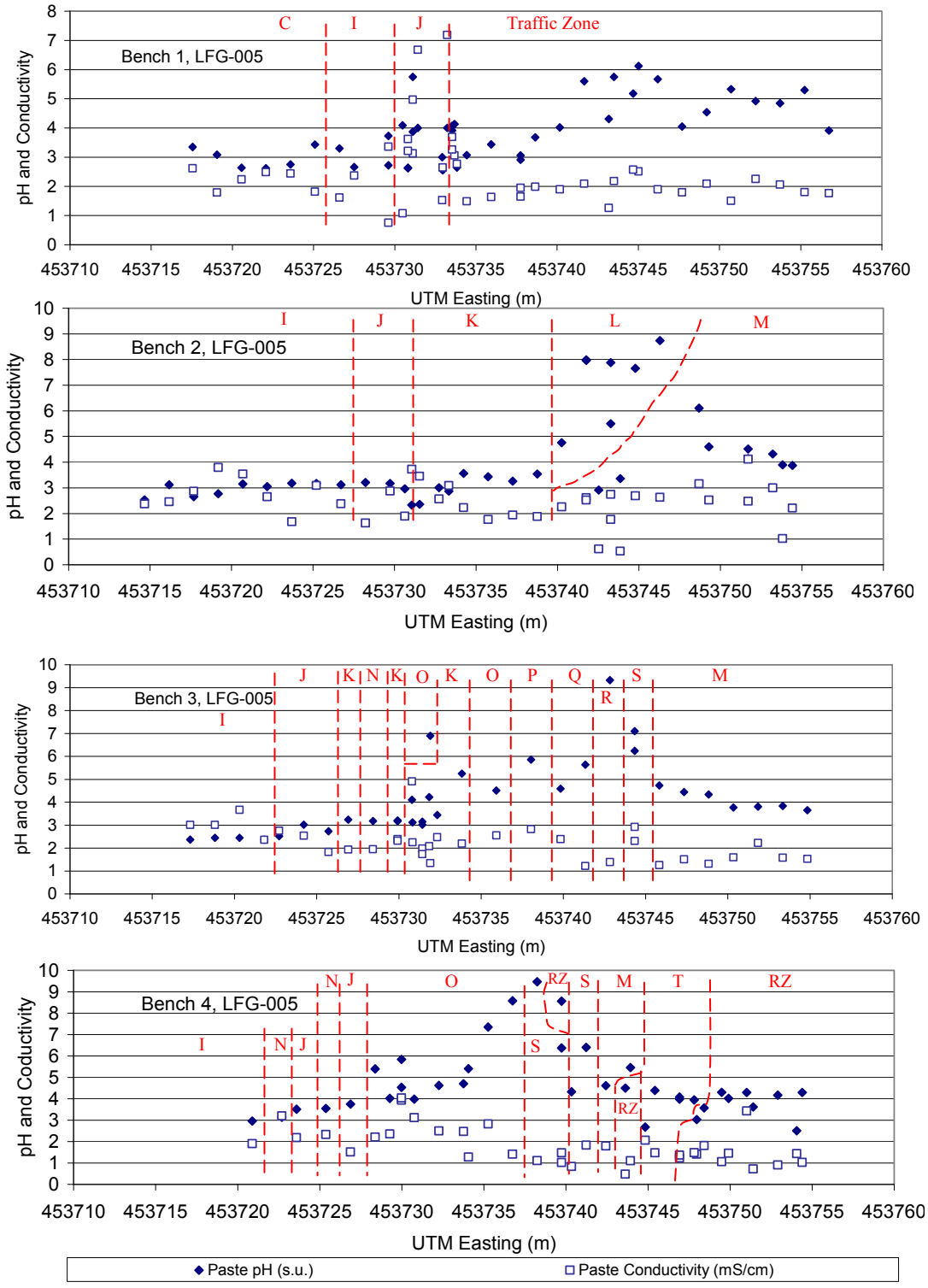

FIGURE 94. Plots of paste pH and paste conductivity along benches in Trench LFG-005. The red dotted lines and labels represent geologic units. RZ = rubble zone. The outer (C, I, J, and N) and basal (T, M and RZ) units have the lowest pH. The middle units (e.g. K, L, S and O) have the highest pH, although O is quite variable. Paste conductivity is not clearly linked to the units.

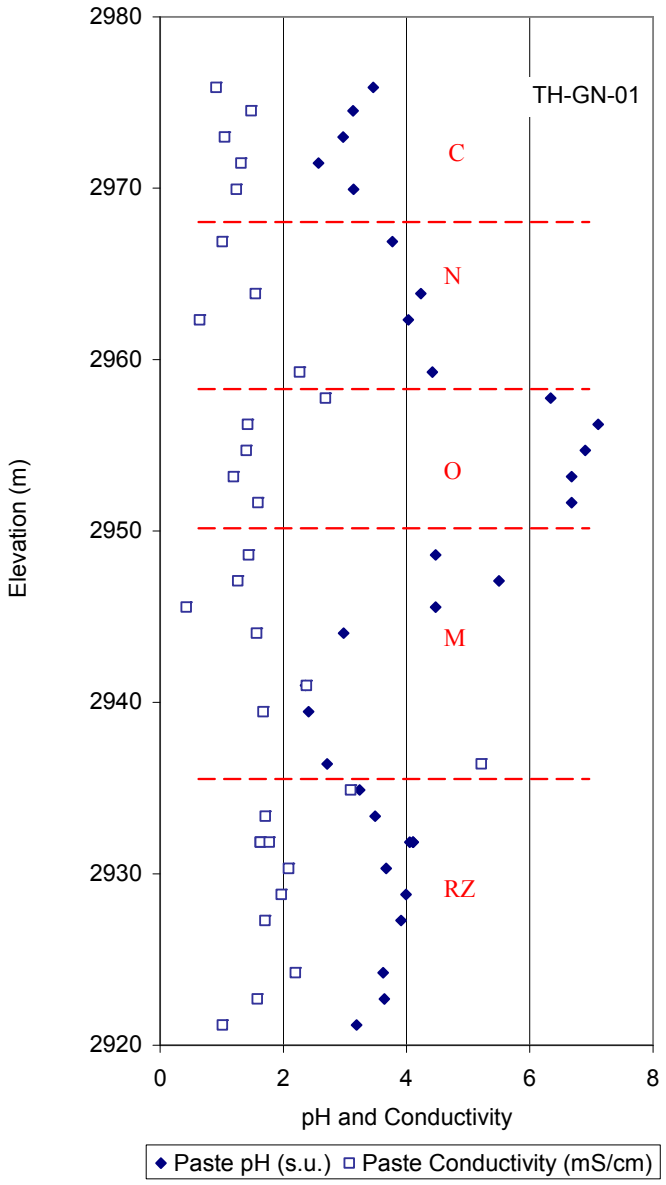

FIGURE 95. Plot of paste pH and paste conductivity down drill hole TH-GN-01. The red dotted lines and labels represent geologic units. RZ = rubble zone. The outer units (C and N) and basal units (M and RZ) have the lowest pH. Unit O in the middle has the highest pH. Paste conductivity does not change significantly from unit to unit.

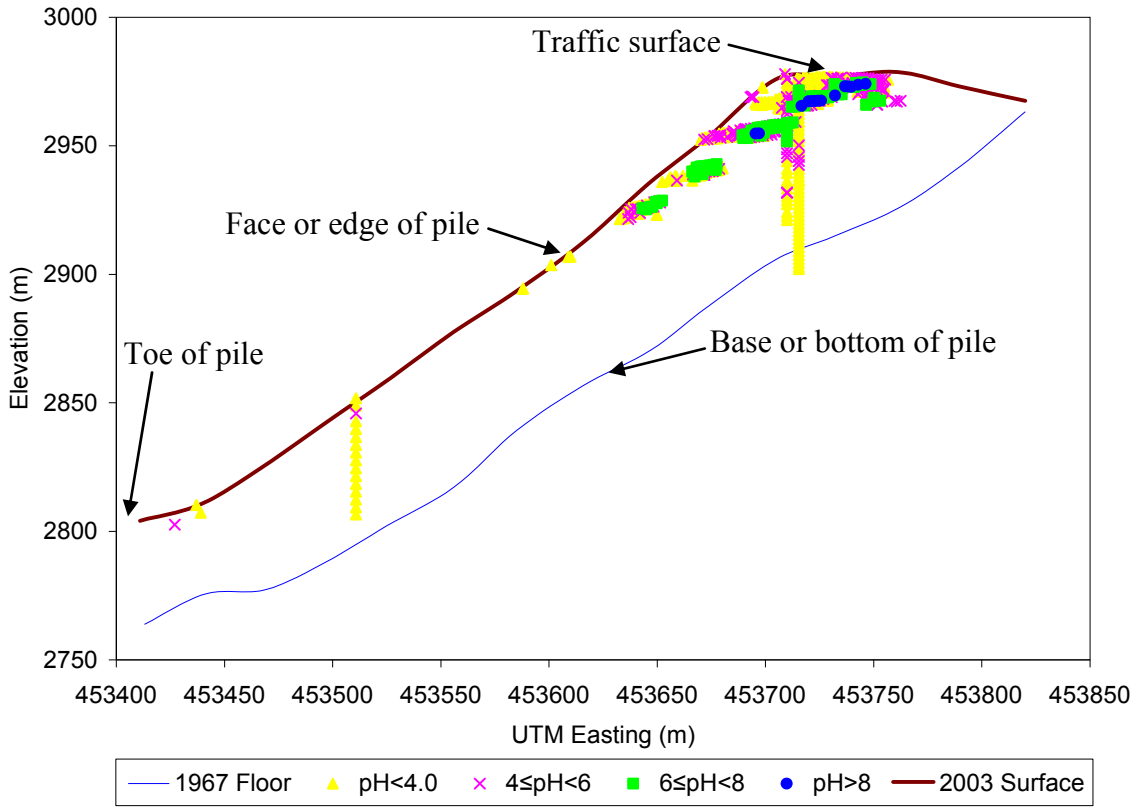

FIGURE 96. Longitudinal cross-section through the stable portion of GHN rock pile showing samples with different ranges of paste pH. The two continuous lines represent the surface and bottom of the stable portion of the pile as determined from 2003 and 1967 contour maps, respectively. The plot shows that there is a high pH zone below the traffic surface and subparallel to the pile face. The high pH zone is sandwiched between two low pH zones, one close to the surface and the other close to the base. The concentration of high pH samples decreased with decreasing elevation from the top of the pile down.

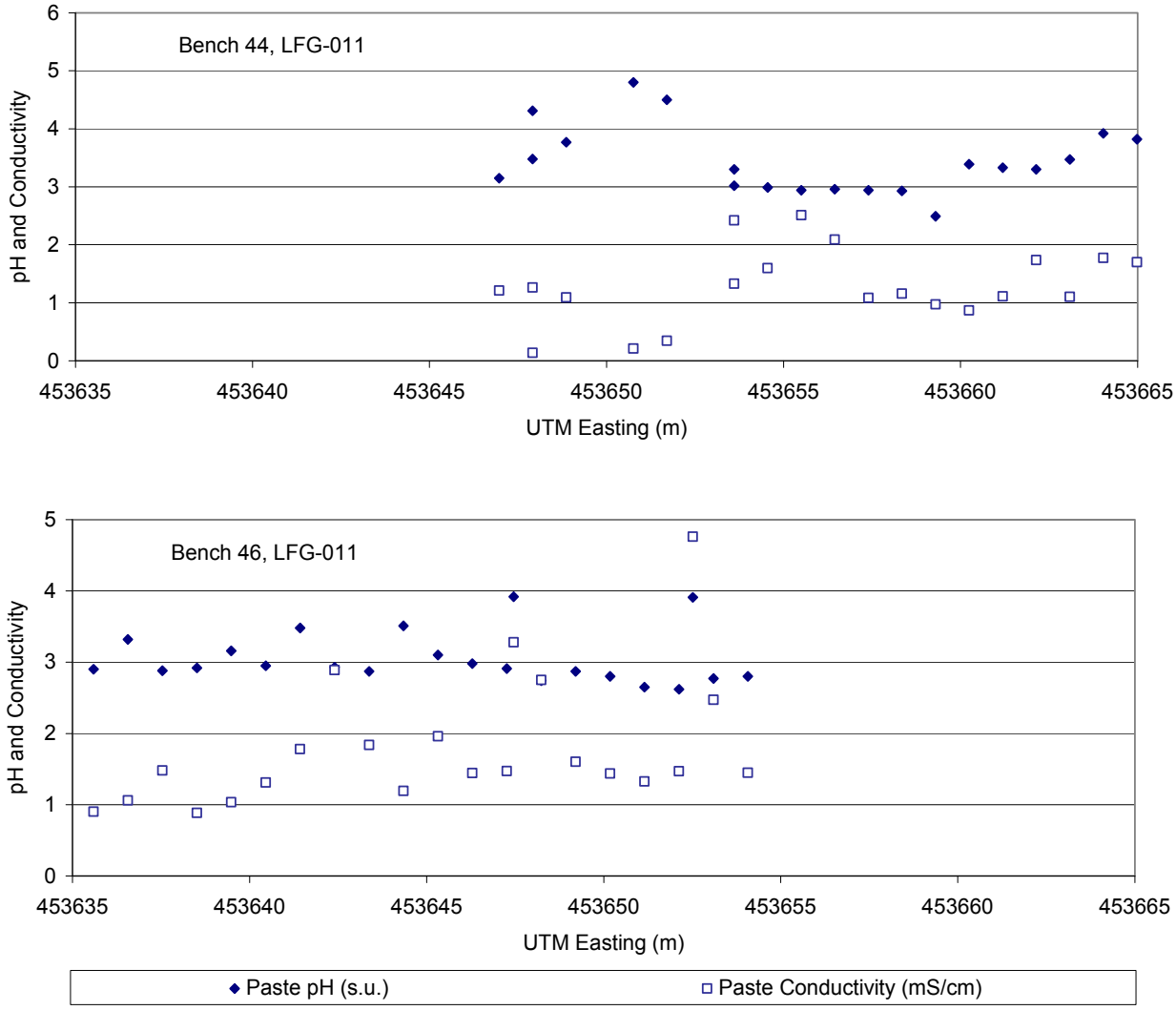

FIGURE 97. Plots of paste pH and paste conductivity along benches in Trench LFG-011 in the unstable portion of GHN rock pile. The pH values are mostly less than 4.0 and do not show any correlation to distance from the edge of the pile.

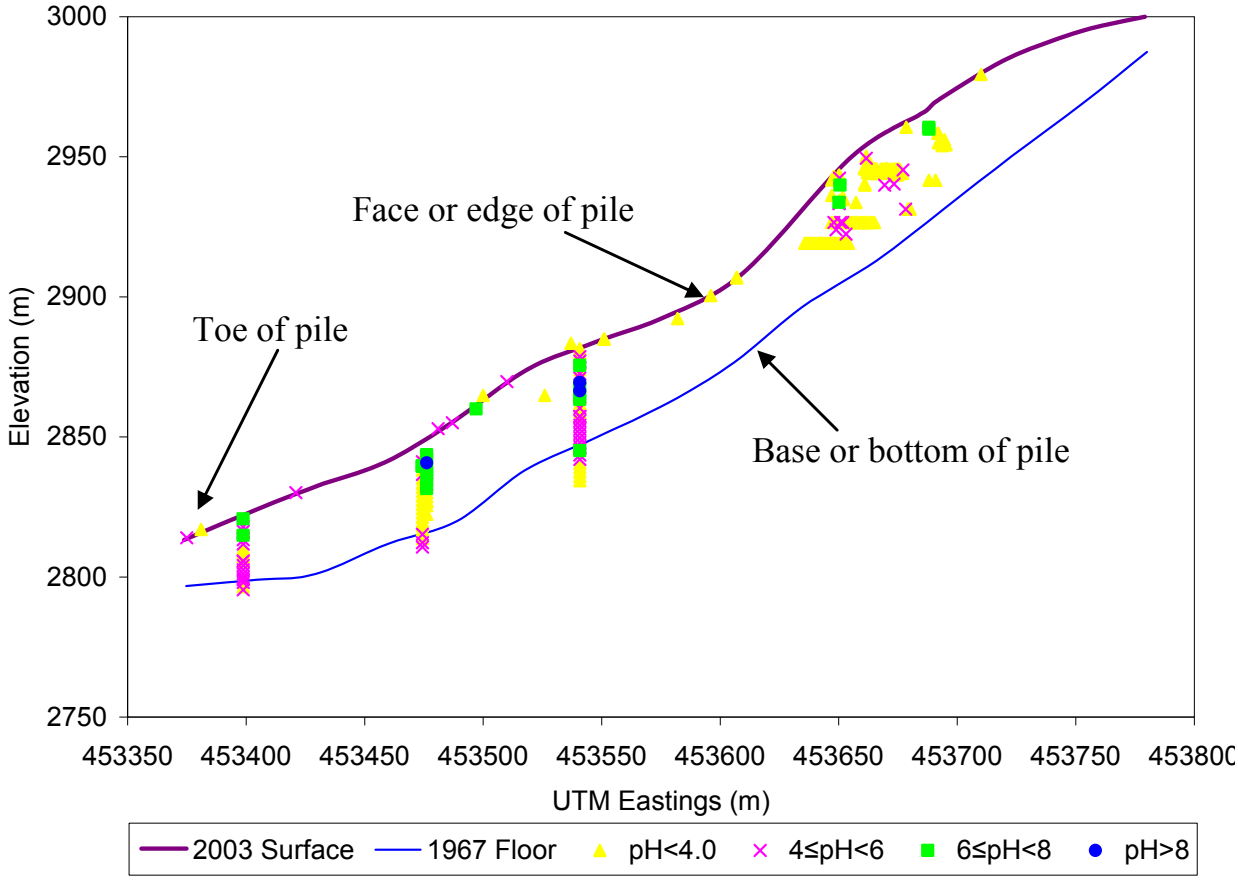

FIGURE 98. Longitudinal cross-section through unstable portion of GHN rock pile showing samples with different ranges of paste pH. The two continuous lines represent the surface and bottom of the unstable portion of the pile as determined from 2003 and 1967 contour maps, respectively. Generally, the samples in the upper part of the rock pile have lower paste pH values than those in the boreholes at the lower part.

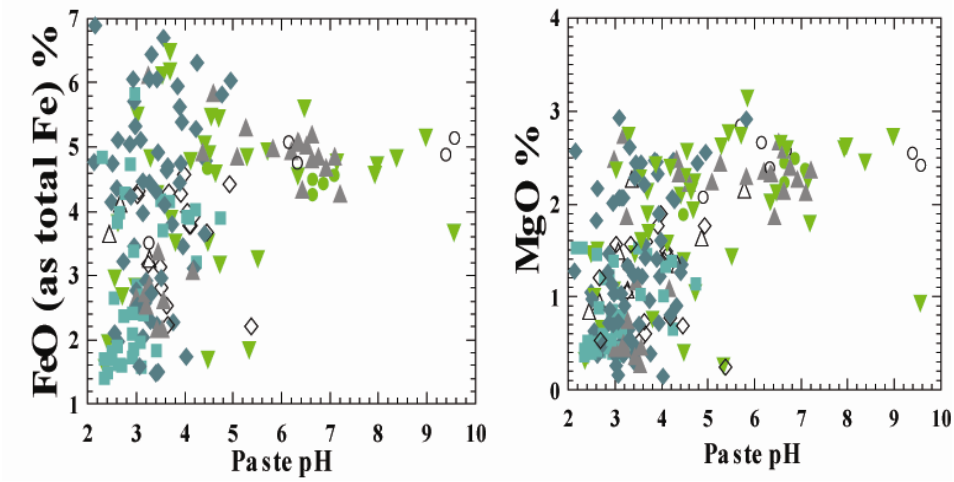

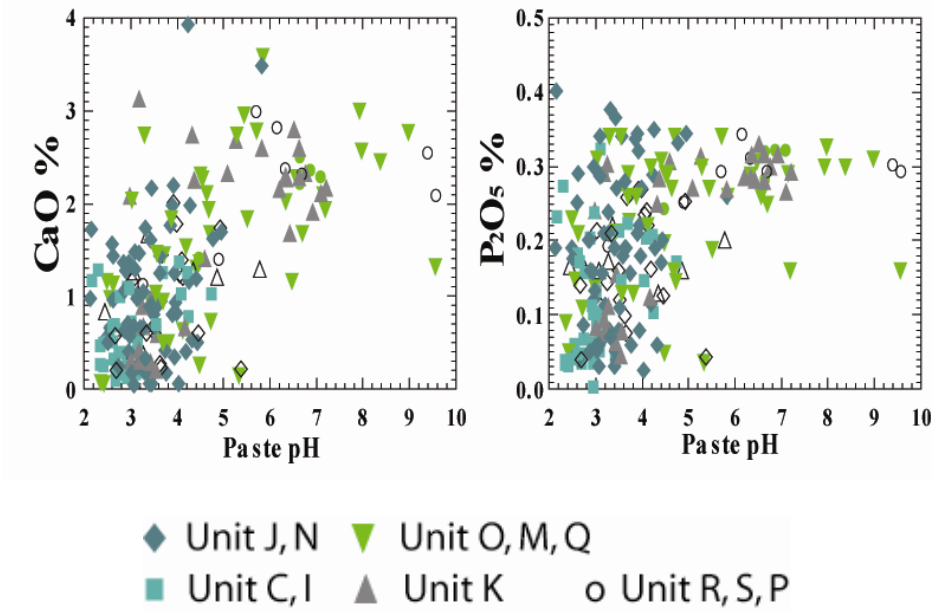

FIGURE 99. Scatter plots of FeOT, MgO, CaO, and P_2O_5 vs. paste pH. More weathered samples (units I, J, N, S) have lower FeOT, MgO, CaO, and P_2O_5. Refer to Table 20 for description of the geologic units.

NAG AND ABA TESTS

Net acid generation (NAG) and acid-base accounting (ABA) tests have been completed on samples from GHN (Tachie-Menson, 2006) and are summarized in Tables 27-29 and Figures 100-104. The samples from the stable portion of the rock pile had an average paste pH of 5.3 and NNP (net neutralizing potential) of 5.4 kg $CaCO_3$/t. For the unstable portion, the averages for the same parameters are 4.8 and -1.3 kg $CaCO_3$/t, respectively. For all the samples tested, the averages are 5.2 and 4.6 kg $CaCO_3$/t, respectively. The samples from the stable portion of the rock pile have an average NAG pH of 5.2 and $NAG_{4.5}$ of 2.7 kg $CaCO_3$/t. For the unstable portion of the rock pile, the averages are 4.0 and 3.7 kg $CaCO_3$/t, respectively. For all the samples from the rock pile, the averages are 4.9 and 2.9 kg $CaCO_3$/t, respectively. The results showed an increase in NAG pH, paste pH and net neutralization potential from the surface of the stable portion of GHN to the interior of GHN (Fig. 101-104). Samples from the outer units are potentially acid producing, whereas samples from the interior units are non-acid generating or unclassified (Fig. 100). It also was observed that paste pH values were higher for powdered samples than for unprocessed samples. Samples that have low paste pH values have higher net acid producing potentials or lower net acid neutralization potentials. Portions of the rock pile still have the potential to produce acid, and even though there are acid-consuming minerals in abundance in the rock pile, the more reactive carbonates are consumed by the acid very quickly, but there are not enough carbonates to neutralize all of the acid that could be produced.

TABLE 27. Summary of ABA results for the stable portion of GHN rock pile (Tachie-Menson, 2006). Paste pH_2 = paste pH on powdered samples; NP = neutralization potential; AP = acid potential; NNP = NP – AP; no = number of samples.

Hole/ Trench	no	Paste pH_2				NNP (kg $CaCO_3$/t)			
		Min.	Max.	Avg.	Stdv	Min.	Max.	Avg.	Stdv.
LFG-005	3	3.98	7.75	5.37	2.07	-1.51	41.03	12.96	24.32
LFG-006	30	3.14	8.08	5.58	1.74	-12.92	47.78	9.23	14.71
LFG-007	3	5.47	7.81	6.47	1.21	0.32	13.33	6.55	6.52
LFG-008	13	4.14	7.69	5.77	1.16	-10.66	28.44	4..38	13.25
LFG-009	16	3.05	6.78	4.46	1.08	-12.81	51.74	2.82	14.02
Surface	2	3.72	4.09	3.91	0.26	-5.59	-5.49	-5.53	0.05
TH-GN-01	32	3.11	8.08	5.23	1.51	-18.8	29.15	3.48	10.64
Overall	99	3.05	8.08	5.30	1.53	-18.8	51.74	5.43	13.25

TABLE 28. Summary of ABA results for the unstable portion of GHN rock pile (Tachie-Menson, 2006). Paste pH_2 = paste pH on powdered samples; NP = neutralization potential; AP = acid potential; NNP = NP – AP; n = number of samples.

Hole/ Trench	no	Paste pH_2				NNP (kg $CaCO_3$/t)			
		Min.	Max.	Avg.	Stdv	Min.	Max.	Avg.	Stdv.
LFG-011	6	3.65	5.48	4.37	0.67	-14.47	3.27	-5.72	6.17
LFG-019	3	3.93	6.75	4.90	1.61	-9.36	14.48	-0.17	12.82
LFG-021	2	3.86	7.21	5.54	2.37	-3.85	14.78	5.47	13.17
LFG-022	1	3.98	3.98	3.98	-	-2.03	-2.03	-2.03	-
Surface	3	4.05	6.51	5.36	1.24	-3.90	11.34	2.36	7.97
Overall	15	3.65	7.21	4.80	1.19	-14.47	14.78	-1.26	8.76

TABLE 29. Summary of NAG test results for the stable portion of the GHN rock pile (Tachie-Menson, 2006). no = number of samples.

Hole/ Trench	no	NAG pH_2				$NAG_{4.5}$ (kg $CaCO_3$/t)			
		Min.	Max.	Avg.	Stdv	Min.	Max.	Avg.	Stdv.
LFG-005	3	2.96	8.99	5.38	3.18	0.00	1.27	0.42	0.73
LFG-006	29	2.42	9.29	6.32	2.06	0.00	29.74	2.02	7.14
LFG-007	3	6.26	8.51	7.27	1.14	0.00	0.00	0.00	0.00
LFG-008	22	2.43	8.62	5.10	1.96	0.00	14.77	1.58	3.70
LFG-009	16	2.03	8.49	4.55	2.10	0.00	25.89	4.99	9.54
Surface	2	2.84	3.00	2.92	0.11	1.66	3.98	2.82	1.64
TH-GN-01	32	1.37	8.06	4.39	2.16	0.00	31.18	3.33	6.44
Overall	107	1.37	9.29	5.16	2.22	0.00	31.18	2.68	6.55

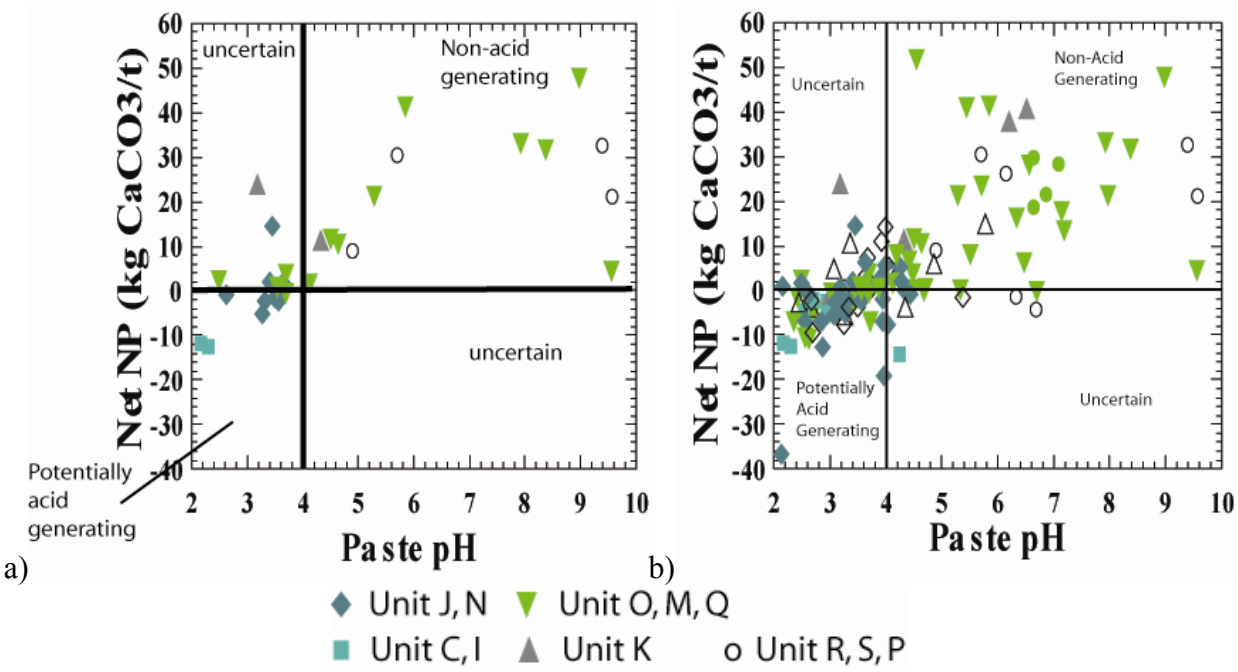

FIGURE 100. Net NP (neutralizing potential) versus paste pH for samples a) along bench 9, GHN and b) for all samples in GHN. Geologic units described in Table 20.

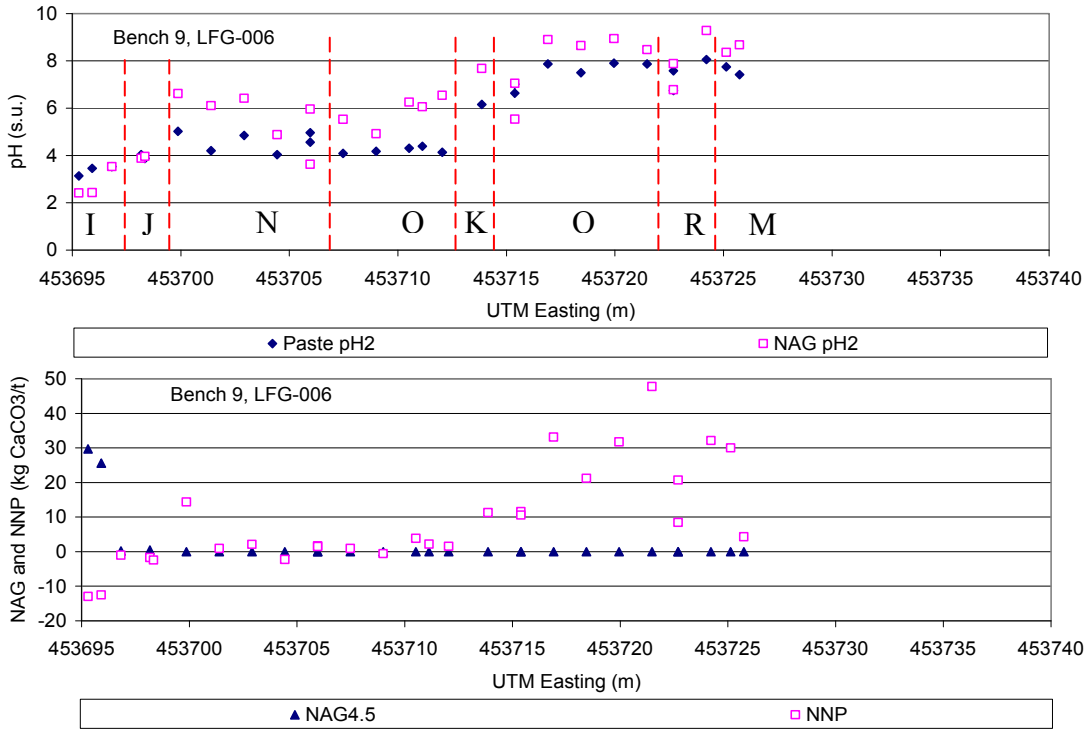

FIGURE 101. ABA and NAG results for Bench 9, Trench LFG-006 (Tachie-Menson, 2006). The top chart is for paste pH_2 and NAG pH_2; and the bottom chart is for $NAG_{4.5}$ and NNP. Red lines represent units.

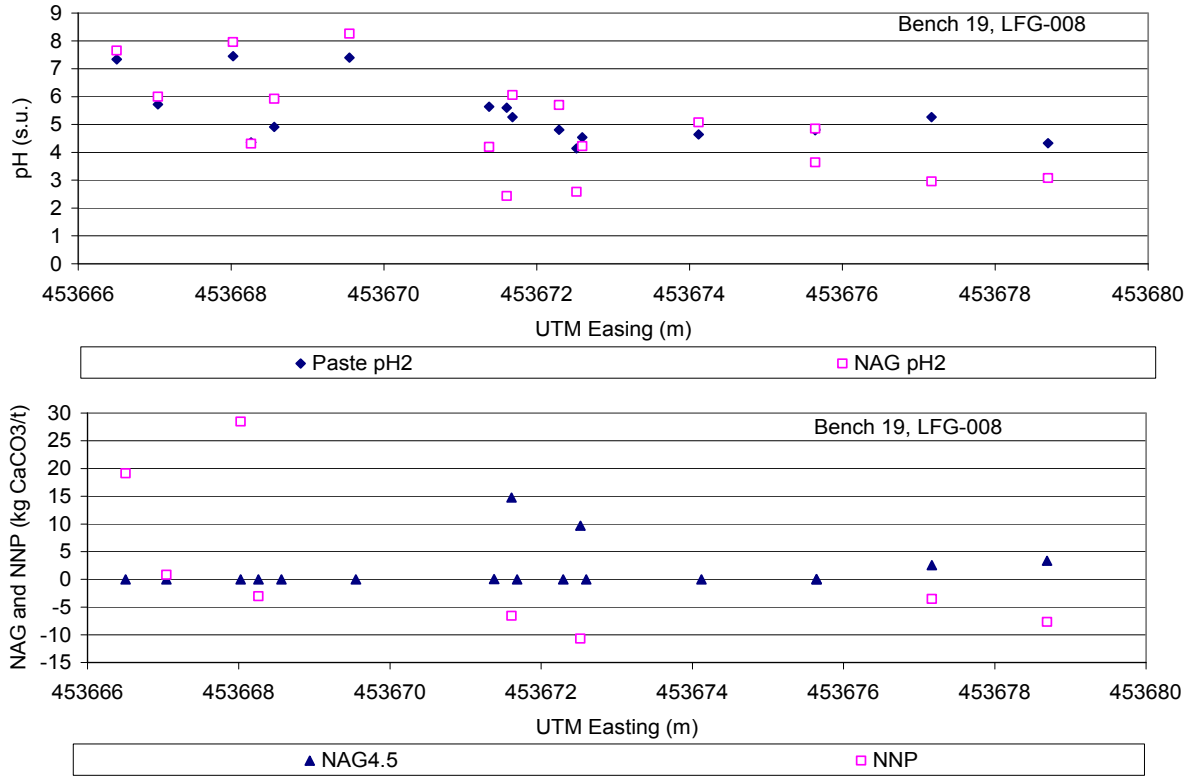

FIGURE 102. ABA and NAG results for Bench 19, Trench LFG-008 (Tachie-Menson, 2006). The top chart is for paste pH_2 and NAG pH_2; and the bottom chart is for $NAG_{4.5}$ and NNP.

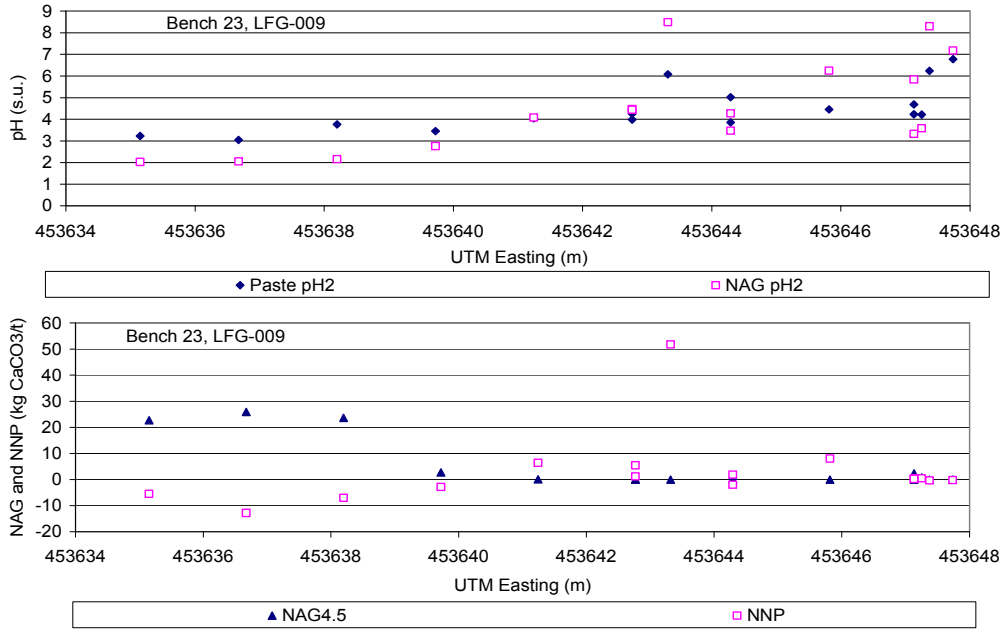

FIGURE 103. ABA and NAG results for Bench 23, Trench LFG-009 (Tachie-Menson, 2006). The top chart is for paste pH_2 and NAG pH_2; and the bottom chart is for $NAG_{4.5}$ and NNP.

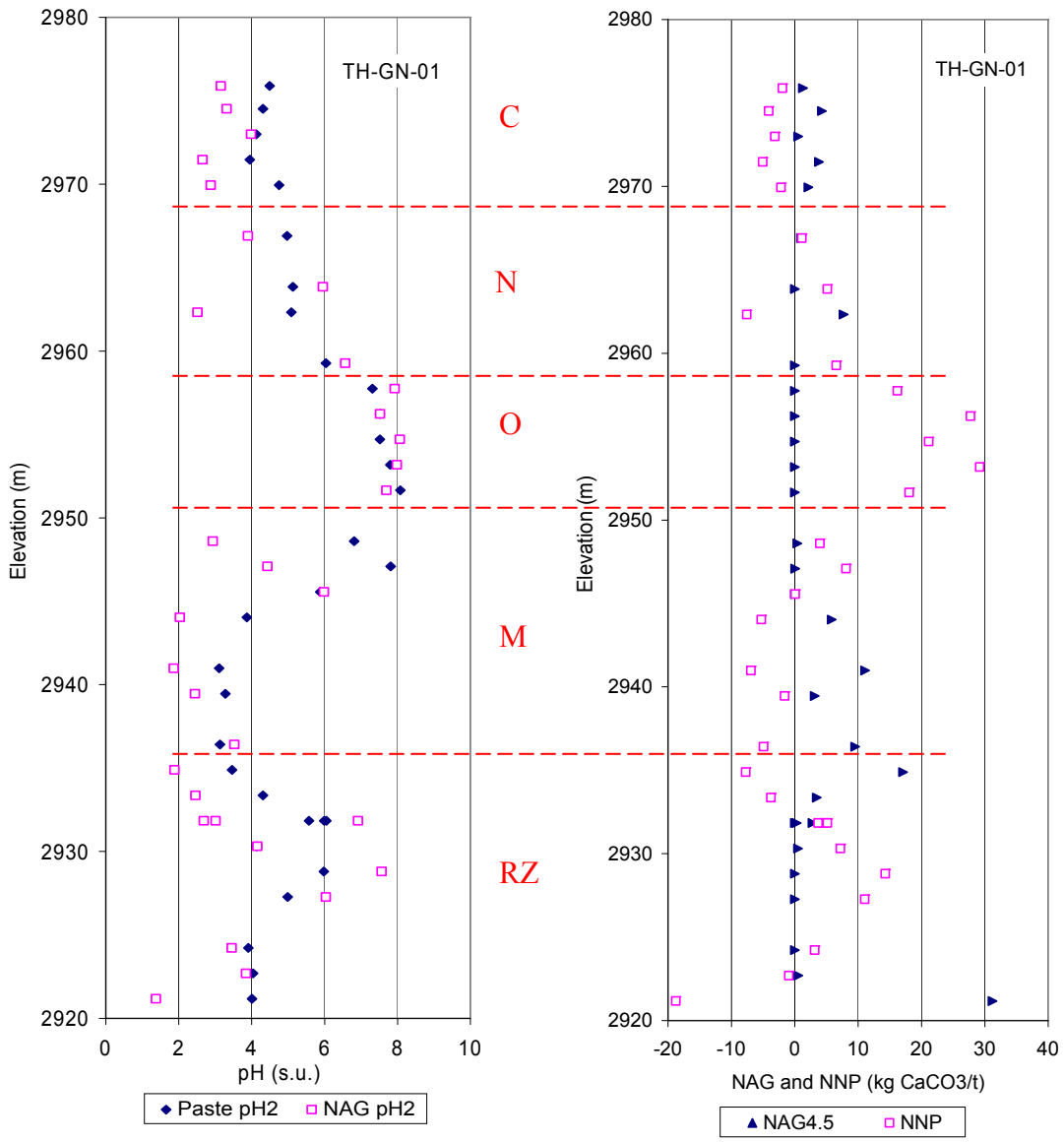

FIGURE 104. ABA and NAG results for borehole TH-GN-01 (Tachie-Menson, 2006). The left chart is for paste pH_2 and NAG pH_2; and the right chart is for $NAG_{4.5}$ and NNP. The red dotted lines represent different geologic units.

PARTICLE SIZE

Particle size analyses, including hydrometer analyses, were performed on trench samples from GHN. Summary statistics are in Table 30 and Figure 105. Most of the samples were classified as poorly-graded or well-graded sandy gravel with small percentage of fines. GHN rock pile consisted of alternating layers of thin cobble supported coarse-grained and thicker layers of matrix-supported finer-grained zones. The layers coarsen down slope in the final trench, LFG-009, where most of the units consisted of coarse sand, gravel, cobbles, and boulders and less fine sand, silt, and clay than the same stratigraphic units up slope in trench LFG-008.

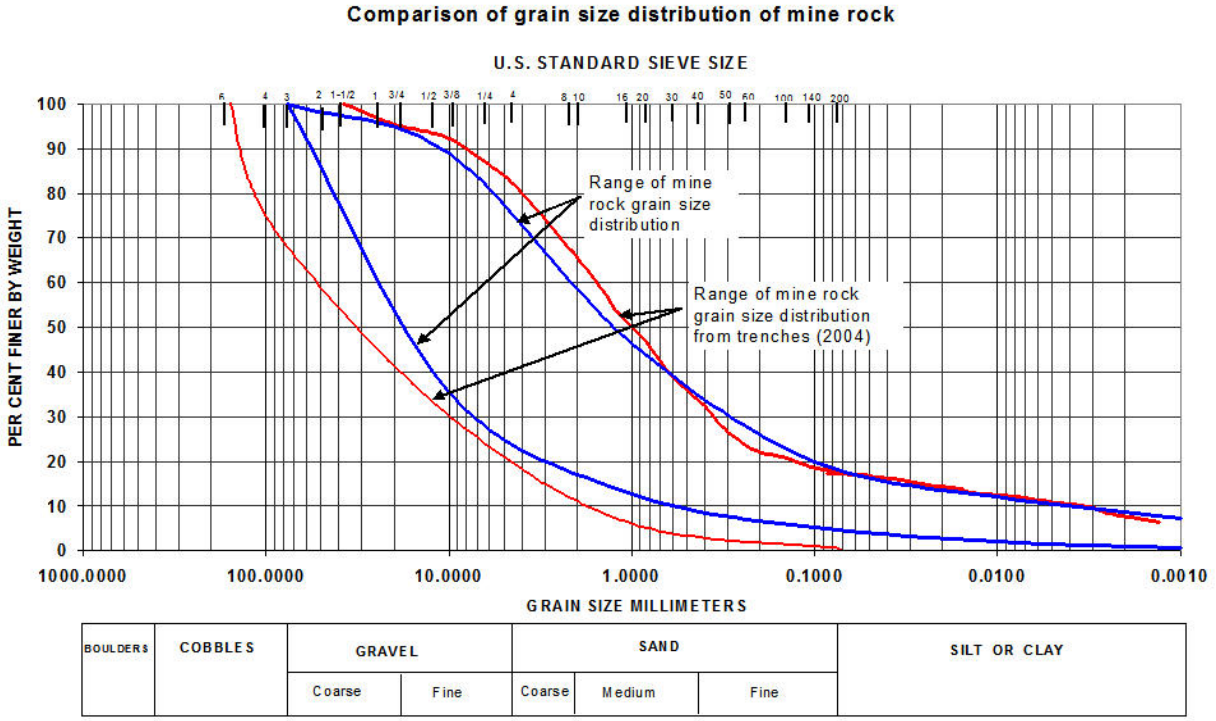

FIGURE 105. Particle size analyses of selected samples from GHN compared to legacy data from company reports. The blue lines are from data in URS Corporation (2003) and the red lines are from data obtained in this study from GHN.

TABLE 30. Summary of particle size analysis of samples from GHN by geologic unit. Descriptions of the geologic units are in Table 20.

Geol. Unit	Gravel %			Sand %			Silt %			Clay %			No. of samples
	Avg	Max	Min	Avg	Max	Min	Avg	Max	Min	Avg	Max	Min	
Oxidized outer zone													
C	41.83			46.95			5.51			5.57			1
I	46.45	55.69	37.21	37.99	43.66	32.32	12.72	14.57	10.87	2.84	4.56	1.12	2
J	56.77	63.40	49.84	35.29	41.01	29.36	6.25	8.34	4.42	1.69	3.97	0.28	5
Intermediate zone													
N	54.55	57.57	51.53	35.88	38.95	32.80	8.13	8.18	8.07	1.46	1.46	1.45	2
Unoxidized, internal zone													
K	54.90	69.62	45.06	35.24	44.20	24.97	6.16	7.97	3.12	3.69	5.71	2.28	4
O	55.25	70.45	41.56	35.45	47.93	24.21	6.26	8.20	3.23	3.04	4.89	2.10	10
M	61.18			28.83			5.58			4.41			1
R	54.51	63.12	45.90	35.09	41.12	29.07	7.41	8.78	6.05	2.89	4.20	1.77	2
S	64.90	74.83	54.98	26.64	33.68	19.59	5.87	7.04	4.70	2.59	4.31	0.88	2
U	69.49	87.39	60.60	24.10	32.33	9.66	3.77	5.05	1.70	2.63	3.61	1.25	3
V	61.44	65.12	58.75	30.69	33.31	28.11	4.97	5.31	4.57	2.90	3.58	2.20	3

ATTERBERG LIMITS (LIQUID AND PLASTIC LIMITS)

Atterberg limits were performed on samples taken from GHN and various locations on and around the Questa mine (Table 31). Seventeen samples were tested in duplicate for quality control purposes. The samples were plotted on Casagrande's Plasticity chart where they generally plot as CL or ML samples with some CL-ML samples (Fig. 106). This indicates the samples are inorganic clays with little swelling potential (CL) to inorganic silts (ML). The sample which plots as CH with the highest plasticity index was taken from Fourth of July Canyon and contains the highest percentage of fines and silt in this sample set. The other CH sample was taken from Goathill Scar while the one MH sample was taken from Straight Creek Scar.

When all bench 9 samples are plotted, there is a slight trend toward a decrease in the liquid limit (LL) and plasticity index (PI) from the outside to the inside of the rock pile (Fig. 107). There is little change in the plastic limit (PL) across bench 9. Samples from bench 14 have a trend similar to bench 9 for all three parameters, however, there is little change in LL, PL or PI across bench 18 (Fig. 108).

There is no discernable difference in liquid limits between the GHN geologic units (statistical analysis is in Appendix 11). The median liquid limit of the debris flows is lower than the median liquid limit of other Questa materials and the median liquid limit of the colluvium is larger than the other Questa material (statistical analysis is in Appendix 11).

TABLE 31. Descriptive statistics of Atterberg Limits by geologic unit for stable portion of GHN rock pile. Histograms are in Appendix 11. Data are results obtained from NMIMT sampling and testing on Questa rock piles 2004-2007 (Appendix 7 and project Access database) and from URS Corp. (2003).

Liquid Limit

Unit	Mean	Median	Standard Deviation	Standard Error	Minimum	Maximum	Number of Cases
unit C	32.2						1
unit I	35.0	35.3	4.9	2.8	30.0	39.8	3
unit J	34.9	35.2	3.4	1.3	28.7	38.4	7

Unit	Mean	Median	Standard Deviation	Standard Error	Minimum	Maximum	Number of Cases
unit N	34.7						2
unit K	30.9	31.3	3.4	1.7	26.5	34.7	4
unit M	30.0						1
unit O	35.1	33.8	3.9	1.0	29.6	43.5	16
unit P	36.0						1
unit R	35.3	35.6	2.0	1.2	33.1	37.2	3
unit S	28.1						1
unit U	31.5	31.2	1.1	0.6	30.7	32.7	3
unit V	33.1	34.5	3.1	1.8	29.5	35.3	3
rubble zone	33.0						2
Entire GHN	33.0	33.5	5.5	0.7	3.3	43.5	61
Middle	28.4	28.7	2.5	0.8	22.9	31.7	10
Spring Gulch	23.4	24.0	3.5	0.8	18.6	30.6	18
Sugar Shack South	31.3	31.6	4.0	1.0	2.7	37.0	15
Sugar Shack West	28.8	28.0	3.3	0.5	24.4	39.3	41
Capulin	28.0	22.0	4.5	0.8	22.0	43.0	34
Sulfur Gulch South	32.5	32.1	3.8	1.9	28.7	37.0	4
Questa rock piles	30.4	30.0	5.0	0.2	3.3	46.0	473
colluvium	34.6	33.59	4.3	1.0	29.9	43.9	19
Alteration scars	33.1	32.3	6.3	1.2	20.1	50.5	30
Debris flows	25.1	24.7	2.9	0.7	20.7	30.5	16

Plastic Limit

Unit	Mean	Median	Standard Deviation	Standard Error	Minimum	Maximum	Number of Cases
unit C	17.9						1
unit I	23.9	24.7	1.8	1.0	21.9	25.1	3
unit J	19.6	19.5	2.6	1.0	15.6	23.4	7
unit N	22.7						2
unit K	17.6	18.2	2.2	1.1	14.5	19.6	4
unit M	19.0						1
unit O	20.1	19.8	2.5	0.6	16.6	24.0	16
unit P	22.4						1
unit R	18.3	18.4	1.5	0.9	16.8	19.8	3
unit S	20.9						1
unit U	19.1	18.3	2.0	1.1	17.7	21.4	3
unit V	23.5	25.6	4.5	2.6	18.3	26.5	3
rubble	21.6						2

Unit	Mean	Median	Standard Deviation	Standard Error	Minimum	Maximum	Number of Cases
zone							
Entire GHN	20.2	19.8	2.7	0.3	14.5	26.5	61
Middle	21.6	20.6	2.8	0.9	17.4	26.3	10
Spring Gulch	18.1	16.9	4.2	1.0	13.1	26.7	18
Sugar Shack South	23.8	22.6	5.0	1.3	17.9	36.0	15
Capulin	17.9	18.0	2.0	0.3	15.0	26.0	34
Sulfur Gulch South	26.0	24.5	7.7	3.8	19.2	36.0	4
Questa rock piles	19.1	19.0	3.0	0.1	11.4	36	473
colluvium	21.7	20.7	3.4	0.8	17.4	30.8	19
Alteration scar	21.2	21.6	3.7	0.7	11.1	28.3	30
Debris flows	18.3	10.2	2.6	0.7	10.2	21.6	16

Plasticity Index

Unit	Mean	Median	Standard Deviation	Standard Error	Minimum	Maximum	Number of Cases
unit C	14.3						1
unit I	11.1	10.2	6.4	3.7	5.3	17.9	3
unit J	15.4	16.4	3.0	1.1	9.3	17.7	7
unit N	12.1						2
unit K	13.3	13.7	3.9	2.0	8.5	17.6	4
unit M	11.0						1
unit O	14.9	14.6	3.7	0.9	6.7	20.4	16
unit P	13.6				13.6		1
unit R	17.0	18.8	3.1	1.8	13.4	18.8	3
unit S	7.1						1
unit U	12.4	13.0	2.4	1.4	9.8	14.4	3
unit V	9.7	8.1	6.7	3.9	3.9	17.0	3
rubble zone	11.3						2
Entire GHN	13.3	13.7	4.1	0.5	3.9	20.7	61
Middle	6.1	6.7	3.4	1.1	1.6	11.1	10
Spring Gulch	5.3	6.2	2.8	0.7	0.2	9.9	18
Sugar Shack South	7.6	7.7	2.3	0.6	1.0	10.5	15
Sugar Shack West	8.8	8.2	3.1	0.5	2.0	15.5	41
Capulin	10.1	10.0	4.1	0.7	5.0	25.0	34
Sulfur Gulch	6.4	7.6	3.9	2.0	1.0	9.4	4

Unit	Mean	Median	Standard Deviation	Standard Error	Minimum	Maximum	Number of Cases
South							
Questa rock piles	11.3	11.0	4.2	0.2	0.2	25.0	473
colluvium	13.0	13.1	4.4	1.0	5.5	22.5	19
Alteration scar	11.9	10.5	5.3	1.0	5.3	24.8	30
Debris flows	6.8	6.2	3.0	0.8	3.1	13.8	16

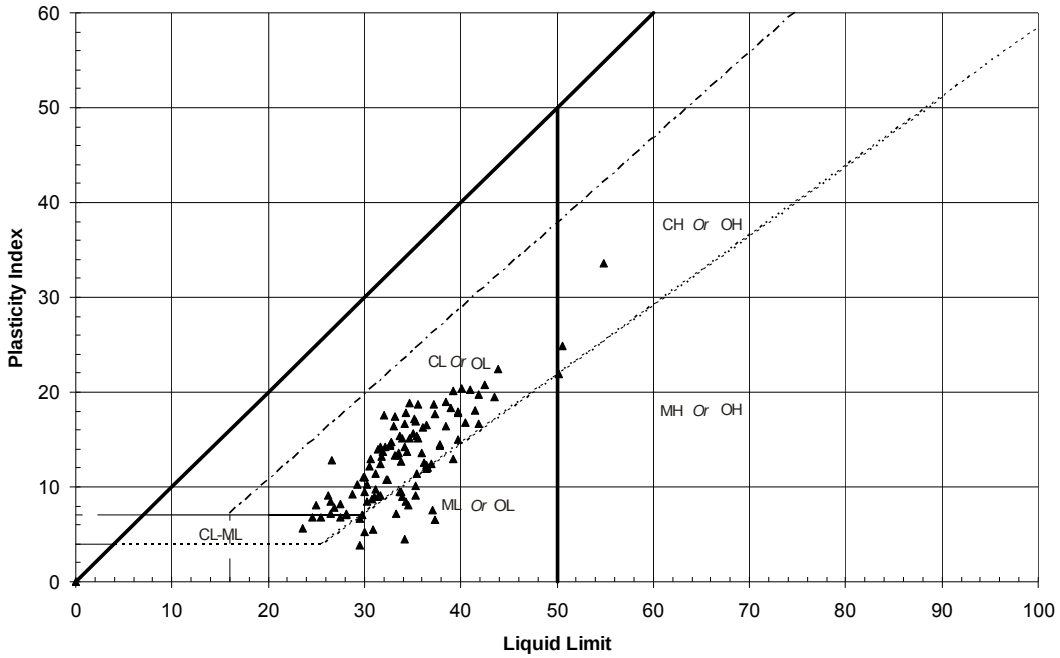

FIGURE 106. Plot of Plasticity Index vs. Liquid Limit for GHN samples. The sample plotted as CH with the highest plasticity index is from Fourth of July Canyon. The other CH sample and the one MH sample are from Goathill Scar and Straight Creek Scar, respectively.

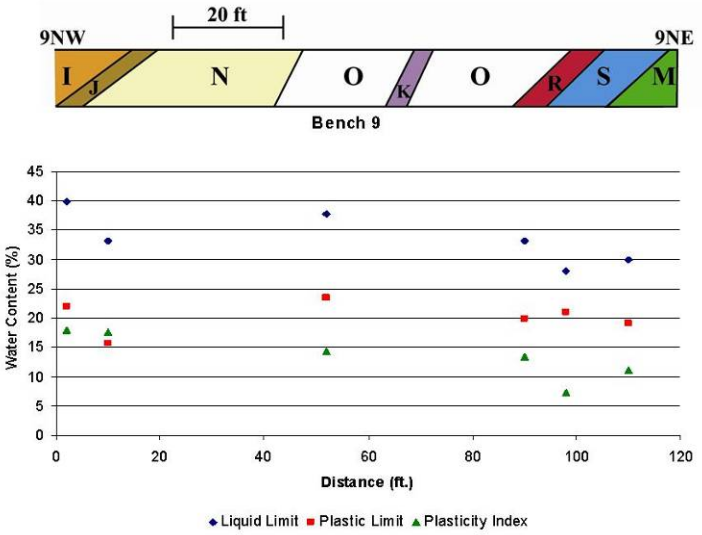

FIGURE 107. Atterberg limit results for samples taken from bench 9. The liquid limit and plasticity index decreases from the outside (more weathered, left) to the inside (less weathered, right) of the rock pile while the plastic limit varies little.

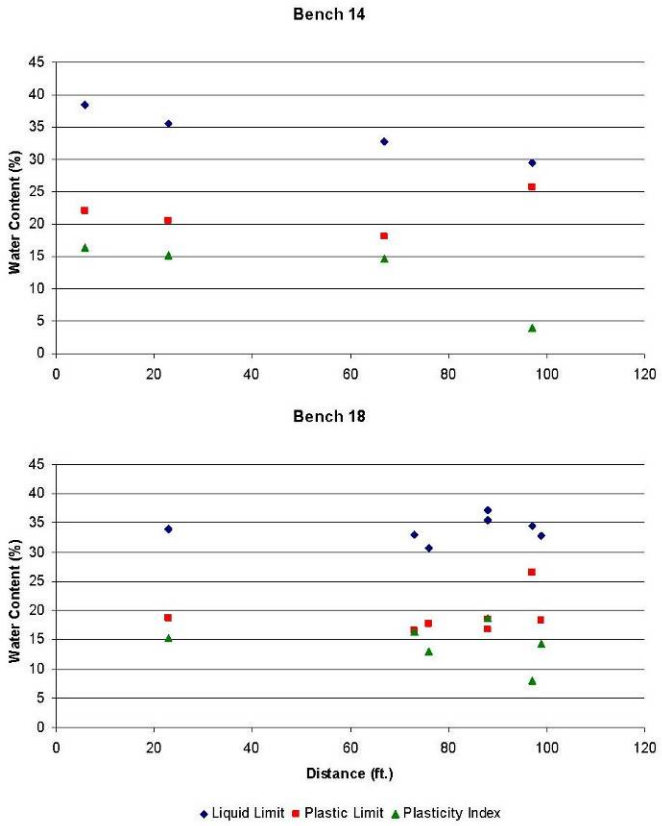

FIGURE 108. The liquid limit, plastic limit and plasticity index for bench 14 are similar to those for bench 9 and also decreases from the outside to the inside of the rock pile. However, samples show little change in plasticity across bench 18.

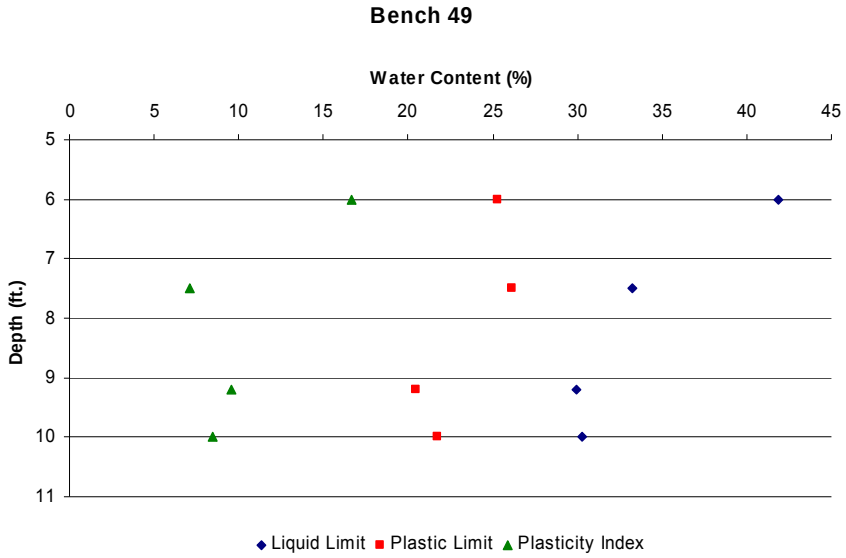

FIGURE 109. Atterberg limit results for the samples from the clay zone and the saprolite are significantly lower than the values from the lower portion of the rock pile.

POROSITY AND PERMEABILITY

The porosity from drill hole samples from company reports varies from 0.2 to 0.47% (project database). The void ratio varies from 0.52 to 0.89. The permeability of drill hole samples from company reports varies from 0.0136 to 2.09 cm/sec using rigid wall permeability test results. Tables 32-34 summarize the data on GHN.

TABLE 32. Volume-mass properties of the soils/tailings collected from Golder Associates (2005a, b).

ID	Soil region	Degree of saturation, *S* (%)	Specific gravity, *G*	Gravimetric water content, *w* (%)	Porosity, *n* (%)
1	TP-4	100	2.65	10.64	22.0
2	TP-5	100	2.65	25.1	39.9
3	TP-6	100	2.65	19.9	34.5
	Average			18.54	32.12

TABLE 33. Volume-mass properties of the soils/tailings collected from Norwest Corporation (2004).

ID	Soil region	Degree of saturation, *S* (%)	Specific gravity, *G*	Gravimetric water content, *w* (%)	Porosity, *n* (%)
1	SSU-3 (TP-5)	100	2.65	8.7	18.7
2	TP-4-2B	100	2.65	19.6	34.2
3	SG-2	100	2.65	19.6	34.2
	Average			14.5	29.03

TABLE 34. Volume-mass properties of the soils/tailings measured using Tempe Cell measurements (M. Fredlund, written communication, April 13, 2006).

ID	Soil region	Degree of saturation, *S* (%)	Specific gravity, *G*	Gravimetric water content, *w* (%)	Porosity, *n* (%)
1	GHN KMD 0016	100	2.65	35.2	48.3
2	KMD 018	100	2.65	21.1	35.9
3	KMD 053	100	2.65	23.7	38.6
4	GHN KMD 0065	100	2.65	29.2	43.6
5	LFG SCS 005	100	2.65	31.3	45.3
6	GHN LFG 001	100	2.65	35.9	48.8
7	LFG 003	100	2.65	24.6	39.5
8	GHN LFG 004	100	2.65	35.1	48.2
9	GHN LFG 006	100	2.65	36.5	49.2
10	PIT LFG 001	100	2.65	32.3	46.1
11	PIT LFG 003	100	2.65	25.4	40.2
12	PIT LFG 005	100	2.65	32.7	46.4
13	PIT LFG 007	100	2.65	23.1	38.0
14	PIT LFG 009	100	2.65	20.2	34.9
15	PIT LFG 0013	100	2.65	36.0	48.8
	Average			29.5	43.5

DENSITY/SPECIFIC GRAVITY

Density is the weight of unit volume of soil; dry density is for dry materials. The dry density is the ratio that connects the volumetric side of the phase diagram with the mass side. In natural soils, the magnitude of the total density or wet density will depend on how much water happens to be in the voids as well as the density of the mineral grains themselves. Measurements of in-situ dry density were made by NMIMT at the Questa mine from 2004 to 2007 using four methods: sand-cone, sand replacement, water replacement, and nuclear emissions density test (see SOPs). Each method of determining the in-situ dry density followed ASTM guidelines or was adapted from ASTM procedures as described in the appropriate SOP (Table 16). Results agree on different tests performed on the same sample. Samples include a mixture of rock fragments (0.3 m to <1 mm in diameter) and soil matrix. Most GHN samples were collected from the trenches in the upper half of the GHN rock pile (Fig. 27).

Dry density measurements have been made in other studies of the Questa rock piles and other materials. URS Corporation (2003) indicated a range in dry density of 1.5 to 2.3 g/cm^3 for rock-pile material. The Norwest front rock pile report (Norwest Corporation, 2005) indicated a range in dry density between 1.5 and 1.7 g/cm^3 and an average of 1.5 g/cm^3 for rock-pile material, 1.3-1.6 g/cm^3 for debris flow, and 1.3 g/cm^3 for Red River colluvium. The dry density calculations indicate that the GHN rock-pile material varied between 1.5 and 2.5 g/cm^3 (URS Corporation, 2003; Norwest Corporation, 2004). Table 35 summarizes the descriptive statistics for the GHN and other Questa materials; histograms and summary of statistical analyses are in Appendix 11. There is not a statistically significant difference between the dry densities of various geologic units within GHN (Appendix 11). The average density for GHN rock piles is

1.8 g/cc (Table 35). The density of the GHN samples is statistically similar to other Questa rock piles, debris flows and alteration scars (Appendix 11).

Specific gravity measurements were performed on samples from the GHN rock pile and elsewhere in the Questa area (Table 35). The material used for testing passed a no. 4 sieve and sample sizes were generally between 100 and 110 grams. Specific gravity measured between 2.6 and 3.0 g/cm^3 for all samples with approximately two thirds falling between 2.6 and 2.7 g/cm^3.

TABLE 35. Descriptive statistics of density (g/cc) by geologic units for GHN and for Questa materials. Histograms are in Figure 110 and Appendix 11.

Unit	Mean	Median	Standard deviation	Standard error	Minimum	Maximum	Number of Samples
Traffic	1.88	1.86	0.11	0.03	1.72	2.06	12
Unit C	1.73	1.76	0.12	0.06	1.57	1.85	4
Unit I	2.00						1
Unit J	1.81	1.85	0.12	0.03	1.59	1.94	12
Unit N	1.81	1.81	0.12	0.04	1.63	1.99	9
Unit K	1.77	1.78	0.16	0.04	1.51	1.96	14
Unit O	1.83	1.81	0.11	0.02	1.53	2.48	35
Unit M	1.91	1.97	0.11	0.05	1.61	2.07	9
Unit U	1.82	1.86	0.07	0.03	1.71	1.89	6
Unit V	1.89	1.86	0.08	0.04	1.83	1.99	4
Unit RUB	1.70	1.71	0.04	0.02	1.64	1.75	7
All GHN (including unstable GHN)	1.84	1.83	0.15	0.01	1.51	2.49	118
Middle	2.12						1
SGS	1.75						1
SPR	1.79	1.83	0.26	0.08	1.43	2.19	11
SSS	1.90	1.92	0.12	0.05	1.68	2.09	7
SSW	1.95	1.90	0.27	0.07	1.40	2.43	15
All rock piles	1.85	1.84	0.14	0.01	1.40	2.49	153
Debris Flow	1.87	1.94	0.34	0.11	1.27	2.46	11
Alteration scars	1.90	1.90	0.21	0.06	1.51	2.27	12
All Questa materials	1.8	1.8	0.18	0.01	1.3	2.4	176

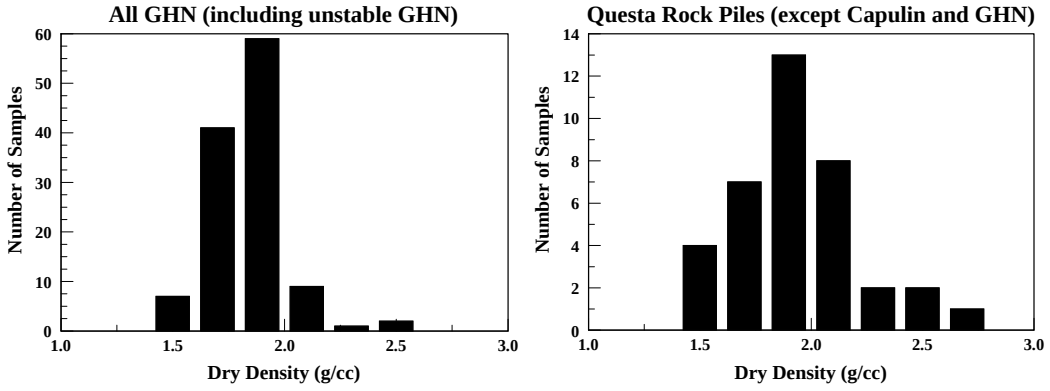

FIGURE 110. Histograms of dry density (g/cc) of Questa rock piles.

GRAVIMETRIC MOISTURE CONTENT

Results of gravimetric moisture contents are presented in Table 36. Gravimetric moisture contents ranged from 2 to 24% near the surface of the rock piles, but values measured in trenches within the GHN rock pile were typically between 6 and 20% (Table 35; Figs. 111, 112). Moisture contents as high as 25.5% are reported in previous studies (Table 6; URS Corporation, 2003). The top of GHN rock pile appears to have higher moisture contents than the base of the rock pile (Figs. 111, 112). Appendices 5 and 6 contain logs of the individual trenches and drill holes with their distribution of moisture content. There is no stastical difference between the gravimetric moisture content of the outer units (units C, I, J) from the interior units (units K, N, O, M, R, S, T, U, V, and W) and the basal rubble zone (unit RUB; Appendix 11). The debris flows materials have a lower gravimetric moisture content median than the other samples and the colluvium and weathered bedrock materials have higher median gravimetric moisture contents than the other samples.

TABLE 36. Summary of moisture contents (percent) of samples from GHN by geologic unit (described in Table 20) and other Questa materials (Appendix 11).

Geologic Unit	Average	Standard deviation	Maximum	Minimum	Number of samples
Oxidized, outer zone					
C	7.0	2.1	9.3	5.5	3
I	15.5	5.0	23.9	10.7	5
J	10.4	3.0	17.1	6.6	16
Interior zone					
N	13.1	2.5	17.3	9.6	17
K	10.2	1.2	11.8	8.3	9
L	8.6				1
O	11.2	2.3	18.0	6.2	50
M	10.3	2.5	15.1	5.5	14
R	10.5	0.8	11.5	9.9	3
S	10.4	2.0	13.4	7.4	6
U	10.6		13.2	8.0	2
V	9.2		9.6	8.6	3
W	9		9.6	8.4	2
Basal rubble zone	11.2	2.9	18.5	7.1	14
Colluvium	14.4	3.0	20.8	9.3	13
Bedrock	15.1	2.7	18.3	8.9	9
GHN (excluding unstable zone)	11.0	2.8	23.9	5.5	170
GHN (including unstable zone)	10.5	3.3	23.9	2.4	227
Middle rock pile	8.1	1.4	10.0	6.6	4
Sulfur Gulch South rock pile	10.2	4.4	9.8	4.1	36
Spring Gulch rock pile	6.3	1.8	8.9	3.8	18
Sugar Shack South rock pile	8.1	3.3	23.1	2.7	51
Sugar Shack West rock pile	7.5	2.2	12.1	2.7	40
Alteration scars	9.2	3.9	18.7	0.1	48
Debris flow	5.2	4.3	28.6	1.0	36

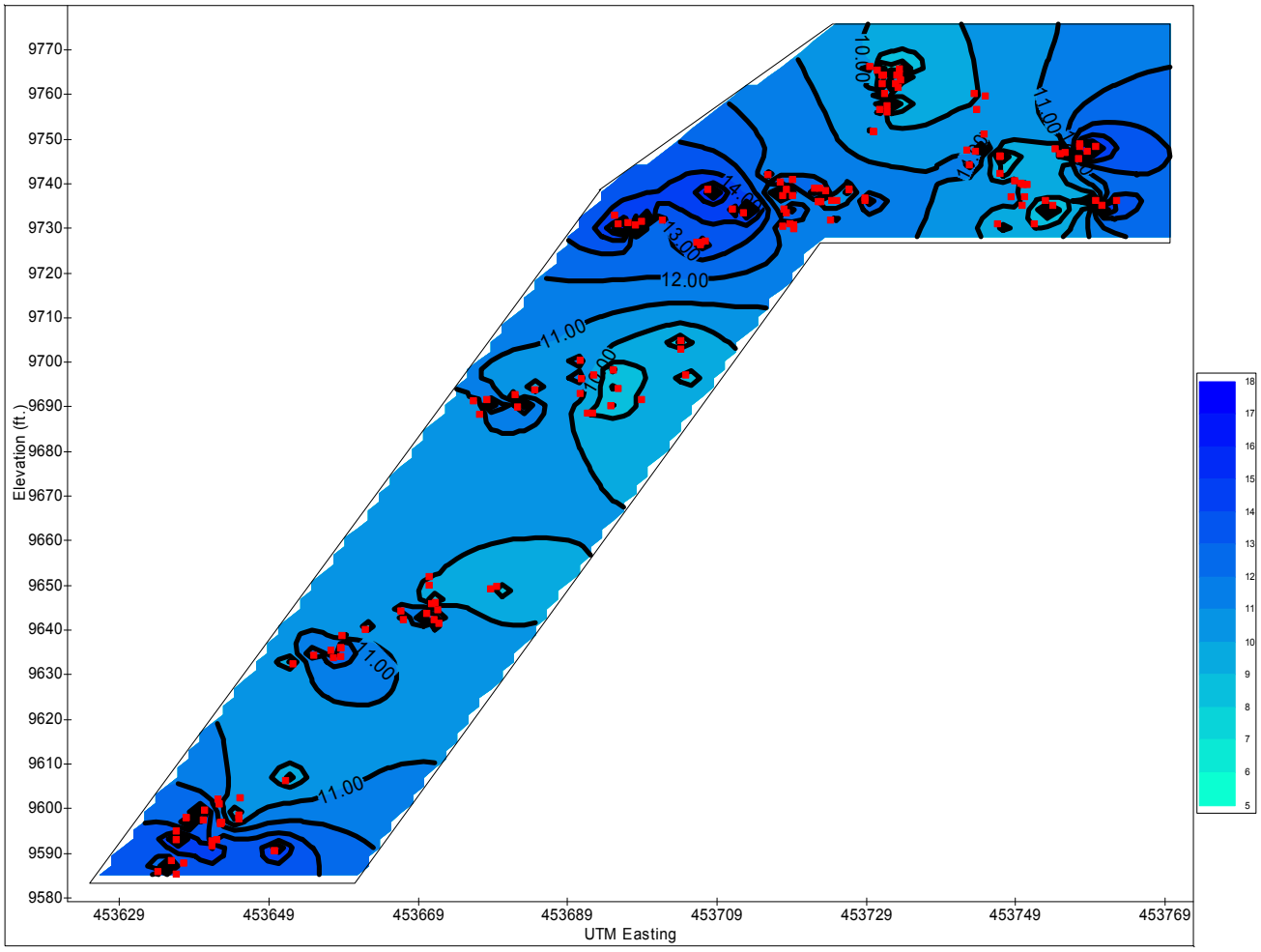

FIGURE 111. A contour diagram of a cross section of the top of the stable portion GHN showing the variation of gravimetric moisture content in the area of trenches LFG-0003 through LFG-009. The red points identify sampling locations. The top of the rock pile shows higher gravimetric moisture content values than the inner portion.

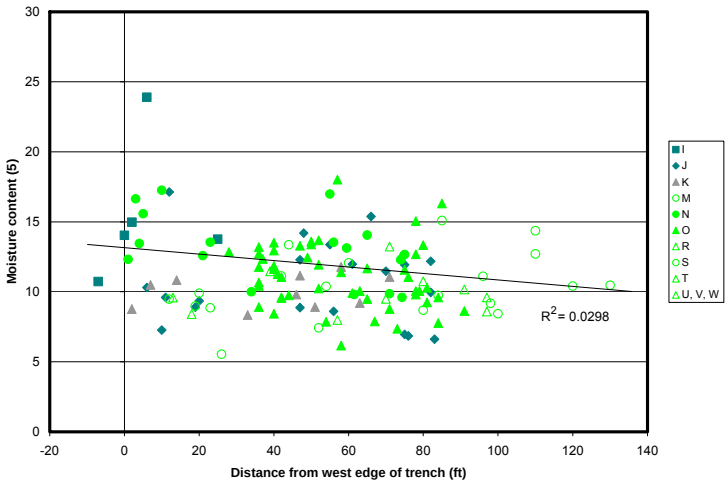

FIGURE 112. Moisture content versus distance from west edge of trench showing slight trend of increasing moisture content towards the interior of the rock pile.

INFILTRATION AND HYDRAULIC CONDUCTIVITY

The term infiltration generally refers to the portion of precipitation that penetrates the surface of a rock pile and excludes the precipitation used by vegetation, that collected on the surface (ponded water), and surface runoff. Net infiltration typically refers to that portion of the infiltration that is not lost by evapotranspiration. Fluid transport occurs by uniform unsaturated flow, preferential channeling, saturated flow below the water table (not present at GHN), and vapor transport through the rock pile. Most numerical models can account for uniform unsaturated flow but the other types of infiltration within a rock pile can be difficult to quantify and model numerically. Infiltration can be directly measured by tensiometers, infiltrometers, guelph permeameters, and lysimeters. Infiltration is an important component of the weathering of rock piles. If little or no water enters the rock piles, then weathering and the generation of acid drainage is limited. Both the volume of the infiltration and elapsed time between infiltration rates effect the intensity and rate of weathering within the rock pile (Morin and Hut, 1994).

Tensiometers were installed on the top of GHN in June 2004 in hand-dug holes in two nests, one in an uncompacted region and one in a compacted region to provide information about the matric potential response of the rock pile to precipitation events. The matric potential response would be used to indicate how quickly the precipitation infiltrated into the variably saturated pile and how well the water was being held in the soil and rock. The tensiometers were installed with temperature sensors to increase our knowledge of the thermal sensitivity of the mine soil to influxes of water. The sensors recorded continuous data during a period between June and September 2004. The temperature of the mine soil at the depths monitored varied between 4 and 20° C and the matric potential varied between –80 and +30 cm. The data recorded by the data loggers indicates several infiltration events, which correspond to precipitation events recorded at the Red River NWS meteorological station. The two tensiometers at the shallowest depths recorded the diurnal temperature variation and responded more quickly to precipitation events than the deeper tensiometers. All tensiometers responded quickly to a large infiltration event in late June. The data collected from the tensiometers revealed changes in the matric potential and temperature that correspond with events recorded at the Red River NWS meteorological station.

The infiltration rates that were measured on several different surfaces using the tension infiltrometer ranged between 0.07 and 3.0 cm/min (Fig. 113). The infiltration rates were measured at different matric suctions, ranging from near saturation at approximately –1.5 cm of suction (saturation is at 0 cm) to –30 cm of suction. The higher matric suctions resulted in the lowest infiltration rates, whereas the lower matric suctions resulted in the highest infiltration rates. Therefore, when the rock pile is drier (higher matric suctions), it is more difficult to infiltrate water into the system than when the pile is wetter (lower matric suctions; Shannon, 2006).

The guelph permeameter measures saturated hydraulic conductivity, whereas the tension infiltrometer can be used to measure the saturated and unsaturated hydraulic conductivity. Twenty-one tension infiltrometer measurements were made in 2004 at GHN (Fig. 113; Appendix 7). The measurements were made to determine the infiltration rate of the piles and to determine the unsaturated hydraulic conductivity or the hydraulic conductivity as a function of the matric suction (Table 37). The data collected were used to estimate the saturated hydraulic conductivity (Ksat = K(h), where h = 0 cm). The proper instrumentation for measuring saturated hydraulic conductivity directly with the tension infiltrometer was not available when the data was collected. The measurements were made on the top and middle bench of the GHN rock pile prior to the regrading phase. There was significant variability in the measurements made on the different parts of the pile. The guelph permeameter was used to make 47 measurements of the saturated hydraulic conductivity. The measurements were made in 2003-2005. Numerous tension infiltrometer measurements were made at the same and different locations in the trenches as prior guelph permeameter measurements.

TABLE 37. Comparison of tension infiltrometer and guelph permeameter measurements. See project database for specific data. Ksat is hydraulic conductivity.

Station id (guelph)	Ksat (m/sec)	Station id (infiltrometer)	Ksat (cm/sec)
GP9-A	0.00007	TI01-080604	0.000757
GP-11A	0.0000084	TI13-82804	0.000635
GP-11A	0.0000084	TI14-82804	0.00658
GP5-A	0.011	TI18-062404	0.000496
GP5-A	0.011	TI19-062404	0.0138
GP-3A	0.0023	TI20-062904	0.00127
GP9-A	0.00007	TI2-080704	0.000627
GP-10A	0.0072	TI3-080704	0.0046
GP-11A	0.0000084	TI4-080704	0.00169
GP-12A	-0.0025	TI5-080704	0.00166

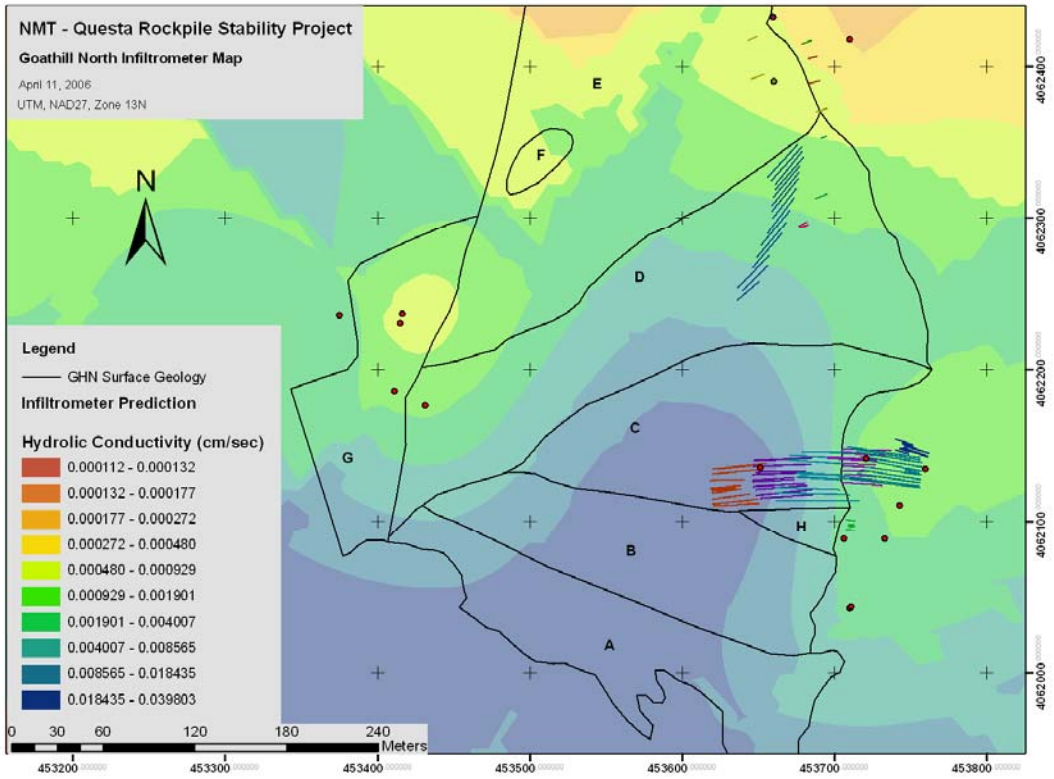

FIGURE 113. Infiltration at the surface of GHN before reclamation. Units A-H are surface geologic units described in Table 20. Red circles are locations of field measurements using Guelph and tension infiltrometer measurements (original data are in the project database). Red, blue, and green lines are trench locations.

Comparison of saturated hydraulic conductivity values from tension infiltrometer and Guelph permeameter measurements at nearby locations show that the tension infiltrometer values are locally an order of magnitude less than those measured by the Guelph permeameter (Shannon, 2006). Possible causes for these differences include different dates of measurement, spatial variability (measurements are accurate but hydraulic conductivity varies widely in space), scale (the volume of rock pile material interrogated by the tension infiltrometer is much smaller than the volume interrogated by the Guelph instrument), methodology (infiltrometer applies water directly to an undisturbed land surface whereas the Guelph permeameter applies water to an excavated hole), and procedural (saturated hydraulic conductivity is estimated from other tension infiltrometer measurements whereas the Guelph permeameter makes measurements closer to 0 cm of matric potential).

EVAPORATION

A literature review was performed to determine the annual evaporation or potential evapotranspiration in the Questa mine vicinity. Numerous studies that were previously completed on the mine facilities estimated the annual evaporation rates using pan evaporation techniques, lysimeter data, and meteorological data. Wels et al. (2001) estimated annual pan

evaporation for the region near the tailings facility as approximately 65-70 inches. After installing a meteorological station, the cumulative potential evapotranspiration was estimated to be 14.04 inches from Aug. 9, 2000 to Jan. 6, 2001. A summary of the four lysimeter test plots for the first year of monitoring (July 2000–July 2001) determined that cumulative potential evaporation reported in inches for each station is as follows: TP-4 = 47.8, TP-5 = 36.7, TP-6/TP-7 = 45.0 (Robertson GeoConsultants, 2003). Evapotranspiration (in inches) was estimated as: TP-4 = 6.54, TP-5 = 3.43, TP-6 = 4.44, and TP-7 = 4.90 (Robertson GeoConsultants, 2003). Golder Associates, Inc. (2005a, b) estimated the annual evaporation for the rock piles from 1965-2003 as 12.6 inches (Table 3).

Stable isotopes and modeling indicate that evaporation at and near the surface is an important process in moving water out of the rock pile (Fig. 114). Stable isotopes (δD and $\delta^{18}O$) in water samples help constrain certain aspects of the hydrology of the rock piles. The investigation focuses on the seasonality of recharge, the degree of evaporation, and the vapor transport within the pile. The first task was to establish the stable isotopic composition of the local precipitation. This is important because this is the source of water in the piles. Nine precipitation collectors were installed across the property and sampled on intervals of 1 to 3 months from 2004 to 2007. The isotopic composition of precipitation varies seasonally, as well as on shorter time scales, but always displays a covariation generally defined as $\delta D = 8\ \delta^{18}O + 10$, known as the Global Meteoric Water Line (MWL). Winter precipitation as snow tends to be isotopically light compared to summer precipitation. The precipitation data from this study (Fig. 114) defines a good local meteoric water line which serves to define the starting point for water entering the rock pile. Samples of the rock-pile material were sampled for stable isotopic analysis. Water is extracted from these samples by distillation and then analyzed. These pore waters originate as precipitation but undergo some evaporation as they infiltrate into the pile. This is seen in Figure 114 by the shift of these samples to the right of the local precipitation. This effect is due to the fractionation of the stable isotopes during evaporation. During evaporation, the light isotopes (H and ^{16}O) are preferentially partitioned into the vapor phase while the heavy isotopes (D and ^{18}O) are retained in the liquid phase. For this reason the residual water gets isotopically heavier and shifts to the right of the precipitation values.

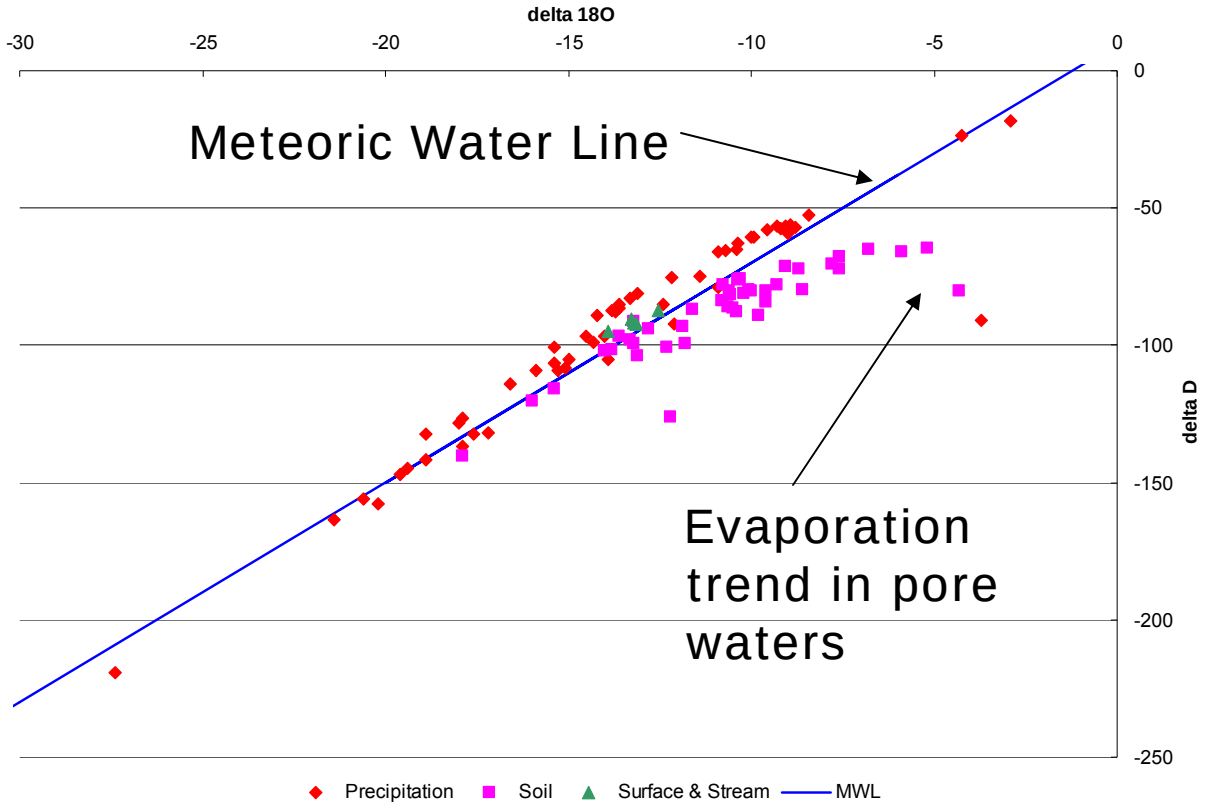

FIGURE 114. Stable isotope analyses of precipitation, pore water, seeps, and stream flow in the GHN area.

MATRIC SUCTION

Handheld tensiometers were used to collect 144 matric potential values from GHN in 2004 and 2005 and other areas in the mine site from 2004 to 2007 (Appendix 7). The data were used to provide an understanding of the hydraulic properties of the distinguishable layers in the trenches. The matric potential values in the trenches ranged between –20 kPa and –1 kPa and the median matric potential was –5 kPa. The values vary significantly and do not provide any information about how the matric potential will vary with time in a particular place; they simply provide useful information for the present state of the pile at the time of the measurement. There is no correlation between matric suction and gravimetric moisture content (Fig. 115). Appendix 5 contains logs of the individual benches with their distribution of matric suction.

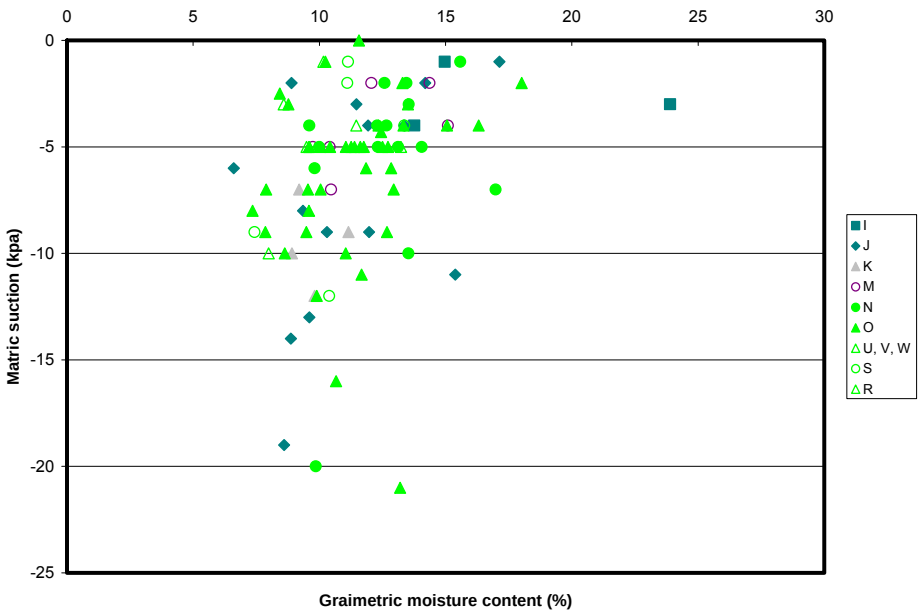

FIGURE 115. Scatter plot of gravimetric moisture content (%) versus matric suction (kPa) showing no correlation.

SLAKE DURABILITY INDEX

The slake durability test is a simple test used to rank rock masses according to their resistance to weathering and deterioration levels after a standard cycle of drying and wetting; an index of alteration is provided by this test. The mechanisms associated with slake durability are subject to permeability, porosity, and the action of fluids and the capacity of the rock to resist turbulent forces (Franklin and Chandra, 1972). Also, ion exchange, capillary effect and stress relief have important effects on slake durability. A series of slake durability tests for soft rocks were performed on four types of soft rocks and the results showed that the slake durability index of weathered soft rocks was influenced by the degree of weathering (Agustawijaya, 2004) and that weathered rock features are compromised by mechanical properties (Gupta and Rao, 2000).

The assessment of weathering processes and slaking properties is important, because the durability of rocks is affected by short and long-term weathering. Thus, it is important to examine the petrographic and chemical properties of the rocks while assessing the slaking properties. Furthermore, it is essential to interpret and correlate these properties with rock alteration processes (Dhakal et. al., 2002).

The slake durability indices from GHN are high to extremely high (Table 38) according to the slake durability index classification (Franklin and Chandra, 1972). Samples from the GHN rock pile are relatively similar in slake durability regardless of the geologic layer and location within the rock pile. However, some samples located in the outer units of the rock pile (units C, I) disintegrated more and have lower durability than similar rocks from the same unit and elsewhere in the Questa area (Figs. 116-118; Table 38). These same samples also have lower paste pH and higher SWI (Fig. 119). This suggests that slake durability index of the GHN rock pile samples decreased as the degree of weathering and hydrothermal alteration increased in some samples from the outer units, but not all. However, the decreases were still quite small and suggest that 25-40 years of weathering have not substantially affected the shear strength properties of these rock pile materials (Viterbo, 2007; Gutierrez et al., 2008).

TABLE 38. Summary statistics of the slake durability indices for GHN rock-pile samples, grouped by geologic units.

Units	Statistics	Slake Durability Index
Traffic	No. of Samples	2
	Mean (%)	97
	Standard Deviation (%)	NA
	Minimum (%)	96
	Maximum (%)	98
	Coefficient of Variation (%)	NA
Unit C	No. of Samples	1
	Mean (%)	97.9
	Standard Deviation (%)	NA
	Minimum (%)	97.9
	Maximum (%)	97.9
	Coefficient of Variation (%)	NA
Unit I	No. of Samples	4
	Mean (%)	87.9
	Standard Deviation (%)	5.5
	Minimum (%)	82.2
	Maximum (%)	95
	Coefficient of Variation (%)	6.3
Unit J	No. of Samples	7
	Mean (%)	95.8
	Standard Deviation (%)	1.9
	Minimum (%)	94
	Maximum (%)	98.5
	Coefficient of Variation (%)	2
Unit N	No. of Samples	5
	Mean (%)	96.3
	Standard Deviation (%)	1.4
	Minimum (%)	94
	Maximum (%)	98.5
	Coefficient of Variation (%)	1.5
Unit K	No. of Samples	5
	Mean (%)	96.2
	Standard Deviation (%)	2.2
	Minimum (%)	93.6
	Maximum (%)	98.4
	Coefficient of Variation (%)	2.3
Unit O	No. of Samples	18
	Mean (%)	96.5
	Standard Deviation (%)	1.4
	Minimum (%)	93.6
	Maximum (%)	98.1
	Coefficient of Variation (%)	1.5
Unit R	No. of Samples	2

Units	Statistics	Slake Durability Index
	Mean (%)	96.4
	Standard Deviation (%)	NA
	Minimum (%)	95.5
	Maximum (%)	97.3
	Coefficient of Variation (%)	NA
unit S	No. of Samples	3
	Mean (%)	97.4
	Standard Deviation (%)	1.6
	Minimum (%)	95.6
	Maximum (%)	98.4
	Coefficient of Variation (%)	1.6
Unit P	No. of Samples	1
	Mean (%)	96.7
	Standard Deviation (%)	NA
	Minimum (%)	96.7
	Maximum (%)	96.7
	Coefficient of Variation (%)	NA
Unit U	No. of Samples	5
	Mean (%)	97.7
	Standard Deviation (%)	0.6
	Minimum (%)	97.1
	Maximum (%)	98.5
	Coefficient of Variation (%)	0.6
Unit UV	No. of Samples	3
	Mean (%)	96.7
	Standard Deviation (%)	0.8
	Minimum (%)	95.9
	Maximum (%)	97.4
	Coefficient of Variation (%)	0.8
Unit M	No. of Samples	1
	Mean (%)	96.6
	Standard Deviation (%)	NA
	Minimum (%)	96.6
	Maximum (%)	96.6
	Coefficient of Variation (%)	NA
Rubble	No. of Samples	7
	Mean (%)	97.4
	Standard Deviation (%)	1.1
	Minimum (%)	95.2
	Maximum (%)	98.5
	Coefficient of Variation (%)	1.1
Unit H	No. of Samples	1
	Mean (%)	96.5
	Standard Deviation (%)	NA
	Minimum (%)	96.5

Units	Statistics	Slake Durability Index
	Maximum (%)	96.5
	Coefficient of Variation (%)	NA
Colluvium	No. of Samples	9
	Mean (%)	95.7
	Standard Deviation (%)	1.7
	Minimum (%)	93
	Maximum (%)	98.5
	Coefficient of Variation (%)	1.8
Unstable GHN	No. of Samples	11
	Mean (%)	95.7
	Standard Deviation (%)	5.1
	Minimum (%)	80.9
	Maximum (%)	99.2
	Coefficient of Variation (%)	5.3

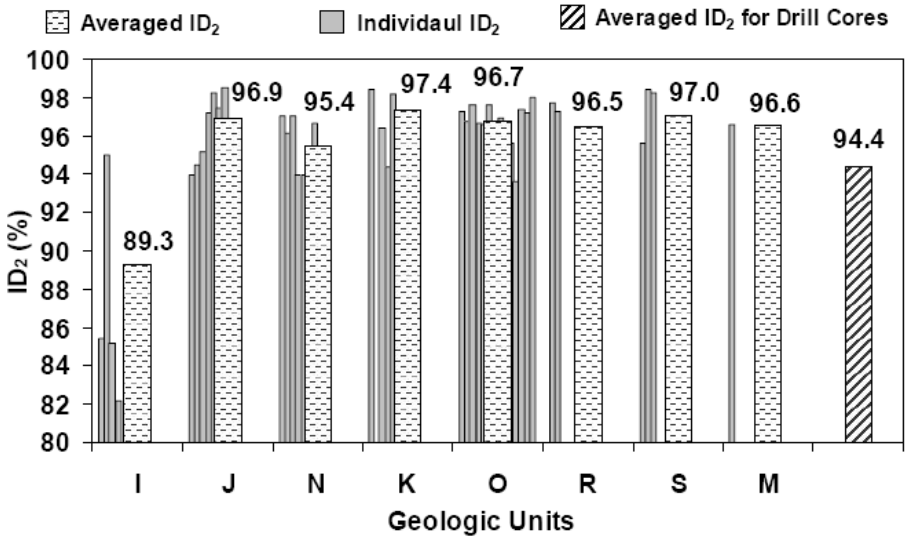

FIGURE 116. Bar graph of slake durability index (ID_2) by geologic unit, GHN. The oxidized samples (unit I) tend to have lower slake durability indices than samples from the inner units of the rock pile. Drill core samples are unweathered samples of the open pit deposit before mining.

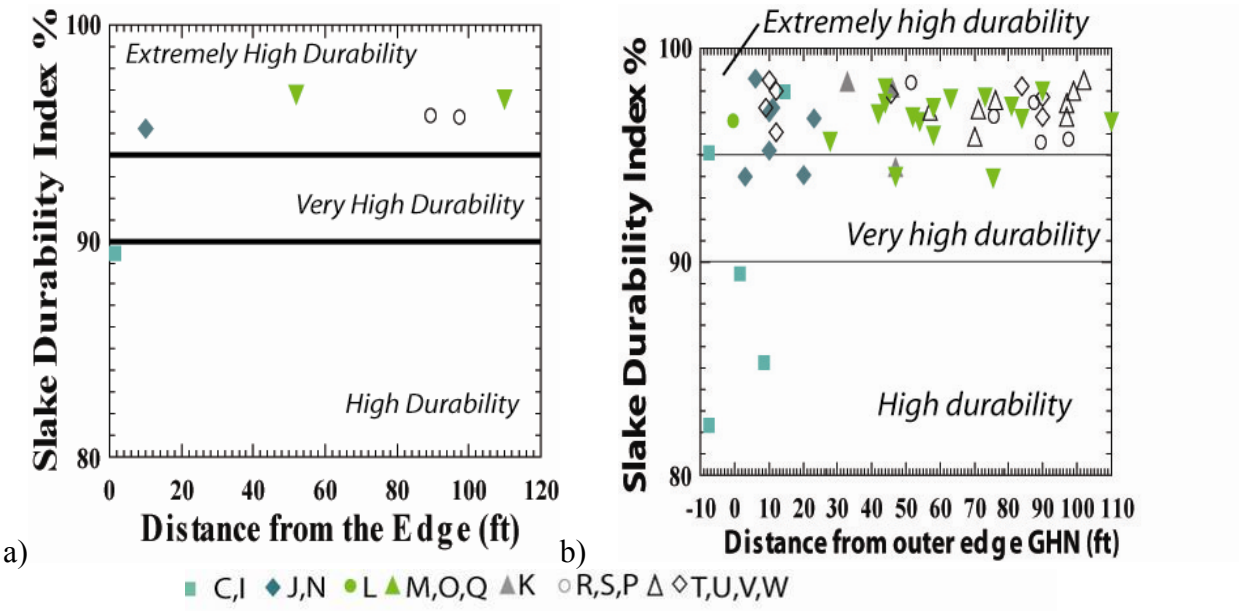

FIGURE 117. Variations in slake durability index for geologic units a) across bench 9, GHN and b) all samples from GHN. See Figure 46 for geologic section and Table 20 for descriptions of the geologic units.

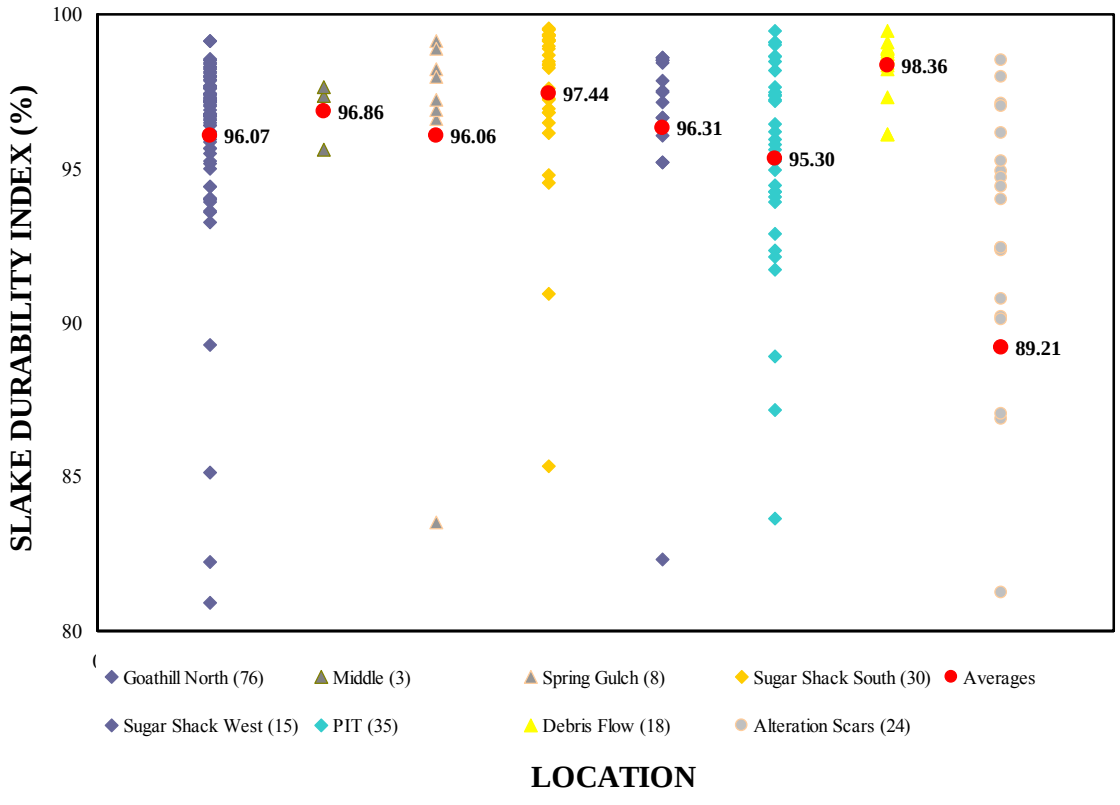

FIGURE 118. Slake durability index values for the Questa rock piles, alteration scars, and debris flows. The average slake durability index for each location is shown with a circle. The number of samples for each location is shown in parenthesis.

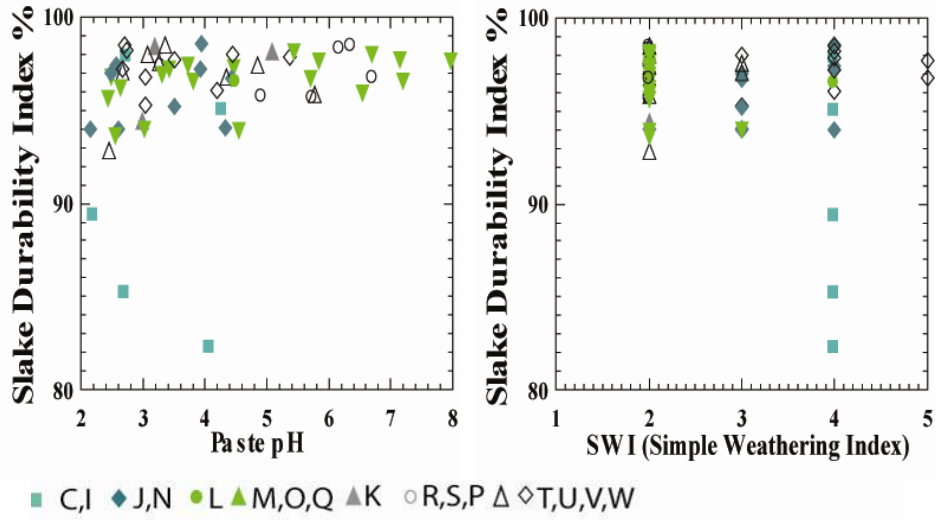

FIGURE 119. Scatter plots of slake index vs. paste pH and SWI for samples from GHN. Refer to Table 20 for descriptions of the geologic units.

POINT LOAD TESTS

The point load test is a simple test used to estimate strength of rocks. The testing machine used consists of a loading frame, which measures the force required to break the sample, and a system for measuring the distance between the two platen contact points. One of many advantages of the point load test is that rock sample failures occur at much lower applied loads than when they are under compression. Therefore, a tester with a lower load capacity is required (Fookes, et. al., 1971). In addition, the point load test can be performed on samples with different shapes, either core or irregular shaped samples. GHN samples have been used for the point load tests and proved most suitable for this purpose because of the nature of the samples as previous work has shown (Broch and Franklin, 1972). The point load index (Is), obtained with the point load test, is adequate as a standard to classify rock strength. Therefore, the point load equipment is being used on samples from GHN rock pile.

Point load tests were performed on samples from GHN and elsewhere in the Questa mine area (Table 39). The point load indices are medium to very high (Fig. 120, 121) according to the point load strength index classification (Broch and Franklin, 1972). Samples from the GHN rock pile are similar in point load index regardless of geologic layer and location within the rock pile, except that some, but not all samples located in the outer edge of the rock pile (units C and I) that are weaker and have lower point load indices (Fig. 121, 122). There are no correlations between point load index and paste pH or SWI (Fig. 121). Samples from the GHN have similar point load indices as samples from other rock piles and materials in the Questa area (Fig. 120). However, after 25-40 years of weathering, the majority of the rock fragments within the rock piles still present high strength.

TABLE 39. Summary statistics of the point load strength for GHN rock pile samples.

Location	Statistics	Point Load Strength Index
Unit I	No. of Samples	2
	Mean (MPa)	1.1
	Standard Deviation (MPa)	NA
	Minimum (MPa)	0.6
	Maximum (MPa)	1.6
	Coefficient of Variation (%)	NA
Unit J	No. of Samples	6
	Mean (MPa)	5.0
	Standard Deviation (MPa)	1.7
	Minimum (MPa)	3.3
	Maximum (MPa)	7.0
	Coefficient of Variation (%)	34.0
Unit N	No. of Samples	4
	Mean (MPa)	2.6
	Standard Deviation (MPa)	1.4
	Minimum (MPa)	1.1
	Maximum (MPa)	4.5
	Coefficient of Variation (%)	53.8
Unit K	No. of Samples	4
	Mean (MPa)	5.3
	Standard Deviation (MPa)	2.0
	Minimum (MPa)	3.7
	Maximum (MPa)	8.2
	Coefficient of Variation (%)	37.7
Unit O	No. of Samples	4
	Mean (MPa)	3.5
	Standard Deviation (MPa)	1.3
	Minimum (MPa)	2.4
	Maximum (MPa)	5.4
	Coefficient of Variation (%)	37.1
Unit R	No. of Samples	2
	Mean (MPa)	5.8
	Standard Deviation (MPa)	NA
	Minimum (MPa)	4.3
	Maximum (MPa)	7.3
	Coefficient of Variation (%)	NA
Unit S	No. of Samples	3
	Mean (MPa)	4.0
	Standard Deviation (MPa)	1.0
	Minimum (MPa)	3.4
	Maximum (MPa)	5.3
	Coefficient of Variation (%)	25.0
Unit U	No. of Samples	1
	Mean (MPa)	6.1
	Standard Deviation (MPa)	NA
	Minimum (MPa)	6.1

Location	Statistics	Point Load Strength Index
	Maximum (MPa)	6.1
	Coefficient of Variation (%)	NA
Unit UV	No. of Samples	2
	Mean (MPa)	5.3
	Standard Deviation (MPa)	NA
	Minimum (MPa)	4.5
	Maximum (MPa)	6.1
	Coefficient of Variation (%)	NA
Unit M	No. of Samples	1
	Mean (MPa)	3.7
	Standard Deviation (MPa)	NA
	Minimum (MPa)	3.7
	Maximum (MPa)	3.7
	Coefficient of Variation (%)	NA
Rubble	No. of Samples	1
	Mean (MPa)	6.5
	Standard Deviation (MPa)	NA
	Minimum (MPa)	6.5
	Maximum (MPa)	6.5
	Coefficient of Variation (%)	NA

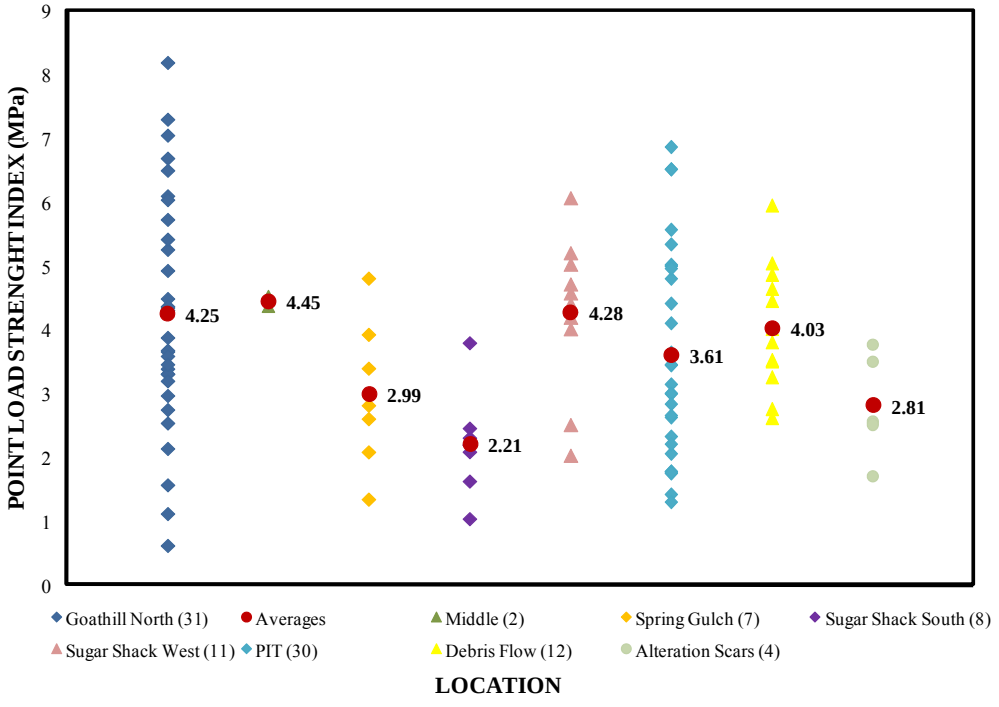

FIGURE 120. Point load strength index values for the rock piles, alteration scars and debris flows.

The average point load strength index for each location is shown with a circle. The number of samples for each location is shown in parenthesis.

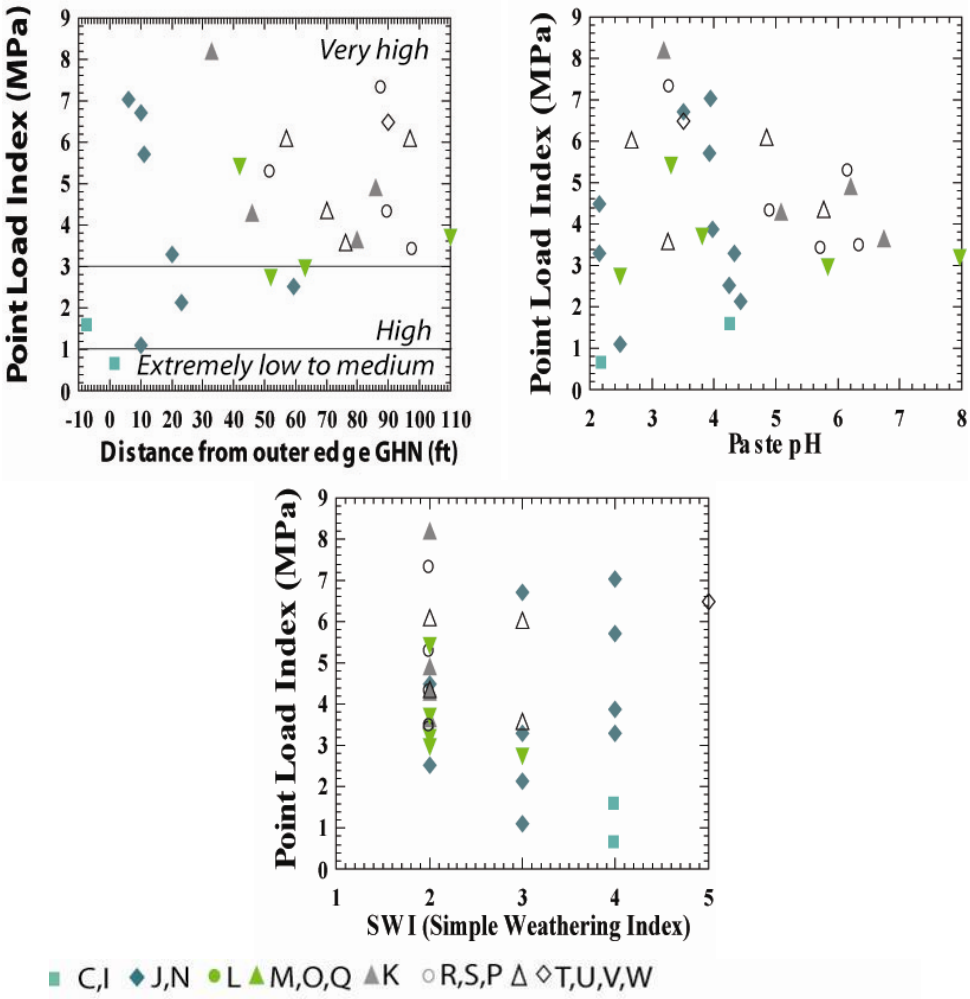

FIGURE 121. Variations in point load index for geologic units, paste pH and SWI for samples from GHN. See Table 20 for descriptions of the geologic units.

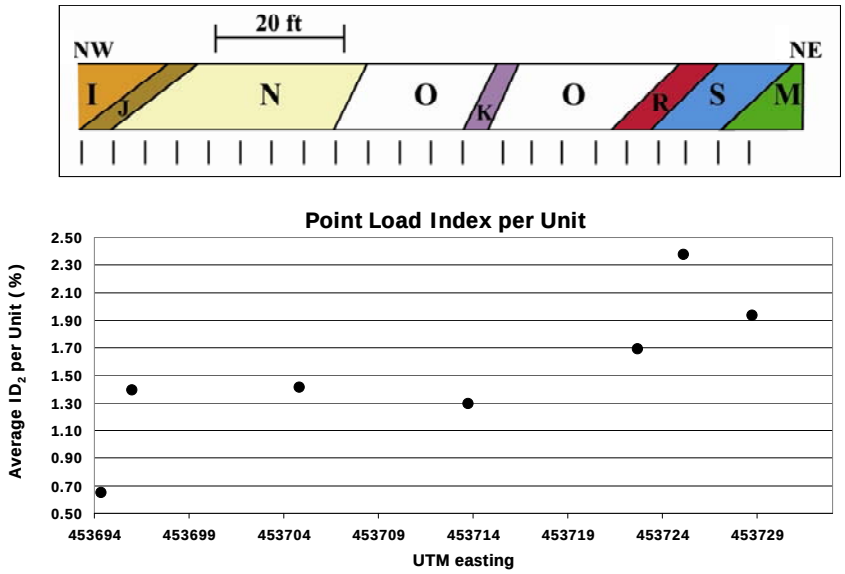

FIGURE 122. Variations in point load index for geologic units across bench 9, GHN. See Figure 46 for geologic section and Table 20 for descriptions of the geologic units.

DIRECT SHEAR TESTS

Direct shear tests were performed on samples from the GHN rock pile and other locations on and around the Questa mine. Representative samples were collected based upon visible changes in the weathering characteristics and were not collected for the purpose of slope stability analysis.

URS Corporation (2003) reports the results of a number of shear tests on Questa rock-pile material using 12 inch wide and 2.4 inch diameter shear boxes that were conducted by AMEC geotechnical laboratory and Advanced Terra Testing in Arizona and Colorado, respectively. The tests were performed under different normal stresses ranging from 119.7 to 478.8 kPa (2.5 to 10 ksf) and 98.6 to 526.7 kPa (2.06 to 11 ksf) for 12-inch and 2.4-inch samples, respectively. The materials of minus 1.5 inch for the 12-inch box and minus No. 4 sieve for 2.4-inch diameter box were used for the shear tests. The materials for 12-inch samples were prepared using dry densities ranging from 1522 to 1682 kg/m^3 (95 to 105 pcf) at water contents ranging from 8 to 12%. The 2.4-inch samples had dry densities of 1522 to 1890 kg/m^3 (95 to 118 pcf) and water contents of 10 to 14%. The friction angle and cohesion for 12-inch shear box ranged from 26° to 59^o and 0 to 111 kPa, respectively. For the 2.4-inch shear box, the friction angle and cohesion ranged from 30° to 41^o and 0 to 34 kPa, respectively. Based on the above shear test results, URS Corporation (2003) concluded that as larger particles are allowed to be present in the shear box, higher shear strengths are obtained; therefore scalping of the Questa rock-pile material causes reduction in the measured shear strengths. These results have been confirmed by additional studies by the QRPWASP (Boakeye, 2008; Nunoo, 2009).

The shear zone beneath the GHN rock pile had friction angles ranging between 16º and 31º, with an average of 23º (Norwest Corporation, 2004). The foundation soils (natural soils in the vicinity of the rock piles) had friction angles that varied from 33 to 44º with an average of 40º (Norwest Corporation, 2004). Samples from a residual weathered profile of the weathered

bedrock beneath the unstable portion of GHN had high peak internal friction angles between 38º and 42º (McLemore, 2009, fig. 4). The friction angle of samples from the weathering profile increased slightly from the middle to the top (more weathered) of the weathering profile (McLemore, 2009, fig. 23).

The peak friction angle for GHN samples run at NMIMT varies from 38 to 48° with ultimate (residual) friction angles ranging from 34 to 44° (Tables 40, 41). These high values of peak friction angle are attributed mostly to grain shape (subangular to very angular) and relative density of the test samples (Gutierrez et al., 2008). Samples from unit I of GHN rock pile (φ =40.8°) have the lowest average peak friction angle (Table 41; Fig. 123). Unit I is near the surface and has been exposed to more intensive weathering, which resulted in a lower point load strength (1.1 MPa) and slake durability index of the rock fragments (87.9%) in some but not all samples of this unit (Tables 38-39). The NMIMT values for internal friction angle are higher than the values reported for saturated conditions ($\phi_{average}$ = 31º and 36º) in past geotechnical studies at GHN rock pile (Robertson GeoConsultants Inc., 2000b; Norwest Corporation, 2004). This difference in friction angle is expected between dry and saturated conditions.

Comparisons between peak friction angle and various geotechnical properties do show some correlations. Specifically, as the percent fines increased, the peak friction angle decreased (Fig. 123). This has been documented in the literature (Norwest Corporation, 2005; McLemore et al., 2009c) and is a result of the decrease in interlocking grain contacts as the percent fines increases. Also as expected, the peak friction angle decreases with increase in plasticity index, for the GHN samples (Fig. 123). As the point load index increases, the friction angle increases (Fig. 123). The trend between peak friction angle and slake durability index is not strong. In general, the lower friction angles correspond to the lower slake durability and point load indices (Fig. 123; Gutierrez et al., 2008).

There is no strong correlation between peak friction angle and lithology (Fig. 124). However, a weak negative trend exists between friction angle and QSP alteration (Fig. 124). This is attributed, in part, to an increase in the clay mineral sericite (illite), which is associated with QSP. Samples with lower amounts of prophylitic alteration tend to have lower friction angles (Fig. 124). But these differences in friction angles are small.

The peak friction angles are high for samples from GHN and are similar to other Questa materials (Table 40). The lower friction angles are, in general, from the outer part of the rock pile (more weathered), more weathered samples in the interior, and the foundation soils beneath GHN (Fig. 125, Table 33). A similar trend is observed in paste pH values and weathering textures are consistent with this trend. This supports previous suggestions and other studies where friction angle decreased with increase in weathering (Arel and Tuğrul, 2001; Bryant, 2003; Tuğrul and Gürpinar, 1997; Moon and Jayawardane, 2004). However, the differences in friction angle between the outer and interior units are relatively small. These results and other studies suggest that changes in physical properties (i.e. particle size, texture and fabric) have a larger effect than mineralogic and chemical changes on the friction angle than do mineralogic and chemical changes (Arel and Tuğrul, 2001; Moon and Jayawardane, 2004). The high friction angles of Questa mine materials are due to (a) angularity of the particles (Nunoo et al. 2009), (b) high strength as determined by point load strength and slake durability of the rock fragments (Viterbo et al., 2007), and (c) presence of low amount of fines material in the rock piles. Since the analogs are older than the rock piles, it appears that weathering so far has not caused noticeable reduction of the friction angles at the test locations. Friction angle, point load strength index and slake durability index of the GHN rock-pile samples decreased as the degree of

hydrothermal alteration and weathering increased in some samples but not all (Gutierrez, 2006; Gutierrez et al., 2008).

TABLE 40. Summary of peak friction angle form direct shear tests of samples from GHN by geologic units, normal stress of 160-750 kPa (modified from Gutierrez, 2006; Gutierrez et al., 2008; Boakye, 2008). Histograms and statistical analysis are in Appendix 11.

Location	No of Samples Tested	Min (degrees)	Max (degrees)	Range (degrees)	Mean (degrees)	Standard Deviation (degrees)	Coefficient Of Variation (%)
All Andesite samples	10	38.7	43.7	5.0	41.0	1.8	4.5
All Rhyolite samples (Amalia Tuff)	9	37.8	45.7	7.9	42.7	2.6	6.1
All Colluvium samples	22	36.9	46.1	9.2	41.4	2.5	6.0
All Debris Flow samples	12	39.2	50.1	10.9	44.3	3.9	8.8
All alteration scars	22	33.4	54.3	20.9	40.7	4.8	11.8
Oxidized, outer zone (GHN rock pile)							
Unit C	1	45.7	45.7	na	45.7	na	na
Unit I	5	38.8	42.1	3.3	40.8	1.3	3.2
Intermediate zone (GHN rock pile)							
Unit J	5	43.7	45.8	2.1	44.9	0.8	1.8
Unit N	3	41.7	42.8	1.1	42.1	0.6	1.4
Unoxidized, internal zone (GHN rock pile)							
Unit K	3	39.6	46.9	7.3	42.3	4.0	9.5
Unit O	15	39.9	47.8	7.9	42.8	2.2	5.1
Unit M	1	42.7	42.7	na	42.7	na	na
Unit R	2	43.4	45.8	2.4	44.6	NA	NA
Unit S	1	43.3	43.3	NA	43.3	NA	NA
Unit P	1	43.8	43.8	NA	43.8	NA	NA
Unit U	4	41.5	46.2	4.7	43.0	2.2	5.1
Unit V	3	42.0	47.8	5.8	44.5	3.0	6.7
Unit RUB	2	39.3	42.1	2.8	40.7	na	na
Samples from the Unstable portion of GHN	11	37.8	45.3	7.5	41.7	2.2	5.3
All Questa materials tested	178	33.4	54.3	20.9	42.0	3.3	7.8

TABLE 41. Summary of ultimate (or residual) friction angle form direct shear tests of samples from GHN by geologic units, normal stress of 160-750 kPa (modified from Gutierrez, 2006; Gutierrez et al., 2008; Boakye, 2008).

Location	No of Samples Tested	Min (degrees)	Max (degrees)	Range (degrees)	Mean (degrees)	Standard Deviation (degrees)	Coefficient Of Variation (%)
All Andesite samples	10	34.1	42.2	8.1	37.4	2.3	6.1
All Rhyolite samples (Amalia Tuff)	9	32.1	38.8	6.7	37.1	2.0	5.3
All Colluvium samples	22	35.7	43.7	8.0	38.6	1.9	4.9
All Debris Flow samples	12	33.8	42.3	8.5	36.9	2.5	6.8
Oxidized, outer zone (GHN rock pile)							
Unit C	1	43.2	43.2	NA	43.2	NA	NA
Unit I	5	34.6	39.9	5.3	37.4	2.0	5.3
Intermediate zone (GHN rock pile)							
Unit J	5	33.7	43.2	9.5	38.3	3.2	8.4
Unit N	3	38.7	40.0	1.3	39.5	0.7	1.8
Unoxidized, internal zone (GHN rock pile)							
Unit K	3	37.5	44.3	6.8	39.9	3.8	9.5
Unit O	15	33.8	43.0	9.2	39.1	2.3	5.9
Unit M	1	42.0	42.0	NA	42.0	NA	NA
Unit R	2	40.7	40.7	0.0	40.7	NA	NA
Unit S	1	39.3	39.3	NA	39.3	NA	NA
Unit P	1	35.0	35.0	NA	35.0	NA	NA
Unit U	4	36.9	42.4	5.5	39.1	2.3	5.9
Unit V	3	35.9	41.6	5.7	38.6	2.9	7.5
Scars	22	26.9	44.8	17.9	36.2	3.4	9.4
Samples from the Unstable portion of GHN	11	34.2	41.7	7.5	38.2	2.3	6.0
All Questa material tested	178	26.9	44.8	17.9	38.0	2.6	6.8

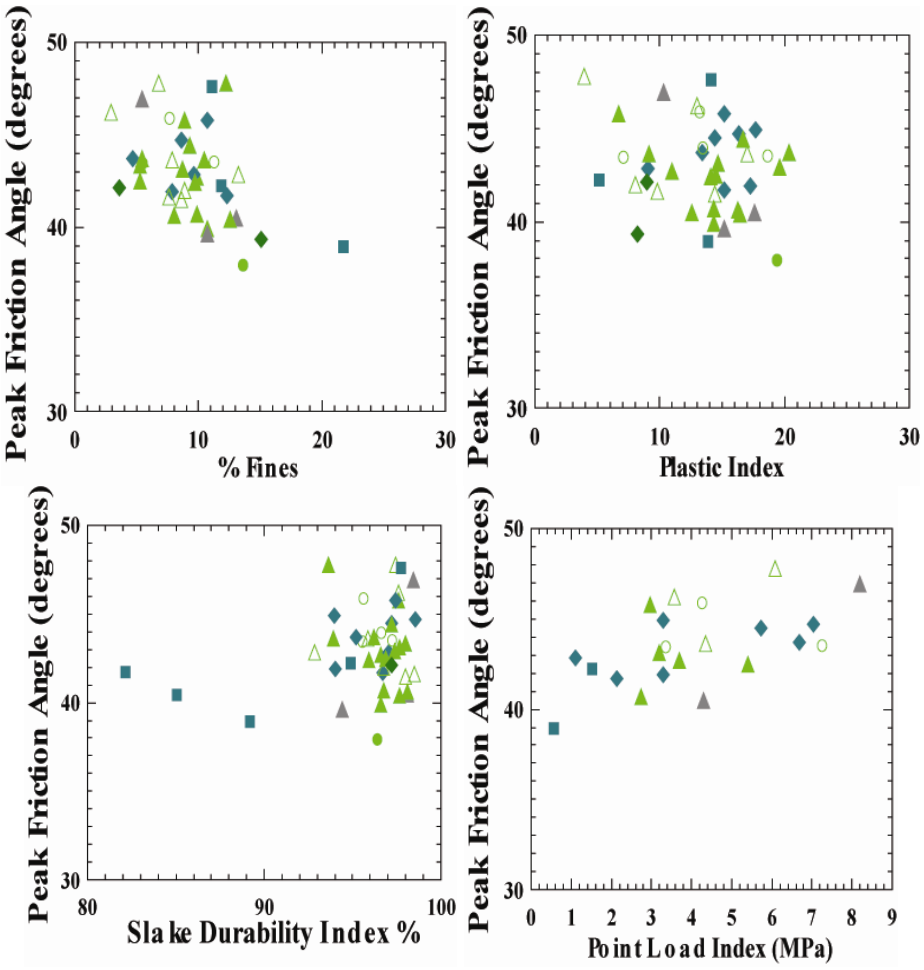

FIGURE 123. Scatter plots of peak friction angle versus geotechnical properties (percent fines, plasticity index, slake durability index, point load index) by geologic unit. Refer to Table 20 for descriptions of the geologic units.

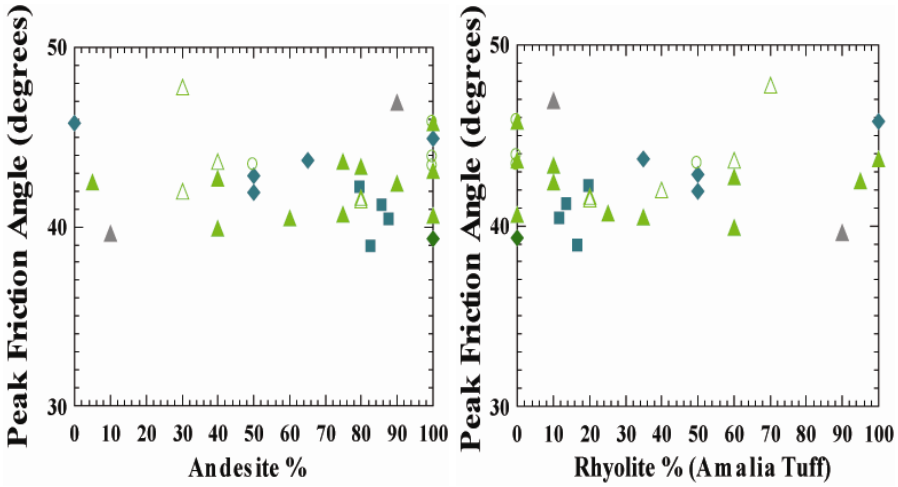

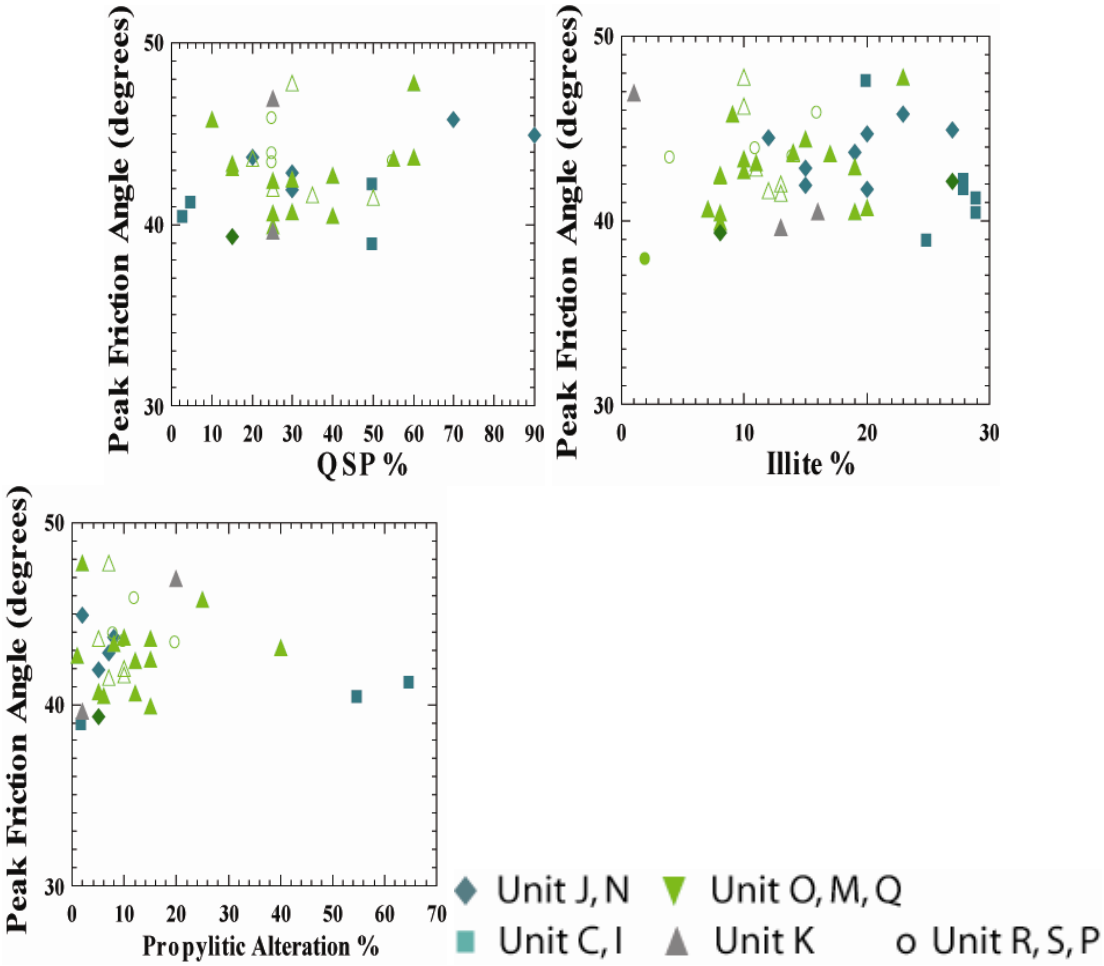

FIGURE 124. Variations between peak friction angle and lithology and alteration. These scatter plots show weak positive correlation of friction angle with QSP alteration. This correlation is related, in part, to an increase in the amount of sericite (a form of illite) in the samples. Refer to Table 20 for descriptions of the geologic units.

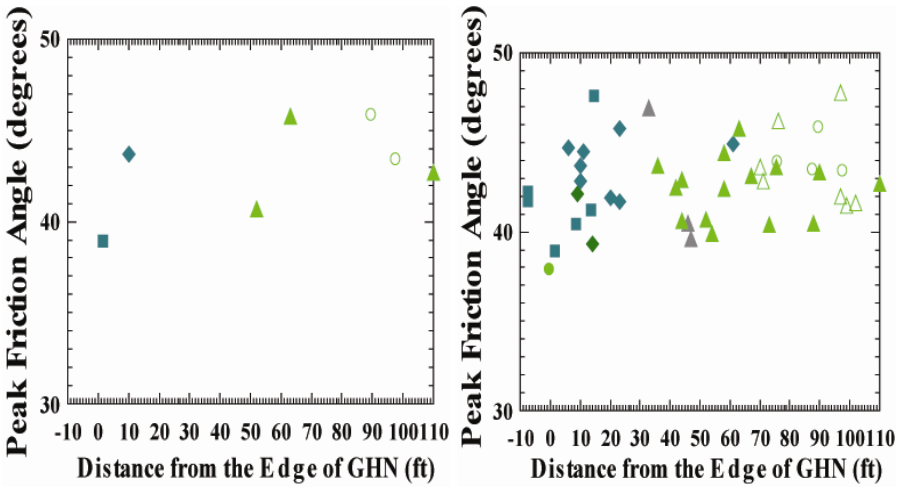

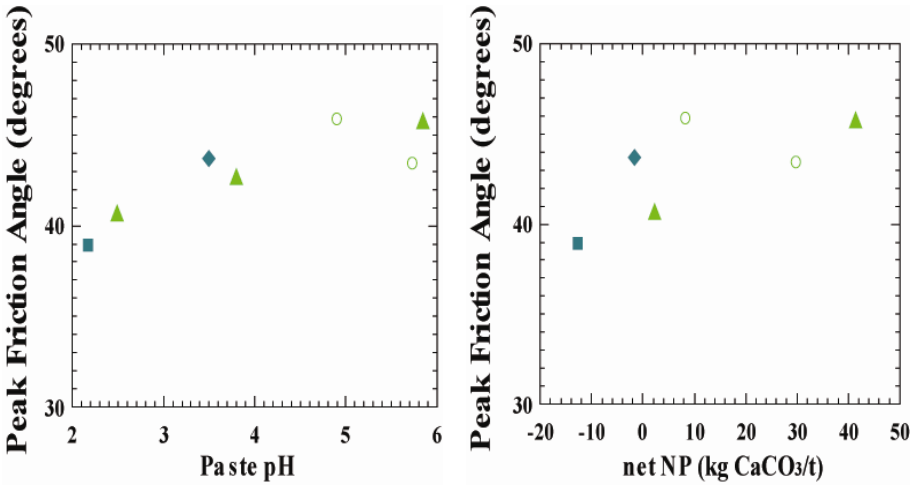

FIGURE 125. Variation of peak friction angle across bench 9 of trench LFG-0006 and all samples from GHN. The lower friction angles are from the outer part of the rock pile (more weathered), more weathered samples in the interior, and the foundation soils beneath GHN. The higher friction angles are from the interior (least weathered) part of the rock pile. A similar trend is observed in paste pH and net NP (neutralizing potential) values. Refer to Figure 46 for geologic section and Table 20 for descriptions of the geologic units.

HOT ZONE GAS AND TEMPERATURE DATA

Air flow through rock piles has the capacity to increase the rate of oxidation and weathering of pyrite by continuing the supply of oxygen and water as humidity. The principle mechanisms of air flow through rock piles include (Wels et al., 2003; Dobchuk et al., 2004):

- diffusion
- advection (thermal, wind pressure gradients, barometric pumping)
- convection.

Some researchers believe that diffusion is probably restricted to the near surface of the rock piles (Wells et al., 2003), but advection and convection have the potential to move air throughout the entire rock pile. Dobchuk et al. (2004) advocate that additional studies are required to understand diffusion through rock piles. The magnitude of air flow is controlled by complex interaction of the daily weather conditions and physical and chemical properties, including the stratigraphy and structure of individual layers of the rock piles (Reiter, 2009). The first step in understanding the importance of air flow in rock piles is to identify, characterize, and field monitor known conditions.

Venting gases or water vapor have been observed from several sites at the Questa mine, mostly from drill holes in the front rock piles (Figs. 126-129) and from cracks at the surface of GHN prior to regrading. Air venting from coarse layers in GHN during sampling of the trenches was observed (Fig. 128). Elevated temperatures and relative humidities explain these venting gases, often called fumaroles, which are common at other mine sites (Ritchie, 2003; Wels et al., 2003; McLemore et al., 2009c). Recent experimental studies by Jerz (2002; Jerz and Rimstidt, 2004) have confirmed earlier work by Morth and Smith (1966) that shows pyrite oxidizes faster in moist air than under saturated conditions, thereby accelerating the weathering of the rock piles, at least locally, and producing hot spots.

Shaw et al. (2003) described the results of one years' monitoring of temperature, CO_2, and O_2 from instrumented drill holes in the rock piles at the mine (Robertson GeoConsultants, 1999). CO_2 decreased with depth and temperature and O_2 increased with depth in the Robertson GeoConsultants data. NMIMT obtained the data from these instrumented drill holes for 1999-2004, which is summarized below from Tachie-Menson et al. (2005). New drill holes drilled in 2004 on the front rock piles are venting gases as well, but were not instrumented for temperature or gases. Unfortunately, there is no temperature or gas concentration data from GHN. However, observed trends from instrumented holes in the front rock piles can be used as an analog to understand air and water vapor flow in GHN.

Temperature, oxygen and carbon-dioxide data collected from nine boreholes monitored from October 1999 to December 2004 were analyzed with plots of each of the three parameters against time, depth profiles of mean monthly values, and calculation of means, standard deviations and correlation coefficients. Oxygen concentrations were lower but carbon-dioxide concentrations were considerably higher than ambient air values. Concentrations of oxygen and carbon-dioxide had a negative correlation that manifested themselves in both the depth profiles and time plots (Tachie-Menson et al., 2005). The highest oxygen and lowest carbon-dioxide concentrations occurred during the colder months. Temperatures varied with the seasons at less than 20 to 30 ft. Below 30 ft depths, temperatures did not show seasonal variations, but rather decreased slightly over the five-year period with a maximum decrease of approximately 10°F. Over the same period, mean oxygen concentrations increased by up to 10% and mean carbon dioxide concentrations decreased by up to 1%. Three of the rock piles (Spring Gulch, Sugar Shack South and Sugar Shack West) had higher average temperatures and lower oxygen concentrations in boreholes at higher elevations. Two rock piles (Spring Gulch and Sugar Shack South) showed higher carbon-dioxide concentrations at higher elevations.

Detailed temperature logs from 18 drill holes in the front rock piles provide estimates of vertical and horizontal flow within the rock piles (Reiter, 2009). The analyses indicate that the predominant flow is by advection from large amounts of air flowing within the rock pile. The heat is generated by pyrite oxidation. The flow patterns are complex and likely change with time.

The interpretations suggest that ample air enters the rock piles through the toe and flows upward through rubble zones and other coarse layers by advection and convection to higher elevations (Wels et. al., 2003; Reiter, 2009). Cool air flows through many of the coarse gravel-cobble zones within the interior units of GHN, as observed during the sampling and mapping of the trenches. There are minor air entry and exit points along the slopes of the rock piles. This phenomenon is observed at a road cut in Sulphur Gulch, where warm air exits the pile along the slope (Fig. 127). However, the mass flow of air from the toe to the top of the piles is the predominant flow mechanism (Fig. 127). Oxygen is used up from the air by oxidation processes, mostly pyrite oxidation catalyzed by micro-organisms, and carbon-dioxide is produced by decomposition of carbonates. Pyrite oxidation is strongly exothermic and produces the heat that controls the temperature of the piles at depth (Shaw et. al., 2003). With time, the chemical processes are slowing down due to reduction of reactants and/or coating of mineral surfaces by reaction products, resulting in decreasing temperatures and carbon dioxide concentrations and increasing oxygen concentrations. In other words, the rock pile material is approaching chemical equilibrium. The flow of air into the rock pile is controlled in part by the difference in temperature between ambient air and the interior of the rock pile and, therefore, there is greater influx of air during the colder months (Wels et. al., 2003). This accounts for the seasonal variation of oxygen and carbon-dioxide concentrations even at depths where temperature does

not change with the seasons. Table 42 shows the elevation and mean values of temperature, oxygen and carbon-dioxide for each borehole in the four monitored piles.

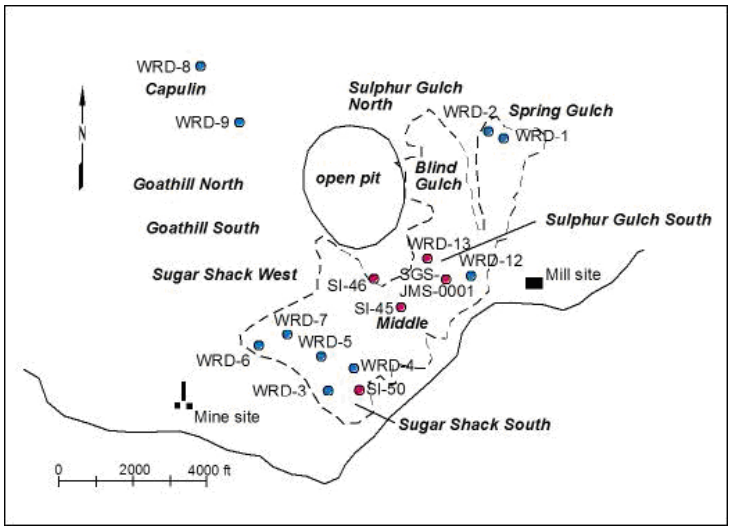

FIGURE 126. Location of venting drill holes and surface vent area. Blue indicates drill holes drilled in 1999 that contain monitoring instruments for temperature, O_2, and CO_2. Red indicates drill holes and surface vent area (SGS-JMS-0001) that do not contain temperature and gas instrumentation and are sites monitored by the NMIMT team.

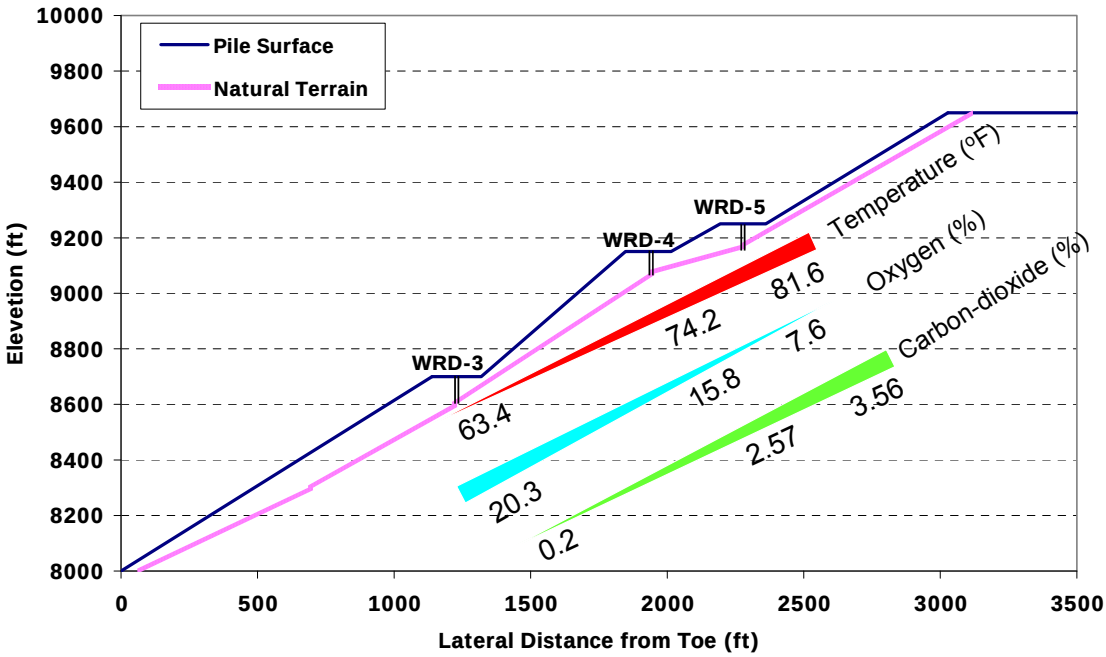

FIGURE 127. Section through monitored drill holes in Sugar Shack South showing the relationship between O2, CO2, and temperature within the rock pile. The thicker line indicates increase in the parameter.

FIGURE 128. Photo of venting gases venting from SGS-JMS-0001 at Sulphur Gulch South rock pile.

FIGURE 129. Photo of venting gases in GHN using a smoke bomb (GHN-LFG-0003-H019).

TABLE 42. Mean temperatures and oxygen and carbon dioxide concentrations by drill hole.

Rock Pile	Drill Hole Number	Elevation	Temperature	Oxygen	Carbon Dioxide
		(ft)	^{o}F	(%)	(%)
Spring Gulch	WRD-1	9100	50.8	20.00	0.33
	WRD-2	9250	71.5	12.23	0.52
Sugar Shack South	WRD-3	8700	63.4	20.32	0.20
	WRD-4	9150	74.2	15.83	0.80
	WRD-5	9250	81.6	7.60	2.57
Sugar Shack West	WRD-6	9000	55.2	10.20	3.56
	WRD-7	9400	62.4	5.46	2.40
Capulin	WRD-8	9810	66.1	18.50	0.24
	WRD-9	9800	60.3	17.77	0.20

WATER CHEMISTRY

Water samples were collected from seeps at the toe of GHN before reclamation and from trench LFG-021 from the colluvium/bedrock during reclamation of the unstable portion of GHN and analyzed for major and trace elements (Table 42). A sample of the stream flowing through the Narrows of Goathill Gulch also was collected and analyzed for major and trace elements (Table 38). The water samples from the toe of GHN likely represented combined flow from the colluvium/bedrock below the GHN rock pile and GHN rock pile. The sample from trench LFG-021 represents flow from the colluvium/bedrock beneath the unstable portion of GHN. The sample from the stream flowing through the Narrows represents combined seepage and runoff from the Capulin and GHN rock piles and runoff from the alteration scar area in Goathill Gulch.

The chemical analyses of these samples are characterized by acidic, high sulfate, high TDS (total dissolved solids), and high metal concentrations (Table 41). Sulfate is the predominant anion and Al, Mg, Fe, and Mn are the predominant cations. The chemical compositions of the water samples collected for this study are similar to water samples collected by SRK in the same area (SRK, 2004). The GHN water samples are lower in pH and contained more sulfate and metals than many of the water samples collected from the Red River and alteration scars above the Questa mine (LoVetere et al., 2004; Naus et al., 2005; Nordstrom et al., 2005).

The chemical analyses of the GHN waters reflect the dissolution of calcite, gypsum, pyrite, and sphalerite as shown by Figures 130-133. The high Mg is related to chlorite and epidote being dissolved by the acidic waters. The high Mn is related to Mn-bearing carbonate (calcite, dolomite, rhodochrosite), chlorite, and epidote (Table 21). The high fluorine is related to dissolution of fluorite, illite, and smectite, which contain anomalous fluorine concentrations (Fig. 130). Similar chemical trends and relationships to dissolution of minerals were found in surface and ground waters upstream of the Questa mine by the USGS study (Nordstrom et al., 2005; Nordstrom, 2007).

TABLE 42. Chemical analyses of water from GHN and surrounding area. Additional analyses are in the project database. Analyses are in mg/l.

Sample	Area	pH	TDS	Hardness	Cl	F	SO4	Na	K	Mg	Ca
GHN-VTM-0020	toe of GHN rock pile	2.75	19740	5798	33	83	17000	12	bd	1170	400
GHN-VTM-0021	toe of GHN rock pile	2.72	20526	5609	36	85	17800	13	bd	1130	390
GHN-VTM-0025	toe of GHN rock pile	2.76	21569	5897	40	80	18750	16	bd	1200	390
GHN-VTM-0026	toe of GHN rock pile	2.77	21778	5847	20	65	19000	13	bd	1170	420
GHN-VTM-0617	Trench LFG-021	4.3	6936	4019	16	22	5500	29	11	720	430
GHS-VWL-0009	Narrows	2.76	15794	4793	16	75	13400	15	bd	920	410
F-2	Goathill Gulch surface flow	2.8	15000		39	80	14000	12	5	683	403
F-1	Goathill-below subsidence	6	5200		19	50	3450	29	20	478	538
P-2	Goathill-below subsidence	6.8	3850		14	23	2675	54	21	310	475
P-3	Goathill-below subsidence	7.1	3450		14	19	2300	56	20	275	458
P-8	old workings	7.3	2800		18	6	1775	56	8	135	565
P-9	old workings	7.1	3075		21	7	1875	49	7	155	608
C-3	rainforest	7.6	2750		20	2	1665	53	8	160	710
P-6	rainforest	7.8	3000		24	2	1825	55	6	118	655
P-7	rainforest	7.7	2550		24	2	1650	49	5	87	610

Sample	Al	Be	Cd	Co	Cu	Fe	Mn	Mo	Ni	Zn	Reference
GHN-VTM-0020	1480	0.41	0.65	4.1	8.9	325	610	0.014	10	138	this report
GHN-VTM-0021	1550	0.43	0.66	5.1	9.1	335	645	0.014	10	140	this report
GHN-VTM-0025	1690	0.42	0.7	5.3	9.4	350	640	0.014	11	142	this report
GHN-VTM-0026	1620	0.44	0.72	5.4	9.5	355	630	0.015	11	145	this report
GHN-VTM-0617	210	0.111	0.189	0.854	0.929	2.523	195	0.004	2.707	34.49	this report
GHS-VWL-0009	1090	0.34	0.6	3.6	9.3	400	455	0.014	8.3	110	this report
F-2	1008	0.28	0.39	2.7	8.2	303	380	0.094	6.3	85	SRK (2004)
F-1	20	0.084	0.024	0.97	0.053	48	198	3.3	1.4	21	SRK (2004)
P-2	3.6	0.042	0.015	0.42	0.02	12	91	4.9	0.65	7.8	SRK (2004)
P-3	1.6	0.034	0.011	0.35	0.02	7.2	76	4.4	0.53	6	SRK (2004)
P-8	0.14	0.013					13	4.4	0.022	0.057	SRK (2004)
P-9	0.27	0.019					19	5.3	0.021	0.035	SRK (2004)
C-3	0.05						1.5	8.4			SRK (2004)
P-6	0.056						1	8		0.045	SRK (2004)
P-7	0.055						1	7.1		0.078	SRK (2004)

a)

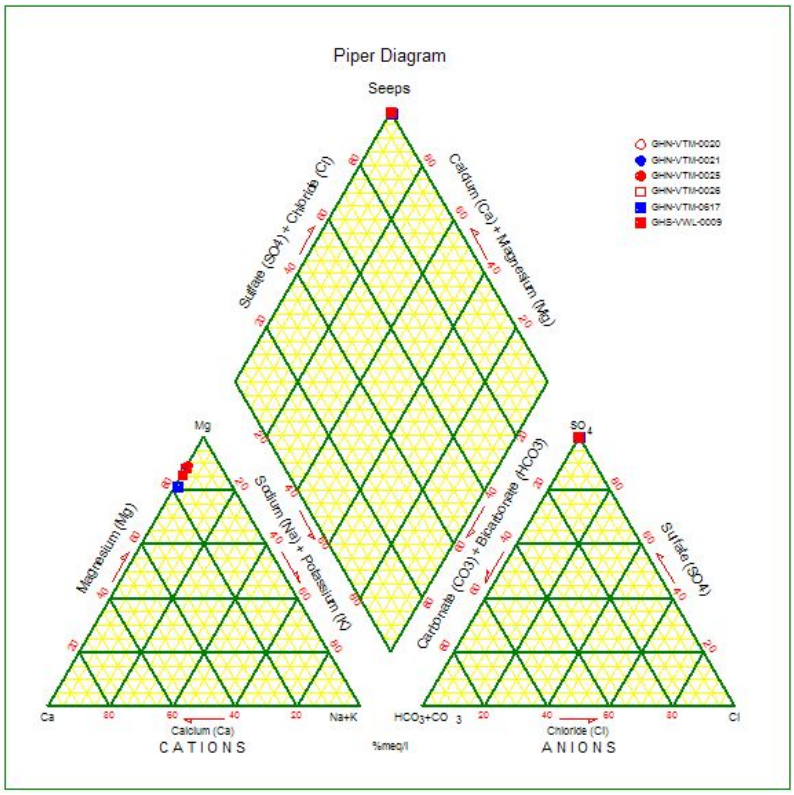

b)

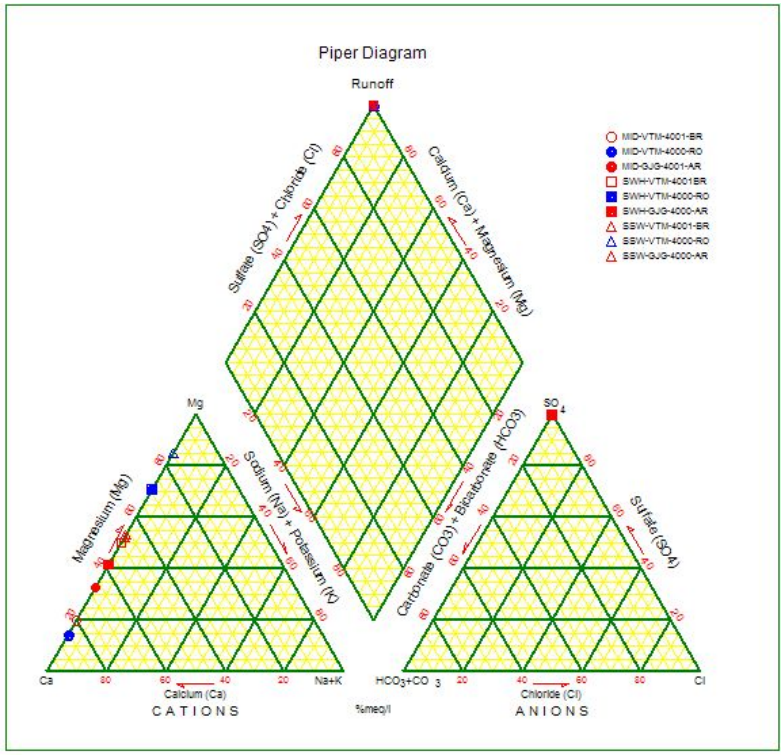

FIGURE 130. Piper diagrams of a) water samples from GHN toe and b) runoff samples during a precipitation event.

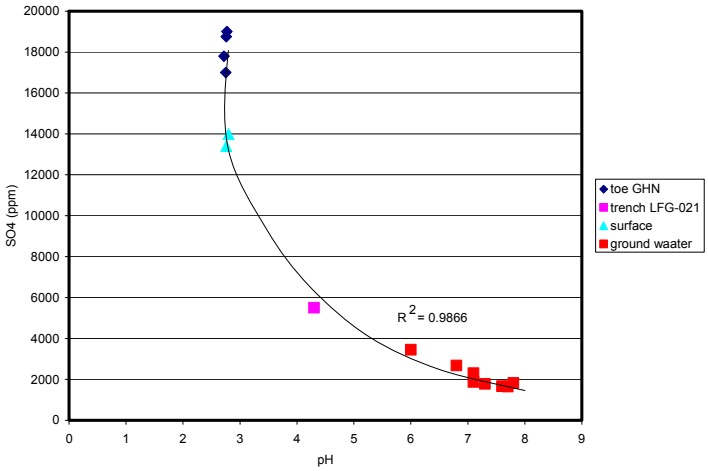

FIGURE 131. SO_4 vs. pH plot indicating that water samples from GHN (toe, this project) and Goathill Gulch (Narrows, surface, this project, SRK, 2004) are higher in SO_4 and lower in pH than GHN trench and ground water (SRK, 2004) samples from Goathill Gulch. Data are in Table 42.

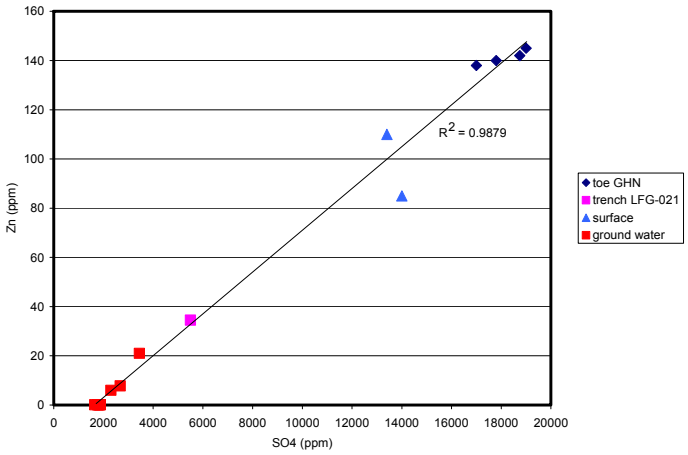

FIGURE 132. Good correlation of Zn vs. SO4 of GHN waters is related to dissolution of sphalerite.

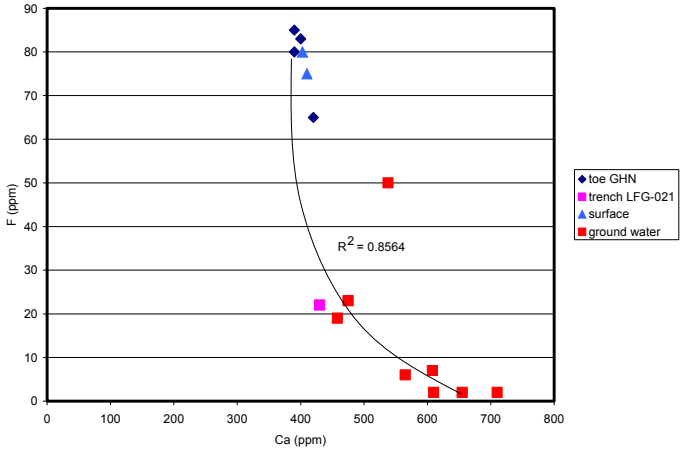

FIGURE 133. Plot showing negative correlation between Ca and F, suggesting that minerals, such as illite and smectite in addition to fluorite are a source of dissolution of F.

CONCEPTUAL GEOLOGIC/GEOCHEMICAL/HYDROLOGIC MODEL

A geologic cross section of the upper portion of GHN is shown in Figure 134. Four different zones of weathering can be distinguished at GHN:

- outer oxidized zone (includes the surface and geologic units C, I and J)
- intermediate zone (includes unit N)
- inner, less oxidized, weathered zone (includes units K-W)
- basal oxidized zone (includes geologic units R and rubble zone).

Weathering decreased from the outside to the inside of the stable portion of GHN. The base of GHN also is oxidized and weathered. The evidence for weathering includes (McLemore et al., 2006a, b):

- Change in color from darker brown and gray in less weathered samples (original color of igneous rocks) to yellow to white to light gray in the weathered samples (Fig. 28-30, 39-42)
- Thin yellow to orange, "burnt" layers within the interior of GHN, where water and/or air flowed and oxidized the rock pile material
- Paste pH, in general, is low in oxidized, weathered samples and paste pH is higher in less weathered samples (Fig. 93)
- Presence of gypsum, jarosite, iron oxide minerals and Fe soluble salts (often as cementing minerals), and low abundance to absence of calcite, pyrite, and epidote in weathered samples (Fig. 64, 65-68)
- Tarnish or coatings of pyrite surfaces within weathered samples (Fig. 58, 59)
- Dissolution textures of minerals (skeletal, boxwork, honeycomb, increase in pore spaces, fractures, change in mineral shape, accordion-like structures, loss of interlocking textures, pits, etching) within weathered samples (Fig. 55, 56, McLemore et al., 2009b)
- Chemical classification as potential acid-forming materials using acid base accounting methods (Tachie-Menson, 2006)
- Chemical analyses of water samples characterized by acidic, high sulfate, high TDS, and high metal concentrations (Al, Ca, Mg, Fe, Mn, SO_4, Table, 42).

Chemical processes operating inside the main volume of the rock pile appear to be fairly uniform, whereas heat and fluid/vapor flow are probably restricted to the basal rubble zone, other coarse layers within the pile, and along interfaces between layers (Fig. 127). Cool air flowed through many of the coarse gravel-cobble zones within the interior units of GHN as observed during the sampling and mapping of the trenches. These internal processes appear to be mainly reflected in the formation of gypsum needles within the rock-pile material. This authigenic gypsum probably formed by oxidation of pyrite to form sulfuric acid and then the neutralization of the acid by calcite.

A zonation of the rock pile consistent with depth is illustrated in Figures 25, 49 and 90 (Phillips et al., 2005; McLemore et al., 2005, 2006b). Typically, the interior, unoxidized units (east, units K-W, excluding unit N, units defined in Table 20) of the piles are uniformly dark to light brown or gray with visible pyrite that are interbedded with occasional yellow to gray zones of oxidation associated with little or no pyrite. The outer surface-atmosphere interface represents a zone with the most active geochemical processes noted in the rock piles. The inner, unoxidized zone typically contains abundant calcite, chlorite, and clay minerals and accordingly, has high paste pH values and low acid generating potential. Apparently chemical reactions within the main portion of the pile are controlled by the availability of oxygen and water. The outer,

oxidized units consist of highly leached and oxidized rock comprised mainly of quartz and secondary iron sulfates, with smectite and mixed layer illite-smectite and some pyrite. This zone is characterized by low paste pH, low acid neutralizing potential, and high acid generating potential. Extensive interchange of water and oxygen occurs in this zone, which enhances pyrite oxidation. Inside the leached zone (J) is a zone of clay-sized material accumulation. The clay minerals are predominantly illite and smectite with increasing chlorite toward the center of the pile. The origin of this clay-sized material accumulation is problematic, and it is not known if the clays represent originally mined and dumped high-clay material or an accumulation of material washed into the pile from the upper zone. This unit is typically green to orange with moderate to low paste pH. Below the zone of clay-sized material accumulation is a zone of sulfate mineral accumulation. Jarosite and gypsum become more abundant and the zone is typically orange. In between the outer, oxidized and interior, unoxidized zone is an intermediate zone (Unit N) of light to dark brown material that is well cemented by clay minerals. It contains local zones of bright orange to punky yellow oxidized sandy clay. Clays are dominated by illite, smectite, and chlorite. Proximal to the interface are zones of dark brown to black accumulation of iron or manganese oxide material that coats grains and clasts. This accumulation of iron and manganese oxides could possibly represent a zone of reduction. Many of the mineral and chemical trends in Figures 89-91 are consistent with this pattern of weathering.

The majority of geochemical activity appears to be confined to the interface regions of the rock pile. These are the surface-atmosphere and bedrock-rock pile (rubble zone) areas. Geochemical activity is typically distributed with respect to the surface configuration and to specific depths effectively mimicking the shape of the pile. The bedrock-rock pile interface is the least explored interface within the rock piles, especially at depth. Drill holes have intersected portions of the base that contain ferricrete that is confined to zones of high water content, possibly as local saturated zones, oxygen availability and ferric ion activity. The nature of this interface at the top of the GHN rock pile was merely rock-pile material sitting on top of a poorly developed soil horizon. The relative distribution of ferricrete along the entire interface is poorly known at this time.

There was no free water in the drill holes or trenches in the rock pile material, supporting previous conclusions (URS Corporation, 2003) that the rock piles are unsaturated. The water table is below the bottom surface of the GHN rock pile (URS Corporation, 2003; Norwest Corporation, 2004; Shannon, 2006). At GHN a local water table is approximately 14-30 ft deep in the bedrock below the toe of the rock pile (Norwest Corporation, 2004; unpublished monthly reports during regrading found at http://www.emnrd.state.nm.us/Mining/Moly_default.htlm; October 2005).

Water in the rock pile is derived predominantly from precipitation (rainfall and snow melt). However, it is unknown how much water in the rock pile was derived from precipitation during emplacement of the rock pile trapped by subsequent dumping or from water trapped in the rock pile from the actual mined and dumped material. From trench activities in the unstable portion of the rock pile, local zones of preferential water flow are found in the upper portion of the colluvium and fractured bedrock underlying the rock pile material. There is humid air flow into the rock pile through coarse cobble layers, which in terms of the water balance is insignificant. However, humid air does provide the moisture needed for the geochemical reactions observed in some zones of the rock piles (Jerz, 2002, Jerz and Rimstidt, 2004).

Some water is lost to evaporation as shown by pan evaporation tests, lysimeter tests, analysis of climatic data (Wels et al., 2001, 2002; Robertson GeoConsultants Inc., 2000b, 2001,

2003) and the stable isotopes studies (Fig. 114). Rates of infiltration were calculated from infiltrometer and guelph permeameter tests (Fig. 113), and gravimetric moisture content analyses indicate the presence of water in the rock piles.

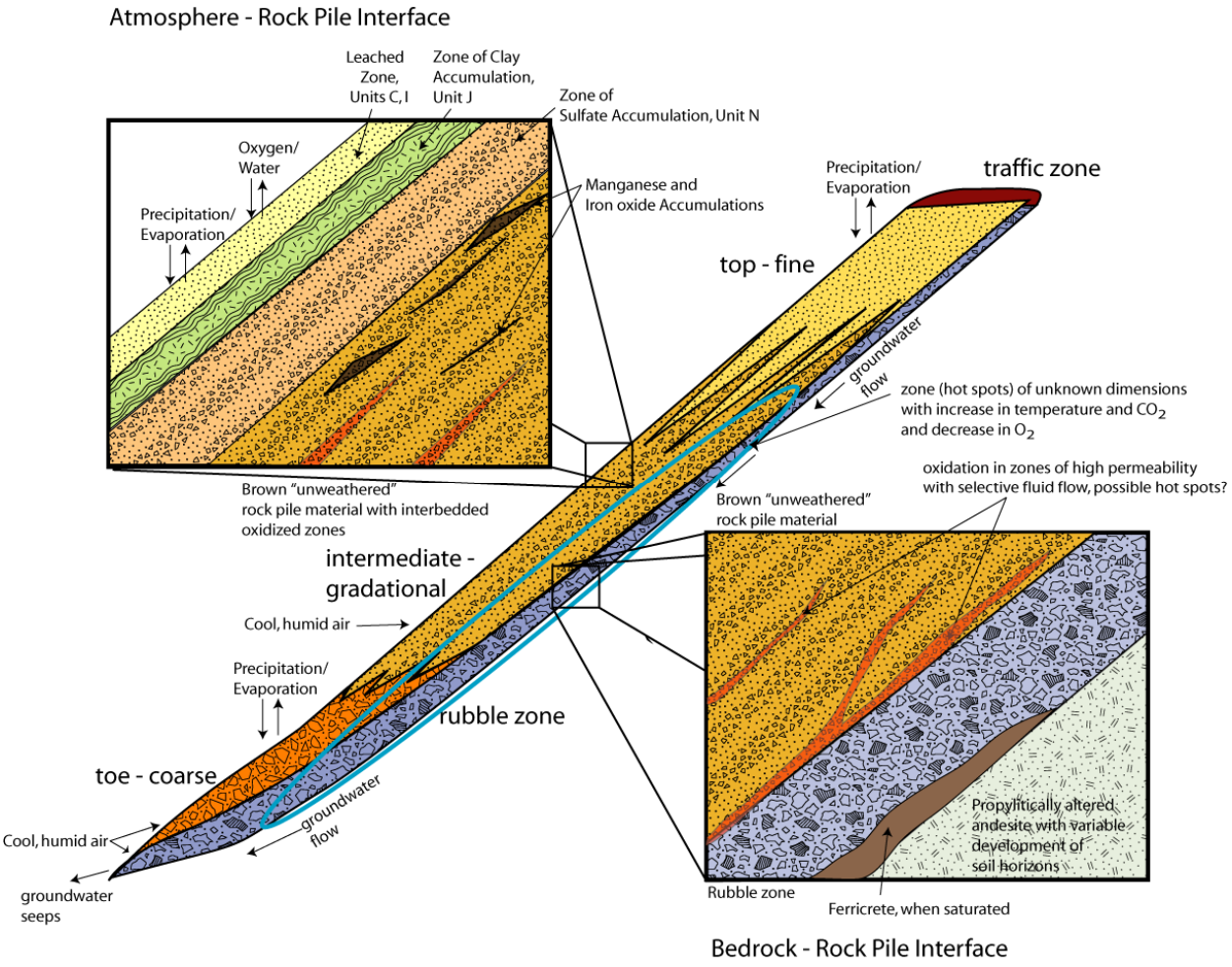

FIGURE 134. Conceptual model of the Questa rock piles (from field studies at GHN and from Nichols, 1987). See text for explanation of zones and processes. The ground water indicated in the figure is from perched zones not from the local ground water table.

Water flows differently in an unsaturated system, such as in these rock piles, then it does from a saturated system, such as found in aquifers. A porous medium's abilities to transmit or retain water under unsaturated conditions are functions of the medium's particle size distribution, original composition, and the weathering it has undergone. The pore networks on which these properties depend can change significantly with saturation because the amount of highly soluble sulfate minerals present as a solid phase can change with saturation. In the rock piles, water will better infiltrate into coarse layers (sand size) that have a high saturated hydraulic conductivity than into clay layers with a low hydraulic conductivity. However, after the water has infiltrated into the system, the flow regime will depend upon the matric suction within the rock pile material. In a system where matric suction is near zero (close to saturation), the water will preferentially flow through a sand layer rather than a clay layer. As the matric suction changes to

be more negative (drier), flow will more likely prevail in a clay layer rather than a sand layer. Based upon field measurements of matric suction (by tensiometers and guelph pememeaters), which indicate relatively moist matric suction values, water in the rock piles flows preferentially down dip along sandy layers that are bounded below by clay layers. In an unsaturated system the presence of cobbles and boulders acts as a flow barrier (Hendrickx et al., 1991; Jury et al., 1972; Hillel, 1998). Water flow will not occur between large rocks, unless they are compacted in a fine matrix with soil. Water flows down hill and eventually exits the rock pile at the toe. The toe of the rock piles will not be saturated and will still allow humid, air to flow into the pile via coarse permeable layers. The humid hot air flows throughout the rock pile by advection and convection.

The hydrological system is characterized as being variably saturated. Figure 12 is a simplified conceptual hydrologic model of GHN for numerical modeling purposes. The five zones based upon particle size distribution (traffic, top-fine, intermediate, toe-coarse, rubble zone) are shown in relation to the trenches and drill holes. A thin colluvium is defined based upon field observations and drilling done by Norwest. Hydrologic properties were estimated from company reports and field data (Tables 30-33) for the numerical model (Table 43).

TABLE 43. Volume-mass properties of the rock pile material in the 7 hydrologic zones in GHN (Fig. 12).

ID	Soil region	Degree of saturation, S (%)	Dry density, ρ_d, (kg/m^3)	Specific gravity, G	Gravimetric water content, w (%)	Porosity, n (%)
1	WR1 (top-fine)	100	1850	2.65	16.32	30.19
2	WR2 (intermediate)	100	1760	2.65	19.08	33.58
3	WR3 (toe-coarse)	100	1690	2.65	21.44	36.23
4	Rubble zone	100	1690	2.65	21.44	36.23
5	Colluvium	100	1700	2.65	21.09	35.85
6	Traffic	100	1940	2.65	13.81	26.79
7	Bedrock	100	1630	2.65	23.61	38.49

CONCLUSIONS

The regrading of GHN provided a rare opportunity to examine, map, and sample the interior of this rock pile. The GHN rock pile is stratified and the strata can be correlated down slope through the rock pile. Rock fragment lithology is generally consistent within mapped units and correlates well with mineralogy and chemistry. The majority of geochemical activity appears to be confined to the interface regions of the rock pile, but not all of these regions exhibit weathering effects. The areas most affected by weathering processes are the 1) surface-atmosphere, 2) bedrock-rock pile (rubble zone) areas and 3) interfaces between fine- and coarse-grained layers in the interior zones where water and/or humid air flow and oxidize the rock pile material. Weathering generally decreased from the outer edge of the rock pile to its interior and then increased toward the base of the rock pile. Where water and oxygen are available, pyrite and calcite are being dissolved by weathering to form gypsum, jarosite and other soluble Fe salts. Oxygen and water are available at and near the surface of the rock piles, at and near the base of the rock pile, in permeable strata within the rock pile, and along cracks and crevasses cutting across the strata that have been formed by slope movement and possibly other means. Stable

isotopes of pore water and precipitation indicate that evaporation at and near the surface is an important process in moving water out of the rock pile. Clays are not being generated by weathering in the rock pile, but were formed by hydrothermal alteration of the rocks before mining. Electron microprobe work, mineralogy and chemistry changes within GHN, and chemistry of waters draining from the rock pile have established that incongruent (residue remains or new phase forms) and congruent (dissolution) mineral dissolution have occurred. Authigenic gypsum, jarosite soluble efflorescent salts, Fe oxide minerals and to a lesser extent, clay minerals liberated from the mined rock material during construction of the rock piles (i.e. pre-mining clay minerals), have cemented parts of GHN rock pile material.

It is difficult, but possible to distinguish between pre-mining hydrothermal alteration and post-mining weathering, by using detailed field observations and petrographic analysis that includes defining the paragenesis (sequence of events), especially using microprobe analyses. The evidence for weathering in the Questa rock piles includes (McLemore et al., 2006a, b; McLemore et al., 2009b):

- Change in color from darker brown and gray in less weathered samples (original color of igneous rocks) to yellow to white to light gray in the weathered samples (Figs. 29-30, 39-42). However, the mineralogical effect of the fast-reacting (less than 40 yrs) weathering pyrite system is to produce precipitates of secondary reaction minerals on the surface of existing rock fragments and within the soil matrix, which result in the yellow to orange color, reflecting the role of ferric iron in the mineral structures. The secondary precipitates form coatings on exterior surfaces, rims, and fill macro- and micro-fractures. Thus, the macro-scale impression of weathering, caused by the discoloration from the observed secondary precipitates is exaggerated.
- Thin yellow to orange, "burnt" layers within the interior of GHN, where water and/or air flowed and oxidized the rock-pile material.
- Paste pH, in general, is low in oxidized, weathered samples and paste pH is higher in less weathered samples.
- Increase abundance of jarosite, gypsum, Fe-oxide minerals and soluble efflorescent salts (locally as cementing minerals), and low abundance to absence of calcite, pyrite, and epidote in weathered samples.
- Tarnish or coatings of pyrite surfaces within weathered samples (Figs. 58-59; Heizler et al., 2007).
- Dissolution textures of minerals (skeletal, boxwork, honeycomb, increase in pore spaces, fractures, change in mineral shape, accordion-like structures, loss of interlocking textures, pits, etching) within weathered samples (McLemore et al., 2009b).
- Change in bulk textures of the rock-pile material including increase in soil:rock ratio, piping or stoping within the rock pile, and decrease in grain size due to physical weathering.
- Chemical classification as potential acid-forming materials using acid base accounting methods (Tachie-Menson, 2006).
- Chemical analyses of water samples characterized by acidic, high sulfate, high TDS, and high metal concentrations (Al, Ca, Mg, Fe, Mn, SO_4).

Friction angle, point load strength index and slake durability index of the GHN rock pile samples decreased as the degree of weathering increased in some samples but not all (Figs. 125, 117, 120; Gutierrez et al., 2008). However, the decreases were still quite small and suggest that 25-40 years of weathering have not substantially affected the shear strength properties of these

rock-pile materials. Some, but not all samples located on the outer edge of the rock pile disintegrated more and presented lower durability. Comparison of slake durability and point load indices of fragments in the rock pile to values of un-weathered drill cores of rocks with similar lithologies to those in the pile shows that rock fragments in the GHN rock pile have not experienced considerable weathering after emplacement. Therefore, lower values of friction angle, point load strength index and slake durability index of samples from the outer edge of the pile are likely due to post-deposition oxidation and hydrothermal alteration, which is consistent with the change in color, loss or obscuring of original igneous texture on the edges and within many rock fragment grains, and increase in weathered minerals (i.e. gypsum, jarosite). Conversely, the point load strength index and slake durability index values of samples on the interior of the pile are similar to the values of un-weathered drill core samples. Consequently, the samples from the interior of the GHN rock pile are not more weathered since its emplacement. However, the differences in friction angle between the outer and interior units are relatively small. These and other studies suggest that changes in physical properties (i.e. particle size, texture and fabric) have a larger effect than mineralogic and chemical changes on the friction angle than do mineralogic and chemical changes (Arel and Tuğrul, 2001; Moon and Jayawardane, 2004). The shear strength would be expected to increase with increase in cementation. Cementation in the short term is controlled by gypsum, jarosite, and other salts. These less stable minerals could form the building blocks (sites) for further stronger cementation consisting of hematite and goethite. Collectively, these results suggest that future weathering will not substantially decrease the friction angle of the rock piles with time.

ACKNOWLEDGEMENTS

This project was funded in part by Chevron Mining Inc. (formerly Molycorp, Inc.) as a subcontract between the University of Utah and the New Mexico Bureau of Geology and Mineral Resources (NMBGMR), a division of New Mexico Institute of Mining and Technology (NMIMT). We would like to thank the professional staff and students of the large multi-disciplinary field team, many of whom are listed on the title page, for their assistance in mapping, sampling, and laboratory analyses. Discussions with Mark Logsdon proved invaluable in bettering our understanding of weathering and statistics. Assistance and oversight of the geotechnical analyses by Cathy Aimone-Martin and Ali Fakhimi were appreciated. We also would like to thank Bruce Walker, Dave Jacobs, Jim Vaughn, and Mike Ness of Molycorp, Inc. and John Purcell of Golder Associates for their training and assistance in this study. Dave Jacobs and several anonymous reviewers commented on earlier published papers cited in the reference section and their insightful comments are appreciated. The ADTI-MMS review committee consisting of Dennis Turner, David Williams, Art Rose, Charles Alpers, Tom Kelly, and Gordon McKenna reviewed portions of this and other project reports and their comments are appreciated. George Robinson reviewed the SOPs and QA/QC report (Appendix 8; McLemore and Frey, 2009). This report is part of an on-going study of the environmental effects of the mineral resources of New Mexico at NMBGMR, Peter Scholle, Director and State Geologist.

REFERENCES

ASTM, 1998, Standard test method for direct shear test of soils under consolidated drained conditions: D3080, American Society for Testing and Materials publication.

ASTM, 2001a, Standard laboratory determination of water (moisture) content of soil, rock, and soil-aggregate mixtures: D2216, American Society for Testing and Materials publication, 482 p.
ASTM, 2001b, Standard test method for liquid limit, plastic limit, and plasticity index of soils: D4318, American Society for Testing and Materials publication, 482 p.
ASTM, 2001c, Standard Test Method for Slake Durability of Shales and Similar Weak Rocks: D464487 (Reapproved 1992), American Society for Testing Materials publication, 482 p.
ASTM, 2002a, Standard test method for particle-size analysis of soils (D422), American Society for Testing and Materials publication.
ASTM, 2002b, Standard test methods for specific gravity of soil solids by water pycnometer (D854), American Society for Testing and Materials publication.
Agustawijaya, D.S., 2004, Modeled Mechanisms in the Slake-durability Test for Soft Rocks: Dimensi Teknik Sipil, vol. 6.
Arel, E. and Tuğrul, A., 2001, Weathering and its relation to geomechanical properties of Cavusbasi granitic rocks in northeastern Turkey: Bulletin of Engineering Geology and the Environment, v. 60, p. 123-133
Bauer, P.W., Kelson, K.I., and Koning, D.J., 2004, Plate 7: Cenozoic geologic timeline—Taos area: New Mexico Geological Society Guidebook, 55, p. 122.
Beauvais, A., 1999, Geochemical balance of lateritization processes and climatic signatures in weathering profiles overlain by ferricretes in Central Africa: Geochimica et Cosmochimica Acta, vol. 63, p. 3939-3957.
Blowes, D.W. and Jambor, J.L., 1990, The pore-water geochemistry and the mineralogy of the vadose zone of sulphide tailings, Waite Amulet, Quebec, Canada: Applied Geochemistry, v. 5, p. 327-346.
Boakye, K., 2008, Large In Situ Direct Shear Tests on Rock Piles at The Questa Mine, Taos County, New Mexico: M.S. thesis, New Mexico Institute of Mining and Technology, Socorro, http://geoinfo.nmt.edu/staff/mclemore/Molycorppapers.html, accessed on October 16, 2008.
Borden, R., 2001, Geochemical evolution of sulphide-bearing waste rock soils at the Bingham Canyon mine, Utah: Geochemistry: Exploration, Environment, Analysis, v. 1, p. 15-22.
Briggs, P.H., Sutley, S.J., and Livo, K.E., 2003, Questa Baseline and Pre-mining Ground Water Investigation: 11. Geochemistry of composited material from alteration scars and mine-waste piles: U. S. Geological Survey Open-File Report 03-458, 17 p.
Broch, E. and Franklin, J.A., 1972, The Point Load Strength Test: Int. J. Rock Mech. Min. Sci., Grain Britain 9, p. 669-697.
Browne, P.R.L., 1978, Hydrothermal alteration in active geothermal fields: Annual Reviews of Earth and Planetary Science, v. 6, p. 229–250.
Bryant, L.D., 2003, Geotechnical problems with pyritic rock and soil: M.S. thesis, Virginia Polytechnic Institute and State University, Blacksburg, 252 p.
Caine, J.S., 2003, Questa Baseline and Pre-Mining Ground-Water Quality Investigation 6: Preliminary Brittle Structural Geologic Data, Questa Mining District, southern Sangre de Cristo Mountains, New Mexico: U.S. Geological Survey, Open-file Report 02-0280, 31 p.
Campbell, A.R. and Lueth, V.W., 2008, Isotopic and textural discrimination between hypogene, ancient supergene, and modern sulfates at the Questa mine, New Mexico: Applied Geochemistry, v. 23, no. 2, p. 308- 319.

Campbell, A.R., Lueth, V.W., and Pandey, S., 2005, Stable Isotope Discrimination Of Hypogene And Supergene Sulfate Minerals In Rock Piles At The Questa Molybdenum Mine, New Mexico (abstr.): Geological Society of America, Abstracts with programs (October), v. 37(7), p. 394.

Carbone, C., Di Benednetto, F., Marescotti, P., Martinelli, A., Sangregorio, C., Cipriani, C., Lucchetti, G., and Romanelli, M., 2005, Genetic evolution of nanocrystalline Fe oxide and oxyhydraoxide assemblages from the Libiola mine (eastern Liguria, Italy): structural and microstructural investigations: European Journal of Mineralogy, v. 17, p. 785-795.

Carey, S.K., Barbour, S.L., and Hendry, M.J., 2005, Evaporation from a waste-rock surface, Key Lake, Saskatchewan: Canadian Geotechnical Journal, v. 42, p. 1189-1199.

Carpenter, R.H., 1968, Geology and ore deposits of the Questa molybdenum mine area, Taos County, New Mexico: *in* Ore deposits of the United States, 1933-1967, Granton-Sales, J.D., Ridge, ed., AIME, p. 1328-1350.

Clark, K.F., 1968, Structural controls in the Red River District, New Mexico: Economic Geology, v. 63, p. 553-566.

Cline, J.S., 1991, Salinity variation in magmatic-hydrothermal fluids in the Questa, New Mexico, U.S.A., porphyry molybdenum deposit: A product of pressure fluctuation: PLINIUS, Supplemento italiano all'Europan Journal of Mineralogy, v. 5, p. 45-46.

Cline, J.S. and Vanko, D.A., 1995, Magmatically generated saline brines related to molybdenum at Questa, New Mexico, USA; in Thompson, J.F.H., ed., Magmas, fluids, and ore deposits: Mineralogical Association of Canada, Victoria, short course series, p. 153-174.

Craig, H., 1961, Isotopic Variations in Meteoric Waters: Science, v. 133, p. 1702-1703.

Czamanske, G.K., Foland, K.A., Hubacher, F.A., and Allen, J.C., 1990, The $^{40}Ar/^{39}Ar$ Chronology of Caldera Formation, Intrusive Activity and Mo-ore Deposition near Questa, New Mexico: New Mexico Geological Society Guidebook 41, p. 355-358.

Dawson, R.F., 1994, Mine waste geotechnics: University of Alberta, Edmonton, PhD thesis, 262 p.

Davis, B., 1998, What is a sample? What does it represent? Australian Institute of Geoscientists Bulletin, v. 22, p. 39-34.

Delvigne, J.E., 1998, Atlas of micromorpholgy of mineral alteration and weathering: Canadian Mineralogist, Special Publication 3, 494 p.

Diehl, S.F., Hageman, P.L., and Smith, K.S., 2006, What's weathering? Mineralogy and field leach studies in mine waste, Leadville and Montezuma mining districts, Colorado; in *7th ICARD*, March 26-30, 2006, St. Louis MO. Published by American Society of Mining and Reclamation, Lexington, KY. CD-ROM, pp. 507-527.

Dhakal, G., Yoneda, T., Kato, M., and Kaneko, K., 2002, Slake Durability and Mineralogical Properties of some Pyroclastic and Sedimentary Rocks: Engineering Geology, v. 65, p. 31-45.

Dobchuk, B.S., Barbour, S.L., MASCE, and Zhou, J., 2004, Prediction of water vapor movement through waste rock: Journal of Geotechnical and Geoenvironmental Engineering, March, p. 293-302.

Donahue, K.M., 2008, Clay Minerals Sulfuric Acid Leach Experiment: unpublished report to Chevron Mining Inc. 13 p.

Donahue, K.M., Dunbar, N.W., and McLemore, V.T., 2007, Origins of clay minerals in the Molycorp Mine Goathill North Rock pile, Questa NM: Society of Mining, Metallurgy and Exploration Annual Convention, Denver, Feb 2007, no. 07-100, 8 p.

Donahue, K.M., Dunbar, N.W., and McLemore, V.T., 2009, Clay mineralogy of the Goathill North rock pile, Questa mine, Taos County, NM: Origins and indications of in-situ weathering: Society of Mining, Metallurgy and Exploration Annual Convention, Denver, Feb 2009.

Downing, B., 2008, ARD sampling and sample preparation: http://technology.infomine.com/enviromine/ard/sampling/intro.html, accessed August 7, 2008.

Farkas, I.M., Weiszburg, T.G., Pekker, P., and Kuzmann, E., 2009, A half-century of environmental mineral formation on a pyrite-bearing waste dump in the Matra Mountains, Hungary: The Canadian Mineralogist, v. 47, p. 509-524.

Ferrage, E., Kirk, C. A., Cressey, G., and Cuadros, J., 2007, De-hydration of Ca-montmorillonite at the crystal scale. Part 1: Structure evolution: American Mineralogist, v. 92, p. 994-1006.

Fines, P., Wilson, G.W., Williams, D.J., Tran, A.B., and Miller, S., 2003, Field characterization of two full-scale waste rock piles; in ICARD 2003—Proceedings from the 5th international conference on acid rock drainage: The Australasian Institute of Mining and Metallurgy, Melbourne, p. 903-909.

Fontes, M.P.F. and Carvalho, Jr., I.A., 2005, Color attributes and mineralogical characteristics, evaluated by radiometry, of highly weathered tropical soils: Soil Sci. Soc. Am. J. v. 69, p. 1162–1172.

Fookes, P.G., Dearman, W. and Franklin, J.A., 1971, Some Engineering Aspects of Rock Weathering with Field Examples from Dartmoor and Elsewhere: Q. J. Eng. Geol, v. 4, p. 139-185.

Franklin, J.A. and Chandra, R., 1972, The Slake-durability Test: International Journal of Rock Mechanics and Mining Science, vol. 9, pp. 325-341.

Galbraith, J.M., 2004, Proposed changes to soil taxonomy that may affect mine soil classification; in 2004 National Meeting of the American Society of Mining and Reclamation: American Society of Mining and Reclamation, CD-ROM, 14 p.

Golder Associates, Inc., 2005a, Mine rock water balance study, Questa mine, New Mexico: unpublished report to Molycorp, Inc., 53 p.

Golder Associates, Inc., 2005b, Fourth Monitoring and Modeling Report: unpublished report to Molycorp, Inc.

Graf, G.J., 2008, Mineralogical and geochemical changes associated with sulfide and silicate weathering, natural alteration scars, Taos County, New Mexico: M.S. thesis, New Mexico Institute of Mining and Technology, Socorro, 193 p., http://geoinfo.nmt.edu/staff/mclemore/Molycorppapers.html, accessed April 28, 2008.

Gupta, A.S. and Rao, K. S, 2000, Weathering effects on the strength and deformational behavior of crystalline rocks under uniaxial compression state: Eng. Geol., v. 56, p. 257-274.

Gutierrez, L. A. F., 2006, The Influence Of Mineralogy, Chemistry And Physical Engineering properties On Shear Strength Parameters Of The Goathill Rock Pile Material, Questa Molybdenum Mine, New Mexico: M. S. thesis, New Mexico Institute of Mining and Technology, Socorro, 201 p., http://geoinfo.nmt.edu/staff/mclemore/Molycorppapers.html.

Gutierrez, L.A.F., Viterbo, V.C., McLemore, V.T., and Aimone-Martin, C.T., 2008, Geotechnical and Geomechanical Characterisation of the Goathill North Rock Pile at the Questa Molybdenum Mine, New Mexico, USA; *in* Fourie, A., ed., First International

Seminar on the Management of Rock Dumps, Stockpiles and Heap Leach Pads: The Australian Centre for Geomechanics, University of Western Australia, p. 19-32. http://geoinfo.nmt.edu/staff/mclemore/Molycorppapers.html, accessed August 20, 2008

Haby, V.A., Leonard, A.T., and Davis, J.V., 1997, A laboratory method to eliminate seasonally variable soil pH: A laboratory method to eliminate seasonally variable soil pH: Res. Cntr. Tech. Rep. 96-1:29-30. Texas A and M University Agricultural Research and Extension Service WWW service.

Haering, K.C., Daniels, W.L., and Galbraith, J.M., 2004, Appalachian Mine Soil Morphology and Properties: Effects of Weathering and Mining Method: Soil Science Society America Journal, v. 68, p.1315–1325.

Hagan, L.B., 2001, Natural and Mining-related sources of metal contamination, Red River, Northern New Mexico: A hydrogeochemical investigation of surface water and groundwater; M. S. Thesis; University of New Mexico, Albuquerque, 192 p.

Hall, J.S. 2004, New Mexico Bureau of Mines and Mineral Resource's Clay Laboratory Manual: Unpublished New Mexico Bureau of Geology and Mineral Resources report.

Hawley, P.M., 2001, Site selection, characterization, and assessment, *in* W.A. Hustrulid. Slope Stability in Surface Mining. M.K. McCarter and D.J.A. Van Zyl (Ed), Society for Mining, Metallurgy, and Exploration, Inc., Littleton, p. 267-274.

Heizler, L., Dunbar, N., and Sweeney, D., 2007, Summary of Investigation of Tarnish on Pyrite Grains in Questa Rock Pile Samples: Unpublished report to Molycorp, Inc, Task B1.1, 3 p.

Hendrickx, J.M.H., Khan, A.S., Bannink, M.H., Birch, D., and Kidd, C., 1991, Numerical analysis of groundwater recharge through stony soils using limited data: Journal Hydrol., v. 127, p. 173-192.

Henley, R.W. and Ellis, A.J., 1983, Geothermal systems, ancient and modern: a geochemical review: Earth Science Reviews, v. 19, p. 1–50.

Herasymiuk, G.M., 1996, Hydrology of a sulphide waste rock dump: M.S. thesis, University of Saskatchewan, Saskatoon.

Hillel, D., 1998, Environmental Soil Physics: Academic Press, New York, 771 p.

Hoefs, J.H., 2004, Stable Isotope Geochemistry: Fifth and Updated Version, Springer, New York, New York, 206 p.

Holtz, R.D. and Kovacs, W.D., 2003, An introduction to geotechnical engineering, Pearson Education Taiwan publication, 733 p.

International Society for Rock Mechanics-ISRM, 1979, Suggested methods for determination of the slake durability index, Int. J. Rock Mech. Min. Sci. Geomech., v. 16, p. 154-156.

Jerz, J.K., 2002, Geochemical Reactions in Unsaturated Mine Wastes: Ph.D. dissertation, University of Virginia, Blacksburg, 115 p.

Jerz, J.K. and Rimstidt, J.D., 2004, Pyrite oxidation in humid air: Geochimica Cosmochimica Acta, v. 68, p. 701-714.

Joeckel, R.M., and Ang Clement, B.J., 1999, Surface features of the Salt Basin of Lancaster County, Nebraska: Catena, v. 34, p. 243-275.

Joeckel, R.M., Ang Clement, B.J., and Van Fleet Bates, L.R. 2005, Sulfate-mineral crusts from pyrite weathering and acid rock drainage in the Dakota Formation and Graneros Shale, Jefferson County, Nebraska: Chemical Geology, v. 215, p. 433-452.

Johnson, C.M., Lipman, P.W., and Czamanske, G.K., 1990, H, O, Sr, Nd, and Pb isotope geochemistry of the Latir volcanic field and cogenetic intrusions, New Mexico and

relations between evolution of a continental magmatic center and modifications of the lithosphere: Contributions to Mineralogy and Petrology, v. 104, p. 99-124.
Jury, W.A., Gardner, W.R., and Gardner, H.G., 1972, Soil Physics: John Wiley and Sons, Inc., New York, 328 p.
Klemm, L.M., Pettke, T., and Heinrich, C.A., 2008, Fluid and source magma evolution of the Questa porphyry Mo deposit, New Mexico, USA: Mineralium Deposita, v. 43, p. 533-552.
Koch, G.S., Jr. and Link, R.F., 1971, Statistical analysis of geological data: Dover Publications, Inc., New York, ISBN 0-486-64040-X, 438 p.
Komdel, P., Bujdak, J., Madejova, J., Sucha, V., and Elsass, E., 1996, Effect of non-swelling layers on the dissolution of reduced-charge montmorillonite in hydrochloric acid: Clay Minerals, v. 31, p. 333-345.
Kwong, Y.T.J., 1993, Prediction and prevention of acid rock drainage from a geological and mineralogical perspective: MEN project report 1.32.1, 67 p.
Lahee, F.H., 1961, Field geology: McGraw-Hill Book Company, New York, 926 p.
Lipman, P.W., 1988, Evolution of silicic magma in the upper crust: the Min-Tertiary Latir Volcanic Field and its cogenetic granitic batholith, northern New Mexico, U.S.A., Transactions of the Royal Society of Edinburgh: Earth Sciences, v. 79, p. 265-288.
Lipman, P.W. and Reed, J.C., Jr., 1989, Geologic map of the Latir volcanic field and adjacent areas, northern New Mexico: U.S. Geological Survey, Miscellaneous Investigations Map I-1907, scale 1:48,000.
Linklater, C.M., Sinclair, D.J., and Brown, P.L., 2005, Coupled chemistry and transport modeling of sulphidic waste rock dumps at the Aitik mine site, Sweden: Applied Geochemistry, v. 20, p. 275-293.
Little, A.L., 1969, The engineering classification of residual tropical soils; in Proceedings 7th International Conference Soil Mechanics Foundation Engineering: Mexico City, v. 1, p. 1-10.
Livo, K.E. and Clark, R.N., 2002, Mapped Minerals at Questa, New Mexico, using airborne visible-infrared imaging spectrometer (AVIRIS) data - preliminary report for: First quarterly report of the U. S. Geological Survey investigation of baseline and pre-mining ground-water quality in the Red River valley basin, New Mexico, November 13, 2001: U.S. Geological Survey, Open-file Report 02-0026, 13 p., http://pubs.usgs.gov/of/2002/ofr-02-0026/
Ljungberg, J. and Ohlander, B., 2001, The geochemical dynamics of oxidizing mine tailings at Laver, northern Sweden: Journal of Geochemical Exploration, v. 74, P. 57-72.
LoVetere, S.H., Nordstrom, D.K., Maest, A.S., and Naus, C.A., 2004, Questa baseline and pre-mining ground-water quality investigation. 3. Historical ground-water quality for the Red River valley, New Mexico: U.S. Geological Survey, Water Investigations Report 03-4186, 238 p.
Ludington, S., Plumlee, G., Caine, J., Bove, D., Holloway, J., and Livo, E., 2005, Questa baseline and pre-mining ground-water quality Investigation, 10. Geologic influences on ground and surface waters in the lower Red River watershed, New Mexico: U.S. Geological Survey, Scientific Investigations Report 2004-5245, 46 p.
Maest, A.S., Nordstrom, D.K., and Lovetere, S.H., 2004, Questa Baseline and Pre-Mining Ground-Water Quality Investigation. 4. Historical Surface-Water Quality for the Red

River Valley, New Mexico. U.S. Geological Survey, Scientific Investigations Report 2004-5063.

Marston, T.M., 2009, An evaluation of annual net infiltration to bedrock for waste rock piles near Questa, New Mexico and the development of a method for examining tritium in clay minerals: M.S. thesis, University of Utah, Salt Lake City, 123 p.

Martín-Garcia, J.M., Delgado, G., Parraga, J.F., Gamiz, E., and Delgado, R., 1999, Chemica, mineralogical and (micro)morphological study of coarse fragments in Mediterranean red soils: Geoderma, v. 90, p. 23-47.

Martineau, M.P., Heinemeyer, G.R., Craig, S.D., and McAndrews, K.P., 1977, Geological report: Questa Project 1975-1977: unpublished mine report, Questa Molybdenum Company.

Mascaro, I., Benvenuti, B., Corsini, F., Costagliola, P., Lattanzi, P., Parrini, P., and Tanelli, G., 2001, Mine wastes at the polymetallic deposit of Fenice Capanne (southern Tuscany, Italy). Mineralogy, geochemistry, and environmental impact: Environmental Geology, v. 41, p. 417-429.

McLemore, V.T., 2008, Characterization of a Weathering Profile Through Bedrock Beneath Goat Hill North Rock Pile, New Mexico: unpublished report to Chevron Mining, Inc., Task B1.4, 30 p.

McLemore, V.T., 2009, Geologic Setting and Mining History of the Questa mine, Taos County, New Mexico: New Mexico Bureau of Geology and Mineral Resources, Open-file Report 515, 29 p., http://geoinfo.nmt.edu/publications/openfile/details.cfml?Volume=515

McLemore, V.T., Anim, K., Fakhimi, A., Dickens, A.K., and Nunoo, S., 2008a, Characterization of Questa rock piles, New Mexico: Unpublished report to Chevron Mining, Inc and the QRPWASP, Task B1.1.

McLemore, V.T., Donahue, K.M., Phillips, E., Dunbar, N., Walsh, P., Gutierrez, L.A.F., Tachie-Menson, S., Shannon, H. R., Wilson, G. W., and Walker, B. M., 2006a, Characterization Of Goathill North Mine Rock Pile, Questa Molybdenum Mine, Questa, New Mexico: National Meeting of the 7th ICARD, SME, and American Society of Mining and Reclamation, St. Louis, Mo., March, CD-ROM.

McLemore, V.T., Donahue, K.M., Walsh, P., Tachie-Menson, S., Phillips, E.H., Gutierrez, L.A. F., and Shannon, H.R., 2005, Trench Sampling of the Molycorp Goathill North rock piles, Questa Rock Pile Stability Study, New Mexico: National Meeting of the American Society of Mining and Reclamation, Breckenridge, Colo, June, CD-ROM, 26 p., http://geoinfo.nmt.edu/staff/mclemore/Molycorppapers.html.

McLemore, V.T., Donahue, K., Phillips, E., Dunbar, N., Smith, M., Tachie-Menson, S., Virtbo, V., Lueth, V.W., Campbell, A.R. and Walker, B.M., 2006b, Petrographic, mineralogical and chemical characterization of Goathill North Mine Rock Pile, Questa Molybdenum Mine, Questa, New Mexico: 2006 Billings Land Reclamation Symposium, June, 2006, Billings, Mt. Published by Published by American Society of Mining and Reclamation, 3134 Montavesta Rd., Lexington, KY CD-ROM, http://geoinfo.nmt.edu/staff/mclemore/Molycorppapers.html, accessed October 17, 2008.

McLemore, V.T., Donahue, K., Dunbar, N., and Heizler, L., 2008b, Characterization of physical and chemical weathering in the rock piles and evaluation of weathering indices for the Questa rock piles: unpublished report to Chevron, Task 1.3, B1.1.

McLemore, V.T., Fakhimi, A., van Zyl, D., Ayakwah, G.F., Boakye, K., Anim, K., Ennin, F., Felli, P., Fredlund, D., Gutierrez, L.A.F., Nunoo, S., Tachie-Menson, S., and Viterbo,

V.C., 2009c, Literature review of other rock piles: characterization, weathering, and stability: New Mexico Bureau of Geology and Mineral Resources, Open-file Report 517, 101 p., http://geoinfo.nmt.edu/publications/openfile/details.cfml?Volume=517

McLemore, V.T. and Frey, B., 2008, Quality control and quality assurance report: unpublished report to Chevron, Task B1 (appendix 8 of this report).

McLemore, V.T., Hoffman, G.K., Wilks, M., Raugust, J.S., and Jones, G.R., 2004a, Use of Databases in Characterization at mine Sites: 2004 National Meeting of the American Society of Mining and Reclamation, Morgantown, WV, April 2004, CD-ROM.

McLemore, V.T. and Mullen, K.E., 2004, Mineral resources in Taos County, New Mexico: New Mexico Geological Society, Guidebook 55, p. 383-390.

McLemore, V.T., Russell, C.C., Smith, K.S. and the Sampling and Monitoring Committee of the Acid Drainage Technology Initiative—Metals Mining Sector (ADTI—MMS), 2004b, Sampling and Monitoring for Closure: Society of Mining, Exploration, and Metallurgy, SME Preprint No. 04-62, CD-ROM, 10 p.

McLemore, V.T. and the Questa Rock Pile Weathering and Stability Team, 2008, Descriptive and conceptual rock pile models: revised unpublished report to Chevron, Task B1.3.2.

McLemore, V.T., Sweeney, D., and Donahue, K., 2009a, Lithologic atlas: New Mexico Bureau of Geology and Mineral Resources, Open-file Report 516, 73 p., http://geoinfo.nmt.edu/publications/openfile/details.cfml?Volume=516

McLemore, V., Sweeney, D., Dunbar, N., Heizler, L., and Phillips, E., 2009b, Determining quantitative mineralogy using a combination of petrographic techniques, whole rock chemistry, and MODAN: Society of Mining, Metallurgy and Exploration Annual Convention, preprint 09-20, 19 p.

Meyer, J.W., 1991, Volcanic, plutonic, tectonic and hydrothermal history of the southern Questa Caldera, New Mexico: University Microfilms, Ph.D. dissertation, 348 p.

Meyer, J. and Foland, K.A., 1991, Magmatic-tectonic interaction during early Rio Grande rift extension at Questa, New Mexico: Geological Society of America Bulletin, v. 103, p. 993-1006.

Meyer, J.W., and Leonardson, R.W., 1990, Tectonic, hydrothermal and geomorphic controls on alteration scar formation near Questa, New Mexico: New Mexico Geological Society, Guidebook 41, p. 417-422.

Mineral Services Canada, Inc., 2008, Petrographic and mineralogical characterization of 14 samples from the rock piles of the Questa molybdenum mine (New Mexico, USA): unpublished report to Mark Logsdon, 80 p.

Molling, P.A., 1989, Applications of the reaction progress variable to hydrothermal alteration associated with the deposition of the Questa molybdenite deposit: Ph. D. dissertation, Johns Hopkins University, Baltimore, MD, 227 p.

Moon, V. and Jayawardane, J., 2004, Geomechanical and geochemical changes during early stages of weathering of Karamu Basalt, New Zealand: Engineering Geology, v. 74, p. 57-72.

Moore, O.M. and Reynolds, R.O., Jr. 1989, X-ray diffraction and the identification and analyses of clay minerals: Oxford University Press, New York.

Morin, K.A., Gerencher, E., Jones, C.E., and Konasewich, D.E., 1991, Critical literature review of acid rock drainage from waste rock: MEND 1.11.1, 176 p.

Morin, K.A., and Hutt, N.M., 1994, An empirical technique for predicting the chemistry of water seeping from mine-rock piles; in International Land Reclamation and Mine Drainage

Conference and the 3rd International Conference on the Abatement of Acidic Drainage: Pittsburg, PA, April 24-29, p. 12-19.
Morin, K.A., Hutt, N.M., and Hutt, S.G., 1997, History of Eskay Creek mine's waste-rock dump from placement to disassembly: MEND Project 1.44.1, 419 p.
Morth, A.H. and Smith, E.E., 1966, Kinetics of the sulfide-to-sulfate reaction: Am. Chem. Soc. Div. Fuel Chem. Preprints, no. 10, p. 83.
Munroe, E.A. and McLemore, V.T., 1999, Waste rock pile characterization, heterogeneity and geochemical anomalies in the Hillsboro mining district, Sierra County, New Mexico: Journal of Geochemical Exploration, v. 66, p. 389-405.
Munroe, E.A., McLemore, V.T., and Dunbar, N.W., 2000, Mine waste rock pile geochemistry and mineralogy in southwestern New Mexico, USA; *in* ICARD 2000—Proceedings from the 5th international conference on acid rock drainage: Society for Mining, Metallurgy, and Exploration, Inc., Littleton, Colo., p. 1327-1336.
Mutschler, F.E., Wright, E.G., Ludington, S.D., and Abbott, J.T., 1981, Granitic molybdenite systems: Economic Geology, v. 76, p. 874-897.
Naus, C.A., McCleskey, R.B., Nordstrom, D.K., Donohue, L.C., Hunt, A.G., Pailet, F.L., Morin, R.H., and Verplank, P.L., 2005, Questa baseline and pre-mining ground-water investigation 5. Well installation, water-level data, and surface- and ground-water geochemistry in the Straight Creek drainage basin, Red River valley, New Mexico, 2001-03: U.S. Geological Survey, Scientific Investigations Report 2005-5088, 228 p.
Neuendorf, K.K.E., Mehl, J.P., Jr., and Jackson, J.A., 2005, Glossary of Geology: American Geological Institute, 5th ed., Alexandria, Virginia, 779 p.
Nichols, R.S., 1987, Rock segregation in waste dumps; *in* Flow-through rock drains: Proceedings of the International symposium convened at the Inn of the South, Cranbrook, B.C., September 8-11, 1986.
Nordstrom, D.K., 1982, Aqueous pyrite oxidation and the consequent formation of secondary iron minerals; chapter 3 in Acid Sulphate Weathering: SSSA Special Publication no. 10, Madison, Wisconsin, p. 37-60.
Nordstrom, D.K., Jenne, E.A. And Ball, J.W., 1979, Redox equilibria of iron in acid mine waters; chapter 3 in Chemical modeling in aqueous systems: ACS Symposium Series 93, E. A. Jenne, ed., American Chemical Society, Washington, D. C., p. 50-79.
Nordstrom, D.K., McCleskey, R.B., Hunt, A.G., and Naus, C.A., 2005, Questa baseline and pre-mining groundwater investigation. 14. Interpretation of ground-water chemistry in catchments other than the Straight Creek catchment, Red River Valley, Taos County, New Mexico, 2002-2003: U.S. Geological Survey, Scientific Investigations Report 2005-5050, 94 p.
Norwest Corporation, 2004, Goathill North Slide Investigation, Evaluation and Mitigation Report: Norwest Corporation report, 56 p., http://www.emnrd.state.nm.us/Mining/Moly/final/Final%20Goathill%20North.pdf
Norwest Corporation, 2005, Questa Roadside Rock piles 2005 Operation Geotechnical Stability Evaluation: unpublished report to Molycorp Inc., 210 p., 3 vol.
Nunoo, S., 2009, Geotechnical evaluation of Questa mine materials, Taos County, New Mexico: M.S. thesis, New Mexico Institute of Mining and Technology, Socorro, 161 p., http://geoinfo.nmt.edu/staff/mclemore/Molycorppapers.html.

Nunoo, S., McLemore, V.T., Fakhimi, A., and Ayakwah, G., 2009, The effect of weathering on particle shape of Questa mine material: Society of Mining, Exploration, and Metallurgy, SME Preprint, CD-ROM, 21 p.

Oerter, E., Brimhall, G.H., Jr., Redmond, J., and Walker, B., 2007, A method for quantitative pyrite abundance in mine rock piles by powder X-ray diffraction and Rietveld method: Applied Geochemistry, v. 22, p. 2901-1915.

Paktunc, A.D., 1998, MODAN: An interactive computer program for estimating mineral quantities based on bulk composition: Computers and Geoscience, v. 24 (5), p. 425-431.

Paktunc, A.D., 2001, MODAN—A Computer program for estimating mineral quantities based on bulk composition: Windows version. Computers and Geosciences, v. 27, p. 883-886.

Pandey, S., 2004, Discrimination between Hypogene and Supergene Sulfates: Questa Mine Site, Taos County, New Mexico MS Independent Study, New Mexico Tech, Socorro NM.

Perkins, E.H., Nesbitt, H.W., and Gunter, W.D., 1995, Critical review of geochemical processes and geochemical models adaptable for prediction of acidic drainage from waste rock: MEND project report 1.42.1, 283 p.

PetraScience Consultants Inc., 2001, Reconnaissance study of waste rock mineralogy: Questa, New Mexico; petrography, OIMA spectral analysis and Rietveld analysis: unpublished report to Molycorp, 25 p.

Phillips, E.H., Lueth, V., Campbell, A., McLemore, V., Walker, B., and Tachie-Menson, S., 2005, Soil Petrography Of A Sample Traverse From A Portion Of The Goathill North Rock Pile, Questa Mine, New Mexico (Abstr.): New Mexico Geological Society, Spring Meeting, Abstracts Volume; Also New Mexico Geology(October), v. 37(7), p. 510.

Piché, M. and Jébrak, M., 2004, Normative minerals and alteration indices developed for mineral exploration: Journal of Geochemical Exploration, v. 82, p. 59-77.

Plumlee, G.S., Ludington, S., Vincent, K.R., Verplanck, P.L., Caine, J.S., and Livo, K.E., 2006, Questa Baseline and Pre-Mining Ground-Water Quality Investigation. 7. A pictorial record of chemical weathering, erosional processes and potential debris-flow hazards in scar areas developed on hydrothermally altered rocks. U.S. Geological Survey, Open-File Report 2006-1205.

Powers, M.C., 1982, Comparison chart for estimating roundness and sphericity: AGI (American Geological Institute), Alexandria, Va., data sheet 18.1.

Price, W.A., Morin, K., and Hutt, N., 1997, Guidelines for the prediction of acid rock drainage and metal leaching for mines in British Columbia: Part II. Recommended procedures for static and kinetic testing *in* Proceedings from the Fourth International Conference on Acid Rock Drainage, Vancouver, B.C.: ICARD, p. 15-30.

Quine, R.L., 1993, Stability and deformation of mine waste dumps in north-central Nevada: M.S. thesis, University of Nevada, Reno, 402 p.

Reed, M.H., 1994, Hydrothermal alteration in active continental systems; *in* Lentz, D. R., Alteration and alteration processes associated with ore-forming systems: Geological Society of Canada, Short Course Notes, v. 11, p. 315-337.

Reed, M.H., 1997, Hydrothermal alteration and its relationship to ore fluid composition; in Barnes, H.L., ed., Geochemistry of hydrothermal ore deposits: 3rd edition, John Wiley and Sons, New York, New York, p. 303-365.

Reed, J.C., Jr., Lipman, P.W., and Robertson, J.M., 1983, Geologic map of the Latir Peak and Wheeler Peak Wilderness and the Columbine-Hondo Wilderness Study Area, Taos County,

New Mexico: U. S. Geological Survey, Miscellaneous Field Studies Map MF-1570-B, scale 1:50,000.
Reiter, M., 2009, Fluid flow estimates in molybdenum mine rock piles using borehole temperature logs: Environmental and Engineering Geoscience, v. 15, no. 3, p. 175-195.
Reyes, A.G., 1990, Petrology of Philippine geothermal systems and the application of alteration mineralogy to their assessment: Journal of Volcanology and Geothermal Resources, v. 43, p. 274–309.
Ritchie, A.I.M., 1994, The waste rock environment: D.W. Blowes and J.L. Jambor, eds., Environmental geochemistry of sulphide mine wastes: Mineralogical Society of Canada, Short Course Handbook, v. 22, p. 133-161.
Ritchie, A.I.M., 2003, Oxidation and gas transport in piles of sulfidic waste; in Environmental aspects of mine wastes: Mineralogical Association of Canada, Short Course Series, v. 21, p. 73-94.
Roberts, T.T., Parkison, G.A., and McLemore, V.T., 1990, Geology of the Red River district, Taos County, New Mexico: New Mexico Geological Society, Guidebook 41, p. 375-380.
Robertson, A.M., 1982, Deformation and Monitoring of Waste Dump Slopes, p. 16.
Robertson GeoConsultants, Inc., 1999, Interim Report: Questa Waste Rock Pile Drilling, Instrumentation and Characterization Study, Open-file Report No. 052007/1 for Molycorp Inc.
Robertson GeoConsultants, Inc., 2000a, Progress report: Results of phase 1 physical waste rock characterization, Questa, New Mexico: unpublished report to Molycorp, Inc., 052007/4, June.
Robertson GeoConsultants, Inc., 2000b, Interim mine site characterization study, Questa Mine, New Mexico: unpublished report to Molycorp, Inc., 052008/10, November.
Robertson GeoConsultants, Inc., 2001, Initial Soil Atmosphere Modeling For Mine Rock Piles, Questa Mine, New Mexico, RGC Report 052008/14 prepared for Molycorp Inc., January 2001.
Robertson GeoConsultants, Inc., 2003, 1st Year Modeling Report Water Balance Study For Mine Rock Piles, Questa Mine, New Mexico, RGC Report 052015/2 prepared for Molycorp Inc., March 2003.
Ross, P.S., Jebrak, M., and Walker, B.M., 2002, Discharge of hydrothermal fluids from a magma chamber and concomitant formation of a stratified breccia zone at the Questa porphyry molybdenum deposit, New Mexico: Economic Geology, v. 97, p. 1679-1699.
Rowe, A., 2005, Fluid evolution of the magmatic hydrothermal breccia of the Goat Hill orebody, Questa Climax-type porphyry molybdenum system, New Mexico—a fluid inclusion study: M.S. thesis, New Mexico Institute of Mining and Technology, Socorro, 134 p.
Scheinost, A.C., and Schwertmann, U., 1999, Color Identification of Iron Oxides and Hydroxysulfates: Use and Limitations: Soil Sci. Soc. Am. J., v. 63, p.1463–1471
Schilling, J.H., 1960, Mineral resources of Taos County, New Mexico: New Mexico Bureau of Mines and Mineral Resources, Bulletin 71, 124 p.
Schilling, J.H., 1990, A history of the Questa molybdenum (moly) mines, Taos County, New Mexico: New Mexico Geological Society, Guidebook 41, p.381-386.
Shannon, H.R., 2006, Fluid Transport through a Variably Saturated Rock Pile hill slope system: M.S. thesis, New Mexico Tech, New Mexico, Socorro, http://geoinfo.nmt.edu/staff/mclemore/Molycorppapers.html, accessed November 19, 2006.

Shannon, H., Sigda, J., van Dam, R., Hendrickx, J., and McLemore, V.T., 2005, Thermal Camera Imaging of Rock Piles at the Questa Molybdenum Mine, Questa, New Mexico: National Meeting of the American Society of Mining and Reclamation, Breckenridge, Colo, June, CD-ROM.

Shaw, S., Wels, C., Robertson, A., and Lorinczi, G., 2002, Physical and geochemical characterization of mine rock piles at the Questa mine, New Mexico; *in* Tailings and Mine Waste '02: Proceedings of the Ninth International Conference on Tailings and Mine Waste: Fort Collins, Colorado, USA, 27-30 January, p. 447-458, also at http://www.robertsongeoconsultants.com/papers/shapag.pdf, accessed November 19, 2006.

Shaw, S., Wels, C., Robertson, A., Fortin, S., and Walker, B., 2003, Background characterisation study of naturally occurring acid rock drainage in the Sangre de Cristo Mountains, Taos County, New Mexico; in ICARD 2003—Proceedings from the 5th international conference on acid rock drainage: The Australasian Institute of Mining and Metallurgy, Melbourne, p. 605-616.

Sheppard, S.M.F. and Gilg, H.A., 1996, Stable Isotope Geochemistry of Clay Minerals: Clay Minerals, v. 31, p. 1-24.

Shum, M.G.W., 1999, Characterization and dissolution of secondary weathering products from the Gibraltar mine site: M. S. thesis, University of British Columbia, Vancouver, 310 p.

Shum, M. and Lavkulich, L.M., 1999, Use of sample color to estimate oxidized Fe content in mine waste rock: Environmental Geology, v. 37, p. 281-289.

Sidenko, N.V., Lazareva, E.V., Bortnikiva, S.B., and Kireev, A.D., 2005, Geochemical and mineralogical zoning of high-sulfide mine-waste at the Berikul mine-site, Kemerovo region, Russia: Canadian Mineralogist, v. 43, p. 1141-1156.

Simmons, S.F., Browne, P.R.L., and Brathwaite, R.L., 1992, Active and extinct hydrothermal systems of the North Island, New Zealand: Society of Economic Geologists, Guidebook Series, v. 15, 121 p.

Smith, K.S., Briggs, P.H., Campbell, D.L., Castle, C.J., Desborough, G.A., Eppinger, R.G., III, Fitterman, D.V., Hageman, P.L., Leinz, R.W., Meeker, G.P., Stanton, M.R., Sutley, S.J., Swayze, G.A., and Yager, D.B., 2000a, Tools for the rapid screening and characterization of historical metal-mining waste dumps, in Proceedings of the 2000 Billings Land Reclamation Symposium, Billings, Montana, March 20-24, 2000: Bozeman, Montana State University, Reclamation Research Unit Publication No. 00-01 (CD-ROM), p. 435-442, http://crustal.usgs.gov/minewaste/pdfs/ksmith_billings.pdf, accessed October 19, 2008.

Smith, K.S., Ramsey, C.A. and Hageman, P.L., 2000b, Sampling strategy for rapid screening of mine-waste dumps on abandoned mine lands: in proceedings; *in* ICARD 2000—Proceedings from the 5th International Conference on Acid Rock Drainage: Society for Mining, Metallurgy and Exploration, Inc., v. II, p. 1453-1461.

SRK, 2004, Hydrogeologic characterization of the caving induced subsidence areas: SRK project Number 009216.00, 184 p.

Stormont, J.C. and Farfan, E., 2005, Stability evaluation of a mine waste pile: Environmental and Engineering Geosciences, Vol. XI, No. 1, February 2005, p. 43–52.

Tachie-Menson, S., 2006, Characterization Of The Acid-Producing Potential And Investigation Of Its Effect On Weathering Of The Goathill North Rock Pile At The Questa Molybdenum Mine, New Mexico: M. S. thesis, New Mexico Institute of Mining and

Technology, Socorro, 209 p., http://geoinfo.nmt.edu/staff/mclemore/Molycorppapers.html, accessed October 19, 2008.

Tachie-Menson, S., McLemore, V. T. and White, T., 2005, Analysis of Five-Year Temperature and Gas Data from Rock Piles at the Molycorp Questa Mine, New Mexico: Rock Pile Stability Project Report, Molycorp Project Managers and Weathering Stability Team, Task 1.4.3, 44 p.

Tamura, K., Yamada H., and Nakazawa, H., 2000, Stepwise hydration of high-quality smectite with various cations: Clays and Clay Minerals, v. 48, no. 3, p. 400-404.

Tonui, E., Jones, R.L., Scott, K.M., 2002. Regolith mineralogy and geochemical dispersion at the Northparkes Cu–Au deposits, NSW, Australia. Geochem. Explor. Environ. Anal. 2, p. 345– 361.

Tran, A.B., Miller, S., Williams, D.J., Fines, P., and Wilson, G.W., 2003, Geochemical and mineralogical characterization of two contrasting waste rock dumps—The INAP waste rock dump characterization project; in ICARD 2003—Proceedings from the 5th international conference on acid rock drainage: The Australasian Institute of Mining and Metallurgy, Melbourne, p. 939-947.

Tuğrul, A. and Gürpinar, O., 1997, The effect of chemical weathering on the engineering properties of Eocene basalts from northeastern Turkey: Environmental and Engineering Geosciences, v. 3, p. 225-234.

URS Corporation, 2003, Mine rock pile erosion and stability evaluations, Questa mine: Unpublished Report to Molycorp, Inc. 4 volumes.

van Dam, R.L., Gutierrez, L.A., McLemore, V.T., Wilson, G.W., Hendrickx, J.M.H., and Walker, B.M., 2005, Near surface geophysics for the structural analysis of a mine rock pile, northern New Mexico: 2005 National Meeting of the American Society of Mining and Reclamation, Breckenridge, Colorado, June, CD-ROM.

Van der Plas, D. and Tobi, A.C., 1965, A chart for judging the reliability of point counting results: American Journal of Science, v. 263, p. 87-90.

Viterbo, V.C., 2007, Effects of pre-miming hydrothermal alteration processes and post-mining weathering on rock engineering properties of Goathill North rock pile at Questa mine, Taos County, New Mexico: M.S. thesis, New Mexico Institute of Mining and Technology, Socorro, 274 p., http://geoinfo.nmt.edu/staff/mclemore/Molycorppapers.html, accessed December 06, 2007.

Viterbo V., McLemore, V., Donahue, K., Aimone-Martin, C., Fakhimi, A., and Sweeney, D., 2007, Effects of Chemistry, Mineralogy, Petrography and Alteration on Rock Engineering Properties of the Goathill North Rock Pile at the Molycorp Questa Mine, New Mexico: Society of Mining, Metallurgy and Exploration Annual Convention, Denver, Feb 2007, no. 07-099, 8 p.

Wagner, A.M. and Harrington, J.T., 1995, Revegetation report for Molycorp, Inc. Questa mine site: unpublished report for Vail Engineering, 45 p.

Weber, P.A., Stewart, W.A., Skinner, W.M., Weisener, C.G., Thomas, J.E., and Smart, R.St.C., 2004, Geochemical effects of oxidation products and framboidal pyrite oxidation in acid mine drainage prediction techniques: Applied Geochemistry, v. 19, p. 1953-1974.

Wellmer, F.W., 1989, Statistical evaluations in exploration for mineral deposits: Springer-Verlag, New York, ISBN 3-540-61242-4, 379 p.

Wels, C., O'Kane, M., and Fortin, S., 2001, Storage Cover Test Plot Study for Questa Tailings Facility, New Mexico: 18th Annual National Meeting, American Society for Surface Mining and Reclamation, June 3-7, 2001, Albuquerque, New Mexico.

Wels, C., Loudon, S., and Fortin, S., 2002, Factors influencing net infiltration into mine rock piles at Questa Mine, New Mexico; *in* Tailings and Mine Waste '02: proceedings of the Ninth International Conference on Tailings and Mine Waste: Fort Collins, Colorado, USA, 27-30 January, p. 469-477, also at http://www.robertsongeoconsultants.com/papers/welfin.pdf, accessed November 19, 2006.

Wels, C., Lefebvre, R., and Robertson, A.M., 2003, An overview of prediction and control of air flow in gas acid-generating waste rock dumps; in ICARD 2003—Proceedings from the 5th international conference on acid rock drainage: The Australasian Institute of Mining and Metallurgy, Melbourne, p. 639-650.

Western Regional Climate Center, April 11, 2006, Historical Climate Data, Climate Extremes by State, http://www.wrcc.dri.edu/htmlfiles/state.extremes.html, accessed April 11, 2006.

Wildeman, T.R., Ranville, J.F., Herron, J., and Robinson, R.H., 2003, Development of a simple scheme to determine the chemical toxicity of mine wastes, in Proceedings, 2003 National Meeting of the American Society of Mining and Reclamation and 9th Billings Land Reclamation Symposium, Billings, MT, June 3-6, 2003: Lexington, Kentucky, American Society of Mining and Reclamation.

Wilson, J.A., 2003, Numerical modeling of unsaturated flow in vertical and inclined waste rock layers using the Seep/w model: Ph.D. dissertation, University of Saskatchewan, Saskatoon, 195 p.

Yager, D.B., Church, S.E., Verplanck, P.L., and Wirt, L., 2005, Ferricrete, Manganocrete, and Bog Iron Occurrences with Selected Sedge Bogs and Active Iron Bogs and Springs in Part of the Animas River Watershed, San Juan County, Colorado: U.S. Geological Survey Miscellaneous Field Studies Map MF-2406.

Yokota, S. and Iwamatsu, A., 1999, Weathering distribution in a steep slope of soft pyroclastic rocks as an indicator of slope stability: Engineering Geology, v. 55, p. 57-68.

Yokoyama, T. and Nakashima, S., 2005, Color development of iron oxides during rhyolite weathering over 52,000 years: Chemical Geology, v. 219, p. 309-320.

Zahl, E.G., Biggs, F., Boldt, C.M.K., Connolly, R.E., Gertsch, L., and Lambeth, R.H., 1992, Waste Disposal and Contaminant Control, *in* Hartman, H.L., ed., SME Mining Engineering Handbook: Littleton, CO, Society for Mining, Metallurgy and Exploration Inc., p. 1170-1180.